2014

Investigation of Laser Clad Bead Geometry to Process Parameter Settings for Effective Parameter Selection, Simulation, and Optimization

Kush Aggarwal
University of Windsor

Investigation of Laser Clad Bead Geometry to Process Parameter Settings for Effective Parameter Selection, Simulation, and Optimization

By

Kush Aggarwal

A Thesis
Submitted to the Faculty of Graduate Studies
through the Department of Mechanical, Automotive and Materials Engineering
in Partial Fulfillment of the Requirements for
the Degree of Master of Applier Science
at the University of Windsor

Windsor, Ontario, Canada

2014

Investigation of Laser Clad Bead Geometry to Process Parameter Settings for Effective Parameter Selection, Simulation, and Optimization

By

Kush Aggarwal

APPROVED BY:

_____

Dr. Z. Pasek
Industrial and Manufacturing Systems Engineering

_____

Dr. B. Minaker
Mechanical, Automotive and Materials Engineering

_____

Dr. R. J. Urbanic, Advisor
Mechanical, Automotive and Materials Engineering

June 23, 2014

DECLARATION OF ORIGINALITY

I. Co-Authorship Declaration

I hereby declare that this thesis incorporates material that is result of joint research, as follows:

This thesis incorporates the outcome of a joint research undertaken in collaboration with Kush Aggarwal, Luv Aggarwal and Syed Saqib under the supervision of Professor, Dr. Ruth Jill Urbanic. The collaboration with Luv Aggarwal and Dr. Ruth Jill Urbanic is covered under partial sections of Chapter 4 & 5; the collaboration with Syed Saqib and Dr. Jill Ruth Urbanic is covered under partial sections of Chapter 5 and Chapter 6. In all cases, the key ideas, primary contributions, experimental designs, data analysis and interpretation, were performed by the author. The contribution of co-authors was primarily through the provision of comments, suggestions and recommendations.

I am aware of the University of Windsor Senate Policy on Authorship and I certify that I have properly acknowledged the contribution of other researchers to my thesis and have obtained written permission from each of the co-author(s) to include the above material(s) in my thesis.

I certify that with the above qualification, this thesis, and the research to which it refers is the product of my own work.

II. Declaration of Previous Publication

This thesis includes excerpts, citations and partial sections from the papers that have been previously published/submitted for publication in peer reviewed journals, as follows:

Thesis Chapter	Publication title/full citation	Publication status
Chapter 6	Aggarwal, K., Urbanic, R., and Aggarwal, L., "A Methodology for Investigating and Modelling Laser Clad Bead Geometry and Process Parameter Relationships," *SAE Int. J. Mater. Manf.* 7(2):2014, doi: 10.4271/2014-01-0737.	Published

Chapter 6 & 7	Saqib, S., Urbanic, R. J., & Aggarwal, K. (2014). Analysis of layer morphology in additive manufacturing process to develop functional parts by using laser cladding method. The 47th CIRP Conference on Manufacturing Systems. Windsor: Elsevier Ltd.	Published
Chapter 5, 6 & 7	Aggarwal, K., Urbanic, R. J., & Saqib, S. (2014). Analysis of laser cladding bead morphology for developing additive manufacturing travel paths. Rapid Prototyping Journal. Emerald Group Publishing Limited.	Accepted for publication
Chapter 7	Aggarwal, K., Aggarwal, L., & Urbanic, R. J. (2014). Identifying relative importance of input parameter(s) in developing predictive models for laser cladding process. International Mechanical Engineering Congress & Exposition. Montreal, Canada: American Society of Mechanical Engineers (ASME).	Accepted for publication

I certify that I have obtained a written permission from the copyright owner(s) to include the above published material(s) in my thesis in appendix A. I certify that the above material describes work completed during my registration as a graduate student at the University of Windsor.

I declare that, to the best of my knowledge, my thesis does not infringe upon anyone's copyright nor violate any proprietary rights. Any ideas, techniques, quotations, or any other material from the work of other people included in my thesis, published or otherwise, are fully acknowledged in accordance with the standard referencing practices. Furthermore, to the extent that I have included copyrighted material that surpasses the bounds of fair dealing within the meaning of the Canada Copyright Act, I certify that I have obtained a written permission from the copyright owner(s) to include such material(s) in my thesis.

I declare that this is a true copy of my thesis, including any final revisions, as approved by my thesis committee and the Graduate Studies office, and that this thesis has not been submitted for a higher degree to any other University or Institution.

ABSTRACT

Laser cladding is an additive manufacturing technique involving deposition of powdered clad metal in successive 2D layers onto a substrate thereby creating surface coatings with enhanced material properties. Process and shape parameters contribute in defining the geometry of the clad bead; however, due to the highly coupled nature of the process, it is difficult to determine the relationship between parameters. This research predicts such parameters through development of a cognitive artificial intelligence system using artificial neural networks. A robust experimentation design process applying response surface methodology technique is adopted to collect the bead geometry data for various process configurations. Furthermore, the research identifies the extent of contribution of each factor and the impact of their interactions on the model output through ANOVA and sensitivity analysis. Lastly, a K-mean clustering algorithm is incorporated to identify optimal number of clusters present in the collected dataset on the basis of bead shape characteristics.

To my parents,

for their unconditional love, endless support, and encouragement.

"A happy family is but an earlier heaven"

– Sir John Bowring

ACKNOWLEDGEMENTS

Foremost, I would like to acknowledge my gratitude and render my warmest appreciations to my advisor and mentor Dr. Ruth Jill Urbanic. A special recognition for her patient guidance, encouragement, enthusiasm, motivation and immense knowledge that she has provided me throughout the years.

I would like to thank the thesis committee members, Dr. Bruce Minaker and Dr. Zbignew Pasek for giving me the honor of being a part of my research committee and allocating valuable time towards my research. Their expert advice, guidance and support during the course of my time as a university scholar contributed a huge encouragement towards this project.

I owe a debt of gratitude to Dr. Jennifer Johrendt for teaching the fundamentals of developing a cognitive artificial intelligence system with use of neural networks. Also, her invaluable assistance and expert knowledge provided a treasured contribution to this research.

I would like to thank Ontario Center of Excellence (OCE) for financially supporting this research project through the Collaborative Research funding program. I would also like to thank the Industry partner for the time and resources endeavored towards this research project.

I would like to thank the University of Windsor for my exceptional education in the field of engineering and providing me with a wonderful platform to shine and showcase my achievements. Also, I would like to acknowledge all my friends who provided me a form of much needed escape from my studies; to keep things in prospective. A special acknowledgement to Avneet Sekhon for helping me edit my thesis work and providing me with constant encouragement to reach my goals.

Lastly, I would like to thank my parents, Dr. Niraj Aggarwal and Dr. Namita Kundra Aggarwal, for helping me realize my own potential and for all the love, support, and unwavering belief in me they have provided over the years. I would also like to thank my brother (Luv Aggarwal) for his love and constant support throughout the years in good and bad times. His friendly guidance has been invaluable throughout all stages of the work. But most of all, I would like to thank him for being such a supportive brother and my best friend.

TABLE OF CONTENTS

LIST OF TABLES

LIST OF FIGURES

LIST OF APPENDICES

LIST OF ABBREVIATIONS/SYMBOLS

Abbreviations

%D	Percentage dilution
2D	Two dimensional
3D	Three dimensional
3DP	Three dimensional printing
4D	Four dimensional
abs	Absolute value
AM	Additive manufacturing
ANFIS	Adaptive network based fuzzy interface system
ANN	Artificial neural network
ANOVA	Analysis of variance
ART	Adaptive resonance theory
ARTMAP	Adaptive response theory of mapping
BP	Backpropagation technique
CAD	Computer-aided design
CAM	Computer-aided manufacturing
CCC	Central composited circumscribed
CCD	Central composite design
CCD Camera	Charged coupled device
CCF	Central face centered
CCI	Central composite inscribed
CFD	Computational fluid dynamics
CH	Calinski Harbasz value
CNC	Computerized numeric control
CT	Clamping technique
CTWD	Contact tip to work-piece distance
CW	Cold wire

D	Matrix design point
DOE	Design of experiments
DOF	Degrees of freedom
FAMNN	Fuzzy ARTMAP neural network
FDM	Fused deposition modelling
FEA	Finite element analysis
FL	Focal length of the lens
FR	Feed rate
GA	Genetic algorithm
GMAW	Gas metal arc welding
GPC	Generalized predictive controller
GTAW	Gas tungsten arc welding
GUI	Graphic user interface
H	Hypothesis condition
HAZ	Heat affected zone
IPG	Semiconductor laser
LC	Laser cladding
LED	Light emitting diode
LM	Layered manufacturing
LM technique	Levenberg Marquardt technique
LOM	Laminate object manufacturing
LS	Laser speed
MIG	Metal inert gas welding
MIMO	Multi-input multi-output
MLP	Multi-layer perceptron
MSE	Mean square error
MSEREG	Regularized mean square error value
MSW	Mean sum of squares of network weights and bias values
OVAT	One variable at a time
P	Penetration
PID	Proportional integral derivative

PSO	Particle swarm optimization
PW	Power
R	Regression value
R&D	Research and development
RBFNN	Radial base function neural network
RH	Reinforcement height
RH_{12}	Reinforcement height between bead 1 and 2
RH_{23}	Reinforcement height between bead 2 and 3
RP	Rapid prototyping
RSM	Response surface methodology
SI	Sensitivity index
SLA	Stereo lithography
SLS	Selective laser sintering
SM	Subtractive manufacturing
Sqrt	Square root value
Std Dev	Standard deviation
STL	Stereo lithography digital file format
T	Total bead height
T_{OUTPUT}	Network target values
TIG	Tungsten inert gas welding
UDF	User defined function
W	Bead width
X	Matrix orientation
X_{INPUT}	Network input values
X-Y-Z	Cartesian co-ordinates

Symbols for Laser Cladding Process

A	Area of the positive bead
B	Area of the negative bead

E	Efficiency of the process
I	Current
Q	Heat input
S	Welding speed
V	Voltage

Symbols for Design of Experiments

I (t)	Current supplied
M	Levels
n	Number of experiments
N	Number of design variables
η	Response surface
n x k	Design matrix
nc	Center points
P(t)	Instantaneous power
V(t)	Potential difference in voltage
X_i	Experimental value
y	Objective function
α	Axial distance from the center point to axial point
β	Co-efficient to linear, square and quadratic terms
ϵ	Noise factor

Symbols for Artificial Neural Networks

a	Lower boundary condition [-1]
b	Bias value
c	Upper boundary condition [+1]
d_m	Total gradient

d_m	First derivative of error
d^s_m	Second derivative of error
e	Natural logarithmic function
g	Improved performance ratio
L(u)	Linear Activation Function
Log(u)	Log sigmoid function
m	Epoch run
N	Number of training cases
t	Targets
Tanh(u)	Hyperbolic tan sigmoid function
w_i	Weight of input(s)
w_m	Input weight
x_i	Inputs to the Network
X_i'	Normalized value
z	Network outputs
λ	Damping factor
σ	Non-linear function

Symbols for Significance of Parameters

μ	Average of response variable
A/B/C/D/E	Manufacturing parameters
C.V.	Co-efficient of variation
H_0	Null hypothesis
$MS_{Pure\ Error}$	Experimental error
n	Number of terms
V	Variation
X	Overall mean
X_i	Mean of the groups
Y	Response variable

β	Co-efficient to linear, square and quadratic terms
δx	Incremental change in inputs
δy	Incremental change in outputs

Symbols for Classification

C	Co-relation value
c_i	Defined cluster
d	Euclidean distance
d(x,y)	Pythagoras co-ordinates
E	Sum of Square Errors
k	Optimal clusters
m	Mean of clusters
m_i	Centroid of each cluster
p	Given element
SS_B	Overall between cluster variance
SS_W	Overall within cluster variance
VRC_k	Variance ratio criterion

CHAPTER 1

INTRODUCTION TO ADDITIVE MANUFACTURING

1.1 Background

The term "manufacturing", refers to a method that converts raw materials into finished products using manual labor or machines, especially on a large scale [1]. Manufacturing is derived from the Latin word "Martus Factus", which means "made by hand" [2].

In general, manufacturing can be categorized according to the technique or the methodology adapted to attain a desired finished product, as follows:

1) Casting process- this is one of the oldest methods of manufacturing. Sand casting is one of the most common examples of the casting process. Here, the molten metal is poured into the metal cavity and it is allowed to solidify to produce the final product. Other examples of the casting process include: investment casting, permanent mould casting, die casting, centrifugal casting etc.
2) Forming process- this is a process that aids in the modifying the shape of a preheated metal. Drop forging is one the most common examples of the forming process. Here, the preheated metal (billet) is placed in the die and a hammer is used to strike the billet. This allows the shape of the die cavity to be obtained. Other examples of the forming process include: press forging, upset forging, wire drawing, rolling etc.
3) Welding process- this process involves joining two or more metallic pieces by applying heat and pressure. Gas welding is one of the most common examples of the welding process in which molten metal wire (with heat and pressure) is used as an adhesive to join metal plates. Other examples of the welding process are: electric arc welding, resistance welding, etc. Soldering, brazing are complementary processes, but the base material is not melted.
4) Subtractive manufacturing (SM) process or material removal process- this is a process that aids in removing the unwanted material from the work piece. Drilling is one of the most common examples of the material removal process in which the unwanted material is removed from the work piece by creating a hole in the work

piece. Other examples of the material removal process include: milling, grinding, broaching, turning etc.

The casting process and the welding process are a few types of the additive manufacturing (AM) processes. On the Contrary, the forming process is a supplemental process to the AM operations that helps generate new parts with no addition to material (parts generated through deformation process). AM is demarcated by the addition of the raw materials to a substrate or a base material. However, SM is demarcated by the removal of the material during a manufacturing/ machining process.

AM defines the future of the manufacturing sector and helps revolutionize the industry as it currently stands. AM techniques not only infuse the idea of "on demand manufacturing", but also have various advantages over conventional methods (SM techniques). This thesis work incorporates an AM approach (laser cladding), which is a budding practice in manufacturing industry today.

1.1.1 Comparison between Additive and Subtractive Manufacturing

Additive Manufacturing (AM) is a modern manufacturing technique to addition or stacking of various successive two-dimensional (2D) layers to form a desired three-dimensional part [3]. Figure 1, displays two additive manufacturing prototypes (figure1 B, source: industry sponsor [4]).

(A) (B)

Figure 1: Additive manufacturing prototypes- (A) FDM and (B) laser cladding operations

On the other hand, subtractive manufacturing (SM) is a traditional manufacturing approach that refers to the process of material removal using various machines such as computer-numeric control (CNC), horizontal/ vertical mills, lathe etc. to achieve a desired finished end product. Again, "subtractive", as the name suggests, refers to loss of material while crafting a desired shape from a basic geometrical shape (such as a cube, a cylinder etc.) [3]. Figure 2, displays a few subtractive manufacturing processes (figure2 (A) source: Gosiger [5]; figure2 (B) source: Florian Schott [6]).

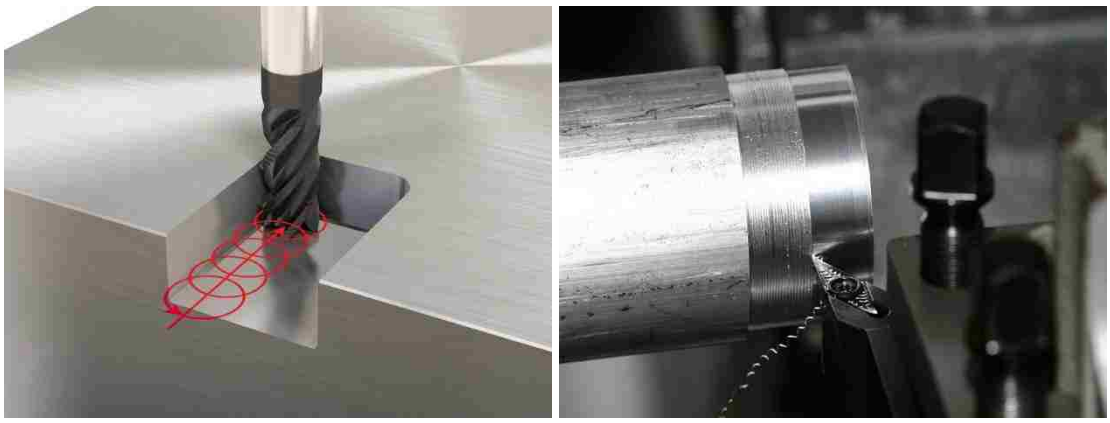

(A) (B)

Figure 2: Subtracting manufacturing processes- (A) milling [5] and (B) lathe [6]

Additive manufacturing (AM) marks a new paradigm shift for the manufacturing field of engineering over various traditional approaches. The industrial revolution was driven by various subtractive manufacturing approaches which led to vast accomplishments in the manufacturing sector. These accomplishments had a major impact on the manufacturing industry but had various limitations in regards to manufacturing capabilities. AM overcomes various manufacturing limitations set by traditional practices and provides better quality and long lasting products [7].

1.1.2 Additive Manufacturing Process

Independent of the process adopted for additive manufacturing, the three sub-components for an additive manufacturing process comprise of:

1) The generation of a computer aided design model (CAD model),
2) The fabrication of a physical layered model, and
3) Post processing of the layered model

These additive manufacturing steps can further be decomposed to six simple procedural step(s): [8]

a) Drafting a 2D/ 3D model utilizing a computer aided design software (CAD)
b) Conversion of a proprietary CAD file to a suitable prototyping file, generally in most cases a '.STL' (stereo lithography) format file.
c) Slicing the generated model/file into 2D cross sectional surfaces
d) Generation of a tool path to create the model in the additive manufacturing machine
e) Creation of the model in real life (physical form)
f) Finishing and post processing operations, for example, removing support materials, cleaning, etching etc.

1.1.3 Additive Manufacturing Applications and Divisions

The systems that manufacture products using principles of additive manufacturing are also known as layered manufacturing (LM) Systems. The prototypes generated by these systems are helpful from the concept visualization phase to the functional and analysis phase of the desired product. These layered manufacturing systems (LM) fabricate components that have applications in diverse fields ranging from manufacturing sector to biomedicine.

The selection of an additive manufacturing process is generally made based on the end use of manufactured prototypes/ products. As seen in figure 3 (adapted from [9]), the maximum (major) share of market for additive prototypes/ products is most prevalent in the consumer products and the automotive industry (approx. 25% each), the second largest share is prevalent in the aerospace industry, business machines and medical industry and the third largest share is prevalent in sectors such as the military/government and various academia institutions. [9]

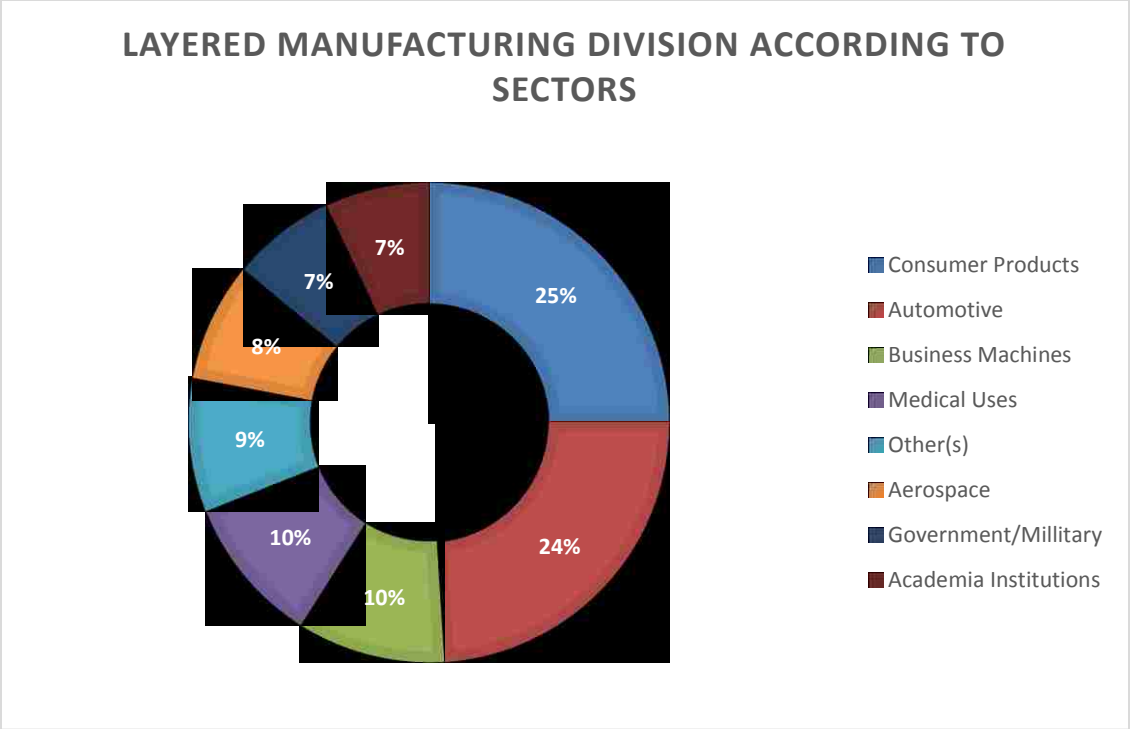

Figure 3: Layered manufacturing division according to sectors adapted from [9]

It can be noted from figure 4 (adapted from [10]) that the primary application of additive manufacturing includes generating functional models, a visual aid tool for engineers, patterns for prototype tooling, and for fit/assembly testing. The secondary application includes building patterns for cast metals, visual aids for toolmakers, and directing tooling inserts. The tertiary applications include using AM prototypes for proposals, ergonomic studies, quoting applications, and others. [10]

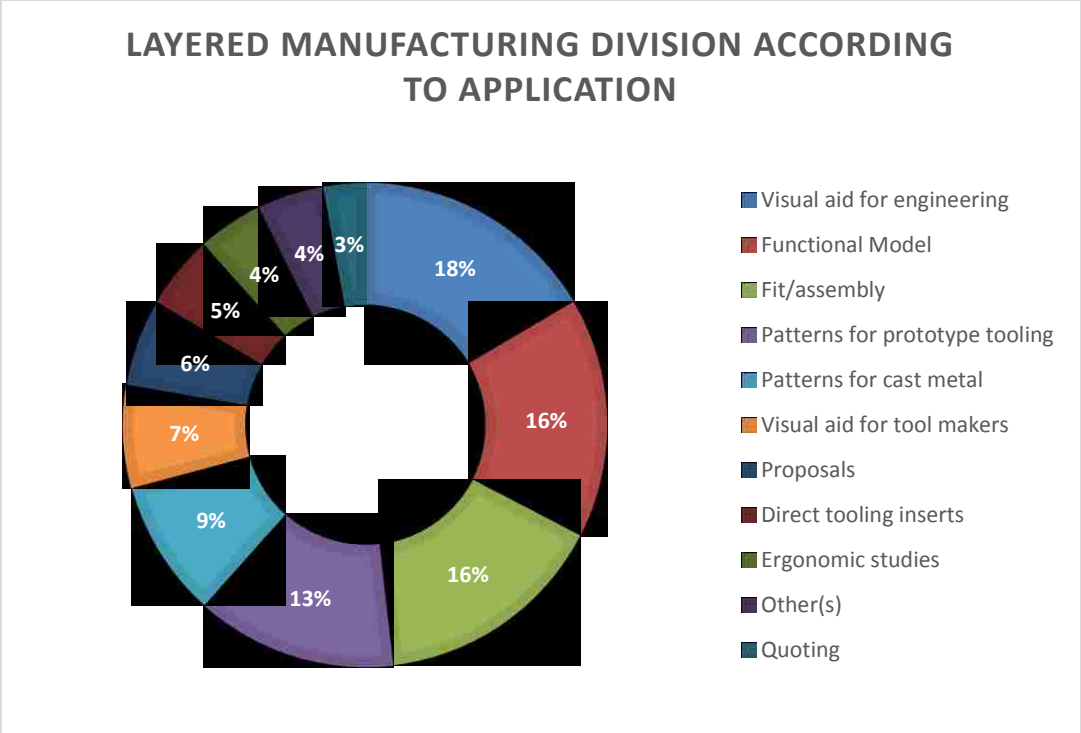

Figure 4: Layered manufacturing division according to application adapted from [10]

1.1.4 Types of Additive Manufacturing Processes

Some of the main AM technologies that exist in today's market/industry and academia are stereo lithography (SLA), selective laser sintering (SLS), fused deposition modelling (FDM), 3D printing (3DP), laminate object manufacturing (LOM) and laser cladding (LC). [8]

These technologies have their unique advantages and disadvantages but are much similar in their overall manufacturing processes, i.e., AM processes consist of six basic fundamental steps to manufacture a component (seen in subsection 1.1.2). Table 1 shows the various layered manufacturing technologies subjected to the raw material utilized for production purposes. [8]

Table 1: Types of layered manufacturing technologies with raw materials

S. No.	Layered Manufacturing technology	Raw Material
1.	Stereo lithography (SLA)	Photopolymer
2.	Selective laser sintering (SLS)	Metal powder, thermoplastics
3.	Fused deposition modelling (FDM)	Thermoplastics/ eutectic metals (ex. silver-gold alloys that transform directly from solid to liquid state or vice-versa).
4.	3D Printing (3DP)	Powder(s)
5.	Laminate object manufacturing (LOM)	Paper (primary raw material), plastics and ceramics
6.	**Laser cladding (LC)**	**Powder metal(s)**

The focus of this thesis work is on the laser cladding technology. This technology is discussed more in detail in chapters 3-6.

1.1.5 Advantages of Additive Manufacturing

Additive manufacturing has various advantages over conventional machining processes, including:

1) Ability to effectively manage increased part complexity without increased process planning time - a major benefit of using an additive approach is the ability to create parts that comprise of complex shapes and are difficult or impossible to manufacture through conventional subtractive practices. For example- additive manufacturing can produce various complex structures that in the past had limitations due to weight or process planning constraints, which are typical applications for the aerospace and automotive industries. Figure 5 (source: Ziad, Abou [11]), displays one such application of structure created through FDM (fused deposition modelling technique), a technique that is extremely challenging to produce through conventional machining operations.

Figure 5: Complex additive manufacturing specimen [11]

2) Digital design and ease of manufacturing- the parts manufactured through the process of additive manufacturing are generally a bi-product of standardized digital files (.STL files). The level of operator expertise and human interaction through a graphic user interface (GUI) required is low as the part is being generated and validated within the CAD/ CAM software. This practice promotes an unmonitored manufacturing approach leading to an increase in production volume and a decrease in lead time. Furthermore, digital manufacturing promotes production through customization [7].
3) Low production cost due to "free complexity"- in subtractive manufacturing, production of a part requires various tool changes along with process planning complications that adds to the complexity of the part. On the other hand, additive manufacturing is a complexity independent process that promotes manufacturing using a single tool for any desired geometry. This proactive approach makes the process complexity free with no additional costs or lead times in manufacturing of the customized parts [7].
4) Instant global production- the products produced with additive manufacturing are created initially through a digital .STL file. Due to this digital nature of the part, these files can be transferred over the web. Once the file is downloaded, it follows the identical process of manufacturing through a compatible production equipment, resulting in similar design characteristics of the 3D part manufactured [7].
5) Waste reduction- additive manufacturing is done through addition of successive 2D layers, hence leading to no wastage of material. In conventional practices, the

material removal process leads to bi-products such as material scraps (ex. metal chips) and other lubrication fluids (ex. coolants and lubrication oils) which are non-biodegradable. Hence, additive manufacturing also promotes "green manufacturing" [7].

1.2 Motivation, Objectives, and Limitations

1.2.1 Motivation

Laser cladding (LC) is an additive manufacturing process that builds a product from thin layers of melted powdered metal(s) through a fusion reaction with help of a laser system. In a particular case of laser cladding, the part's geometrical properties depends on the material's deposition orientation, feed rate of the powder (metal), power of the laser, focal length of the focusing lens, travel speed of the laser to provide fusion reaction and the distance of the nozzle to the workpiece. These factors/ parameters control the meso-structure characteristics of the bead and influence the overall built of clad bead geometry. The dependence of the material's geometrical properties and meso- characteristics on the manufacturing parameters provides the laser cladding (LC) technology an ability to optimize the overall build performance. This approach is well established for similar process like metal inert gas (MIG) and tungsten inert gas (TIG) welding technology; but proves to be a novelty area of research for the laser cladding technology.

There are three main manufacturing strategies for the clad bead structure built or generated by using laser cladding technology: single pass bead, overlapping layers and multi- layer orientation (3D part). Each manufacturing strategy has a significantly unique use in the industry and hence, it is relevant to study these strategies to generate profits. Single bead orientations are generally used in repair work of mold and die sets, overlapping layers are generally used to coat a surface of a metal to enhance the metallurgical properties of a substrate (such as wear, corrosion, thermal etc.) and multi-layer orientations are complex integrations of various overlapping layers which aid in generating a three-dimensional structure. Figure 6 (source: industry sponsors [4]; figure 6 (C), designer- Mr. Syed Saqib), displays uses of each manufacturing strategy.

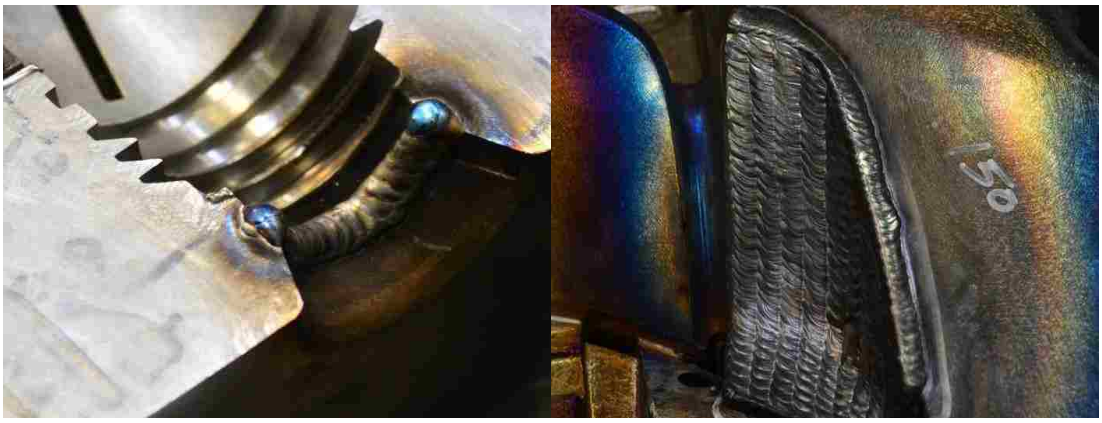

(A) (B)

(C)

Figure 6: Laser cladding operation- (A) single pass, (B) overlap pass, and (C) 3D part [4] – designer Mr. Syed Saqib

The excessive time consumed, financial investments and material wastes are prominently increased when a part is generated in any of the mentioned (A, B, and C) manufacturing strategies due to laser cladding being a novel technology in the additive sector. Research has shown that when various manufacturing parameter configurations are utilized, dilution levels over a diverse range are generated in bead structures. Also, overlapping and multilayer structures tend to possess porosity due to imperfections in the manufacturing process and systems involved. Presence of such impurities during

production is not desirable since such impurities may lead to instability and various structural mishaps. Evidently, it is desirable to standardize the laser cladding process to reduce the manufacturing time and the material wastage. The aforementioned action will be desirable to characterize and ensure the stability of the structure as well as the geometrical behavior for which the desired part is produced.

The shape or geometrical properties established in a laser cladding process are thus governed by the manufacturing parameters. Hence, it is vital to characterize or standardize a methodology that can show linear or non-linear topological relationships between the structural (shape) properties with corresponding manufacturing parameters.

1.2.2 Thesis Objective

The key focus of this research is to standardize and optimize a clad bead structure that relates to a set of manufacturing parameters for the laser cladding additive manufacturing process. This thesis encompasses the following objectives which are necessary to achieve the desired goal of standardization.

1) An experimentation approach for data collection: the objective of defining an experimentation strategy for standardizing the laser cladding technology is to minimize extensive collection of raw data. This raw data results from generating combinations of configurations (manufacturing parameters) that are involved in the LC process varied over five levels. Fabrication of the desired clad bead geometry for various process configurations is highly expensive, as it involves investment of raw materials, financial participation and time resources. Thus, a design of experiments (DOE) technique is hereby applied to this thesis work for data collection, providing a cost- effective means of solving problems and developing new processes.
2) A cognitive artificial intelligence system: the purpose of developing an artificial intelligent cognitive system is to reverse engineer the laser cladding process and to commercialize the product (software package). Here, a neural network application based off a MATLAB workspace is utilized along with the experimental approach

(designed through DOE), to successfully predict manufacturing parameters from shape parameters of a generated clad bead and vice-versa. A neural network uses a supervised learning technique to confidently predict the output variables in the system based on a Levenberg Marquardt (LM) learning algorithm. This prediction tool helps reduce experimentation time by generating outputs for various unknown input datasets for future use.

3) Significant interactions between the manufacturing parameters (feed rate, power, travel speed, focal length of the lens, and contact tip to workpiece distance) and the geometrical shape characteristics (height, width, penetration and percentage dilution): laser cladding is a multi-variable, non-linear behavioral process with interactions among its parameters. The objective here is to identify the extent of the contribution of each variable (parameter) and its impact resulting from interactions on the output. This is essential in developing and manipulating confident predictive models for desired results. Analysis of variance (ANOVA) and sensitivity analysis methodologies are studied through this research to determine the most significant process factors that relate to the various shape parameters for a laser cladding process configuration.
4) Optimization of clad bead geometry: optimization is a vital component of manufacturing industry in today's market. This optimization approach is adopted in this thesis work to generate the clad bead structures that reduce system instability and structural mishaps. To achieve such goals, production impurities, such as percentage dilution is minimized as an objective function. The response optimizer application based of the MINITAB software workspace is utilized to the generated statistical model. The response optimizer also aids in visualizing single and multiple objective optimization results that helps optimize single or multiple parameters at a particular time in space.
5) Clad bead shape classification: classification of clad bead shape geometry is performed to determine and assign a cluster characteristic to the collected raw data points. The objective of classifying the raw data points is to determine various shapes a clad bead possesses with changing levels of percentage dilution. These shapes will eventually help define a class or cluster and determine the cluster

properties to which a bead structure belongs. A combination of MINITAB (Euclidean distance) and MATLAB (classification network) packages are used to classify the collected experimental data.

1.2.3 Limitations

The work presented in this thesis focuses on defining a clad bead shape geometry with respect to various process configurations i.e. combination of manufacturing parameters for a laser cladding operation. This thesis work is limited to the interactions between five manufacturing parameters (power of the laser, feed rate of the powdered metal, travel speed of the laser, focal length of the focusing lens and contact tip of the nozzle to workpiece distance) and four mechanical shape parameters (width of the bead, reinforcement height of the bead, penetration of the bead and percentage dilution).

The thesis work does not incorporate any external mechanical factors (such as heat affected zone, metallurgical properties, chemical properties of metals etc.) except the five manufacturing parameters and the four shape parameters. This research work uses 420 steel (low carbon) clad powder for various single pass and overlap configurations. The overlap configurations are limited to 40%, 50 %, and 60 % overlaps with a three pass bead formation. The thesis does not contribute any significant in-depth knowledge in 3D part production. The equipment used to build the clad samples is selected according to the availability of the machine at the industry sponsor facility. The composition of the 420 steel clad powder used to generate the single pass and the overlap samples is presented in table 2 (source: industry sponsor).

Table 2: Composition of the 420 steel clad powder

Elements	420 powder steel (ferrous)
Carbon (C)	0.25 %
Manganese (Mn)	0.26 %
Silicon (Si)	0.52 %
Chromium (Cr)	13.4 %
Molybdenum (Mo)	0 %
Sulfur (S)	0 %
Phosphorus (P)	0.009 %
Iron (Fe)	85.541 %
Nickel (Ni)	0 %
Cobalt (Co)	0.020 %
Titanium (Ti)	0 %
Vanadium (V)	0 %

CHAPTER 2

LITERATURE REVIEW

2.1 Experimentation

There are several experimental approaches that have been used in the past by researchers for sample collection. There is an enormous paradigm shift in the experimentation process from conventional methods to a formal 'design of experiments' approach. Most of the researchers nowadays adopt the design of experiments approach to gain a maximum amount of information from a single optimized experiment. In adopting a DOE approach, the researchers limit the amount of material wastage, time spent in generating a population of samples and long equipment usage hours. These factors directly have an impact on the financial contribution towards a research and thus, limiting them is the most favorable condition. This sub-section focuses on various DOE techniques adopted by researchers in the past to perform a successful sample collection process.

The L9 Taguchi approach is one technique applied by a research team to investigate effects of conducting polymers composite sensor compositions on the response to a homologous series of alcohol. A 2-4 (2 levels and 4 factors) L9 design is applied to collect experimental data. As compared to the conventional DOE approaches, the Taguchi prospective involve creating a robust design rather than focusing on an average result level. In this research, variation of the raw data is studied and experiments are carried out for controllable design factors and disturbing signal factors (2 or 3 levels). Also, this approach helps in choosing factor levels that help minimize sensitivity against disturbances and noise factors. The Taguchi approach is based on quality loss function by focusing on minimizing losses in quality through achieving target values. Through quality loss, Taguchi developed a method of extending each experiment with an outer array (also called orthogonal array). The outer array helps in simulating the external environment that experiments are exposed to. By applying this approach, the sensors were characterized with a view to improve sensitivity [12]. The Taguchi method through other research works' is also considered relevant in determining the behavioral changes in the shape parameters of a weld bead with fluctuating process parameters. Here, the model is developed using the three basic steps of

a robust design i.e. concept design, parameter design and tolerance design with main focus being on the parameter design. [13]

Another approach that has been applied by Buragohain, M. and Mahanta, C. [14] focuses on using a full factorial design technique in DOE. The research team applied a full factorial design methodology in deciding the size of the input-output data set while developing an adaptive network based fuzzy interface system (ANFIS) for the modelling and controlling of uncertain systems. The main objective of using a full factorial approach is to optimize the number of data points used in the learning process of the network. The paper uses the simplest design of 2 levels and n factors i.e. 2^n factorial design for generating data points. The data points in such a model lie on the corners of an n-dimensional space. Hence, in the presented paper the data points lie on the cube points (3 factors making it 8 experimental points). One of the limitations of this highlighted approach is that in a two dimensional factorial design, it is difficult to distinguish between linear and higher order interaction effects such as the quadratic and the square interactions between factors. To overcome such inabilities, the paper discusses a comparison of a 2-level design with a 3-level (1), 3-level (2) and a 4-level full factorial design. The number of experimental runs for theses designs are defined as 8, 13, 11, and 18 respectively i.e. by calculating a 2^n experimental run and adding the effect of the factors. [14]

V. K. Gupta and R. S. Parmar [15] have also approached the problem of optimizing welding bead shape parameters with the help of design of experiments (DOE) [15]. The paper defines welding processes as a multi- input, multi- output process with various process and shape parameters. Various methods for optimizing shape parameters have been defined such as factorial, response surface methodology, general algorithm, artificial neural network, and Taguchi method. Factorial design in DOE uses a 2^{n-1} approach with n being equal to 5 (process parameters). It is seen through this research that the factorial technique with a 2^{n-1} approach is highly effective in plotting main effects and interactions between different welding process parameters. Also, the factorial technique is helpful in generating mathematical models that can help predict the shape parameters and the high quality weld (when fed into automatic robotic surfacing) in boundary conditions of the factors [15]

One of the most effective and widely used DOE approaches is a response surface methodology (RSM) technique which uses a central composite design (CCD) to define an experimental dataset [16]. Zhang Z. [16] has shown the importance of central composite designs in defining a response surface. One paper presents a comparison between the three CCD's i.e. central composite circumscribed (CCC), central composite inscribed (CCI), and central face centered (CFC) designs. The CCD's are robust designs and overcome the limitations of a full factorial design by studying the interactions of quadratic and squared terms along with linear terms. The advantage of a CCD over any other approach is that the CCD design is rotatable (i.e. axial distances help in the selection of a design region) and has maximum stability due to generation of center points of a system. It is concluded from the paper that the three variations of CCD's have similar efficiency levels in the degree of model but have dissimilarities in terms of the estimation precision, the stability of variance, the uniformity in precision, and the robustness of extrapolation. Also, it is concluded that the central face centered (CCF) design is the simplest variety of CCD as it requires only three levels of each factor. Therefore, it minimizes the deception in the data set due to the experimental error in the data setup and collection process [16].

Also, another approach adopted by Khawas A., Banerjee A., and Mukhopadhyay S. [17] show that D-optimal designs are widely used in a computer generated design of experiments. Use of such a design technique helps in the construction of a quadratic 2^{nd} order model more efficiently than any other approach. The objective of this design is to select the best set of points in an experimental set to maximize the determinant of $|X^T * X|$. Here, X defines a matrix orientation of the design variables. D-optimal design, therefore, helps in minimizing the error of the coefficients of a response model (2^{nd} order model). The advantage of using such a design is the availability of extra design points that can be incorporated into the system. In papers, this approach has been found to be quite effective in analog circuit performance optimization [17]. Another area where the D- optimal technique is used as a DOE approach includes wing design for a high- speed civil transport [18].

Hence, through a detailed literature review a CCD design approach is chosen for the purpose of this thesis and a response surface methodology is carried out to optimize the input parameters at a later stage.

2.2 Artificial Intelligence system(s)

Use of artificial neural networks (ANN's) is one of the few approaches to developing a prediction model that can be termed as an artificial intelligence system. From one of the research papers, it is noted that this approach was applied in an arc welding process to control physical processes. Gas tungsten arc welding (GTAW) experimentation was carried out initially to determine the various shape parameters present in a bead structure. A neural network architecture was then built and studied using the MATLAB toolbox which aided in estimating trends in the shape parameters as well as the errors involved in the GTAW process. Various neural network configurations were built and tested to reach the best performance configuration (2-by-18 i.e. 2 hidden layers with 18 neurons/ activation functions was the best indicated configuration). The four inputs to the system are defined as voltage, current, electrode travel speed and wire feed rate; and the four outputs are defined as the shape parameters (width, penetration, reinforcement height and bead cross sectional area). [19] [20]

Alternatively, Datta S. and Pratihar D. K. [21] approached the similar problem with three approaches to establish input- output relationships in metal inert gas (MIG) welding process. The three defined approaches were different from one another as approach 1 was based on the genetic algorithm (GA) to optimize the radial base function neural network (RBFNN); whereas approaches 2 and 3 structure RBFNN according to two different clustering techniques i.e. the fuzzy c-means algorithm and the entropy based algorithm. The result shows that poor performance was seen while adapting to approach 1 due to permutations in genetic algorithms while, approach 3 was the best approach to establish the input-output relationship due to a combination of one global and one local optimizer approach. Also, it was seen that the entropy based clustering had better fitting and performance results than fuzzy c-means algorithm. [21]

Determining geometrical dimensions of the clad bead in a laser cladding process was adopted by a few researchers. Meriaudeau F., Truchetet F., Grevey D., Vannespresented A.B. [22] presented a unique low cost system using two charge-coupled device (CCD) matrix cameras, a standard acquisition card and a personal computer to gather information on the laser cladding process both in warm-up and actual operational state. Here, one of the CCD matrix camera was used to gather temperature measurements through the use of a spectral thermometer and the other CCD matrix camera was used to gather the shape parameters such as width, length of the tract, power spray distribution etc. The aim of the research was to control the cladding process in a closed loop. The real time temperature measurements were performed using algorithms based on statistical momentum conservation (Wen's algorithm) and it was seen that the temperature range for the cladding process lies between 0.7 and 15 micrometers (Max Planck's equation derivation). The paper also, envelops different methods of involving CCD sensors for the sample collection such as Doppler anemometer, discrete Fourier transform, two or three color imaging velocimerty etc. [22].

Similar research is conducted by Meriaudeau F., Truchetete F., Dumont C., and Renier E. Bolland P. [23] where two CCD cameras are used to determine shape parameters, surface temperature readings to detect variations in powder feed rate and powder distributions. Here, surface temperature is calculated using Beer Lambert's law. For temperature measurements, CCD technology (through Max Planck's Law) interpolates a linear relation between digitalization of optical radiation signal and black body temperature. Furthermore, CCD technology used for geometric measurements through afore displayed curves predicts change of track section (shape) when variations in parameters are introduced. [23]

Amara E. H., Achab L., Boumiahave O. [24] also developed a dynamic mesh method to model the laser cladding process. The major concerns of this study relates to the physical (mechanical) properties of the process i.e. the Marangoni thermocapillary flow, the powder-melt poll interaction, the mass transfers and diffusion, the laser-powder interaction, and the laser work- piece interaction. The aim of the study is to predict various shape parameters involved in laser cladding process. A mathematical approach is applied

to reach the goal where, the heat conditions and the flow dynamic equations relates to the inner and the outer boundary of the clad bead were established. A finite element analysis (FEA) approach is then applied to the generated equations for discretization and through the user defined function (UDF) deformations in the mesh were studied. Hence, these deformations were related as a result/function of the input parameters of laser, substrate material and the injected clad material. [24]

Xiong Z., Zhang Y, and Zeng X. [25] conducted specific experiments using 304 stainless steel thin plates (substrate plate) and a co-axial nozzle for the powder feed rate to demonstrate deformations in the substrate plate through the laser cladding process [25]. Parameters that contributed include the power, the scanning speed, and the line energy on the bending angle. Initially, it was seen through various experiments that there was a significant bending in the substrate plate and the bending was directly proportional to the parameters. It was realized later that the bending rate decreased when parameters reached their critical values. Also, the value of bending angle is related to yield strength of the heat affected zone, the temperature gradient in direction of thickness, and the size of plastic zone. Contrary, it was observed that with too small or too large values of the line energy, the bending angle was of smaller magnitude, but with a moderate line energy value the bending angle was of a larger magnitude [25].

Also, Song L. and Mazumder J. [26] presented a control strategy with the input constraints to stabilize the temperature possessed by a melt pool during the process of laser cladding while forming various clad layers. The instrument used to monitor the temperature reading was a dual-color pyrometer. The sub-space method helped device a dynamic model relating the laser power to the melt pool temperature. A dSPACE real-time controller was implemented to predict the control algorithm with the input constraints. Adjusting the diode laser power helped track the melt pool temperature to a reference temperature profile in a closed loop cladding process. Instead of a PID (proportional integral derivative), controller a generalized predictive controller (GPC) was used to compensate lack of deposition by the adjusting laser power during the cladding process. This is because a GPC can deal with the input constraints systematically and adapt easily to the (multi input- multi output) MIMO system. [26]

Various researchers have explored the field of welding, its processes and the shape parameters for optimization with help of various specialty tools such as DOE and ANN but the field of laser cladding is yet to sprout to its fullest. A few research articles can be found on the single bead shape characteristics through the charged couple device cameras or the image processing techniques with use of the generalized predictive controller for the laser cladding process. No research techniques are developed to tackle the problem of process planning using a single bead, an overlap and a layered approach. Furthermore, no error analysis model has been developed to correct the predictions generated by MATLAB neural network toolbox. Hence, this research should act as a fundamental basis of process planning for the laser cladding process.

2.3 Quadratic Model and Optimization

To optimize the design process Stewart T. and Stiver W.D. [27] have compared the one variable at a time (OVAT) technique to a combination approach of DOE methodologies in conjunction with the numerical inputs from a computational fluid dynamics (CFD) program. The goal of carrying out an optimization process, is to enhance multiple aspects of the thermal performance in this research paper. It is seen through the paper that the OVAT technique fails for any real time application due to the fact that as the number of experimentation points increase, the adjustment is made to one factor while holding other factors as constant. In contrast, the combination approach helps reduce the empirical prototype cycles from four to two. Also, there are considerable improvements in the experimental cycles of producing a cooling solution for the thermal problem. The DOE technique used here is a fractional factorial approach which minimizes the experimentation process from 32,768 to 16 in a model with 15 factors and 2 levels; while the CFD program used is FOTHERM which aids in providing junction temperatures. Once the design points are set for the factors and target values are achieved through the CFD program, an optimizer program through a MINITAB (DOE approach) application is run which aids in eliminating the factors that are not significant to the process. In addition the optimizer provides optimal values for other significant factors (to new design points). Through this technique a rapid evolution of design variations is achieved that is necessary to compete with multiple competitors [27].

Another approach developed for optimization of response variables by Sreeraj, P.K. [28] is use of response surface methodology along with the response optimizer tool. The paper presents a mathematical generation of second order model with linear, squared and quadratic terms to the weld bead geometry in a gas metal arc welding process (GMAW). This model aids in achieving function objectives to predict the bead geometry. Note- the objective in the paper is to obtain a good quality bead with a good corrosion resistant property to reduce the manufacturing cost along with optimizing the bead parameters. The RSM technique uses these predicted results to a construct response surface (surface and contour plots) that illustrates interactions between various factors. The optimization process through the response optimizer in MINITAB is initiated by providing a starting set of points so that an optimal combination of the process factors can be obtained. The optimizer tool also provides two solution types i.e. a local solution and a global solution. The local solution provides the best combination settings for a particular set of starting points whereas a global solution provides the best combination of factor settings for desired response variables i.e. an optimal setting for all local points. [28]

Jahan A., Ismail Y., Noorossana M.R. [29] have presented a novel method of optimization of multiple response problems in DOE. The paper proposes a four step algorithm for the optimization of nonlinear problems. The first step involves creation of a regression model of means and standard deviations for the qualitative responses. The second step focuses on converting the qualitative characteristics of the mean and the standard deviations to a capability processes index. Step three focuses on determining the lower limits of the capability processes according to the desired levels and step four helps in selecting the optimization method to solve a non-linear multi-objective problem. In the paper, the method chosen for carrying out the optimization process is a bounded objective method. This method selects the objective as the main response function and the other goals are converted to limitations according to the desirability targets. Due to the simple nature of this 4-step approach, this method can be widely applied in industry for finding the optimal combinations of parameters for multi response problems. Also, combination of means and standard deviations as capability process in step one reduces the number of objectives. [29]

For the purpose of this thesis work, a combination approach of response surface methodology (RSM) for generating second order model along with a response optimizer tool in MINITAB application is chosen for solving the multi-objective non-linear problem of the laser cladding process. Here, the regression model (2nd order mathematical model) along with various contour and surface plots aids in providing the starting points for the response optimizer tool.

2.4 Classification

Clustering of data points is generally performed to distinguish the sub-sets in a data population according to similar behavioral properties among the various data points. Many research techniques have been adopted by researchers in the past to cluster data points to various classes. This allows the elements of that sub-set to be identified according to the cluster it belongs too. Some of the major clustering techniques used in the past by researchers are explained later in this sub-section.

Kumar M., Verma S., and Singh P.P. [30] have adopted the fuzzy adaptive resonance theory (ART) technique for data clustering in the sensor networks based of the neural network application. This research paper presents a resonance based clustering of the data points technique. A combination of offline and online techniques has been proposed in the research paper. Here, fuzzy ART is used initially to cluster the data points to detect various classes as an offline deployment approach. The advantage to using fuzzy ART logic is that the approach does not require any knowledge of the data behaviour or trends. It only requires knowledge of the parameters or factors (such as range, type etc.) to generate data for clustering. The online approach applied in this research paper is application of fuzzy adaptive resonance theory of mapping (ARTMAP) through neural networks (FAMNN). FAMNN is used to cluster the data points to groups/classes after being classified by the fuzzy ART. Also, FAMNN eliminates the need to regroup data as it is able to distinguish outliers present in the model or any group generated. This combination of offline and online approaches helped researcher's aggregate data to reduce high communication cost at the expense of the low energy computation operations. [30]

Abidi S.S.R and Ong J. [31] have adopted a hybrid clustering technique with a combination of the self-organizing neural network and k-mean clustering approach. The self-organizing neural network help cluster the data points into various classes for interpretation. In this paper, a hybrid technique for clustering is used. This is due to the non-linearity in the dataset. Hence, the neural networks are not able to cluster the data points into distinctive groups. In such cases an additional step of statistical analysis is performed for better classification. This approach has been seen more advantageous than other clustering techniques as it helps discover similarities among the data points, clusters the data into distinctive groups according to cluster properties and aids as a visual tool for a better understanding. Note- one of the limitation of using a k-mean clustering approach is that it requires the user to input the number of clusters (k value) which is addressed by the neural network in this research paper. [31]

Similar problems relating to clustering large amounts of heterogeneous data are tackled by another research group. Alam S., Dobbie G., Koh Y.S., and Riddle P. [32] present a novel technique of clustering by introducing a similarity measure between the heterogeneous attributes of the data points. The output from the similarity measure is used in the particle swarm optimization (PSO) based clustering algorithm. This clustering algorithm aids in classifying such complex data by combining the hierarchical and the partition clustering approaches. The novel similarity measure approach focuses on the web session clustering data. The technique focuses on addressing three basic steps: uneven session lengths, determining the intra-cluster and the inter-cluster distances; and weighing the similarity attributes among various groups. [32]

For the purpose of this research, a k-mean clustering algorithm is used in conjunction with the MATLAB software based clustering approach that uses a Calinski Harabasz algorithm. Also, various dendogram plots and silhouette plots are generated using the MINITAB application and the MATLAB application respectively, to visualize the decomposition of clusters generated.

CHAPTER 3

LASER CLADDING: AN ADDITIVE MANUFACTURING APPROACH

3.1 Background

"Cladding", in engineering is defined as, "the process of protecting one metal by bonding a second metal to its surface" [33]. It can also be defined as a process of bonding dis-similar metals under high pressure and temperature. Therefore, the laser cladding technique is "a process that uses a laser beam to fuse another material, which has different metallurgical properties to a substrate. A very thin layer of the substrate has to be melted in order to achieve metallurgical bonding with minimal dilution of added material and substrate to maintain the original properties of the coating material" [34] [35]. This process proves to be a potential competition to the "selective laser sintering (SLS)" technique, as a three-dimensional process for manufacturing the metallic components with flexibility in the material and the size selection.

The clad material is generally powdered in nature, and can possess similar metallurgical properties to that of the substrate metal (ex. in case of general repair work) or can possess dis-similar metallurgical properties to that of the substrate material to achieve new strengths (ex. creation of new parts with enhanced material characteristics). The powdered clad material is available in various metallic compositions (ferrous and non-ferrous) and in various varieties in accordance to the end user application.

With increasing demands for the metallic prototypes and the tools, the introduction of the laser cladding technology has opened a new scope for the manufacturers. This technology has been well recognized in establishing the repair industry of molds and dies but experiences a growing phase for creation of the new parts i.e. creation of a 3D part through successive 2D layers. Some of the major industrial applications of the laser cladding technique in today's industry include high-pressure gas turbine blade shroud by Rolls Royce (material- triballoy on mimonic) [36]; cylinder and engine valve- Fiat (material- on cast iron) and General Motors (material- stellite, triballoy T-800) [37]; interlocks- Pratt & Whitney etc. [37].

3.2 Essential Elements of the Laser Cladding Process

3.2.1 Process Types

Generally, the laser cladding process is carried out with dis-similar metals (different clad and substrate metal) to enhance the functional characteristics in manufacturing such as corrosion resistance, thermal surface treatments, abrasions and wear. There are two essential parts to the laser cladding process, which are as follows:

1) Melt pool formation and fusion by moving the laser, and
2) Supply of cladding material to the substrate

The first part of the process includes a combination of the degree of mixing (i.e. the controlled heat input by the laser to achieve a good mix of the melt pool between the powdered clad bead and substrate metal) and the dependency on the temperature cycle (i.e. the heating and the cooling rates leading to a favorable fine-grained microstructure) to control the laser energy and the temperature distribution over the substrate surface. [35]

The second part of the laser cladding process deals with the addition of the powdered metal to the substrate metal. According to the literature review, there are two ways (illustrated in figure 7 A & B, source: adapted from Schneider M. [17]) to add or to provide the powdered metal to the substrate metal, which are as follows [35]:

1) Preplacing of the clad metal (2-stage process) – in this case, the formation of the melt pool is established on top of the cladding metal which proceeds downwards to the substrate metal. In this process, the clad layer can be seen once the substrate is melted. Hence, the first stage deals with the application of clad material (through plasma spraying, flame spraying or preplacing the material as a solid plate or paste) and the second stage deals with the fusion process of melting the clad powder.
2) Injecting the clad metal (1-stage process) – in this case, the formation of the melt pool is established in the substrate metal. In this process, the clad layer forms instantaneously while the powdered metal is being fed. This 1-stage process deals with the application of the clad powder (through injection process as powder or wire) with a simultaneous fusion reaction.

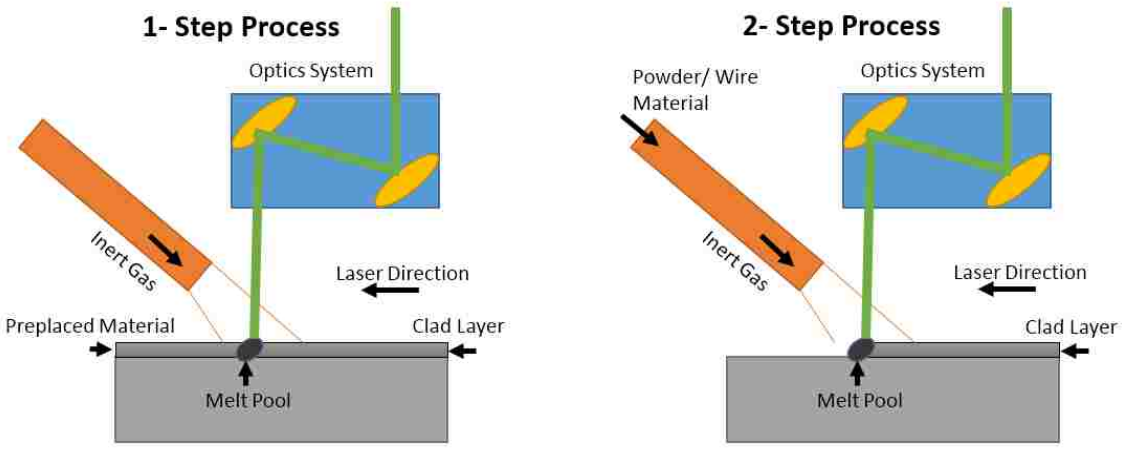

(A) (B)

Figure 7: Laser cladding process- (A) 1-step and (B) 2-step

The research focus in this thesis work targets the injection of the powdered clad metal during the laser cladding process for various two-dimensional and three-dimensional applications. The powdered injection is preferred over the wire injection process (and is a focus of this thesis), as it is considered robust than the wire cladding. This is due to the fact that firstly, there is no direct contact between the clad material (powder) and the melt pool, which in the case of a wire feed touches the metal pool; and secondly, the laser beam can easily pass through the powdered particles due to its granular nature. Hence, the laser beam will not face obstruction as in case of the wire (solid state) feed. [35]

3.2.2 Powder Feeder Types and Principles

According to the literature, there are three evident powder feeder type principles that a powder feeder can be based on, including:

1) The first powder feeder comprises of a funnel shaped hopper through which the powder flows into the slots of a rotating disks by the aid of gravity. This powder is then transported to the suction unit, which helps in dispensing the powder onto the substrate material with the help of a carrier gas. In this case, the feed rate of the powder is dependent on the speed of the disk and the dimensions of the slot. [38]
2) The second powder feeder comprises of a funnel shaped hopper through which the powder is directly transported to the dispensing nozzle with the help of a pneumatic

screw. In this case, the feed rate of the powder is dependent on the rotational speed of the pneumatic screw and its dimensions [39] [40]

3) The third powder feeder also comprises of a funnel shaped hopper through which the powder is transported to the dispensing nozzle through a combination of the pneumatic and the vibrational forces. Here, the vibrational forces are generated through a standard ultra-sonic cleaning device. [41]

For the purpose of this thesis work and for collection of the experimental data, a powder feeder that works on the principle of rotating disks (type-1) is chosen. The carrier gas chosen to dispense the clad powder onto the substrate metal is the argon gas due to its inert nature.

3.2.3 Types of Dispensing Nozzles

Once the powder feeder dispenses the metal powder to the dispensing nozzle through one of the stated principles, it is seen through literature that the dispensing of this metal clad powder can happen through various nozzle types (illustrated in figure 8 A and B, source: adapted from Schneider M. [17]) listed as follows:

1) Co-axial powder supply- this nozzle (integrated with an optical system) dispenses the powdered clad material through the openings co-axially placed with the laser beam and the shielding gas. Advantages of using a co-axial nozzle are that the powder supply to the nozzle is independent of the direction in which the workpiece moves; and secondly that the co-axial nozzle provides a controlled heating environment for the clad powder before it is dispensed onto the melt pool, hence, maintaining a high powder efficiency. A limitation to using a co-axial nozzle is that not all the products (shapes) can be accessed easily with this nozzle type. [17]
2) Lateral supply of powder- this nozzle incorporates dedicated or separate powder nozzles for handling of the part, hence, displaying no limitations. In simple words, the lateral nozzles are tubes (straight or curved) which act as separate commodities and are not integrated within the optical system. Lateral nozzles can reach any geometry for the treatment of parts such as the inner diameters of a tube or the surface of a turbine blade. [17]

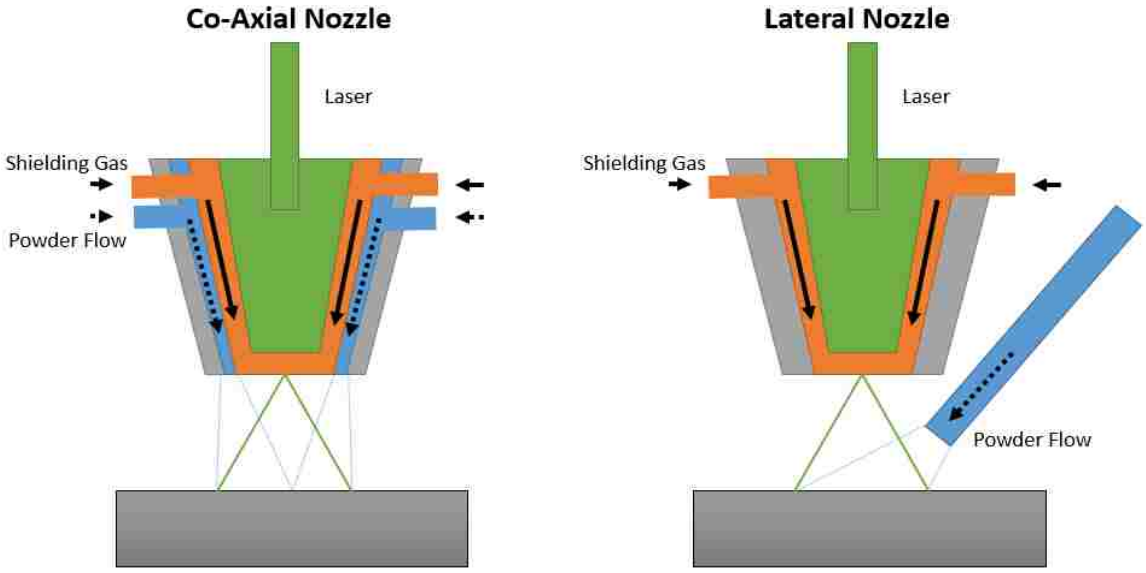

Figure 8: Powder supply nozzle- (A) co-axial and (B) lateral

Nozzle type is chosen according to end user application. For the purpose of this thesis work and experimentation purposes, a lateral type nozzle is chosen due to its advantages over a co-axial nozzle. The importance of choosing a right cladding nozzle is: the high efficiency in the powder utilization; the flexibility with the bead/beam size and the focal lengths; compatibility with various laser systems; the low maintenance and the longer production times. [42]

3.2.4 Types of Lasers Systems

A laser system is a device that generates a laser beam for the fusion reaction to occur between the clad powder and the substrate metal. A laser is defined as "a source of high- intensity optical, infrared or ultraviolet radiation as a result of stimulated emission maintained within a solid, liquid, or gaseous medium. The photons involved in the emission process all have the same energy and phase so that the laser beam is monochromatic and coherent, allowing it to be brought to a fine focus." [43]. In other words, a laser is a device that uses the process of optical amplification to emit the light. The special coherence behaviour of the laser makes it very different from any other light source because unique behaviour focuses the beam of light to converge onto a narrow tight spot. This coherence

nature enables the laser light to perform applications such as laser cutting, fusion, lithography etc. There are many different laser types, such as the solid state laser, the gas laser, the semiconductor laser etc.

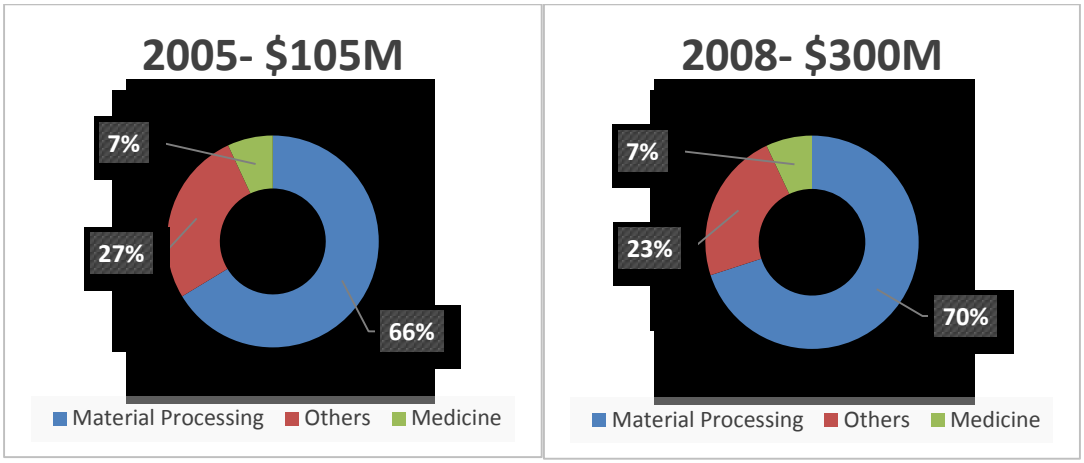

(A) (B)

Figure 9: Applications of laser systems- (A) year 2005 and (B) year 2008

The use of laser systems for the industrial operations has increased over the years due to their high efficiency. It can be seen from figure 9 A and B (adapted from Optech consulting [26]), that over the years (2005-2008), the use of the fiber lasers have increased by 4% margin for the material processing operations. This 4% increase has led to increased revenue of $195 M for the world markets [44]. Also, it can be seen from figure 10 A, B, and C (adapted from Optech consulting [27]), that the amount of market share of the fiber lasers over any other laser types has been on an exponential increase from 4% in 2005; 10% in 2008 and 18% in 2012 [45], hence, presenting a boosting trend for the manufacturing sector in terms of economy.

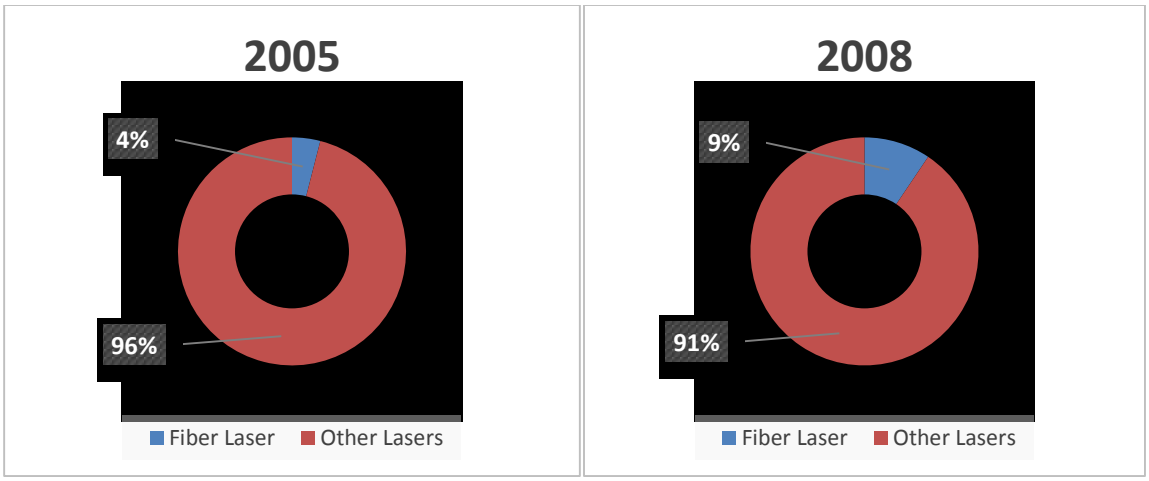

(A) (B)

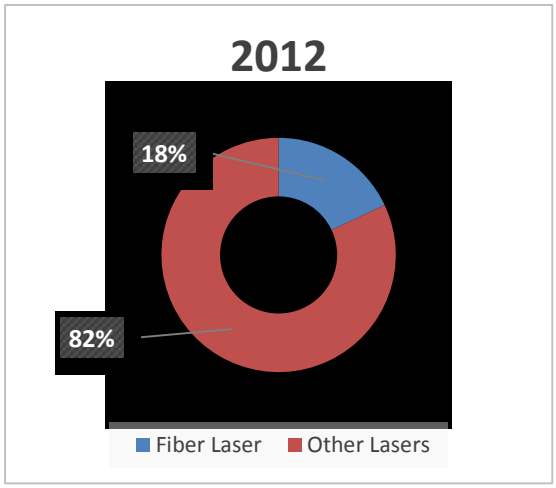

(C)

Figure 10: Application of fiber laser- (A) year 2005, (B) year 2008 and (C) year 2012

For the purpose of this thesis work and experimentation the two lasers that are studied are as follows:

1) Fiber laser- these are a form of the solid state lasers which work on the principle of total internal reflection. Here, the light travels through an optical fiber. The advantage of this kind of fiber material is that it provides better cooling conditions for the light beam as the light travels longer in the gain medium region. Also,

according to the literature it is determined that there is less thermal distortion (of the beam) due to the fiber nature.

Some fiber lasers are designed as double-clad fibers i.e. they contains an inner core, an inner cladding and an outer cladding. This design is greatly preferred in the industrial applications because the inner core acts as a single mode fiber to emit the laser emissions and the outer core acts as a multicore power generator (pump) to generate higher levels of power. Figure 11 (adapted from Stiles, Eric [29]), shows a visual representation of the double clad fiber laser [46] Note- the single pass experiments for the 420 steel clad powder are generated with the fiber laser system for this thesis workup.

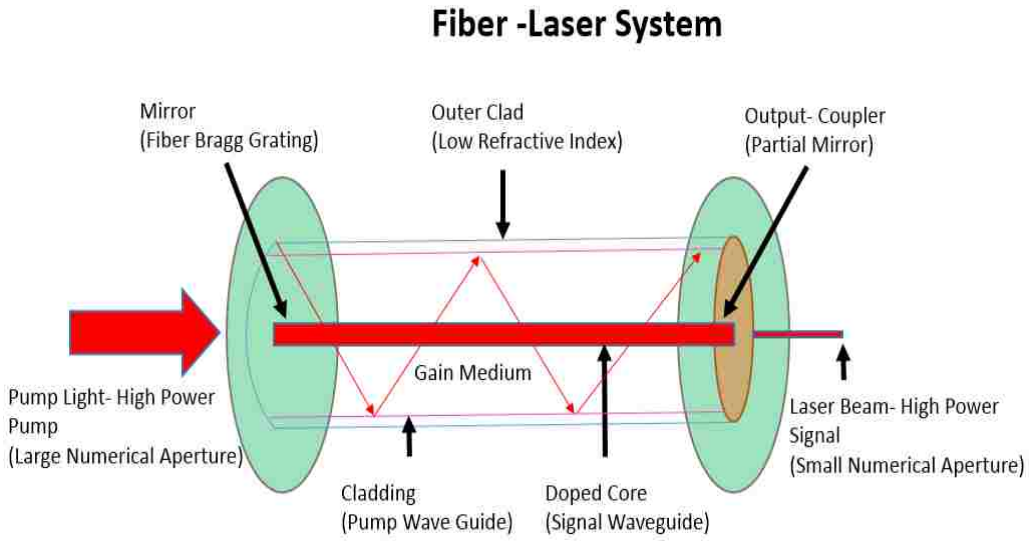

Figure 11: Fiber laser system- schematic diagram

2) Semiconductor laser (IPG laser)- also known as laser diodes; a semiconductor lasers work on the similar principle as the fiber lasers but the power supply for these lasers are the diodes that are electrically pumped. Here, the diodes consists of two outer semiconductor layers (p-n junction) separated by a middle layer (i junction). Due to the interaction between the electrons and the holes generated by (p-i-n) junction, an electric current is generated in the semiconductor diode. This electric current is unidirectional in nature and travels through the i-juction where the p type

silicon (Anode) to the n type silicon (Cathode) meet; similar to a light emitting diode (LED). Figure 12 (adapted from Olympus [47]), shows the visual representation of a laser diode. [48] [49]

Note- overlap pass (40%, 50%, and 60%) experiments for 420 steel are generated with a semiconductor's diode laser system for this thesis workup.

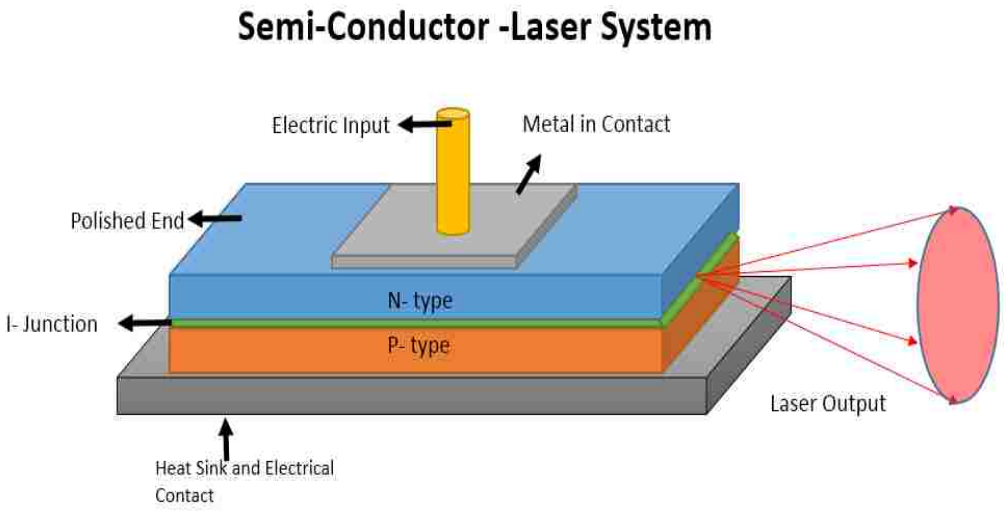

Figure 12: Semi-conductor laser system- schematic diagram

In general there are five major components to a laser system that helps to generate a laser beam (illustrated in figure 13, adapted from: Aldrich, Robert [28]), presented as follows: [50]

1) A gain medium- this material has a unique characteristic to amplify the light emitted through a source by stimulated emission.
2) Pumping- a process by which the energy is supplied to the gain medium. Generally, the energy supplied is either in the form of an electric current or a light with different wavelengths.
3) Optical cavity- a space that occupies the high reflector mirror (opaque) of the laser system that holds the gain medium. The other reflector mirror is called the output coupler that is transparent (slightly) in nature to allow the laser light to escape form

the apparatus setup. The purpose of these mirrors is to reflect the light back and forth through the gain medium to amplify it.

4) Laser beam- this is the final output of the laser apparatus, exiting from the output coupler reflector mirror in the form of a narrow beam of light.

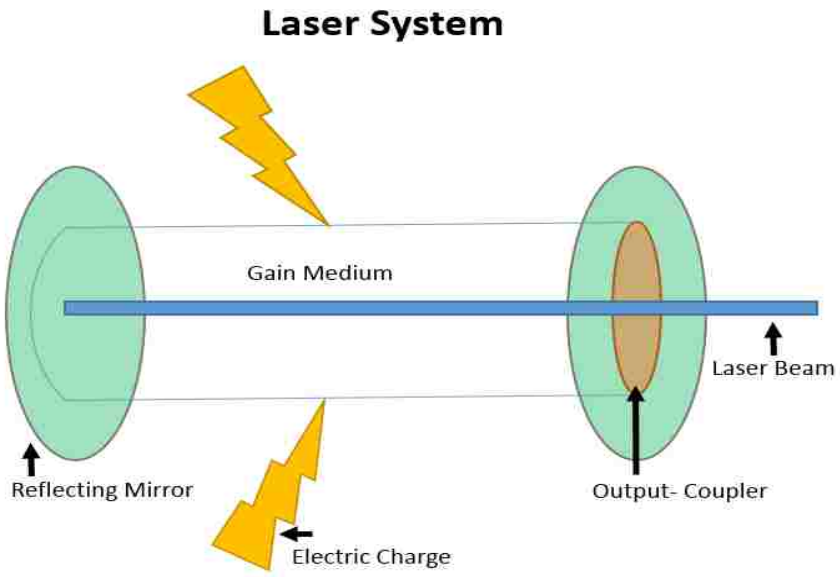

Figure 13: Components of a laser system

3.3 Laser Cladding Apparatus

There are eight basic components to a laser cladding system for industrial production. These components work simultaneously and coherently to form a clad bead structure. The eight components are presented in figure(s) 23 and 24 (source: industry sponsor [4]), and are as follows:

1) A laser system- this is a device that generates a laser beam (either through a fiber or diode source) for the fusion reaction to occur. This fusion reaction takes place between the powdered clad material that is dispensed from the nozzle (carried with a carrier gas) and the substrate metal (base metal- onto which the clad bead is formed).
2) A motion control system- this is one of the mechanical components that is involved indirectly with the laser cladding operation. As the name suggests, it is a system (embedded with a software package by the manufacturer) that controls/ integrates

the X-Y-Z Cartesian co-ordinates between the motion control stage (planer X-Y Cartesian)/ the rotary table and the vertical motion stage.

3) A powder feeder- this is a hopper (container) that provides one of the many input(s) to the laser cladding system and is directly involved in the cladding process. The hopper contains the powdered clad material that is dispensed onto the substrate metal for a clad bead formation.
4) A focusing optics system- this system consists of a set of optical lenses which form an optical cavity. Here, the set of optical lenses are held between a gain medium and the purpose of the reflecting lenses is to reflect the light back and forth through the medium amplifying its effect. The lens towards the output of the laser light is called the output coupler and is slightly transparent in nature, providing an escape to the laser beam.
5) An X-Y motion control stage/ rotary table- this is a mechanical component involved in the laser cladding process. Generally, the motion control stage is either an X-Y Cartesian table or a rotary table for various desirable parts. The purpose of the control stage is to act as housing to the substrate metal i.e. the base metal sits onto the control stage (through clamps). The motion of this control stage defines the motion of the substrate metal on which the clad bead is generated. As mentioned earlier, the control stage is operated by the motion control system.
6) A nozzle- this is a tube that aids in dispensing the powdered clad material onto the substrate material along with a carrier gas. There can be multiple nozzles present at one particular production time. As mentioned earlier, this nozzle can be either co-axial or lateral in nature.
7) A vertical motion stage- this is housing for the optical cavity (i.e. the focusing optics system). As mentioned earlier, the vertical motion stage is controlled by the motion control system. The purpose of the vertical motion stage is to direct/emit the laser beam radiations perpendicularly onto the substrate metal (base metal). Note: if the focusing optics system has re-configurability approach (i.e. can be moved in degree motion at a pivot point), the laser beam will not be perpendicular to the substrate metal.

8) A robotic arm- this is an open kinematic chain onto which the laser system, focusing optics and nozzle are mounted. This industrial robotic arm is selected according to the end user application and the part production. Generally, a 5-axis or 6-axis degree of freedom (DOF) robot is chosen for the laser cladding operation. There are two ways to define the path of the clad bead either by the movement of the motion control stage (on which the substrate metal rests) or by movement of the robotic arm (on which the laser system rests). According to the literature, the best practice for defining the movement/ path of the clad bead generated is by the movement of the robotic arm as it comprises of more degrees of freedom.

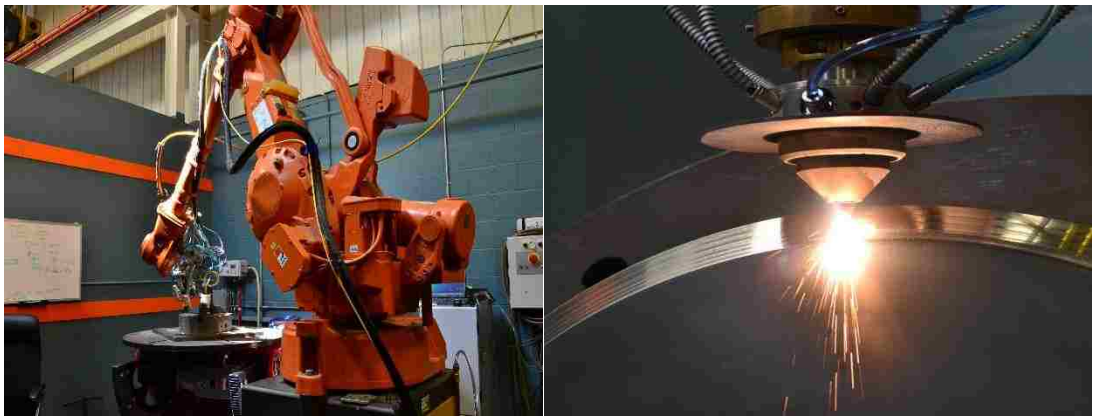

Figure 14: Laser cladding apparatus setup – real time [4]

Figure 15 (adapted from Materialgeeza [51]); displays a schematic view of the laser cladding equipment.

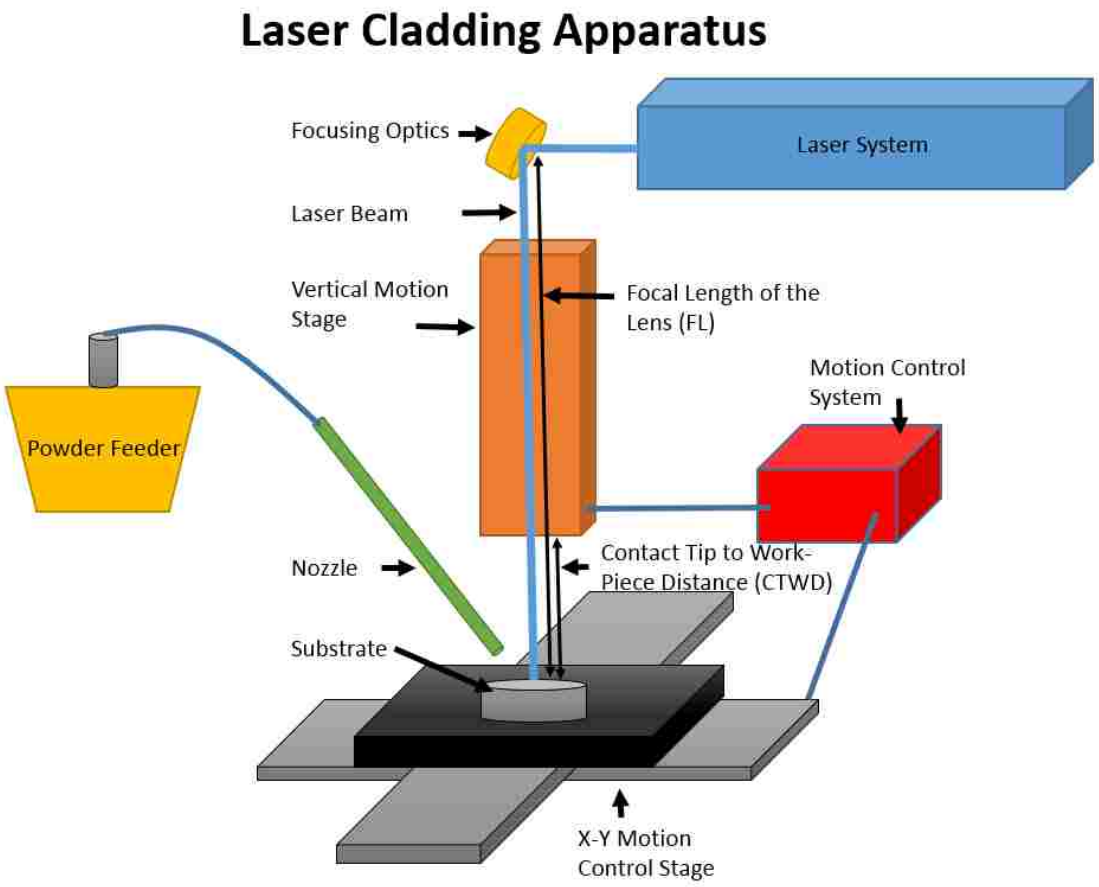

Figure 15: Laser cladding apparatus- schematic view

3.4 Laser Cladding Process

As explained in subsection 3.1, laser cladding is a process in which the metal clad material (wire or powdered) is metallurgically bonded on to the substrate metal. This metallurgical bonding is done with a laser beam through a fusion reaction. This process is performed to enhance the metallurgical properties (such as wear, abrasion, thermal, conductivity, toughness etc.) of the substrate metal. A typical single layer laser bead thickness ranges from 0.2mm - 7.0 mm (source: industry sponsor), which is generated with a low-moderate heat input laser system. According to the literature, the objective of the cladding process is to attain a geometrically perfect bead. This perfect geometry can be

attained only if the percentage dilution with substrate material is controlled (between 2% - 5% for best results).

The cladding process starts with the introduction of the powdered clad metal through the powder feeder (pneumatic flow, gravity flow or hybrid i.e. pneumatic and vibrational). The next step involves the injection of the powdered clad material onto the substrate through a lateral or a co-axial nozzle (presented in figure 26). Once the powder is introduced with the carrier gas onto the substrate (base metal), the laser interacts (fusion reaction) with the clad powder, resulting in the formation of a melt pool. To protect the melt pool (clad area) from interacting with various atmospheric gases, a shielding gas is introduced in the system which is injected along with the powdered clad material (one example of a shielding gas is 'argon'). Thus, a melt pool is created onto the substrate metal. Movement/ motion of the robotic arm onto which the laser system, the focusing optics and the nozzle are mounted helps in creating a metal clad track (single pass). This metal clad track (single pass) is a result of the solidification of the melt pool along the movement of the laser. The melt pool generated is formed in-between the deposited layer and the re-melted zone leading to the formation of the heat affected zone (HAZ) on cooling of the molten clad bead. The HAZ, refers to the area of the substrate metal that has had its microstructure and properties altered due to intensive interaction between the powder clad and the laser but has not melted. According to the literature, for a laser cladding operation the laser intensity (heat input) is generally selected in a range of low to moderate, to have a nominal HAZ [52]. The heat input is generally calculated with the following mathematical expression presented in equation (1):

$$Q = \left(\frac{V * I * 60}{S * 1000}\right) * \mathrm{E} \qquad (1)$$

Here, Q is the heat input expressed in kilo joules per millimeter (KJ/mm)

V is the voltage expressed in volts (V)

I is the current expressed in amperes (A)

S is the welding/travel speed of the laser expressed in millimeter per minute (mm/min)

E is the efficiency of the process used (scale of 0-1)

The powder feed system selected for the laser cladding process is generally precise, hence, reducing the amount of wastage of the powder itself. The laser cladding process is a fully automated process (with CAD/CAM and CNC integration capabilities) with the largest selection of clad materials (ferrous and non-ferrous). According to the literature, the laser cladding process achieves up to a 10 times higher deposition rate than a tungsten inert gas- cold wire (TIG –CW) feeding process [53]. A schematic representation of the process is presented in figure 16 A and B.

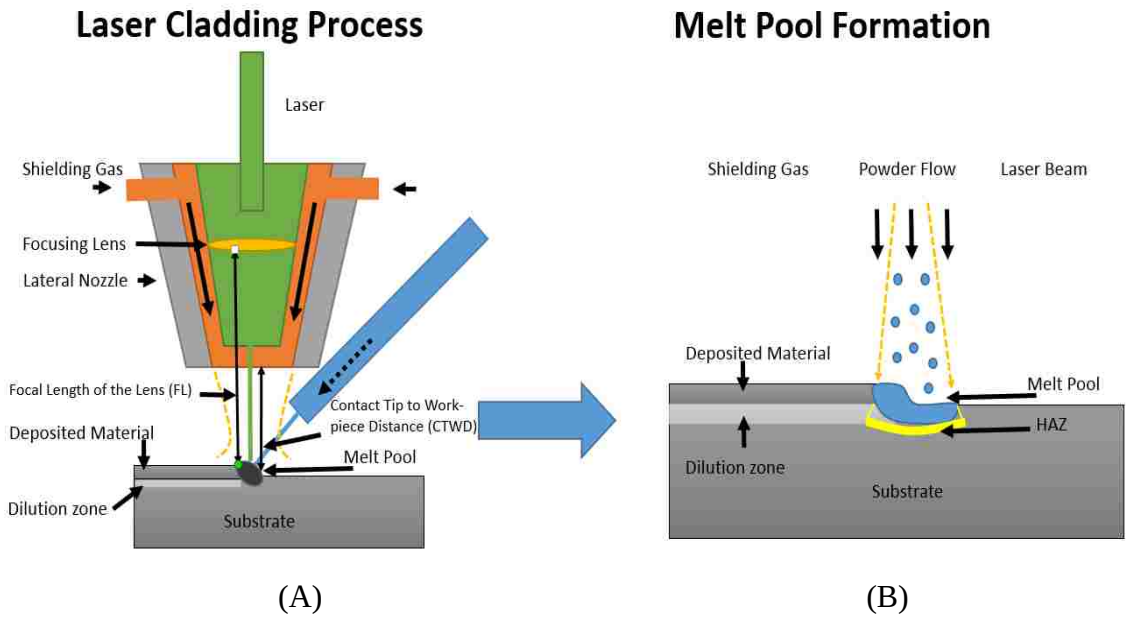

(A) (B)

Figure 16: Laser cladding- (A) process and (B) melt pool formation

Once the solid clad layers are formed, various properties of this clad bead can be studied (classified under four major categories) which are represented in table 3: [35]

Table 3: Various Properties for a clad bead

Geometrical	**Mechanical**	**Metallurgical**	**Qualitative**
Width	Hardness distribution	Microstructure	Roughness
Reinforcement height	Residual stress	Dilution	Cracking
Penetration	Fatigue	Porosity and voids	
Dilution	Wear resistance	Grain size	
	Tensile strength	Homogeneity	
	Compressive strength	Corrosion resistance	
	Torsional properties		
	Bending strength		

This thesis work focuses on understanding the impact of the manufacturing process parameters on the geometrical shape parameters (physical structure of a clad bead), optimizing the geometrical properties and establishing the effects of interdependencies of such properties.

The goals of this research are: (1) to be able to select process parameters with confidence that will generate the desired bead geometry, (2) develop a streamlined methodology to establish process parameter to bead geometry relationships for a wide range of process conditions, (3) develop an error map to illustrate the confidence levels with respect to the predictive model, and (4) classification of data points into classes to determine the approximate bead shape represented by each of the cluster. Goal (3) is especially important for multiple layering scenarios as laser cladding is an open loop process.

3.5 Geometric Properties

3.5.1 Physical Shape Properties for Single Pass and Overlaps

Geometric properties are the properties that define geometry of a structure or shape. To determine the geometry of a clad bead for a single or overlap pass, a detailed process needs to be carried out which involves various steps, including sample preparation, cutting of samples to obtain a cross sectional view, mounting, polishing, and etching. These steps will be explained in detail in the following chapters. Once the sample is prepared, it is analyzed under a metallurgical microscope to determine the bead's geometrical measurements. Depending on the size of the bead and the manufacturing configuration a magnification of 10X or 20X is adjusted in the microscope to get the following shape parameters:

1) Width of the bead (W) – the clad bead width is the maximum width of the clad metal deposited. In other words, it can be expressed as the maximum latitudinal distance of a cross-sectional bead in the positive X Cartesian co-ordinate space. According to the literature for welding or cladding processes, the bead width is directly proportional to the current (I), the voltage (V), the diameter of the electrode or nozzle and indirectly proportional to the welding speed (welding process) or the travel speed of the laser (laser cladding process) [54]. Other researchers have also documented that bead width generally increases with an increase in current input until a certain critical value and then shows a decreasing trend with the increasing current thereafter [55]. Also, it is observed that bead width has no significant affect by the type of power source to the system [56].
2) Reinforcement height of the bead (RH) – the reinforcement height is the maximum distance between the substrate metal and the deposited clad material of the bead. In other words, it can be expressed as the maximum longitudinal measurement from the base metal to the outer boundary of the cross sectional bead in the positive Y Cartesian co-ordinate space. The reinforcement height is known to determine the strength of the clad bead and is highly dependent on the feed rate of the clad powder [54]. According to the literature, the reinforcement height increases with an increase in the feed rate (directly proportional) and has no affect due to the current (I) [57]. Also, it is documented by some researchers that the reinforcement height

is indirectly proportional to the voltage, the travel speed of the laser, and the nozzle diameter (thickness). This increase in the height with increase in the feed rate is a result of more clad metal being deposited onto the substrate per unit length. Decrease in the height due to increase in the voltage is due to the fact that the width of the bead increases, hence, spreading out the clad material instead of stacking [54].

3) Penetration/ depth of the bead (P) – the penetration is the maximum distance between the outer boundary of the substrate material and the boundary of fusion reaction inside the substrate. In other words, penetration is expressed as the maximum longitudinal distance between the top of the base plate to the boundary of the cross sectional bead created by a fusion reaction of the laser (i.e. the boundary just before the starting of the HAZ, in the negative Y Cartesian co-ordinates space [54]. According to the literature, penetration is observed to be directly proportional to the current supplied and inversely proportional to the laser travel speed and the nozzle diameter [58]. This decrease in the penetration with increasing travel speed is due to the fact that the time during which the force is allowed to penetrate decreases. Also, the decrease of penetration with an increase of the nozzle diameter is due to the fact that the current density increases [59].
4) Area of the positive bead (A) – this is the enclosed space between the top boundary of base metal and the extent to which the deposited clad material is present. It is generally affected by the width of the clad bead and its reinforcement height. Hence, it follows similar direct and indirect trends, as the width and the reinforcement height parameters.
5) Area of the negative bead (B) – this is the enclosed space between the top boundary of the base metal and the extent to which the fusion reaction occurs within the substrate/ base. It is generally affected by the width of the clad bead and its penetration. Hence, it follows similar direct and indirect trends, as the width and the penetration parameters.
6) Percentage dilution (%D) – this refers to- “the change in chemical composition of a filler material caused by the admixture of the base material or previously deposited weld material in the deposited bead. It is normally measured by the

percentage or base material or previously deposited weld material in the weld bead" [60]. Please refer to sub- section 3.5.2 for more details.

The above mentioned properties are relevant to a single pass or a single bead configuration. In the case of an overlap configuration (3 single bead passes), there are three beads/ passes that co-inside with each other; with a 40 %, 50% or 60% layover percentage. The sample preparation for the overlaps configuration follows the same parameters as described for a single pass, however, there are two new sets of geometrical parameters which are as follows:

1) Reinforcement height between bead 1 and bead 2 (RH_{12}) – this the maximum distance between the substrate metal and the intersection area of bead 1 and 2; which is created by the deposited clad material of the bead. In other words, it can be expressed as the maximum longitudinal measurement from the base metal to the outer boundary of the cross sectional bead in the positive Y Cartesian co-ordinate at the intersection of bead 1 and 2. It has similar direct and indirect trends as the reinforcement height of the bead.
2) Reinforcement height between bead 2 and bead 3 (RH_{23}) – similarly, the reinforcement height between bead 2 and bead 3 is the maximum distance between the substrate metal and the intersection area of bead 2 and 3; created by the deposited clad material of the bead. In other words, it can be expressed as the maximum longitudinal measurement from the base metal to the outer boundary of the cross sectional bead in the positive Y Cartesian co-ordinate at the intersection of beads 2 and 3. It has similar direct and indirect trends as the reinforcement height of the bead.

It should be noted that, there will be three sets of width (W_1, W_2, and W_3), reinforcement heights (RH_1, RH_2, and RH_3), and penetrations (P_1, P_2, and P_3) in an overlap sample. This is due to the fact that an overlap sample is simply a three pass single bead sample with a layover percentage (40%, 50% or 60%). Hence, six geometrical/ structural shape parameters are studied for this thesis with regards to five manufacturing parameters. In the case of overlap configurations these geometrical shape parameters increase to a total of fourteen. Figure 17 A and B displays a representation of a sample for a single pass and

an overlap pass configuration respectively. The beads presented in the figures 17 A (single pass) and B (40% overlap pass) are generated using the manufacturing parameters- FR: 20 g/min, PW: 2 KW, FL: 400 mm, LS: 10 mm/sec, and CTWD: 23mm.

(A) (B)

Figure 17: Clad bead generation- (A) single pass and (B) overlap pass [4]

3.5.2 Dilution

As explained in sub-section 3.5.1, dilution is the amount of the base metal that is melted due to the fusion reaction of the laser during the laser cladding process [61]. The process of laser cladding is performed to attain a strong fusion bond between the cladding material and the substrate. This bond created between the two materials is due to the formation of a melt pool in the substrate metal. According to the literature, the depth of the melted substrate metal should be minimal in order to obtain a pure surface layer that is not diluted by the substrate material [35]. Thus, the quality of the clad bead is dependent on the dilution of the substrate metal caused by the clad layer.

One of the advantages of the laser cladding (LC) process over the laser welding technique, the metal inert gas (MIG) or the tungsten inert gas (TIG) techniques is that the percentage of dilution levels are much smaller in magnitude. It is generally seen that for a good quality clad bead generation, the percentage dilution should be maintained between 2%- 5%, while for a good weld bead the dilution percentage lies between a range of 20%-40% [61].

There are two ways of calculating the percentage dilution: [62]

1) Clad layer geometry – the first method takes into consideration the overall clad geometry of the bead. Here, dilution is defined as the ratio of the penetration (P) of the bead in the substrate over the total height, (T) (i.e. summation of reinforcement height (RH) and penetration (P)) of the bead. For this method, the distribution of geometrical elements over the cross section of the clad bead is assumed to be homogenous. A mathematical representation of the expression is presented in equation 2 (figure 18- represents a schematic representation for calculation of dilution):

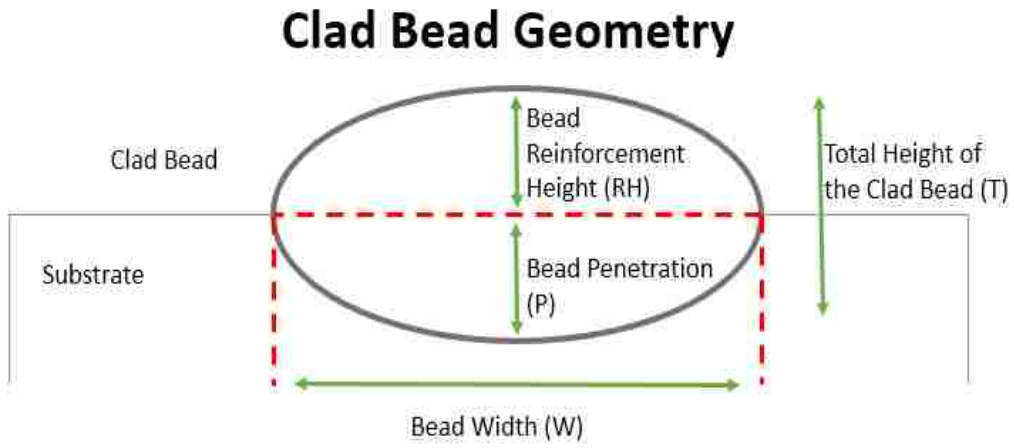

Figure 18: Clad bead geometry

$$D = \left(\frac{P}{RH + P}\right) = \frac{P}{T} \quad (2)$$

Here, D is the dilution expressed in percentage

P is the penetration depth expressed in millimeters (mm)

RH is the reinforcement height expressed in millimeters (mm)

T is the total height of the bead expressed in millimeters (mm)

2) Material composition in clad layer – the second method takes into consideration the material compositions involved in the laser cladding process. Here, a comparison is made between the material composition of the pure coating material and the composition of the substrate. This method is more widely accepted in the industry

and accounts for the variation of dilution over the clad depth. In other words, dilution is calculated using the cross sectional melted area of the base metal compared to the difference between the total area of the weld metal and the cross sectional weld area [63]. A mathematical representation of the expression is presented equation 3 (figure 19 represents a schematic representation for calculation of dilution):

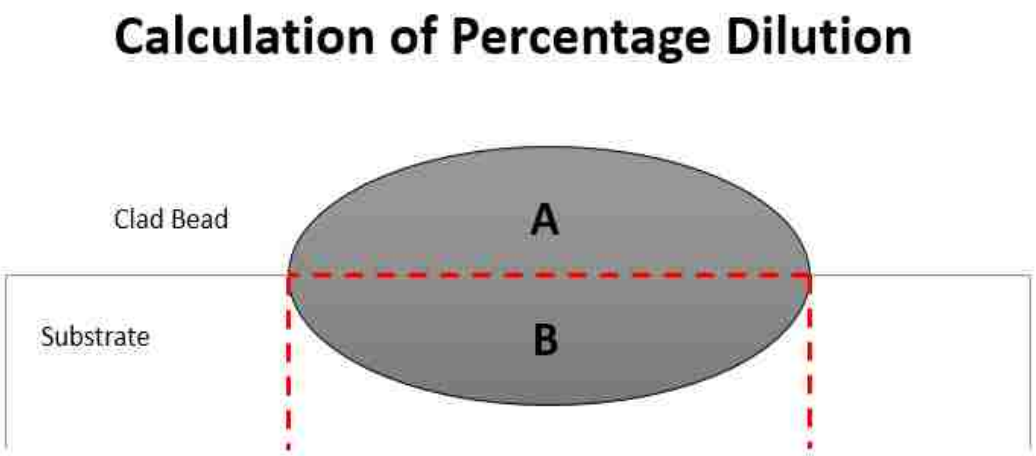

Figure 19: Percentage dilution calculation method

$$D = \frac{B}{A + B} \tag{3}$$

Here, D is the dilution expressed in percentage

B is the area of the negative bead expressed in square millimeters (mm^2)

A is the area of the positive bead expressed in square millimeters (mm^2)

CHAPTER 4

RESEARCH METHODOLOGY

4.1 Proposed Research Methodology

This research work proposes a five step detailed approach for standardizing the laser cladding process. The methodology starts with a detailed literature review that focuses on the various approaches for an experimental strategy, strategies to set up predictive models to generate outputs (results), classification approaches to clustering bead shape according to group (class) characteristics and methodology to determine interdependencies among the shape and manufacturing parameters.

The second step involves selecting an experimental strategy for an effective sample collection process. For this thesis work, this process involves a response surface methodology with the use of a central composite design. Once the experiments are setup and the single pass and overlap beads are generated at the sponsor facility, post processing of samples is carried out. The post processing operations aid in retrieving the shape measurements of the bead structures created through the laser cladding process.

The third step involves the development of a cognitive artificial intelligence system with the help of artificial neural networks to predict various shape parameters from manufacturing parameters and vice versa. Once a successful model is developed and the predictions are generated within a high confidence range (90%- 95%), the model is ready to simulate future trends in the dataset. Sub-section 4.2 presents a 5-step approach to the development of a predictive model.

The fourth step is a vital component in determining the significance of each parameter and their interaction with other parameters. These interactions present in the system make the laser cladding process non- linear in nature. Various contour and surface plots are generated to provide a visual representation of the non-linear behaviour present in the system.

The final step encompasses of a classification approach for the shape analysis of the clad bead structure. Classification of the bead structure aids in determining the group

properties of a class to which a bead belongs. Hence, the classification approach is useful in standardizing the bead shapes according to the geometrical measurements of the bead. A detailed explanation of the stated five steps is provided in the following chapters for a better understanding to this approach.

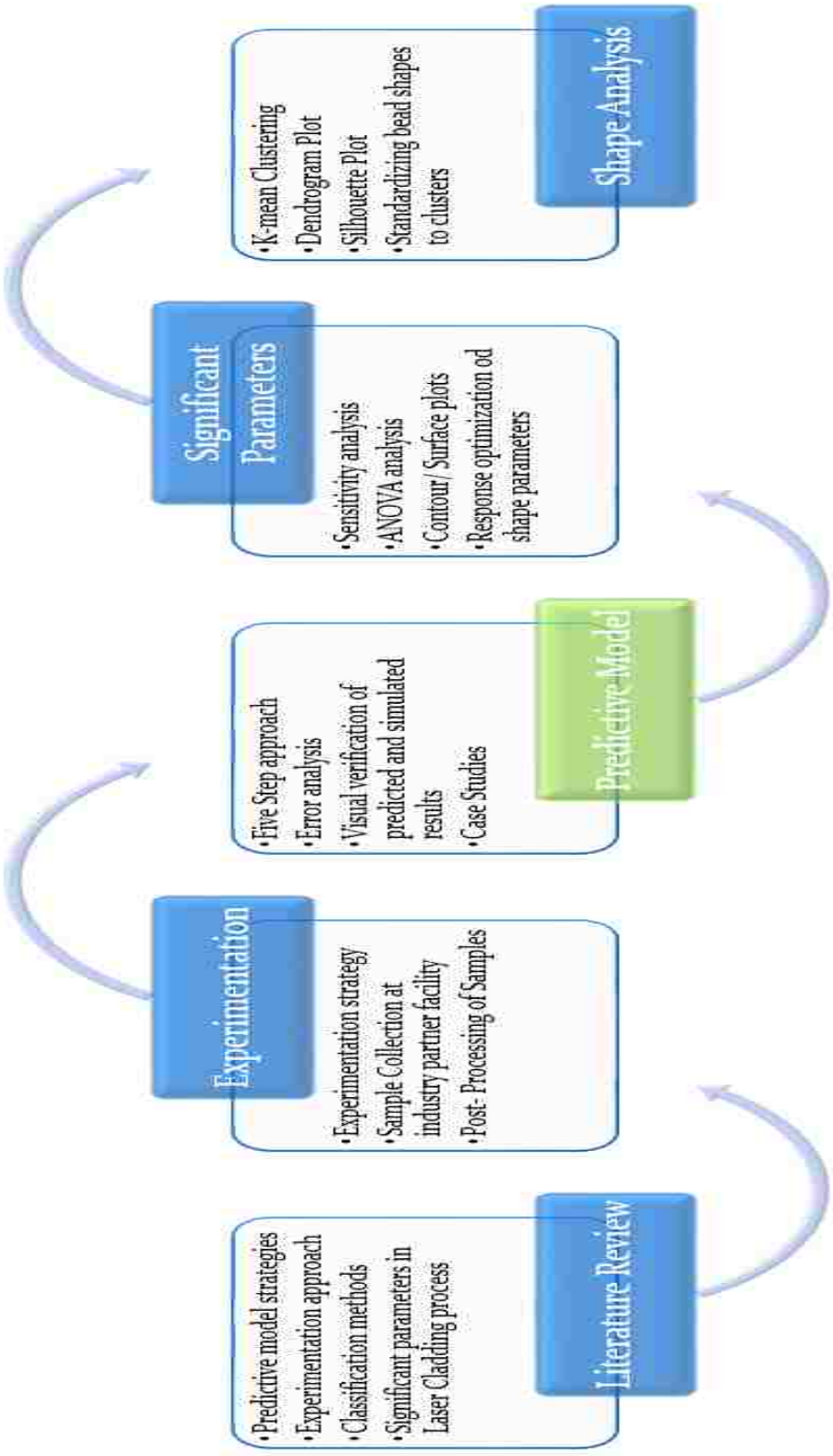

Figure 20: Proposed research methodology

4.2 Proposed Predictive Model Methodology

To develop the cognitive artificial intelligence system, a five step novel methodology is set up for this research. This methodology is applied to both the single pass and the overlap manufacturing configurations. The objective of documenting and devising a methodology is to standardize the process of laser cladding to reduce the lead times during production. This methodology comprises of a five step process and encompasses the five manufacturing parameters and the four shape parameters which are discussed in the previous chapter(s). Figure 21, displays a schematic flow of the five step methodology

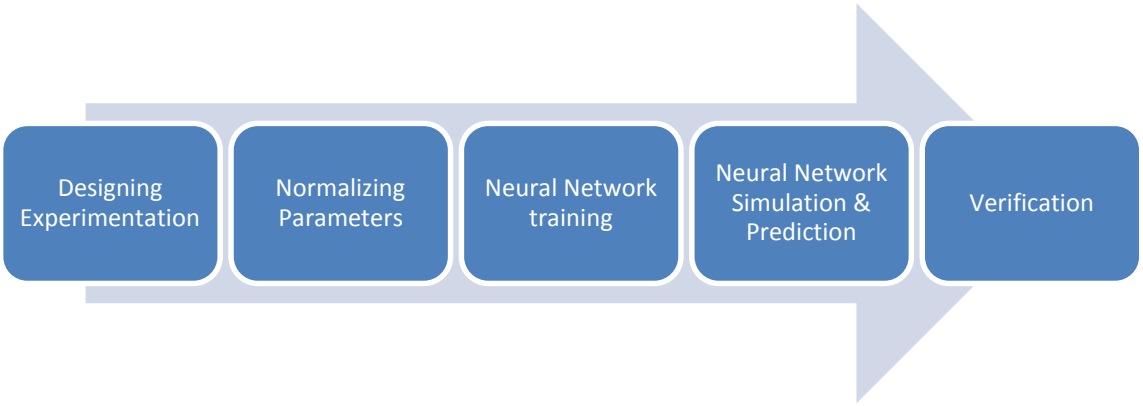

Figure 21: A methodology to development of artificial intelligence system

The methodology follows the following steps:

1) Designing experimentation – the design matrix (D) for experimentation is generated with the aid of the design of experiments (DOE) technique. Here, a response surface methodology approach is applied with a central composite box design (CCD) to help set experimental runs/ configurations.

2) Normalization – this is a process by which all independent variables (the manufacturing and the shape parameters) are brought to a common range of [-1, 1] with a simple ranging scale technique.

3) Neural network training – this incorporates normalized independent parameters and divides them into various input and target sets to carry out a supervised learning

process. The input and the target sets help in overall learning and adaptation to the linear and the non-linear trends through the aid of the network architecture defined for the data points.

4) Simulation and prediction – a test input set consisting of the manufacturing parameters is introduced to the trained network and confident predictions for shape parameters are derived without actually carrying out the experiment physically at the sponsor's facility.

5) Verification – the confident predictions made by the trained neural network are verified both visually and analytically to confirm the level of accuracy. An error percentage (error mapping) is generated for any deviations present in the predicted values from the actual values (shape parameters).

CHAPTER 5

DESIGN OF EXPERIMENTS

5.1 Response Surface Methodology

Response surface methodology (RSM) refers to "a collection of mathematical and statistical techniques useful for modelling and analysis of a problem in which a response (output variable) of interest is influenced by several variables (input parameters) and the objective is to optimize this response variable (output variable)" [64]. In other words, response surface methodology is an empirical model building technique that aids in setting up an experimentation process.

One of the major applications of the RSM technique is the design for optimization. This design aims at reducing the cost of expensive analysis methods such as the finite element analysis technique, the computational fluid dynamics (CFD) technique etc. Here, the smooth functions are utilized to improve convergence of the optimization process to reduce the effects of noise factors and allow the use of derivative based algorithm. [65]

In this thesis, the focus is to find optimal levels of manufacturing parameters (power- PW, feed rate- FR, laser speed- LS, local length- FL, and contact tip to workpiece distance- CTWD), through a response surface methodology and the objective function(s) are our mechanical shape parameters (width- W, reinforcement height- RH, penetration- P and percentage dilution- %D). Here, the RSM technique defines an objective function as presented in the following mathematical equation: [64]

$$y = f(PW, FR, TS, FL, CTWD) + \epsilon \quad (4)$$

Here, y is the objective function

f is a function of the manufacturing parameters

ϵ is a noise/ error observed in the response

Now, if the response is denoted as E(y) then, [64]

$$E(y) = f((PW, FR, TS, FL, CTWD) = \eta \quad (5)$$

Then the surface is represented as ŋ, and is referred to as a response surface. [64]

$$ŋ = f((PW, FR, TS, FL, CTWD) \quad (6)$$

Generally, a response surface (ŋ) is plotted graphically against the different levels of the various response variables (PW, FR, TS, FL, and CTWD). Visualizing of such responses is best perceived within a three- dimensional space or surface and contour plots, which is explained in detail in the following chapters.

While defining a RSM, the relationship between a response and a response variable contained in the system is unknown. Hence, the first step in designing an RSM is to determine an appropriate approximation for a true functional relationship between the objective function(y) and the response variables. In this case, a low-order polynomial function is applied. Once the function is applied and the response seems to be well modeled, the function is the first order model, which is mathematically represented as [64]

$$y = \beta_0 + \beta_1 x_1 + \beta_2 x_2 + \cdots + \beta_k x_k + \epsilon \quad (7)$$

if, the function is unfit to be modeled i.e. if there is a curvature in the system, a second- order model is used, which possess a polynomial function of a higher degree. Note- for the purpose of this thesis, a second order model has been applied to generate the relations between the objective function and the independent response variables (manufacturing parameters) due to the non-linear nature of the laser cladding data. The second order model is mathematically represented as: [64]

$$y = \beta_0 + \sum_{i=1}^{k} \beta_i x_i + \sum_{i=1}^{k} \beta_{ii} x_i^2 + \sum \sum_{i<j} \beta_{ij} x_i x_j + \epsilon \quad (8)$$

In such a case, the method of least squares is generally used to estimate the parameters to approximate the polynomials and the response surface analysis is performed (using fitted surfaces) [66]. Analysis of the fitted surface is considered as the analysis of the actual system only when the fitted surface is a true approximation of the response

function. Note- for effective estimation of the model parameters, a proper experimental design should be applied for experimentation process. [64]

The response surface methodology is considered to be a sequential procedure. The objective is to rapidly and efficiently move along the path of improvement to achieve optimal results for the independent variables of the system. The process starts with a first-order model and moves on to a second-order model gradually. The method used to move along the path of improvement is the method of steepest ascent (in case of maximizing the response variable) or the method of steepest descent (in case of minimizing the response variable). Thus, the method of steepest ascent refers to "a procedure for moving sequentially in the direction of the maximum increase in the response" [67]. It is always assumed that the first-order model can provide an approximation of the true surface. Hence, the experiments are conducted along the path of steepest ascent till the time there is no further improvement in the value of the response. Once there is no improvement recorded for the response value, a second order model is generated (to approximate the response) and a new path of steepest ascent is followed until the response is in close proximity to the optimal result. This final response point that is in very close proximity to the optimal response is generally referred to as the stationary point. [64]

The original application of the RSM technique was to model experimental responses; however, the RSM technique has evolved into a system for modeling numerical experiments [66]. By applying the RSM methodology, a series of tests called runs are set up, in which many variations (in manufacturing parameters) are introduced in various combinations of input parameters to identify the trends/reasons for changes in the response variables (outputs) in a non- linear system.

5.2 Design Properties for Selecting a Design Strategy

For this thesis and research work, the two optimal designs that will be studied are the full factorial approach and the central composite design. Once the design approaches are understood and documented, a selection of the design approach will be made to start the experimentation process at the sponsor's industrial facility. The selection process of the experimentation strategy is solely dependent on two factors- (1) the minimal time and the

financial investment for experimentation process (data collection); and (2) the level of approximation of response (in comparison to the true optimal value).

The following are some design properties that are necessary in selecting the design technique for a particular process/system:

1) Orthogonality – a design (D) is said to be orthogonal- if the combination of the defined matrix (X'X) is a diagonal matrix i.e. there are values present only in the diagonal elements of the matrix (X'X) and the other elements are zero. An advantage of such a design property is the presence of the uncorrelated elements, hence, making it easier to test the significance of the parameters. The design matrix (D) is expressed mathematically as: [68].

$$D = \begin{bmatrix} x_{11} & x_{12} & \cdots & x_{1k} \\ x_{21} & x_{22} & \cdots & x_{2k} \\ \vdots & \vdots & \cdots & \vdots \\ x_{n1} & x_{n1} & \cdots & x_{nk} \end{bmatrix} \quad (9)$$

Here, D is an n x k design matrix and each row of D defines a design point

2) Rotatability – a design (D) is said to be rotatable, if the equidistant points from the design center have a constant prediction variance. The advantage of such a design is that, even on rotation of the co-ordinate axes in a design the prediction variance remains unchanged which indeed helps in comparing the designs on the basis of rotatability. According to the literature, this property was first introduced by Box and Hunter. [69] [68].
3) Uniform precision – a design (D) is said to possess a uniform precision property, if the variance at the center point of a design (origin) is equal to the variance value at any other point at a distance from the origin. The advantage of this design property is that it helps in making the system (in predicting variance) more stable Again, according to the literature, this property was first introduced by Box and Hunter. [49] [68].
4) Design robustness – a design (D) is said to be robust, if the properties of that design are not impacted by the failures of the design. In other words, the failures in design should not affect the assumptions of the model and its error distributions, thus

displaying a lack of fit. According to the literature, this property was first introduced by Box and Draper. [66] [68].

5) Design optimality – a design (D) is said to be optimal depending on the closeness of the predicted response to the mean response over a certain region of interest. These designs are constructed on the basis of a certain optimal criterion such as the variance- related criterion. The objective for such a design is to minimize or maximize the objective function associated with the estimation of the independent factors. [68].

5.3 Proposed Experimental Designs

5.3.1 Full- Factorial Design

A factorial experiment is a design strategy in DOE in which multiple variables are grouped together, instead of one variable at a time. A full factorial design investigates all possible combinations to construct an approximation model that captures interactions between various variables. A factorial design is generally considered the most suitable design for the screening (pre-processing) process. The objective of the screening process is to identify the significant factors relevant to the process being investigated. A factor is considered to be significant if the influence of the factor is greater than the error value [70]. Here, each variable (factor) has a set number of possible levels.

In a factorial design, the total experimental runs are defined using equation 10

$$n = M^N \tag{10}$$

Here, n is the total number of experiments
M is the total number of levels defined for a variable
N is the total number of design variables

Generally, there are two levels (upper bound and lower bound) defined for each of the selected design variables. The total number of experiments can be defined by the expression 2^N (N is the design variables). In cases where there is a midpoint level (0) in-between the upper bound (+1) and the lower bound (-1) levels, then according to equation

12, the total number of experimental runs are 3^N. Figure 22 displays a graphical representation of the full factorial design with 3 levels and 3 factors ($3^3 = 27$ experimental points). [64]

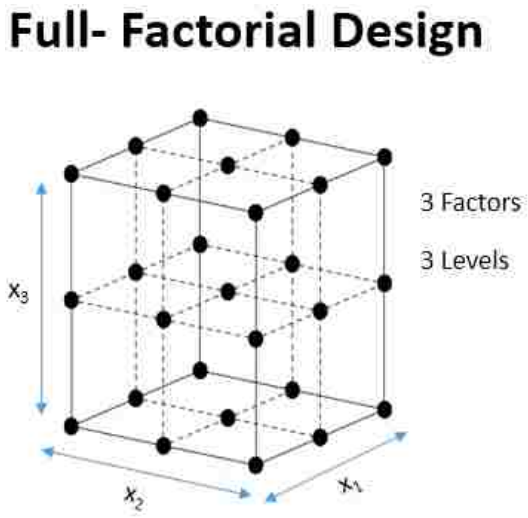

Figure 22: Full factorial design with 3 factors and 3 levels

It should be noted that while defining the full factorial design, the experimental points are always the end points of the cube. According to the literature, a factorial design is generally used for 5 or fewer factors. But in the case of factors greater than 5 (N >5), a fraction of a full factorial design is applied. The aim of a fractional factorial design is to screen only the important design variables that have the maximum influence on the process being investigated. Thus, a fractional factorial approach is used to estimate a few vital combinations of the full factorial approach. [68]

For the stated example (in figure 22) with 3 factors and 3 levels, a fractional factorial design is created using the mathematical equation presented in equation 11

$$n = 3^{N-p} \tag{11}$$

Where, n is the total number of fractional factorial design runs

N is the number of factors

$(1/3)^p$ fraction is constructed, resulting in 3^{N-p} runs/points

Hence, if p=1 then 3^{3-1} (9 points for a one third fraction design is generated). A visual representation of these nine points is presented in figure 23 A, B, and C with various selected combinations. [64]

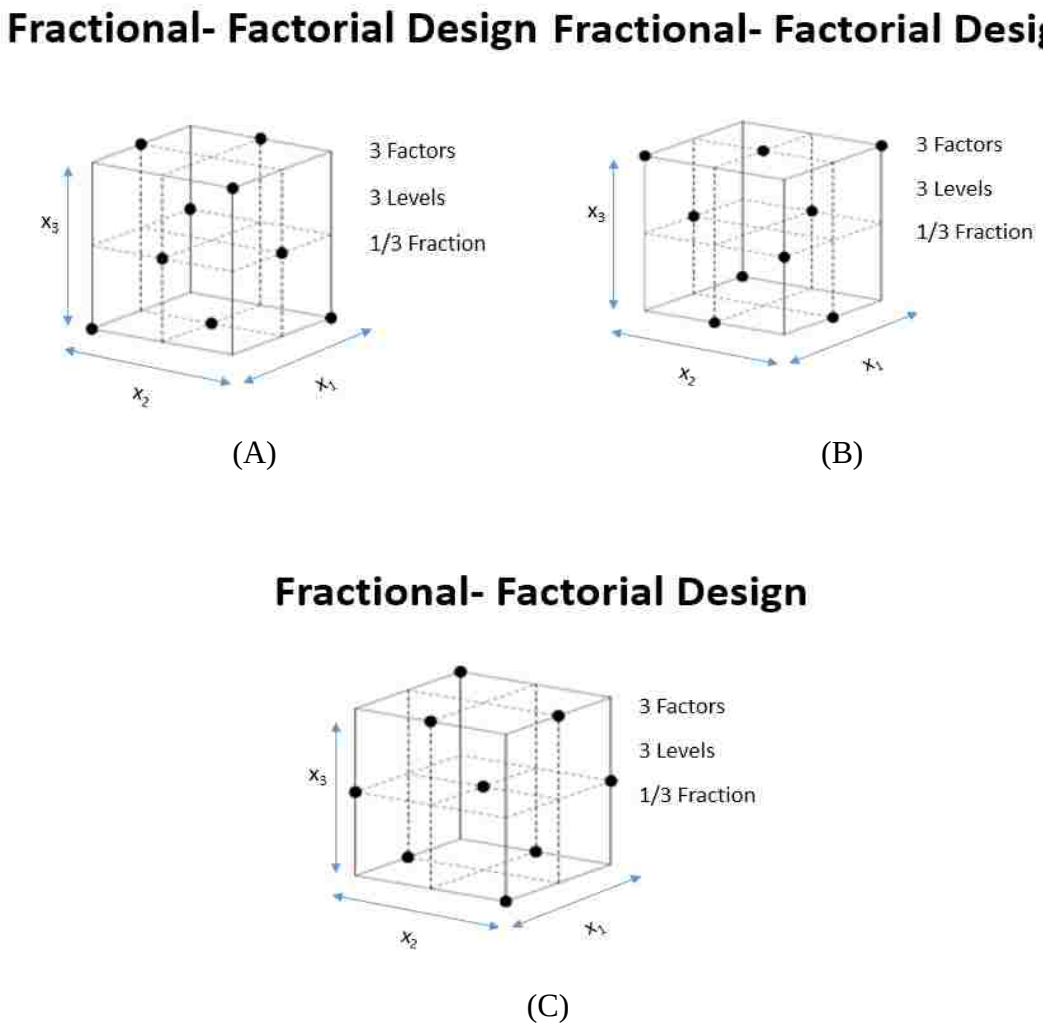

Figure 23: Fractional factorial orientations

5.3.2 Central Composite Design

A central composite design (CCD) is developed to find the optimal settings of the variables and to plot the response surfaces. On the other hand, the use of a factorial design is to provide indications of the significant effects and the interactions between the process variables [70].

A CCD design is considered as the most superior class of design for fitting a second order model [70]. In a CCD, each factor has 5 levels (extreme high, high, center, low and extreme low), which are coded between the ranges of -2 to +2. The total number of experimental runs for a CCD is defined by the following equation 12-

$$n = 2^N \quad (12)$$

Here, n is the total number of experiments

N is the total number of design variables

A CCD consists of end points, axial points and center points. The axial points are mathematically calculated as 2*N i.e. twice the number of design variables. The center points (n_C), according to the literature (with increasing factors), should always be selected between 3 and 6 to maintain maximum stability of the system. Therefore, the remaining points out of total experimental runs are the end points, and are mathematically calculated as n-(2N)-(6). [64]

A system of N factors for a first order system produces a 2^N experimentation set. In the case of a second order model system, an alternative 3^N design is also available. The benefit of such a design for a second order model system is that the total number of experimental runs (n) are comparatively less than that of the full factorial approach. For example, for a system of 3 factors and 3 levels, the total number of design/ experimental runs for a full factorial will be 27 (i.e. 3^3); while the total number of design runs for a CCD will be 15 (2^3=8 end points, 2*3=6 axial points and 1 center point). [64]

Figure 24, represents a CCD of N= 3 factors (called a cube experiment), with 8 end points, 6 axial points and 1 center point in a three dimensional factor space.

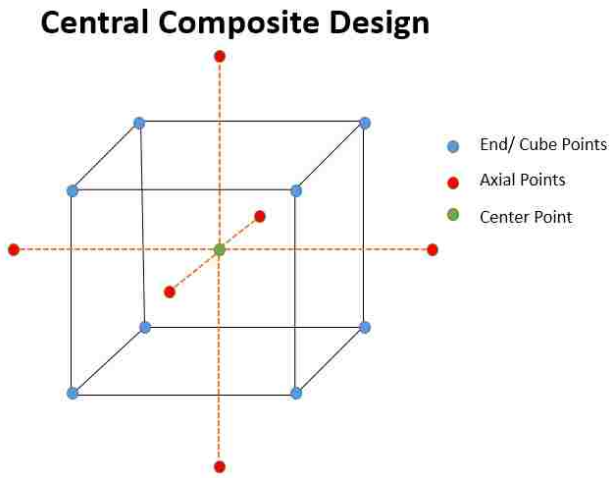

Figure 24: A central composite design demonstration

A CCD experimentation generally shows a lack of fit in a first order model, hence, axial runs or points are added to the design to allow quadratic terms to be incorporated in the model and avoid the fitness problem. The two parameters that are essential in designing a CCD are as follows [64]:

1) The distance α of the axial runs from design center point: a CCD design is made rotatable by the choice of an α value. The value of α depends on the number of points in the factorial portion of the design. Here α is numerically calculated by the expression:

$$\alpha = n^{1/4} \tag{13}$$

Here, α is the distance of the axial run from the design center
n being the number of points in the factorial portion of design

2) Number of center points (n_C): according to the literature, the center points are repeated 3-6 times to enhance the stability of the model along with providing a possibility to calculating standard deviation and exploring the maximum possible accuracy of the model.

5.4 Design Matrix- Setup

This thesis work uses a central composite design (CCD) for the experimentation process. This is due to the fact that the overall expenditure of material, time and financial investment is considerably low for a central composite design over a full factorial approach. Table 4 shows a comparison of experimental runs with both the CCD and the full factorial approaches (total savings of 9279 experiments).

Table 4: Comparison between full factorial and central composite design

	Full Factorial Design	Central Composite Design
Factors	5	5
Levels	5	5
Replicates	3	3
Total Experiments	$3* (5^5) = 9375$	$3* (2^5) = 96$

The experimental setup for this research work consists of five input factors (manufacturing parameters) varied over five levels. These levels are coded over a range of -2 to +2, with -2 being extremely low and +2 being extremely high values of the manufacturing parameters for the laser cladding process. Also, 0 is coded as a base/ mid-point for the laser cladding operation. The combinations of the parameters for the mid-point are chosen with expert advice of the industry partner, the regular production parameters and with careful review of the literature (research projects). As mentioned before there are a total of 96 experiments (i.e. 32 experiments with 3 replicates) setup with a CCD approach. Table 5, represents the design matrix generated for the laser cladding process.

Table 5: Design matrix for the laser cladding process

Design Matrix							
Parameters	Units	Notations	Factor Levels				
			-2	-1	0	1	2
Feed rate	g/min	FR	10	15	20	25	30
Power	KW	PW	1	2	2.5	3	4
Focal length of lens	mm	FL	380	390	400	410	420
Laser speed	mm/sec	LS	5	7.5	10	12.5	15
Contact tip to work distance	mm	CTWD	21	22	23	24	25

The five manufacturing parameters chosen (after a detailed literature review) for the design of a experimentation set are the feed rate of the clad powder (FR), the power of the laser (PW), the focal length of the optic lens (FL), the laser speed (LS) and the contact tip to workpiece distance (CTWD)

1) Power (PW) – power refers to the amount of energy consumer per unit time and is expressed in watt (joules/sec). It is mathematically derived by the following equation 14,

$$P(t) = I(t) * V(t) \quad (14)$$

Here, P (t) is the instantaneous power and is expressed in watts
I (t) is the current supplied to the system and is measure in amperes (Amp)
V (t) is the potential difference in voltage and is expressed in volts (volt)

Hence, power is directly proportional to the current supplied and the voltage drop. According to the literature review, the current is one of the most vital factors in defining the clad bead's geometrical structure. It is documented that with an increasing current, there is an increase in penetration of the bead. This is due to the fact that with an increase in current at a certain travel speed of the laser results in an increase in the depth of the fusion reaction. This increase in fusion reaction may

lead to more penetration and higher dilution percentage due to a melt through the substrate metal [54]. Also, it is noted that with an increase in current, there is an increase of bead width until a certain critical point after which the bead width starts decreasing [58]. Other researchers have also concluded that with an increase in the current, the penetration increases and thus, increases the heat affected zone. Less current leads to inadequate penetration and incomplete fusion in other cases [71].
The shape of the weld bead cross section and the external appearance is determined by the voltage. With an increase in the voltage, the constant current, and travel speed of the laser, it is noticed that a flatter bead is usually generated. This flatness reduces the penetration and there is a less chance of porosity [54]. If the voltage is increased excessively, it is noticed that a wider bead is produced. With an increase in the bead width and with less penetration there is always a chance of cracking failures. But if the voltage is too low, a narrow bead is formed for which slag removal as a post-process is highly difficult (especially along the bead edges). [72] [73]

2) Laser speed (LS) – laser speed defines the overall pattern of the bead. It is documented that with an increase in the speed, the power of the laser decreases. This decrease in the power decreases the heat input which effects the reinforcement height. As less of the filler material is deposited, the reinforcement height is reduced with an increase in speed. Bead penetration is also affected by the laser speed. The penetration is low with a higher speed as less fusion power is experienced. This excessive speed can result in high porosity and cracking failures in the clad bead. High laser speed also leads to a low heat affected zone due to the same reasons (low fusion power on high laser speed) [74]. To improve the failure of the porosity, a slow laser operations should be performed so that there is enough time for gases to escape. Extensively low speed can lead to a rough bead with slags because of a large molten pool formation. It is also reported that the laser speed has a slight effect on the metal deposition rate as well. [75]

3) Feed rate of the clad material (FR) – feed rate of the clad powder with constant power and laser speed has a direct effect on the bead shape. It is noted that with an increase in the feed rate of the powdered clad there is an increase in reinforcement height and a taller bead is generated. The taller the bead, there is more penetration, resulting in a higher dilution. Note that the increase in the laser speed with considerable decrease in the feed rate leads to either no bead formation (just spurs around the laser area) or cracking due to less fusion reaction and no chemical bond formation.

4) Focal length of the lens (FL) – for this thesis work, the focal length of the lens refers to the distance between the outer focusing optical lens and the workpiece. Generally any adjustment to the lens affects the shape of the bead. Focusing lens plays a vital role in overlap configurations. Malfunctioning of the lens or improper positioning of the lens could lead to incorrect layover percentages in the overlaps. It also affects the layering configurations as layers are seen to be disoriented while manufacturing (slightly bend towards one side instead of one over the other) with changing lens distances.

5) Contact tip to workpiece distance (CTWD) – this is the parameter that defines the distance between the nozzle tip and the top of the workpiece (substrate metal). Change in this distance affects the overall shape of the bead. It is documented that with lesser distance (nozzle closer to workpiece) and constant power, the feed rate, and the travel speed; there is an increase in the bead width. On the other hand, if the distance is larger (nozzle far from workpiece), an increase in the reinforcement height is noticed.

Once the factors are selected and are coded between the [-2, 2] range, the next step is choosing a design. As mentioned earlier, a CCD is chosen with the two important parameters α (axial distance from center point of the design) and n_C (number of center points). The value of alpha (α) is computed as the fourth root of the total experiments i.e. 32 experiments (2 approximately). The number of n_C (center points) that are chosen for

constructing a stable design are 6. Figure 25, presents a breakdown of the points in a CCD design for this thesis work.

Central Composite Design

Factors:	5	Replicates:	1
Base runs:	32	Total runs:	32
Base blocks:	1	Total blocks:	1

Two-level factorial: Half fraction

Cube points:	16
Center points in cube:	6
Axial points:	10
Center points in axial:	0

Alpha: 2

Figure 25: Central composite design specifications

Lastly, a MINITAB 16 software environment with a response surface methodology (RSM) application and a central composite design (CCD) approach is used to define the various experimental runs. These experimental runs are combinations of manufacturing parameters which are used to collect four shape parameters for a single bead configuration and 12 shape parameters for an overlap configuration. Table 6 presents the various experimental runs developed with the MINITAB software. (Note- runs 13, 17, 22, 23, 24, and 29 are all set as midpoint runs- center points of the design to increase the stability of the overall system).

Table 6: Experimental configurations for sample collection

Runs	FR	PW	FL	LS	CTD
1	-1	-1	-1	-1	1
2	2	0	0	0	0
3	1	1	-1	-1	1
4	0	0	0	0	-2
5	1	-1	-1	-1	-1
6	1	1	-1	1	-1
7	-1	-1	-1	1	-1
8	-1	1	1	-1	1

9	0	0	0	0	2
10	0	0	-2	0	0
11	0	0	0	-2	0
12	1	-1	1	1	-1
13	0	0	0	0	0
14	1	1	1	1	1
15	0	2	0	0	0
16	-1	-1	1	1	1
17	0	0	0	0	0
18	1	-1	-1	1	1
19	1	1	1	-1	-1
20	-2	0	0	0	0
21	-1	-1	1	-1	-1
22	0	0	0	0	0
23	0	0	0	0	0
24	0	0	0	0	0
25	-1	1	1	1	-1
26	-1	1	-1	-1	-1
27	-1	1	-1	1	1
28	1	-1	1	-1	1
29	0	0	0	0	0
30	0	0	0	2	0
31	0	0	2	0	0
32	0	-2	0	0	0

Once the experiments are set-up, the next step involves the collection of the shape parameters for a single layer and overlap configurations. The following subsections mention in detail the assumptions, the equipment requirements etc. for the sample collection. Also, the post processing procedures are listed to attain the shape characteristics from the generated clad bead(s).

5.5 Assumptions and Equipment Requirements

The table 7 incorporates the list of equipment(s) and work procedures that are kept constant for collection and post- processing of samples for a single bead or overlap configuration.

Table 7: Constant factors for the laser cladding process

S. No.	Constant Factors	Specification/ Manufacturer
1.	Workbench angle	0 (degrees)
2.	Laser torch angle	90 (degrees)
3.	Shielding gas	100 % Argon gas
4.	Shielding gas flow rate	11-35 CFH (cubic feet per hour)
5.	Base material (Substrate)	Cold rolled structural steel coupon(4”x2”x0.5”)
6.	Powdered clad material	420 Steel
7.	Laser system	Fiber Laser; IPG Semi-conductor diode laser
8.	Powder feeder principle	Hybrid
9.	Nozzle type	Co- axial nozzle
10.	Tip- size (diameter)	4.3 (mm) grain size
11.	Metallographic microscope	Olympus SZX12
12.	Abrasive cutter	Buehler, oscillamet
13.	Robotic arm	IRB 4400 (ABB- Manufactures)
14.	Mounting press	Leco, PR-32
15.	Mounting material	EpoMet- hard material with good edge retention,
16.	Flush mount variable	Buehler, Ecomet 12
17.	Polisher and grinder	Speed grinder & polisher with Automet 3000 power head
18.	Etching solution- 420 Steel	Nitric hydrochloric glycerol (10ml HNO_3, 20-50 ml HCL and 30 ml glycerol); spray with methanol
19.	Gas mask	Gas respirator face mask (advantage 3200 full-face piece respirator)
20.	Fume hood	Lincoln electric mobiflex 200-M fume extractor with XFMR- model# K-1653-2

The selection of the equipment is done according to the availability of the equipment at the sponsor industry partner due to financial constraints.

Maintaining all assumptions and equipment requirements, the clad bead samples are generated using the MINITAB devised experimental runs. The samples generated here are incapable of providing the shape characteristics; hence, various post- processing operations are required to procure the shape characteristics for each experimental run (explained in Appendix). These post- processing operations comprise of the abrasive cutting process (to obtain a cross-section of the clad bead), the sample mounting process (performed for easy storage and accessibility of multiple samples onto a single mount head), the polishing, grinding and etching process (to obtain a reflective surface of the sample), and the image processing process (to obtain the geometrical measurements of the clad bead under a metallurgical microscope).

CHAPTER 6

A COGNITIVE ARTIFICIAL INTELLIGENCE SYSTEM

6.1 Background

Neural networks are an emerging and evolving field that has its origin from the science of neurobiology. A neural network imitates the basic information processing mechanism or path carried out by a human brain (similar to a neurobiological system). In simpler words, neural networks are mathematical models that perform similar functions as a human brain to process information. A human brain consists of various neurons that help in processing information from one to another. Similarly, a neural network consists of various perceptrons (neurons) that help transfer (information and pass) numerical data from one to another. Hence, the neural networks are designed to perform complex tasks just like the brain [76]. Figure 26 (source: Quasar Jarosz [77]), presents a structure of a neuron of the human brain.

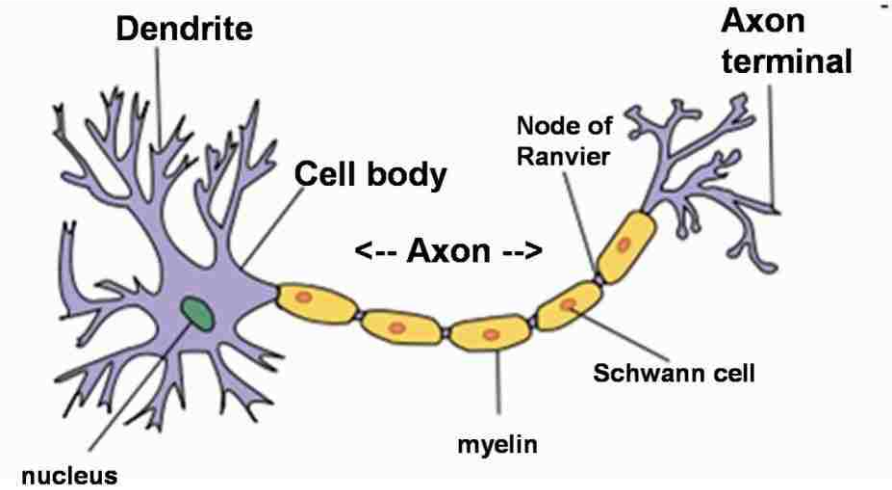

Figure 26: A schematic diagram of a human brain neuron [77]

In statistics, a neural network is a compilation of interconnected neurons that learn from an external environment (raw data supplied as input and target values to the network). These networks adapt to linear and non- linear trends and show incremental change in their structures as the data is processed by each activation center. Learning through the external environment triggers a training phase for the network and thus predictions and simulations

are made accurately according to the fitness (accuracy) of the learning curve. Generally, it is noted that a lower learning rate is achieved if the raw data supplied to the neural network consists of various noise factors. [76] [78]

The data processing operation is carried by neurons that act as basic computing units. A neural network is "a massively parallel distributed processor that has a natural propensity for storing experiential knowledge and making it available for use. It resembles the brain in two respects: 1. knowledge is acquired by the network through a learning process; 2. interconnection strengths between neurons, known as synaptic weights or weights, are used to store knowledge" [79]. In other words, neurons are parallel structures whose function is determined by the network architecture, the connection strengths and the processing mode.

6.1.1 Capability- Neural Network

Neural networks can perform various tasks such as classification, clustering, forecasting and pattern recognition. Some of these tasks are explained as follows:

1) Function approximation – neural networks have a capability to fit both linear and/or non-linear data to a multidimensional space to achieve the desired accuracy. Approximation occurs over a supervised learning set comprising of the known input, the output and the target variables. These prediction networks (predictors) are called the universal approximators as they help follow a pattern over a data range and approximate new data with similar trends. This process of approximation can be time consuming if it is done through conventional methods or by numerical calculations. In terms of functionality, these networks are addition to multivariate techniques for predicting trends such as multiple linear regression and non-linear regression [76]. Figure 27 (adapted from: Samarasinghe [76]) displays a graphical representation of the functional approximation.

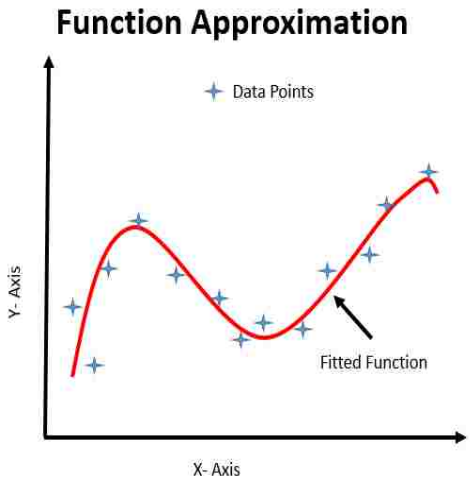

Figure 27: Function approximation graph, adapted from [76]

2) Data and signal classification – neural networks are useful in data classification as they aid in assigning data to a specific class. Linear, non-linear, complex, and multi-categorical data consisting of linear or non-linear classification boundaries can be classified with the help of such networks. Classification networks are most frequently encountered in the manufacturing industry and majorly aid in the decision making process. As classification is encountered frequently, it should be noted that the data used for training should not be over trained to avoid any over fitting circumstances. Over-fitting of data can lead to an undesirable result. Along with data classification, these networks help in classifying signals over a time series range by assigning the raw data to a specific class. Generally, classification is performed by using a pattern recognition tool used for a supervised learning environment. In supervised learning, the input and the target data is well known before training. This supervised learning technique helps the network categorize specific inputs to its target value [76]. Figure 28 A and B (adapted from: Samarasinghe [76]), display a graphical representation of the classification.

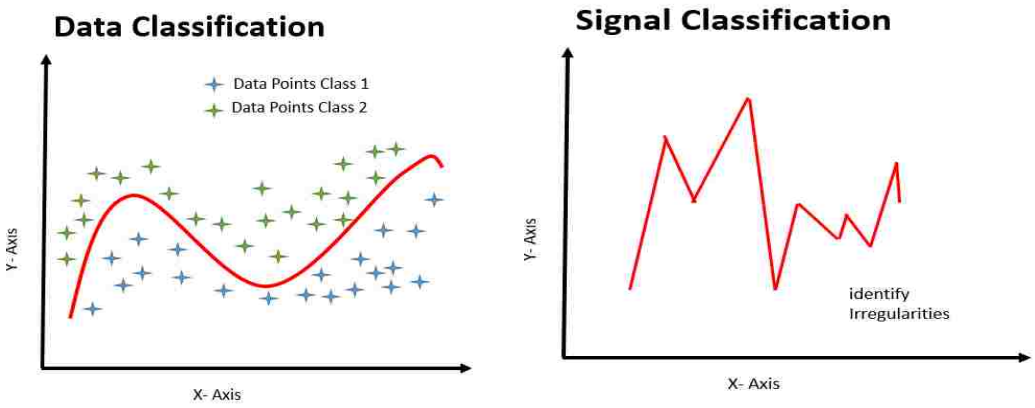

(A) (B)

Figure 28: Classification graphs- (A) data and (B) signal, adapted from [76]

3) Unsupervised clustering – neural networks are also capable of classifying unsupervised complex data and grouping them into classes according to trend similarities. This type of network is generally used in an unsupervised learning environment where the data has inputs but the user/software is unaware of the target values. This unsupervised learning process makes it difficult for the software for meeting convergence criteria. These networks do not include a priori (i.e. no similar trends match to the network in any previous work/trial). Therefore, when training such networks unknown clusters are formed in a given dataset and the network uses internal data properties to discover such clusters. In functionality, these self-organizing networks reveal spatial relations between clusters while discovering other clusters [76]. Figure 29 (adapted from: Samarasinghe [76]), displays a graphical representation of the unsupervised clustering.

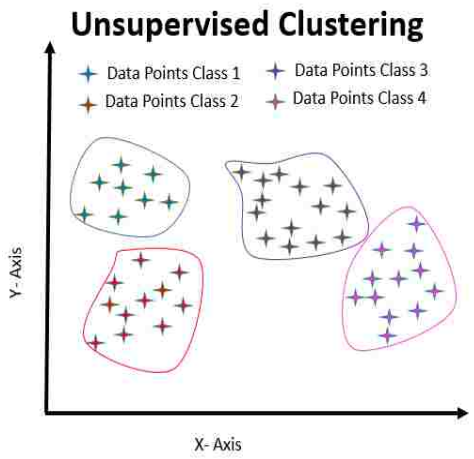

Figure 29: Unsupervised clustering graph, adapted from [76]

4) Forecasting – in forecasting, the data used is time series driven. These networks help determine future outcomes over a time series range by capturing the past memory of the model consisting of various temporal patterns. This past memory aids the network forecast future behaviour or trends on a time series scale [76]. Figure 30 (adapted from: Samarasinghe [76]), displays a graphical representation of the forecasting.

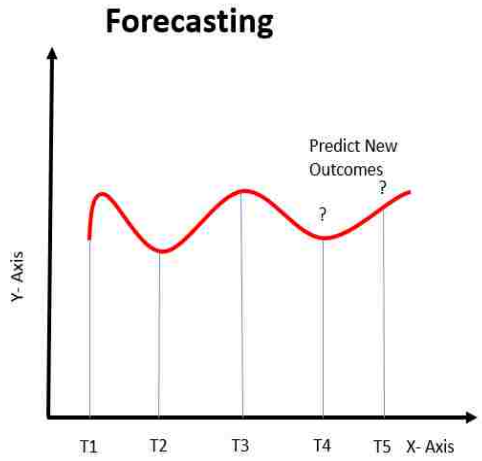

Figure 30: Forecasting graph, adapted from [76]

6.2 Network Essentials

6.2.1 Epoch

"An Epoch is a single pass of all input patterns in a perceptron during the training phase." [76]. In other words, an epoch is a single iteration carried out through the process of training the network. There are two training methods i.e. batch training and example-by-example training, which are explained in detail in the following sub-sections. In each epoch run, the data set is provided to the network defined, which consists of the input weights. Once the training phase starts, these network weights along with their bias values are updated to the lowest mean square value (MSE). Once a low value of MSE is reached the epoch is terminated and the new set of weights is passed onto the next epoch. Thus, the updated weights act as the input weights to the next epoch and the process is carried on until there is no more improvement (i.e. lowest MSE error value is obtained). In most cases, several epochs are required to train a network dataset to reach a desired result/performance with the least mean square value (MSE) [76] [80].

6.2.2 Training methods

There are two types of training methods or algorithms that a neural network training phase is based upon. Both these methods use training techniques for adaptation of the network to the data trend and hence, converge to a common least mean square error value. As mentioned earlier, both methods have several epoch runs but the weight updating method is very different for the same input data set. A detailed explanation of each of this training method is provided as follows [81]:

1) Example by example training – example by example is a method in which, the input weights are adjusted after each appearance of an input pattern (also called the online training). Due to such frequent update in the input weights, the input weights oscillate back and forth. This oscillation happens because the adjustment required by one input vector is cancelled by another input vector. This oscillating phenomenon can generally lead to time wastage while learning, training and minimizing the value of mean square error. In example by example training, the network is trained to minimize error for each example. In most cases the random

movement of weights due to oscillation causes instability to the result as well as to the network. The error calculations for this method use different weights of each input sample for each run [81]. Figure 31 (adapted from: Samarasinghe [76]) displays a graphical view of the example by example learning with the trend in oscillating weights.

Figure 31: Example- by- example training, adapted from [76]

2) Batch training – batch training is a method that is more popular than example by example training. This is due to the fact that it provides a stable solution and there is no oscillation of the weights. In this method, all input patterns are processed at once and later (after each epoch) the weight adjustment takes place in an average sequential form. In batch training, the overall error with respect to the training set decreases incrementally with the adjusting weights. Here, the error is the least in the direction of the greatest descent indicated by a resultant gradient. As the error varies with input, there is always a new error surface leading to new error values and gradients with each epoch [81]. The error across each epoch in this learning is denoted by the following equation 15 : [76]

$$MSE = \frac{1}{2N}\sum_{i}^{N}(t_i - z_i)^2 \tag{15}$$

Here, MSE is the Mean square error value

t is the target value for supervised learning supplied to the network

z is the network output value

N is the number of training cases (Input weights)

The total gradient for an epoch is mathematically expressed as equation 16, [76]

$$d_m = \sum_{n=1}^{N} \left[\frac{\delta MSE}{\delta w_m}\right]_n \tag{16}$$

Here, d_m is the total gradient

m is an epoch run

n is the number of examples of the m^{th} epoch

MSE is the mean square error value

w_m is the input weight

Figure 32 (adapted from: Samarasinghe [76]), displays a graphical view of the batch learning with gradient descent (no oscillations).

Figure 32: Batch training, adapted from [76]

The direction of steepest descent is always opposite direction to the direction of batch gradients in a training set. During the greatest descent, the magnitude of the weights decreases to meet the least point of the error surface. Batch learning is an implementation of the steepest descent method. [81]

6.2.3 Degrees of Freedom

The degrees of freedom for a network generally refer to total number of independent parameters at a certain instance possessed by a system [82]. In the case of neural networks, the degrees of freedom available to a neural network are the number of weights and the biases in the defined network. The degrees of freedom (value) determine the plasticity of the network which is the capability of the system to approximate the training set. Increasing the plasticity helps the network reduce the error generated during the training phase but it can increase the error during the testing phase of a network. Decreasing the plasticity immensely can lead to a large error in testing and training. [83]

6.2.4 Activation Functions

The network architecture for a neural network consists of three different layers. Both the hidden layer and the output layer, contain the activation functions. These activation functions are the mathematical functions that help the network update weight and corresponding bias values. The update in input values helps in superior learning and adaptation to the trends in the data set. The activation functions are non-linear, continuous in nature, and are bound between a higher and a lower value. The non-linearity behaviour refers to the non- linear outputs of the functions as compared to the network inputs. Continuity refers to the sharp peaks or gaps in the function so that the delta rule can be applied to adjust the input-hidden and the hidden-output weights through a backpropagation technique. [76]

Activation functions are generally categorized in two categories i.e. as sigmoid functions S-shaped functions or as Gaussian functions. For this thesis, the main focus is on the sigmoid functions. There are three types of sigmoid functions that are utilized while defining the network architecture, which are as follows:

1) Tan sigmoid activation function – The hyperbolic tan sigmoid function has a lower bound of -1 and an upper bound of +1. Hence, the output range is between the [-1, +1] boundary. Also, according to the literature, the slope of the hyperbolic tan sigmoid function is higher than the log sigmoid function. The mathematical representation of a hyperbolic tan sigmoid function is expressed in equation 17.

$$\tanh(u) = f(u) = \frac{1 - e^{2u}}{1 + e^{2u}} \tag{17}$$

A graphical representation of the hyperbolic tan sigmoid function is seen in figure 33.

Figure 33: Graphical representation of tan sigmoid function

2) Log sigmoid activation function – The log sigmoid activation function has a lower bound of 0 and an upper bound of +1. Hence, the output range is between the [0, +1] boundary. The mathematical representation of a log sigmoid function is expressed in equation 18.

$$y = Log(u) = \frac{1}{1 + e^{-u}} \tag{18}$$

A graphical representation of the hyperbolic tan sigmoid function is seen in figure 34.

Figure 34: Graphical representation of log sigmoid function

3) Linear activation function – The linear activation function is an unbounded function and is present in the output layer of the network architecture. This activation function is best suited as an output neuron function because it provides a one-to-one relationship with the network output. The mathematical representation of a log sigmoid function is expressed in equation 19.

$$y = f(u) = u \tag{19}$$

A graphical representation of the hyperbolic tan sigmoid function is seen in figure 35.

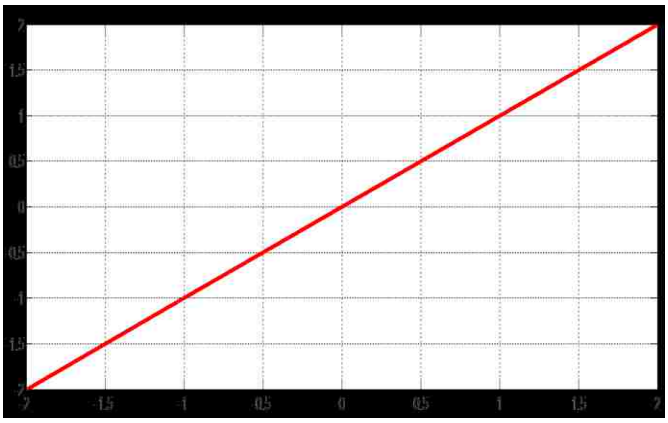

Figure 35: Graphical representation of linear function

6.2.5 Learning Algorithm

There is a wide selection of learning algorithms that a network can adopt for training purposes. For the purpose of this research, a Levenberg Marquardt (LM) method has been adopted for training purposes. A Levenberg Marquardt method is expressed as "a numerical solution to the problem of minimizing a (generally nonlinear) function, over a space of parameters for the function" [84]. According to the literature, LM technique is considered superior to the gauss-newton method as it adjusts the value of learning rate (Є) to unity and adds a new term e^{λ} to the second order equation. This addition of the natural logarithmic term (e) along with a damping factor (λ), helps in reaching a minimum MSE value. Thus, the lower the MSE value, the better the network performance. The LM technique can mathematically be expressed as equation 20. [76] [85]

	$\Delta w_m = \frac{d_m}{d_m^s + e^{\lambda}}$	(20)

Here, m is an epoch run

d_m is the first derivative to the error value

d^s_m is the second derivative to the error value

e is the natural logarithmic function

λ is the damping factor

The LM technique uses a gradient descent method, to reach a global minimum error value by minimizing all first gradient derivative values to zero.

6.2.6 Network Layers

There is a wide selection of network architectures that a neural network can adopt for the learning and training purposes. The focus of this thesis work is the multi-layer perceptron network (with one or multiple hidden layers) architecture that uses a feed forward back propagation technique to update the weights and corresponding bias values.

A multi-layer perceptron (MLP) network refers to a network that possesses various layers in a network architecture. The main function of the MLP network is for the pattern recognition, classification and approximation. The three layers present in a MLP network are as follows [76]:

1) Input layer – this layer contains the inputs to the network, defining the condition for which the network undergoes the training phase. Each input to the network is an independent variable that has an influence on the output of the network. This layer is connected to the hidden layer which helps in passing the input weights to the activation functions for the training (weight adjustment) process.

2) Hidden layer – this layer contains the non-linear activation functions. There could be multiple activation functions present in this layer to process information. For the purpose of this research, the hidden layer contains sigmoid activation functions to

help adapt to the non-linear trends of the input weights supplied by the input layer. This layer is connected to the output layer to pass the output weight of the system.

3) Output layer – this layer contains the linear activation function. There could be multiple activation functions present in this layer to provide various outputs to the system. This layer denotes a second step of weights being fed to the network. The updated weights from the hidden layers act as inputs to the output activation functions. Here, the linear functions bring together the outputs by computing the weighted sum of the updated network weights. Generally, there is a one-to-one relation to the network outputs and the linear activation functions present in the output layer.

Figure 36 displays a schematic view to a MLP network with various layers.

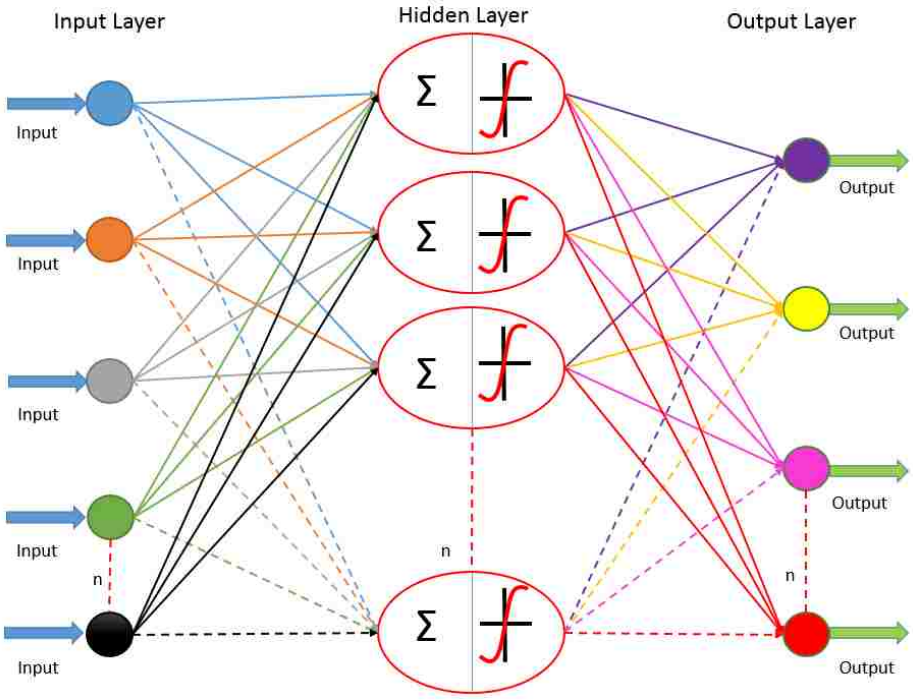

Figure 36: A schematic diagram of artificial neural network

MLP networks are trained using the supervised learning technique. The supervised learning technique refers to the learning adopted by a network when the experimental

output results for particular inputs are introduced to the network. These experimental output sets are referred to as the target sets. A feed forward back propagation behaviour is selected for the MLP networks. Feed forward network behaviour refers to a network in which the flow of information is only in one direction i.e. from the input to the output. There are no feedback loops present in such a MLP network. Backpropagation, refers to the technique of learning from input examples and desired (known) correct output for each case. This backpropagation (BP) technique helps the network adapt to the behaviour of the data that is expected [86].

The weights are updated along with their corresponding bias values using the following mathematical formula presented in equation 21,

$$S = \sum_{i-1}^{n} (w_i - x_i) + b \tag{21}$$

Here, x_i is the inputs to the network

w_i is the weight of each input value

b is the bias value

n is the total number of variables

6.3 Normalization

The technique used to normalize raw data for the thesis work the simple ranging technique. A simple ranging technique can be bound within two boundary conditions.

1) Boundary condition [0, +1] - this technique proves to be highly effective according to the detailed literature review. This technique limits all input and target values to a ranging scale of [0, +1]. Note- the activation function used in the hidden layer is a tan sigmoid function with a ranging scale of [-1, +1]. Hence, this technique is best suited with a log sigmoid activation function due to similar boundary conditions. The mathematical expression of a simple ranging scale is expressed in equation 22,

$$X_i' = \frac{X_i - X_i(\min)}{X_i(\max) - X_i(\min)} \tag{22}$$

Here, i is any defined variable

X'_i is a normalized variable

X_i is the experimental value of the defined variable

X_i (min) is the minimum value for the variable i

X_i (max) is the maximum value for the variable i

2) Boundary condition [-1, +1] - this technique limits all input and target values to a ranging scale of [-1, +1]. For the purpose of this thesis, all variables to the network are normalized using this boundary condition. Also, this condition holds significant for the tan sigmoid activation function due to similar boundary conditions. The mathematical expression of a simple ranging scale is expressed in equation 23,

$$X_i' = a + \frac{\big(X_i - X_i(\min)\big) * (c - a)}{X_i(\max) - X_i(\min)} \tag{23}$$

Apart from the variables explained earlier,

c is the upper boundary condition (+1)

a is the lower boundary condition (-1)

A normalization process proves advantageous as it is highly effective in a condition where the variables of larger magnitudes are combined with the variables of smaller magnitudes in a design matrix. It is generally observed that while training a network in such a condition, the larger magnitude variables mask the effect of the smaller magnitude variables which provides an ineffective result. Thus, normalization brings all variables in a design matrix to a similar ranging scale [-1, +1] so that a true influence of each of the variables can be studied and an effective training result is obtained. [78] [76]

For the purpose of this thesis work, the input set(s) and the training set(s) are initially normalized between the range of [-1, +1] and then fed to the network. It should be noted here that all input and target parameters are assumed to be independent (i.e. no interactions or interdependencies are assumed). In the case of interdependencies, another process called whitening will be utilized over the simple ranging scale.

6.4 Network Training

The training process for a neural network starts with defining the network architecture along with its layers. Once the network architecture is developed the next step involves normalization of the input and the target parameters followed by division of data.

The training process is generally referred to as the process of adaptation. During this stage, the neurons present in the hidden and the output layers of the network architecture perform various steps to align to the pattern of the raw data points presented. This adaptation is necessary and is vital in making the future prediction and the simulations confidently. The neurons present in the hidden layer during this training phase sums the corresponding weighted inputs (denoted as Σ) and then passes these summed weighted inputs to the non-linear activation functions (denoted as σ). The non-linear functions transform the weighted inputs of a neuron to non-linear outputs. The non-linear functions, as described in previous sections can either be sigmoid or Gaussian functions in nature. The output from each hidden neuron is mathematically expressed as in equation 24 [76]

$$Output = \sigma\left(\sum_{j=1}^{n} w_j\, x_j + b\right) \tag{24}$$

Here, n is the receiving inputs to the hidden neurons

$X_1 \ldots X_j$ are the hidden neurons

σ is the non-linear function

b is the bias input value (noise factor)

w_j is the weight of each input

Σ is the initial summation of weights

Once the output is generated by processing the weighted inputs through the hidden layers, these outputs from hidden neurons act as inputs to the output layer neurons. The second sets of weights generated are passed them through the output neurons by computing the weighted sum and then passing through linear functions. The outputs from the linear functions are the outputs to the neural network. Once the outputs to the network are determined the training phase is terminated. Many results/ graphs are generated for the training phase that define the training state and the characteristics of the training process.

For the purpose of this thesis a single hidden layer multi-layer perceptron (MLP) network is utilized. The network contains the hyperbolic tan sigmoid function (neurons) in its hidden layer and the linear output function (neurons) in its output layer to carry out the training phase.

6.4.1 Division of Data Points

As mentioned earlier in this section, the pre- requisite to the training of a network is the division of data. This division of data is done in three categories to address the training efficiently which are as follows [85] [78]:

1) Training data – this data is the part of the dataset that is involved in the actual training of the network. Here, the neurons along with their activation functions help in updating weights based on the mean square value (MSE). Once the lowest MSE value is achieved (best performance), the network stops training. The default value of this data is set to 70% of the entire data set in the neural network application.

2) Testing data – this data is the part of the dataset that is not involved directly with the training phase. However, it provides an independent measure of the network's performance during and after the training has been performed. The default value of this data is set to 15% of the entire dataset in the neural network application. Also, this dataset aids in examination of the overall performance of the neural network.

3) Validation data –this data is the part of the dataset that helps in determining the network generalization. Generalization refers to a state of training where the neurons avoid the over fitting or the under fitting of the dataset. The network training stops once the generalization value stops improving. This data set is used to determine the performance of the network on patterns that are not yet trained during the learning state.

Each data division categories are vital for successful and confident training and prediction phases using the artificial intelligence system. The division of data is generally set to (70-15-15) %, as default value to the neural network toolbox in MATLAB software.

To prove that the default division percentage of data is accurate for this thesis work, one of the sample data test is evaluated (420 steel single pass forward network). Here, the different division percentages are considered in comparison to the default values set by MATLAB. The division that shows the best network performance is thus selected for the thesis work. Table 8 shows a comparison between the various data division percentages for the network training.

Table 8: Division of data for the single pass 420 steel forward networks

Training-Testing-Validation Data division	Fitness Percentage	MSE Error
70-15-15	96.34	0.0172
60-20-20	86.40	0.0173
50-25-25	83.93	0.0215

It is clear that the best network performance is achieved at the default division values (70-15-15) %. This is due to the fact that at (70-15-15) % division, there is maximum fitness of data and a minimum mean square error is encountered. Presence of such trends in the dataset helps gain maximum network performance and thus helps in making confident predictions.

6.5 Network Architecture for Single Pass 420 Steel

The following is the forward network architecture (MLP network) developed for a single pass for a 420 steel (low carbon) configuration, displayed in figure 37.

X_{input}= [FR; PW; FL; LS; CTWD]

T_{output}= [W; RH; P; D]

Hidden layer: tan sigmoid activation function (30 neurons)
Output layer: linear activation function (4 neurons)
Here, a 70-15-15 (training- testing- validation) division of data is used to obtain the best prediction results.

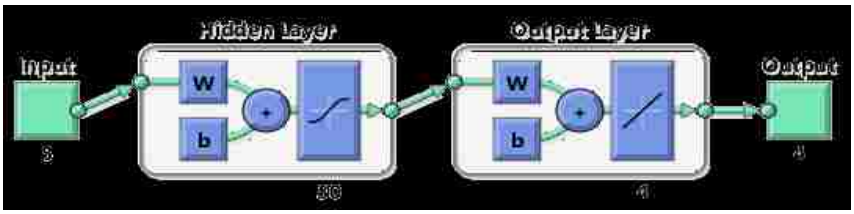

Figure 37: Neural network architecture- forward network 420 steel single pass

The following is the backward network architecture (MLP network) developed for a single pass for a 420 steel (low carbon) configuration, displayed in figure 38.

X_{input}= [W; RH; P; D]

T_{output}= [FR; PW; FL; LS; CTWD]

Hidden layer 1: tan sigmoid activation function (20 neurons)
Hidden layer 2: tan sigmoid activation function (20 neurons)
Output layer: linear activation function (5 neurons)

Note- as compared to the forward network for a single bead generation, the backward network uses a multi-layer perceptron network with multiple hidden layers carrying tan sigmoid activation functions. Also, a division of 80-10-10 (training- testing-validation) in this case provides the best prediction results.

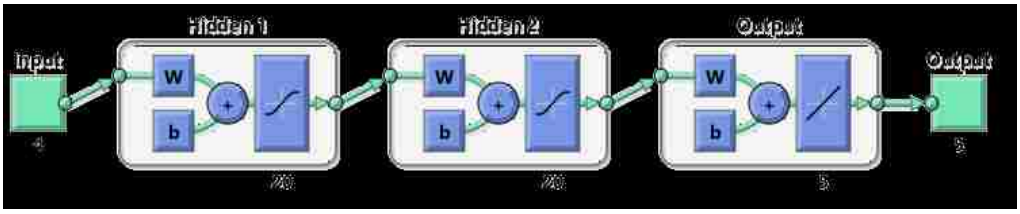

Figure 38: Neural network architecture- backward network 420 steel single pass

6.5.1 Fitness and Accuracy

The following four plots are generated to display a good fitness of the data points resulting in an accurate and precise learning state. Here, the single pass 420 steel forward

network data is used as an example to illustrate the visual trends. The first plot is a performance plot. A performance plot is a graphical plot constructed between the epoch runs and the mean square error values. This plot shows an individual trend in the MSE values for each data set (training, testing and validation) with advancing epochs. The best validation performance is indicated at a certain epoch, once the validation curve starts having a progressive, upward incline trend. While studying a performance plot, it should be noted that to achieve the best fit, the training curve and validation cure should follow similar trends. Any deviations from this trend would either lead to over fitting or under fitting of the data.

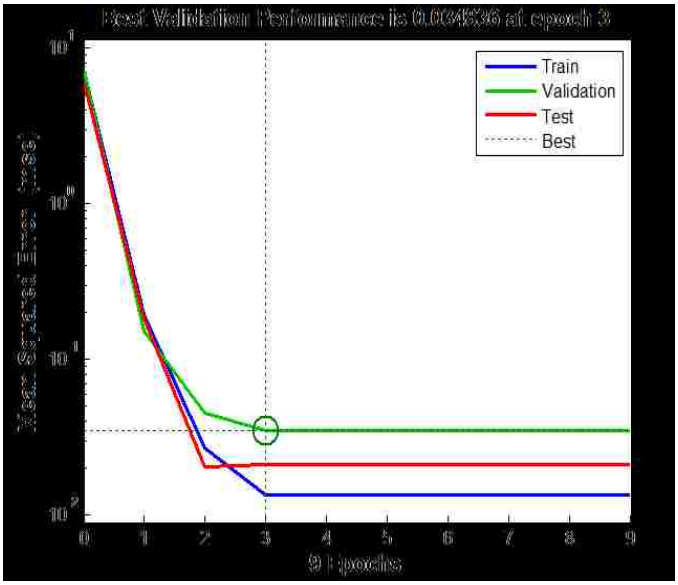

Figure 39: Performance plot for the single pass forward network

It can be seen from figure 39 that the green line (validation curve) starts showing a progressive trend at epoch 3 out of 9 epochs. At epoch 3, the best validation performance (least mean square error) is recorded as 0.034. Also, the performance plot generated here shows that the validation curve and the test curve (red line) are showing a parallel trend after epoch 3. This indicates that there is no over fitting or under fitting of data during the training phase.

The second plot is a training state plot. The training state plots shows the deviations in the default values of training parameters (such as gradient and mu values), during the execution/ training of the neural network. This plot predicts the reason for termination of

the network runs/ epoch(s). It is observed that the network training can only stop due to one of the following reasons:

a) Ran all entered Epochs (default setting in training parameter)
b) The value of Mu/gradient is maxed/minimized out (set in between a range in the training parameter)
c) The Validation checks are maxed out

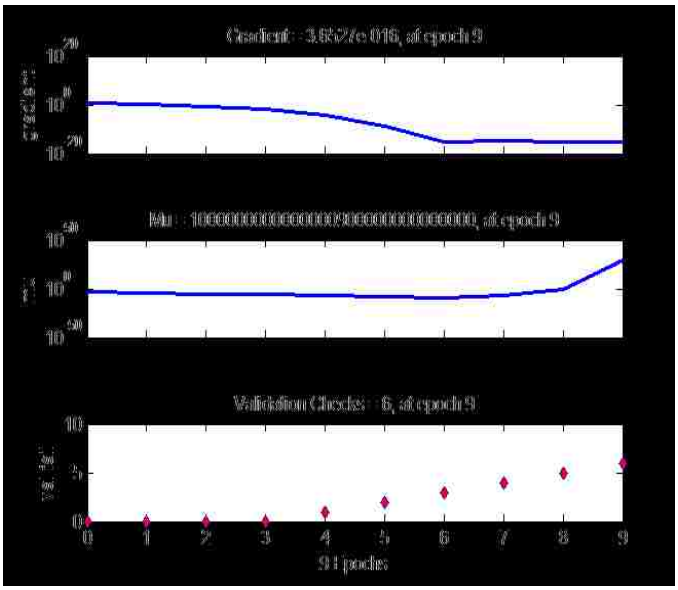

Figure 40: Training state plot for the single pass forward network

It can be seen from figure 40 that the reason for termination of the network training is due to the training parameter mu. The training parameter mu reaches its maximum value of (10^{30}) at epoch 9 and hence terminates the network learning. This plot can generally be validated with the training progress window (figure 41), which displays a mathematical representation of the train state plot training parameters involved in the process.

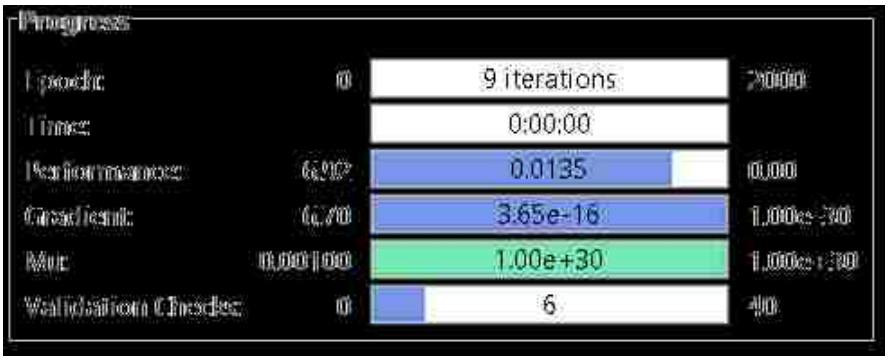

Figure 41: Training progress view for the single pass forward network

The third plot is an error histogram plot. The error histogram plot predicts the frequency of errors concentrated over a range. The x-axis indicates the various error values while the y-axis indicates the number of instances the error was predicted by the network. For a perfect fit/ well fit, the maximum frequency or the concentration of errors should be around the zero value to provide it with a perfect bell shape curve centered at zero.

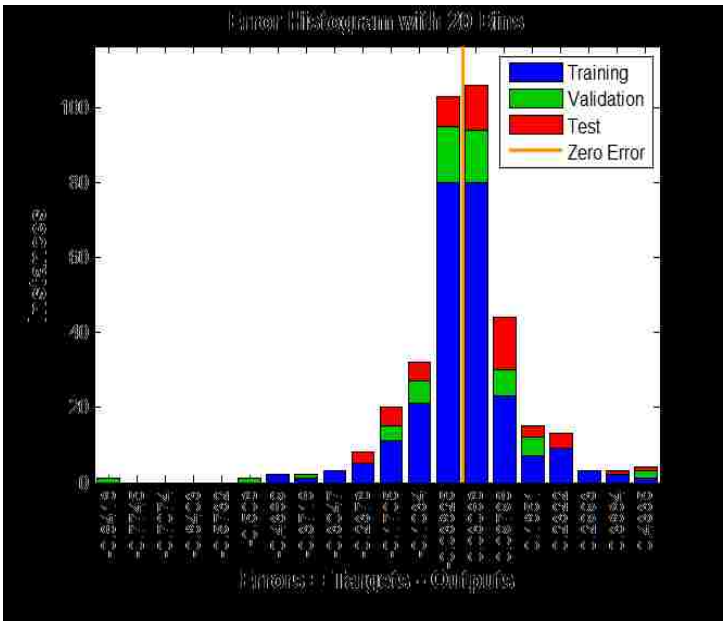

Figure 42: An error histogram for the single pass forward network

It can be seen from figure 42 that, the error histogram for a single pass of 420 steel data is forming a bell shaped curve near the zero value representing a good fit. Here, an individual decomposition of the errors is provided according to the training, validation and

testing datasets. The bar graph generated for this case is centered at 0.03 providing a good bell shape curve with in the 95th percentile window.

The fourth plot is a regression plot. The regression plot is a graphical plot between the target values and the network output values. When there is a perfect linear relationship between the target and the network output values, the value of the regression curve (R) becomes equal to 1 indicating a perfect fit. Here, the small circles in the graph indicate the data points, the blue line indicates the line of fit and the dotted line (hash line) indicates the best fit i.e. 100% accuracy.

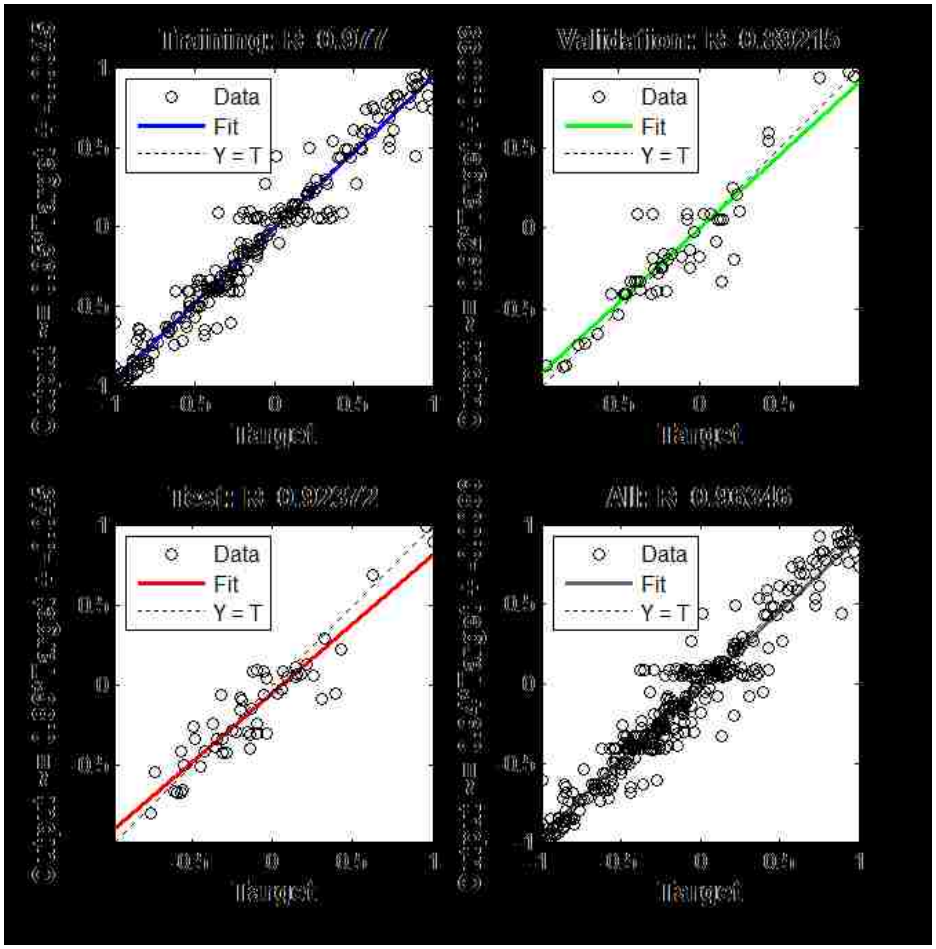

Figure 43: Overall regression plot for the single pass forward network

It can be seen from figure 43 that the overall fitness of the network achieved is at 0.9634. This fit is considered as a good fit as it helps in predicting values for the unknown test data which would be 96.34% accurately trained for future experiments. This plot also

provides an individual breakdown of fitness levels for different data sets involved in the training phase. Note- the graph is generated between -1 to +1 boundary levels due to the normalization process (-1, +1 boundary levels).

Table 9 presents a summary of results generated for a 420 steel single pass (data) laser cladding operation. Note- the mean square error value is the overall performance of the training network. A lower value of mean square error indicates a better prediction and fit and vice versa. In this case, the average mean square error is stabilized at 0.0045, indicating a good prediction and fit.

Table 9: Network results for the single pass 420 steel forward network

Results	Value
Overall mean square error (MSE)	0.0180
Training performance	0.0135
Testing performance	0.0211
Validation performance	0.0348
Overall R value	0.9634
Best validation performance (epoch)	3
Error histogram centered at (bell curve)	0.03086
Total epoch runs	9
Total validation checks (40 checks)	6

Accuracy of fitness is an important step after the training phase to make sure that a similar trend of data values has been predicted by the network as the experimental results. To check the accuracy of fitness, the network targets (actual values of shape parameters) are plotted individually to the network output (predicted values of shape parameters). The graphs (Appendix B and C), show a comparison plot for shape parameters with red curves representing the actual state and blue curves representing the predicted output state. Any deviations noticed from the actual values acts an error. A relative error percentage and an absolute error window is generated for the process.

Figures 44-47 display plots for residual errors present in the shape parameters for the forward network single pass network. It can be observed from the figures that there are no relevant trends present in the residual errors in the shape parameters.

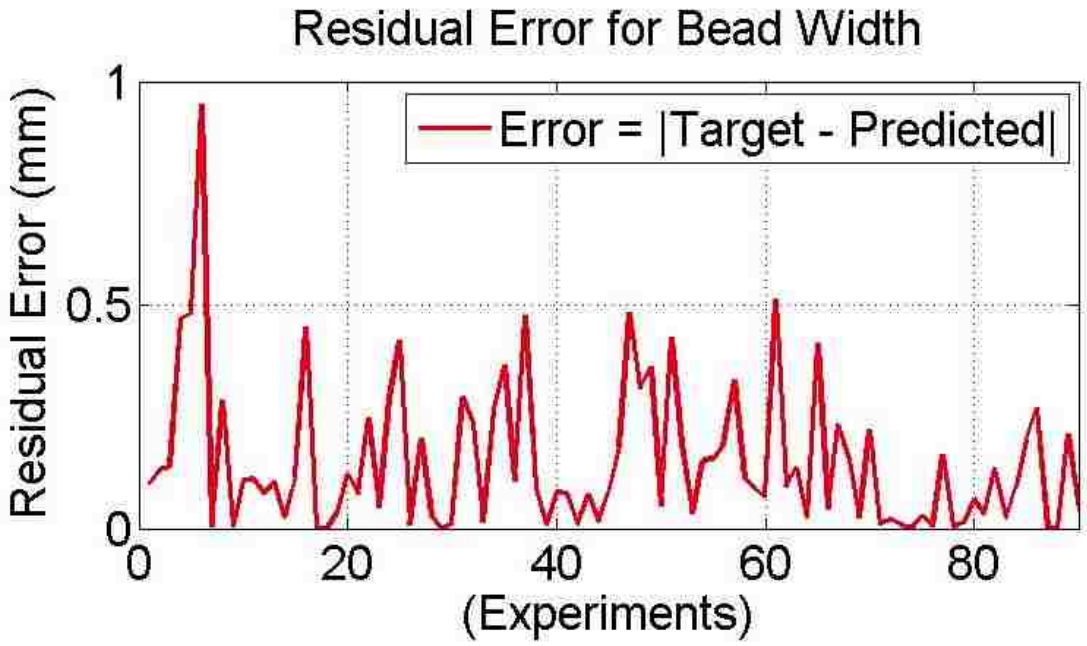

Figure 44: Residual error plot for the bead width for a single pass 420 steel forward network

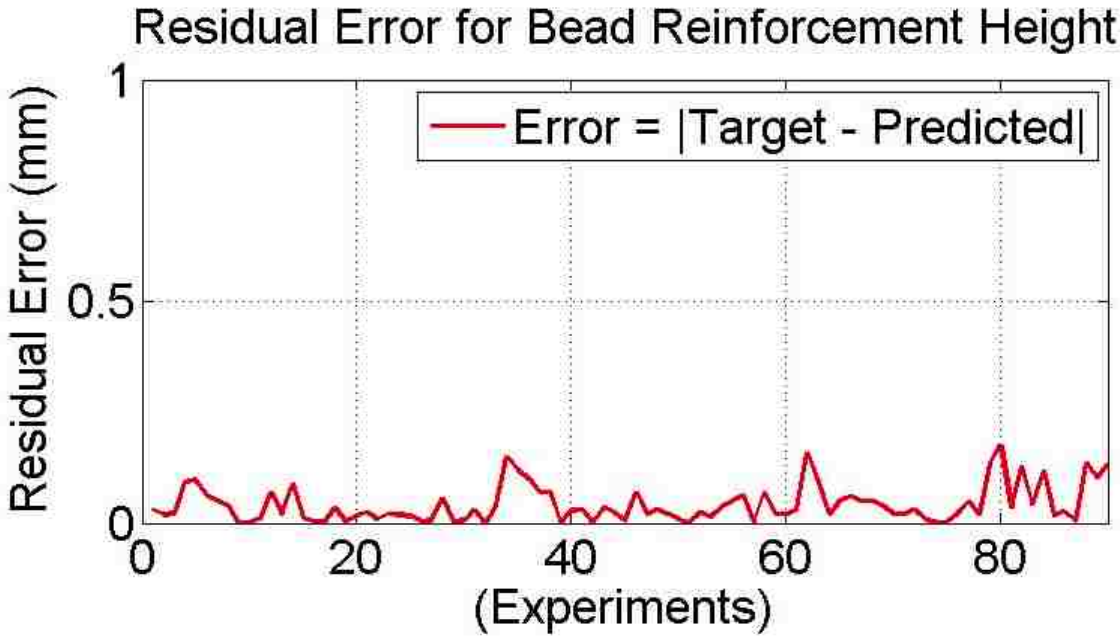

Figure 45: Residual error plot of the bead reinforcement height for a single pass 420 steel forward Network

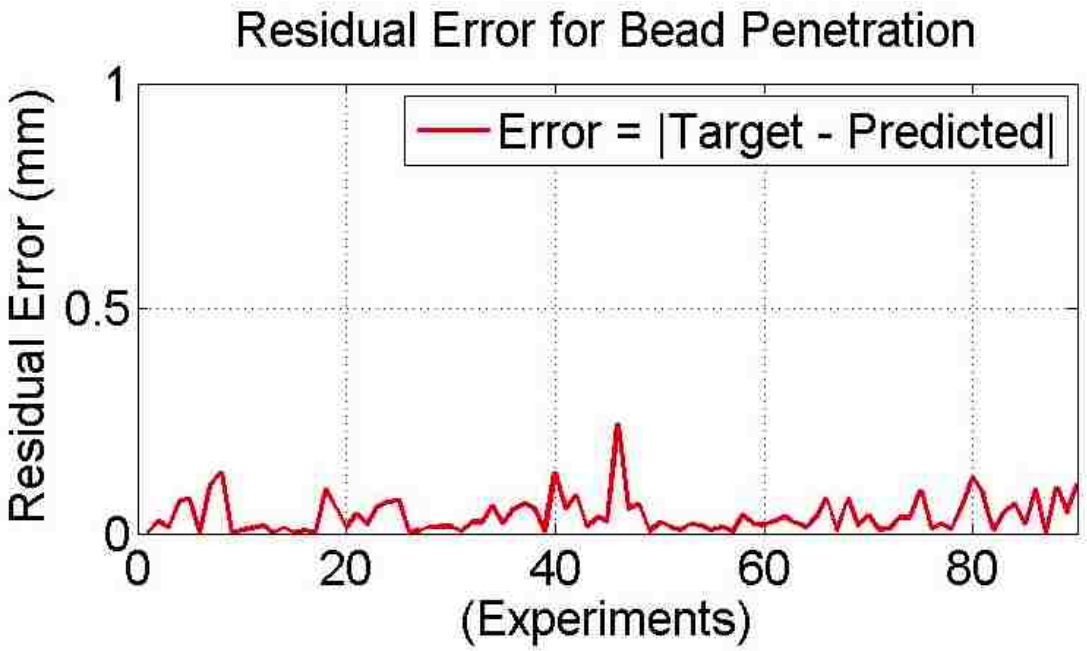

Figure 46: Residual error plot of bead penetration for a single pass 420 steel forward network

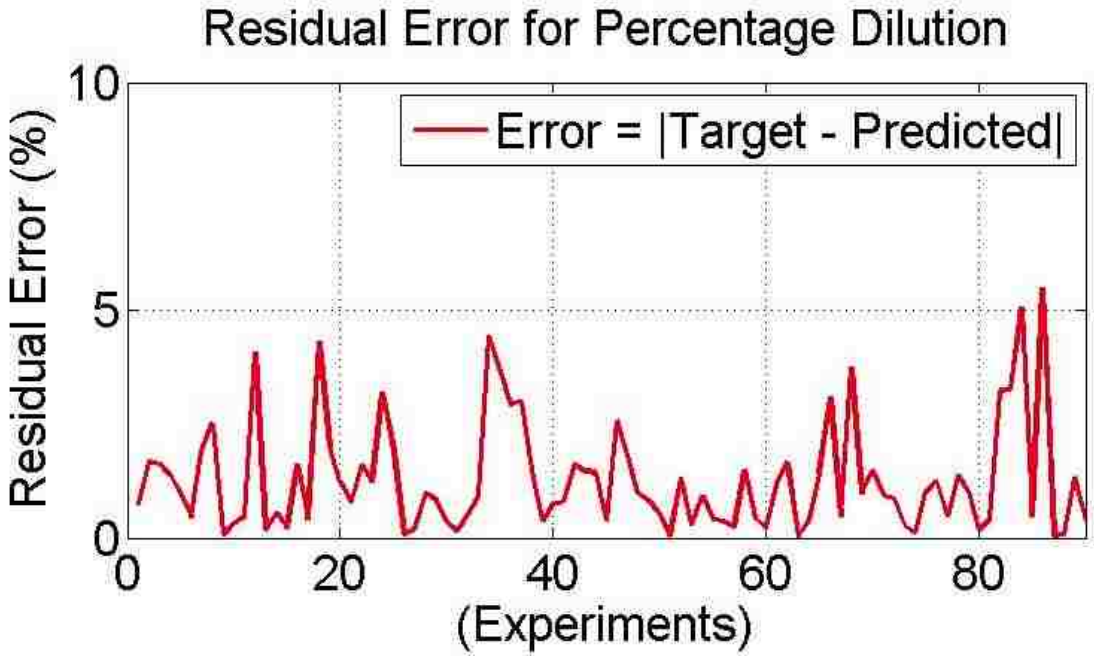

Figure 47: Residual error plot of bead percentage dilution for a single pass 420 steel forward network

Similar plots can be generated for the backward network with a single pass. Note- the residual errors for the basic shape parameters (W, RH, and P) are expressed in mm, whereas the residual error for dilution is expressed in percentage.

For a single pass of 420 steel data forward network, table 10 represents the error(s) relevant in the system (comparison of target input to network output). The red shaded boxes indicate a successful prediction in the output values within a 95th percentile confidence level while the green shaded boxes indicate a successful prediction in the output values within a 99th percentile confidence level.

Table 10: Absolute and relative error values for the single pass forward network

Shape Parameters	Absolute Error Values			Relative Error Percentage
	Maximum Error	Minimum Error	Error Window	
Width (W)	0.950000 mm	0.000077 mm	0.949923 mm	0.17%
Reinforcement Height (RH)	0.180000 mm	0.000360 mm	0.179640 mm	0.11%
Penetration (P)	0.240000 mm	0.000140 mm	0.239860 mm	1.80%
Percentage Dilution (% D)	5.500000 %	0.021000 %	5.479000 %	0.67%

Here, the absolute error (maximum and minimum) is mathematically calculated using equation 25

$$\text{Absolute } Error = abs(Actual\ Value - Predicted\ Value) \tag{25}$$

And, the percentage relative error is calculated using the mathematical expression presented in equation 26

$$\text{Relative } Error\ \% = abs\left(\frac{Actual\ Value - Predicted\ Value}{Actual\ Value}\right) * 100 \tag{26}$$

It can be seen that the absolute error in predicting the values of percentage dilution is maximum, hence, having an error window of almost 5 %. In the case of relative error percentage, the penetration parameter is recoded to be maximum percentage at 1.80%. Also, within the three basic shape parameters (width, penetration and reinforcement

height), the maximum error is recorded in the bead width parameter (approx. 1mm absolute error window) hence, displaying maximum deviations in figure 44.

6.5.2 Simulation and Verification

Once the network architecture is developed and the training phase is completed, the next step involves making successful predictions through the trained neural network. Here, a simulation tab (located in the neural network toolbox), is utilized to input a test raw input data set. While inputting the test raw input data set, it should be noted that the manufacturing parameters are arranged in the same sequence as the input set was used to train the network. Also, it should be noted that the test data set should include values that are in the boundary range for each of the target parameters. Table 11 presents the boundary conditions for shape parameters for a single pass 420 steel data.

Table 11: Boundary conditions for the shape parameters

Target Inputs	Maximum Boundary Condition	Minimum Boundary Condition
Width (W)	5.2 mm	3.03 mm
Reinforcement Height (RH)	1.51 mm	0.43 mm
Penetration (P)	1.06 mm	0.02 mm
Percentage Dilution (D %)	48.57 %	1.11 %

The test input set is then selected with in the boundary conditions and it is introduced to the trained network. The network then makes successful and confident predictions for the unknown combination of the test parameters. One such example for the single pass 420 steel is presented in table 12 for backward network architecture.

Table 12: Simulation data for the single pass 420 steel backward network

	Known Input		Predicted output	Actual output	Relative Error %
FR (g/min)	15	W (mm)	4.01	3.91	0.25%
PW (KW)	2	RH (mm)	0.70	0.67	2.30%
FL (mm)	390	P (mm)	0.46	0.47	3.00%
LS (mm/sec)	7.5	D (%)	27.54	28.27	0.85%
CTD (mm)	24				

It should be noted that the maximum error is seen in the penetration and the reinforcement height parameter(s). The red shaded boxes indicate a successful prediction in the output value within a 95th percentile confidence level while the green shaded boxes indicate a successful prediction in the output value within a 99th percentile confidence level. Hence, the system proves to be a successful method of artificial intelligence.

6.5.3 Results

Table 13 summarizes the error values for the single pass 420 steel network(s)

Table 13: Error analysis for the single pass 420 steel neural networks

Forward Network			Backward Network		
Output Parameter (s)	Relative Error (Training)	Relative Error (Simulation)	Output Parameter (s)	Relative Error (Training)	Relative Error (Simulation)
W	0.17%	0.25%	FR	0.36%	2.50%
RH	0.11%	2.30%	PW	0.48%	0.75%
P	1.80%	3.00%	FL	0.08%	0.17%
D	0.67%	0.85%	LS	4.80%	3.60%
			CTWD	0.51%	0.00%

The graphs for the prediction plots and training plots are presented in appendix A. It is seen that while training the forward network, the maximum deviation or the error value of the output data from the target values is found in the bead penetration (approx. 1.80%). A similar trend is observed for the simulation process where an unknown input set is introduced to the trained forward network. In this case, the maximum recorded error is 3% for the bead penetration value followed by a 2.3% error for the bead reinforcement value. The predictions for the bead width and the percentage dilution are made in with a 99 percent confidence level as compared to the bead penetration and the bead reinforcement height (95 percent confidence). The network performance (MSE overall error) recorded for the forward network is 0.0203 (0.0116- training data set; 0.0413 validation data set; 0.0397 testing data set).

On the other hand, the maximum error value for the training data set is seen in the laser speed data (4.80%) for the backward network. Similar trends are seen in simulating an unknown data set to the trained network where the prediction confidence for the laser speed and the feed rate values are within 95 percent. For the backward single pass network, the predictions for the power, the focal length, and the contact tip to work-piece distance values is within a 99 percent confidence. The graphs relating to the training state and the simulations are presented in appendix B for the backward network. The presented error analysis aids in making adjustments to the final results of the forward and the backward single pass network(s) before generating the final output parameters. The network performance (MSE overall error) recorded for the backward network is 0.0227 (0.0119- training data set; 0.0421 validation data set; 0.0304 testing data set)

6.5.4 Case Study

In this case study, two cases will be premeditated which are presented in figure 48 A and B. Both the cases focus on generating the manufacturing process parameter values (FR; PW; FL; LS and CTWD). The real time experiment cannot be generated due to limitations with the controller and the equipment specifications at the sponsor facility. Hence, parameters are generated using the developed artificial intelligence system to demonstrate the capabilities of the system.

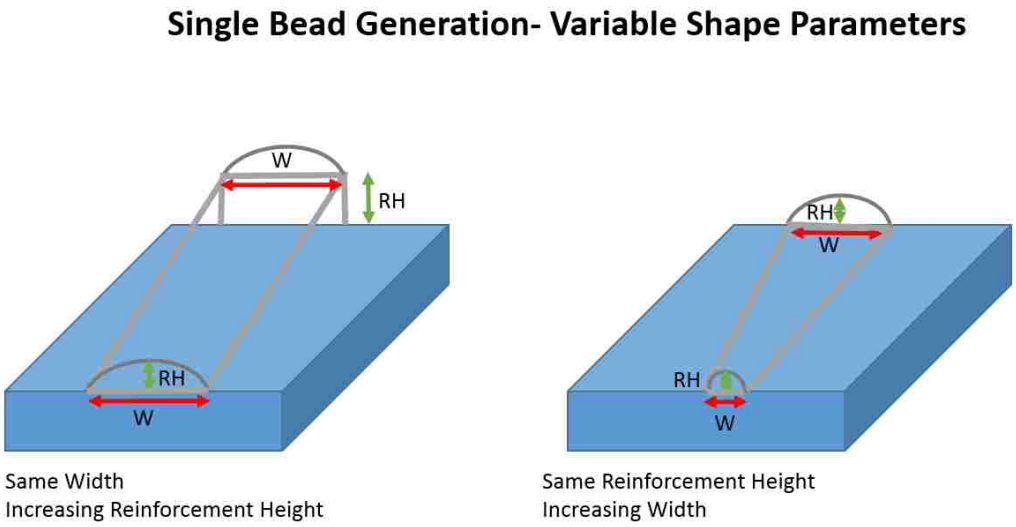

Figure 48: Single pass 420 steel- (A) case study 1 and (B) case study 2

The first case defines a problem in which the bead reinforcement height (RH) plays a critical factor while laying a clad bead onto a substrate metal (especially in slopes or cavities). To address this issue, the artificial intelligence system predicts the manufacturing parameters for positioning the single bead in a way that the width (W) of the bead is maintained constant and the reinforcement height (RH) increases incrementally. Table 14 displays the change in parameter values for a 3 step increase in the value of RH.

Table 14: Case study-1 results

Step- 1		Step-2		Step-3	
Desired Starting Shape parameters	Manufacturing Parameters	Shape Parameters	Manufacturing Parameters	Desired Ending Shape parameters	Manufacturing Parameters
W= 3.00	FR=12.04	W= 3.00	FR= 21.41	W= 3.00	FR= 29.14
RH= 0.50	PW=1.58	RH= 0.75	PW= 1.64	RH= 1.00	PW= 2.27
P= 0.20	FL= 409.25	P= 0.20	FL= 395.31	P= 0.20	FL= 403.76
D= 3.00	LS= 9.76	D= 3.00	LS= 9.44	D= 3.00	LS=10.95
	CTWD= 23.97		CTWD= 23.33		CTWD= 22.86

Similarly in the second case, a problem is presented in which the bead width (W) plays a critical factor while laying the clad bead onto the substrate metal (especially while repairing cracks in the die-sets). To address this issue, the artificial intelligence system predicts the manufacturing parameters for positioning the single bead in a way that the reinforcement height (RH) of the bead is maintained and the bead width (W) increases incrementally. Table 15 displays the change in the parameter values for a 3 step increase in value of the RH.

Table 15: Case study-2 results

Step- 1		Step-2		Step-3	
Desired Starting Shape parameters	Manufacturing Parameters	Shape Parameters	Manufacturing Parameters	Desired Ending Shape parameters	Manufacturing Parameters
W=3.00	FR=28.27	W=3.25	FR=28.88	W =3.50	FR=29.16
RH =1.00	PW =2.16	RH=1.00	PW=2.32	RH =1.00	PW=2.35
P=0.30	FL=401.68	P=0.30	FL=407.79	P =0.30	FL=411.79
D=3.00	LS =9.25	D=3.00	LS=9.76	D=3.00	LS=9.79
	CTWD= 23.11		CTWD= 22.96		CTWD =22.95

6.6 Network Architecture for Overlap Configurations 420 Steel

The following are the forward network architectures (MLP network) developed for an overlap pass (40%, 50%, and 60% overlap) for a 420 steel (low carbon) configuration, displayed in figure(s) 49, 50, and 51 Note- the network architectures for 40%, 50% and 60% are structurally similar but have different values for regression (fitness). Also, a 70-15-15 (training- testing- validation) division of data is used to obtain the best prediction results.

X_{input}= [FR; PW; FL; LS; CTWD]

T_{output}= [W1; W2; W3; P1; P2; P3; RH1; RH2; RH3; RH12; RH23; D]

Hidden layer: tan sigmoid activation function (40 neurons)

Output layer: linear activation function (12 neurons)

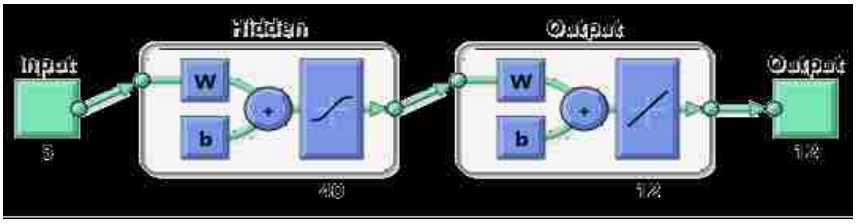

Figure 49: 40% forward overlap configuration neural network

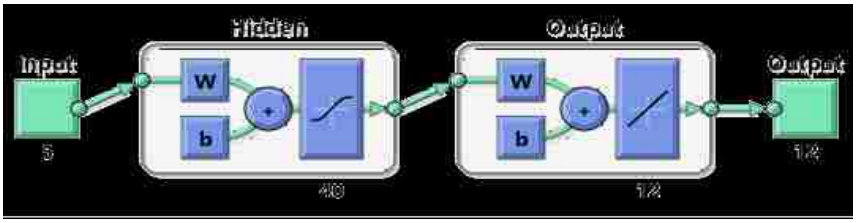

Figure 50: 50% forward overlap configuration neural network

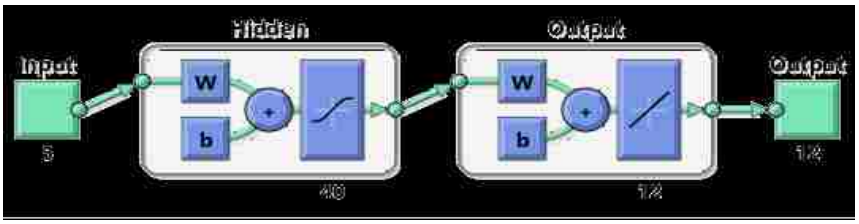

Figure 51: 60% forward overlap configuration neural network

The following are the backward network architectures (MLP network) developed for an overlap pass (40%, 50%, and 60% overlap) for a 420 steel (low carbon) configurations, displayed in figure(s) 52, 53, and 54.

X_{input}= [W1; W2; W3; P1; P2; P3; RH1; RH2; RH3; RH12; RH23; D]

T_{output}= [FR; PW; FL; LS; CTWD]

Hidden layer: tan sigmoid activation function (12 neurons)

Output layer: linear activation function (5 neuron)

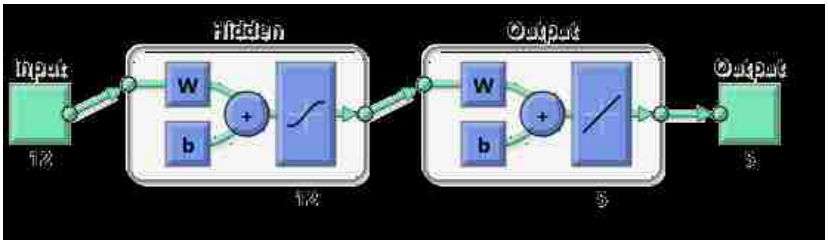

Figure 52: 40% backward overlap configuration neural network

X_{input}= [W1; W2; W3; P1; P2; P3; RH1; RH2; RH3; RH12; RH23; D]

T_{output}= [FR; PW; FL; LS; CTWD]

Hidden layer: tan sigmoid activation function (20 neurons)

Output layer: linear activation function (5 neuron)

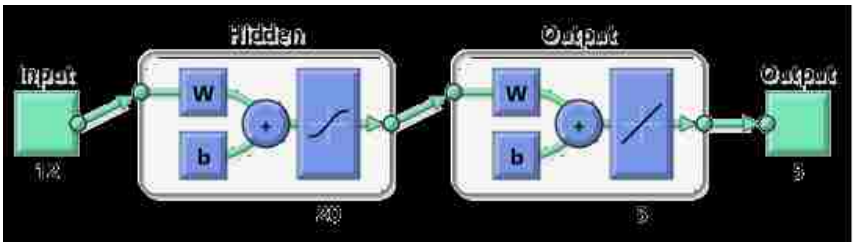

Figure 53: 50% backward overlap configuration neural network

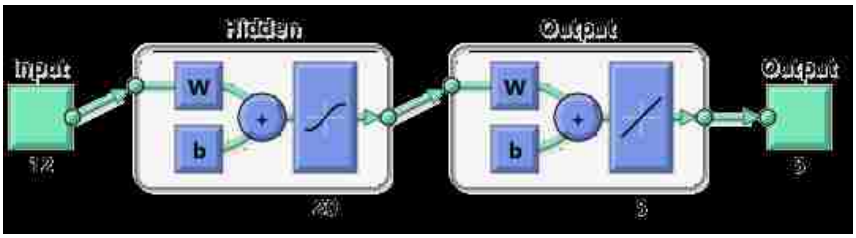

Figure 54: 60% backward overlap configuration neural network

Note- the accuracy, the fitness and the simulation outputs for the backward networks for the various overlap configurations are provided in the appendix for reference.

6.6.1 Results

Figures 55 display plots for residual errors present in the shape parameters for the forward network single pass network. It can be observed from the figure that there is no relevant trends present in the residual errors in the shape parameters.

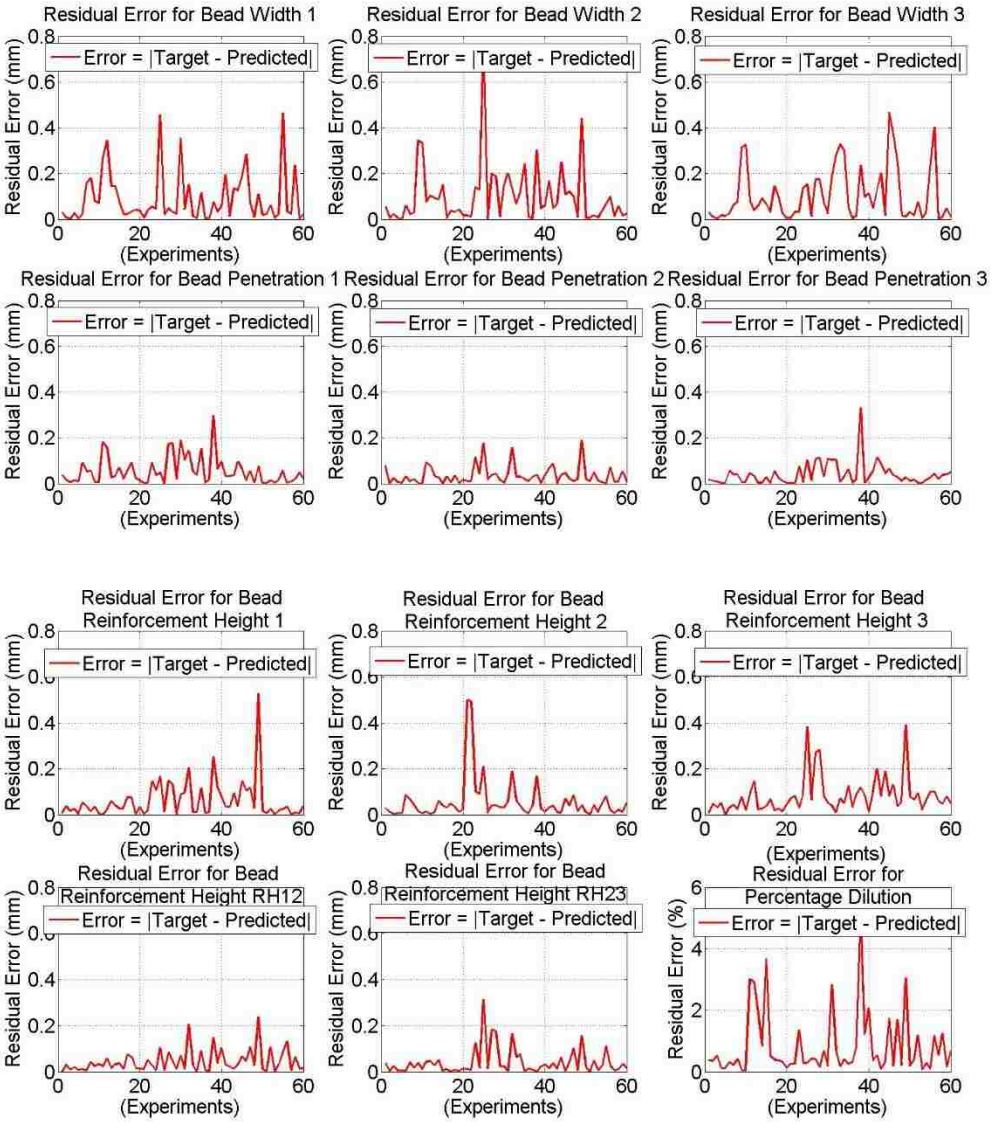

Figure 55: Residual errors for 40% forward overlap configuration network

Similar plots can be generated for the forward and backward networks with a 40%, 50%, and 60% overlap. Note- the residual errors for the basic shape parameters (W, RH, and P) are expressed in mm, whereas the residual error for dilution is expressed in percentage.

Table 16 summarizes the error values for the various (40%, 50%, and 60%) overlap configuration passes for the forward network(s).

Table 16: Error analysis for the overlap passes for forward networks

Forward Overlap Network						
	40% Overlap		50% Overlap		60% Overlap	
Output	Relative Error (Training)	Relative Error (Simulation)	Relative Error (Training)	Relative Error (Simulation)	Relative Error (Training)	Relative Error (Simulation)
W1	0.10%	1.60%	0.47%	2.60%	0.83%	2.70%
W2	0.65%	2.00%	0.40%	1.40%	0.13%	0.34%
W3	0.43%	1.90%	0.11%	0.12%	0.45%	1.90%
P1	1.20%	1.00%	1.40%	2.80%	2.10%	4.70%
P2	0.70%	4.40%	0.13%	5.30%	0.13%	3.10%
P3	2.80%	4.90%	3.80%	4.30%	0.17%	3.00%
RH1	2.20%	5.00%	0.27%	4.70%	1.30%	1.60%
RH2	0.04%	1.10%	0.08%	2.40%	1.80%	2.10%
RH3	4.30%	4.70%	0.11%	3.70%	0.91%	4.00%
RH12	0.36%	2.60%	0.62%	3.50%	1.20%	0.48%
RH23	0.99%	1.90%	0.10%	3.70%	0.46%	0.00%
D	0.38%	1.40%	1.00%	1.50%	0.58%	2.10%

In the table 16, the green shaded boxes specify the error percentages less than or equal to 1% in the training and the simulation process. The red shaded boxes specify the error percentage between an error windows of [1% - 5%]. Here, the error percentage denotes the relative percentage deviation of the networks output values from the target values while training the neural network.

In the case of the 40% overlap configuration for the 420 steel clad powder, the forward network shows a maximum deviation in the values of the reinforcement height 3 (4.30%) followed by the reinforcement height 1 (2.20%) and the penetration 3 (2.80%)

values for the training state. Again, a similar trend is observed in the simulation process whereas the maximum deviation from the predicted results is observed in the reinforcement height 1 (5.00%) followed by the penetration 3 (4.90%) and the reinforcement height 1 (4.70%) values. The graphs for the prediction plots and the training plots are presented in appendices C, D, and E. In the case of the 50% overlap configuration for the 420 steel clad powder, the forward network shows a maximum deviation in the values of the penetration 3 (3.80%) followed by the penetration 1 (3.00%) values. Similar to this trend, the maximum deviation for the predicted results through simulation shows a maximum deviation in the bead penetrations (average- 4.13%). The graphs for the prediction plots and the training plots are presented in appendices C, D, and E. Finally, in the case of the 60% overlap configuration for the 420 steel clad powder, the forward network shows a maximum deviation in the values of penetration 1 (2.10%) which is again similar to the trends in the simulation phase of the predicted values for calculating the relative errors (4.70% for P1). The graphs for the prediction plots and the training plots are presented in appendices C, D, and E.

Table 17 summarizes the error values for the various (40%, 50%, and 60%) overlap configuration passes for the generated backward network(s).

Table 17: Error analysis for the overlap passes for backward networks

Backward Network						
	40% Overlap		40% Overlap		40% Overlap	
Output	Relative Error (Training)	Relative Error (Simulation)	Relative Error (Training)	Relative Error (Simulation)	Relative Error (Training)	Relative Error (Simulation)
FR	2.20%	4.20%	2.10%	1.00%	2.90%	4.70%
PW	1.30%	3.80%	0.63%	0.69%	1.90%	2.00%
FL	0.05%	0.18%	0.04%	0.34%	0.13%	0.37%
LS	0.98%	3.30%	4.00%	2.20%	2.20%	3.70%
CTWD	0.31%	0.82%	0.15%	0.31%	0.04%	0.70%

As mentioned earlier in the 40%, 50%, and 60% overlap forward model, similar trends in relative errors are seen in the training and the simulation phases. Note- the errors are relatively higher in the backward networks as the data is discreet and the generalization arises due to averaging of the results to newer classes as compared to assigning the data points to the predefined classes. The graphs for the prediction plots and the training plots are presented in appendices (F, G, and H).

Once, the error analysis results are determined, the sample cases are presented in the next section to show the applications of the artificial intelligence system proposed for this thesis. The numerical values for the predictions are generated and are adjusted by the network and the true parameters (error adjusted) are presented for the production purposes.

6.6.2 Case Study

Similar case studies are presented in this section but for the various overlap configurations. Instead of the single bead, multiple (3 pass), beads are created through the laser cladding operation. The three passes have a defined layover percentage which is generally referred to as the overlap percentage.

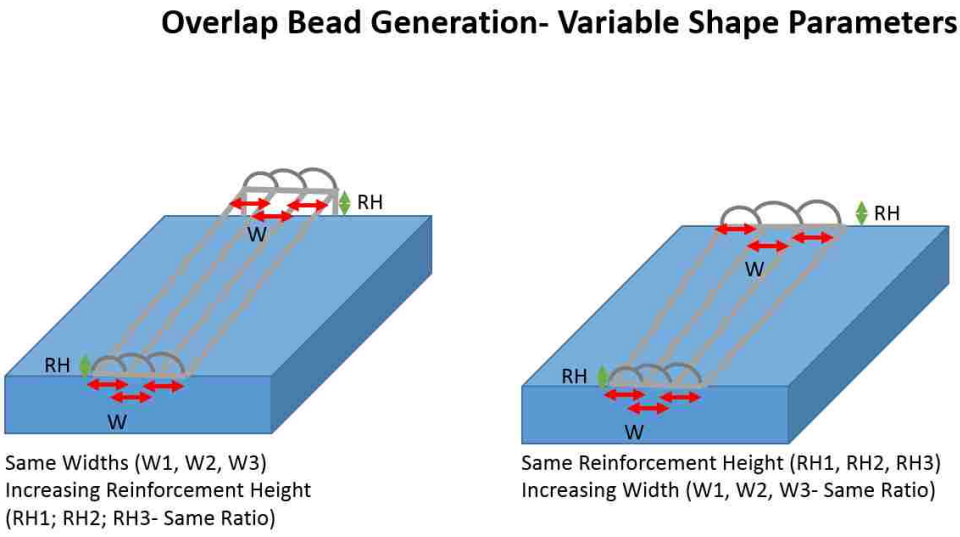

Figure 56: Single pass 420 steel- (A) case study 3 and (B) case study 4

Note- the predictions made for case 3 and case 4, presented in figure 56, are prepared with a 40% overlap configuration. Here, a three step increase in the reinforcement height (RH1, RH2, and RH3) and the width (W1, W2, and W3) values for cases 3 and 4 respectively is carried out. The changes in the manufacturing parameters for the presented cases (3 and 4) are listed in table 18 and table 19 respectively.

Table 18: Case study-3 results

Step- 1		Step-2		Step-3	
Desired Starting Shape parameters	Manufacturing Parameters	Shape Parameters	Manufacturing Parameters	Desired Ending Shape parameters	Manufacturing Parameters
W1=3.00	FR=17.04	W1=3.00	FR=18.75	W1=3.00	FR=19.69
W2=3.00	PW=2.33	W2=3.00	PW=2.41	W2=3.00	PW=2.41
W3=3.00	FL=404.99	W3=3.00	FL=402.91	W3=3.00	FL =401.73
P1=0.20	LS=10.85	P1=0.20	LS=10.20	P1=0.20	LS=9.09
P2=0.20	CTWD=23.10	P2=0.20	CTWD =22.87	P2=0.20	CTWD=22.81
P3 =0.20		P3 =0.20		P3 =0.20	
RH1 =0.50		RH1 =0.70		RH1 =0.90	
RH2 =0.70		RH2 =0.90		RH2 =1.10	
RH3 =0.90		RH3 =1.10		RH3 =1.30	
RH12=0.50		RH12=0.70		RH12 0.90	
RH23=0.70		RH23=0.90		RH23=1.10	
D=5.00		D=5.00		D=5.00	

Table 19: Case study-4 results

Step- 1		Step-2		Step-3	
Desired Starting Shape parameters	Manufacturing Parameters	Shape Parameters	Manufacturing Parameters	Desired Ending Shape parameters	Manufacturing Parameters
W1=2.60	FR=21.48	W1=2.80	FR=20.96	W1=3.00	FR =20.64
W2=2.10	PW =2.81	W2=2.30	PW=2.53	W2=2.50	PW=2.37
W3=2.30	FL=401.34	W3=2.50	FL=404.46	W3=2.70	FL=407.15
P1=0.30	LS=13.59	P1=0.30	LS=13.19	P1=0.30	LS=12.72
P2=0.30	CTWD =22.02	P2=0.30	CTWD=22.15	P2=0.30	CTWD=22.53
P3 =0.30		P3 =0.30		P3 =0.30	
RH1 =0.80		RH1 =0.80		RH1 =0.80	
RH2 =0.80		RH2 =0.80		RH2 =0.80	
RH3 =0.80		RH3 =0.80		RH3 =0.80	
RH12= 0.70		RH12= 0.70		RH12=0.70	
RH23=0.70		RH23=0.70		RH23=0.70	
D=5		D=5		D=5	

6.7 Summary

Figure 57 displays the process that the artificial intelligence system takes in predicting successful and confident results. Here, the blue boxes are the process steps, the grey cylinders are the prerequisites for a certain process, the red arrows show the flow of data for a training phase and the green dashed arrow shows the flow of data for the simulation phase. This model is a schematic representation of the model created through MATLAB coding (.mfile). The inputs to the model are the process parameters and the target parameters (actual bead geometry data collected at the sponsor facility). The outputs to the model are the predicted bead geometry parameters. Design of experiments (DOE) is a prerequisite to the model for designing the various process configurations to collect the target data for the network using a central composite design technique. Accuracy check,

verification and error analysis are the post- processes to the proposed model and are carried out once the network outputs are achieved.

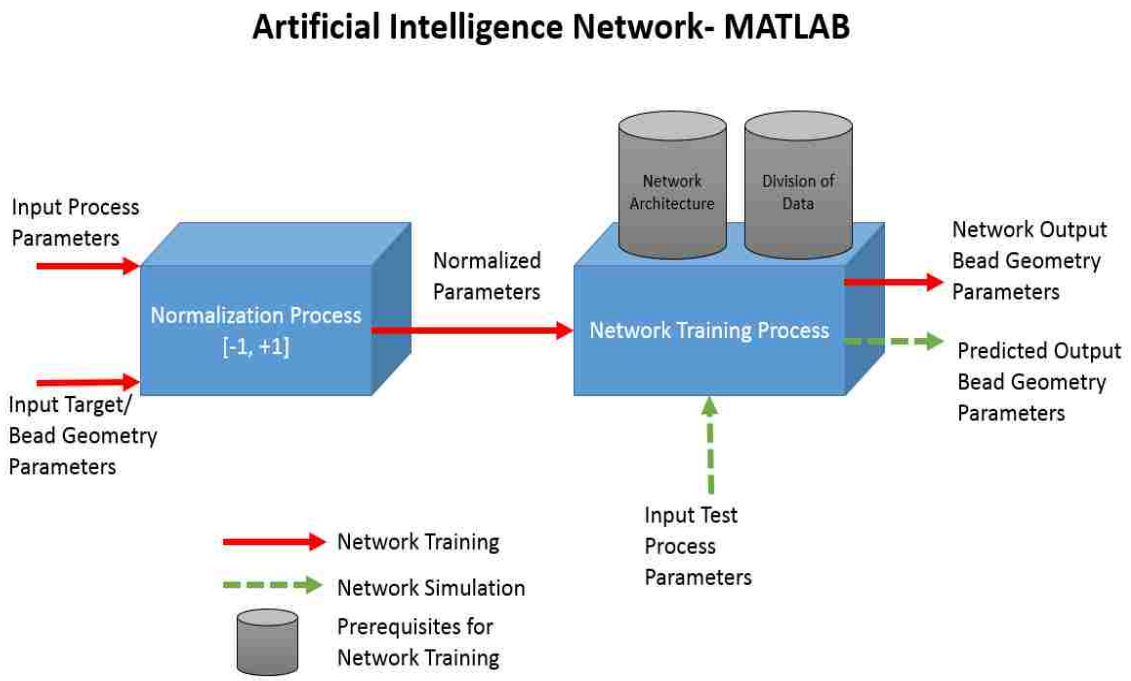

Figure 57: Summary of artificial intelligence system developed in MATLAB

CHAPTER 7

SIGNIFICANCE OF MANUFACTURING PARAMETERS

After development of the artificial intelligence system with the aid of the neural networks, it is evident that the input manufacturing parameters play a vital role in deciding the shape properties of the clad bead. As stated earlier, the laser cladding process is a multiple variable process that involves investment of raw material, financial participation and time. Hence, the significance of parameters is in fact much needed. This chapter focuses on identifying the extent to which each factor or interaction affects the outputs of the predictive system proposed. To study this approach, two separate techniques-sensitivity analysis and analysis of variance (ANOVA) are studied and compared to verify results. A model summary of statistics for all response variables is generated to stimulate confidence in the generated models. Both the contour and the surface plots are created for illustrating the difference in effects over a response variable by a single process parameter as compared to two or more interacting process parameters. Finally, the optimization solver toolbox (response optimizer) with aid of MINITAB is applied to the generated model to visualize the single and the multiple objective optimization results that can be obtained for the response variables.

7.1 Analytical Model Development

A response surface methodology (RSM) of a 2^{nd} order model system has been utilized to develop an analytical method of the single pass 420 steel laser cladding process. The analytical method uses the process of linear regression in making successful predictions in terms of the clad bead shape parameters.

The linear regression model developed helps in optimizing the response variable as a function of the input parameters (manufacturing parameters) to the system. The system is not only able to show the extent of contribution of each factor (manufacturing parameter) but also the influence of the squared and the quadratic terms (various interactions). A response function for a second order equation can be expressed as equation 27:

$$Y = \beta_0 + \beta_1 * A + \beta_2 * B + \beta_3 * C + \beta_4 * D + \beta_5 * E + \beta_{11} * A^2 + \beta_{22} * B^2 + \beta_{33} * C^2 + \beta_{44} * D^2 + \beta_{55} * E^2 + \beta_{12} * AB + \beta_{13} * AC + \beta_{14} * AD + \beta_{15} * AE + \beta_{23} * BC + \beta_{24} * BD + \beta_{25} * BE + \beta_{34} * CD + \beta_{35} * CE + \beta_{45} * DE \quad (27)$$

Here, Y= f (A, B, C, D, E); with Y being the response variable,

A= Feed Rate (FR)

B= Power (PW)

C= Focal Length of the lens (FL)

D= Laser Speed (LS)

E= Contact tip to work distance (CTWD)

β_0= free term (constant) of the regression equation

β_i= Coefficients of linear terms

β_{ii}= Coefficients of square terms

β_{ij}= Coefficients of quadratic terms

The coefficients (β values) are calculated using the MINITAB software and the following equations 28, 29, 30 and 31 (response variables), are generated for the single pass 420 steel laser cladding bead.

$$W = 4.531 - 0.005 * A + 0.646 * B + 0.225 * C - 0.414 * D - 0.116 * E + 0.009 * A^2 - 0.098 * B^2 - 0.171 * C^2 + 0.289 * D^2 - 0.042 * E^2 + 0.015 * AB + 0.181 * AC - 0.200 * AD - 0.212 * AE + 0.296 * BC + 0.115 * BD - 0.229 * BE - 0.185 * CD + 0.033 * CE + 0.120 * DE \quad (28)$$

$$RH = 1.020 + 0.277 * A - 0.051 * B + 0.025 * C - 0.277 * D + 0.133 * E + 0.217 * A^2 - 0.086 * B^2 - 0.134 * C^2 - 0.032 * D^2 - 0.246 * E^2 - 0.135 * AB + 0.068 * AC + 0.000 * AD - 0.138 * AE + 0.107 * BC + 0.145 * BD - 0.137 * BE - 0.098 * CD + 0.130 * CE + 0.181 * DE \quad (29)$$

$$P = 0.558 - 0.243 * A + 0.349 * B - 0.033 * C - 0.263 * D - 0.107 * E + 0.064 * A^2 - 0.0010 * B^2 - 0.040 * C^2 + 0.142 * D^2 - 0.094 * E^2 - 0.047 * AB + 0.061 * AC + 0.115 * AD - 0.090 * AE - 0.020 * BC - 0.050 * BD - 0.137 * BE - 0.040 * CD - 0.033 * CE + 0.115 * DE \quad (30)$$

$$\%D = 24.730 - 21.635 * A + 20.420 * B - 1.633 * C - 2.336 * D - 0.489 * E + 12.418 * A^2 - 1.286 * B^2 + 2.488 * C^2 + 5.921 * D^2 + 8.844 * E^2 - 4.661 * AB + 0.151 * AC + 4.706 * AD - 2.731 * AE - 3.135 * BC + 4.848 * BD - 0.045 * BE + 0.426 * CD - 6.387 * CE + 1.794 * DE \quad (31)$$

Here, W, RH, P and % D are the response functions

And the boundary constraints are defined as:

10≤ A ≤30 (g/min)

1≤ B ≤4 (KW)

380≤ C ≤420 (mm)

5≤ D ≤15 (mm/sec)

21≤ E ≤25 (mm)

Similar models are generated for overlap configurations (attached to the appendix) for validating the influence of the single, the squared and the quadratic terms of the manufacturing parameters over the shape parameters (response variables). Later the above generated equations are run through an optimizer tool based off the MINITAB software to find the optimum results for the desired single or multiple responses.

7.2 Significant Factor Assessment Techniques

The significance of the factor in a mechanical process is vital in making the decisions for future trends. Thus, understanding of uncertainty in a process is important. Uncertainty is generally a behaviour of a parameter when the conditions are unfavorable to generate a desired shape. Conditions here refer to the surrounding factors, interactions among parameters etc.

For the purpose of this thesis work, the significance of each manufacturing parameter is evaluated over its shape parameters. There are two techniques discussed in this chapter (later sub-sections) to illustrate the significance concept namely: sensitivity analysis and analysis of variance (ANOVA). Once the significant factors are discovered, it is easy to manipulate the shape of a clad bead structure by manipulating the most relevant manufacturing parameter to the shape characteristic.

Studying the influence of the manufacturing parameters on the clad bead shape parameters, it is determined that the major influence is due to the linear manufacturing parameters over the squared and the quadratic interactions. A summary of results is provided in table 20, to prove the similarity in both the adopted approaches.

Table 20: Most significant linear factors - sensitivity vs ANOVA

	Most Significant Linear Factors		
Response Variable (Y)	ANOVA	Clamping Technique	Sensitivity Index
Percent Dilution (%D)	FR, PW	FR, PW	FR, PW
Width (W)	PW, LS	PW,LS	PW, LS
Reinforcement Height (RH)	FR, LS	FR, LS	FR, LS
Penetration (P)	FR, PW, LS, CTWD	PW, FL	PW, FL

7.2.1 Sensitivity Analysis

Sensitivity analysis refers to a technique that aids in determining the uncertainty in the output of a system. This ambiguity noticeable in the system arises due to change in the input parameters. Thus, the sensitivity analysis helps in measuring the change in the output parameters of a system with respect to the change in its input parameters.

For the purpose of this thesis work, analysis from two of the sensitivity techniques is compared and the similarities are driven to verify results. The two techniques that are evaluated are the clamping technique and the sensitivity index technique. Each of these techniques are discussed later in this sub-section and the graphical results are generated using the line plot chart.

1) Clamping technique (CT) – this technique is a measure of change in the output with change in its input parameters. The clamping technique provides an uncertainty in the output value of the model with an incremental change in its input parameters. Note- the increment in the input parameter is performed one at a time with keeping all the other input parameters as constants [85] [78]. To calculate the clamping effect, the first order partial derivatives are studied which are mathematically represented in equation 32

$$CT = \frac{\delta y}{\delta x} \tag{32}$$

Here, x and y are the input and output parameters respectively

δ defines the incremental change.

CT is the slope of the curve

Note: the determination of the sensitivity value for the clamping technique should always be done with normalized parameters to obtain a true value that can be compared at a later stage.

2) Sensitivity index (SI) – sensitivity index is a measure of the change in the output value of the model over the output's maximum value. This change in the output value is a computation of the range of the output. This method is computationally

inexpensive over the clamping technique [85] [78]. The mathematical expression for calculation of the sensitivity index is presented in equation 33,

$$SI = \frac{Max(y) - Min(y)}{Max(y)} \tag{33}$$

Here, y is the output to the system

Note: The determination of the sensitivity value for sensitivity index should always be done with normalized parameters.

For the purpose of this thesis, a validation is presented to display similarity in results for both the sensitivity techniques using a single pass 420 steel as an example. Similar results can be generated for the overlap models as well. Note- to obtain true influence of each parameter, the parameters are normalized between the ranges of 0 to +1. Table 21 shows a summary of all the mathematical calculations for the clamping technique and the sensitivity index technique [85] [78].

Table 21: Sensitivity ratios for clamping technique and sensitivity index

	Clamping Technique				Sensitivity Index			
	W	RH	P	% D	W	RH	P	% D
FR	0.16	0.98	0.37	0.99	0.16	0.89	0.31	1.00
PW	0.78	0.63	0.69	0.92	1.00	0.80	0.80	0.95
FL	0.06	0.27	0.65	0.07	0.09	0.37	1.00	0.37
LS	0.36	0.76	0.29	0.32	0.41	0.79	0.28	0.42
CTWD	0.07	0.21	0.14	0.24	0.10	0.41	0.20	0.49

Here, FR, PW, FL, LS and CTWD are the manufacturing parameters (inputs)
W, RH, P and %D are the mechanical shape parameters (outputs)

The following line plot graphs (figure(s) 57, 58, 59, 60 and 61) can be generated using the values from table 21, to prove similarity of both the sensitivity techniques and to verify the results for the significant factors. Note- numeric digits 1, 2, 3, and 4 displayed on the graphs represent the W, RH, P, and % D respectively.

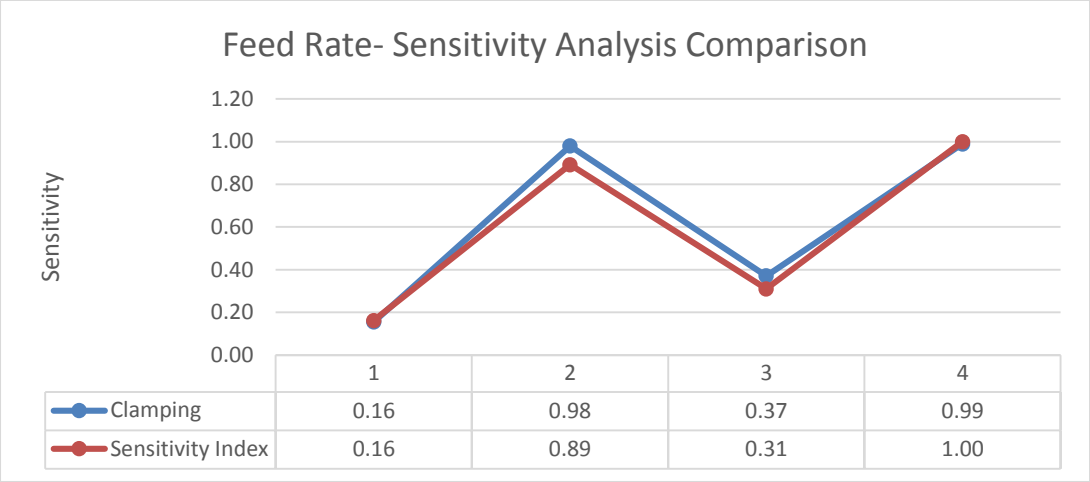

Figure 58: Sensitivity analysis comparison for the feed rate

From figure 58, it can be determined that the feed rate (FR) is the most significant factor for determining the reinforcement height (RH) and percentage dilution (%D) for the clad bead generated with a single pass of 420 steel.

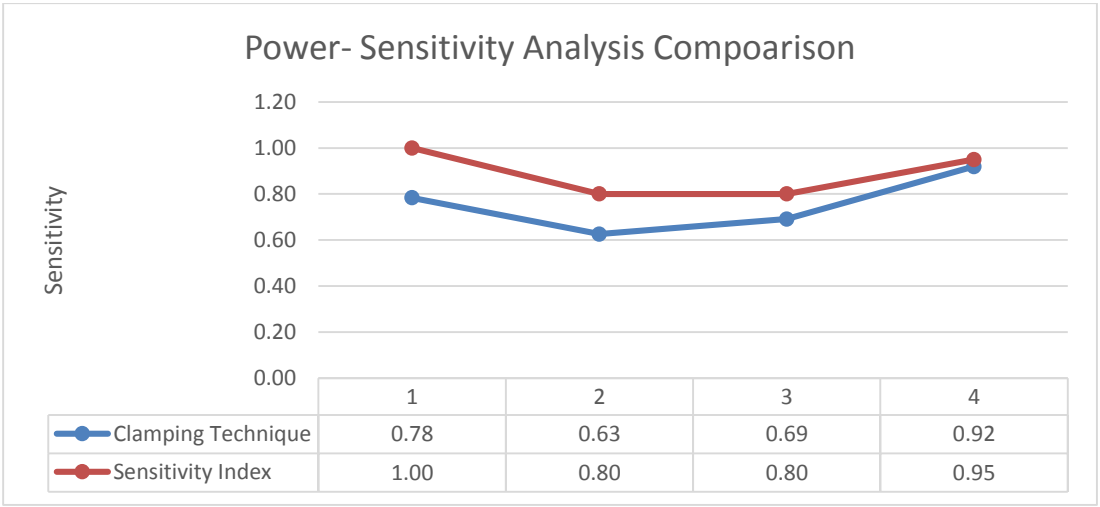

Figure 59: Sensitivity analysis comparison for the power

From figure 59, it can be determined that the power (PW) is the most significant factor for determining the width (W) and the percentage dilution (%D) for the clad bead generated with a single pass of 420 steel.

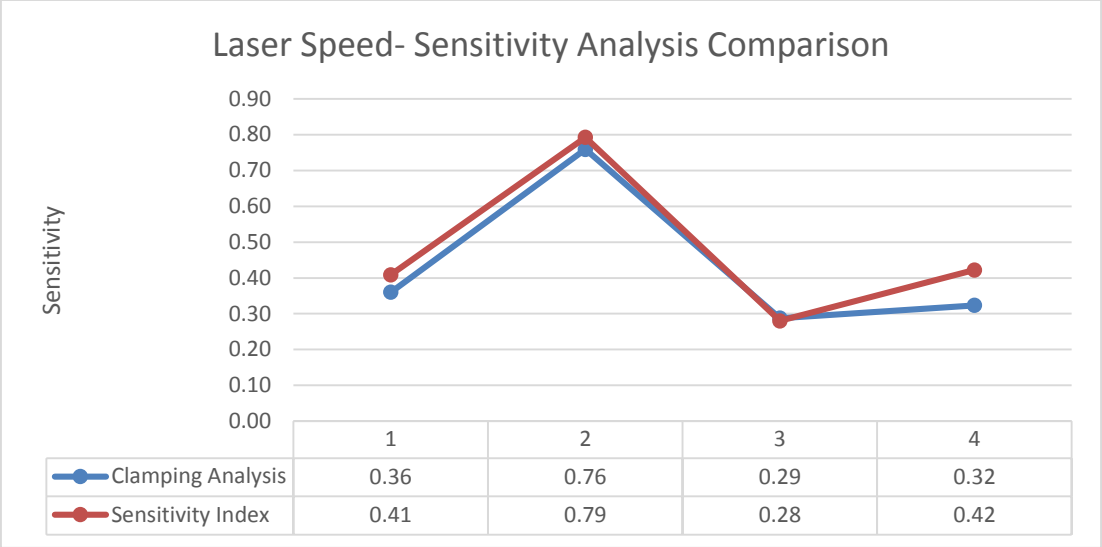

Figure 60: Sensitivity analysis comparison for the laser speed

From figure 60, it can be determined that the laser speed (LS) is the most significant factor for determining the reinforcement height (RH) for the clad bead generated with a single pass of 420 steel.

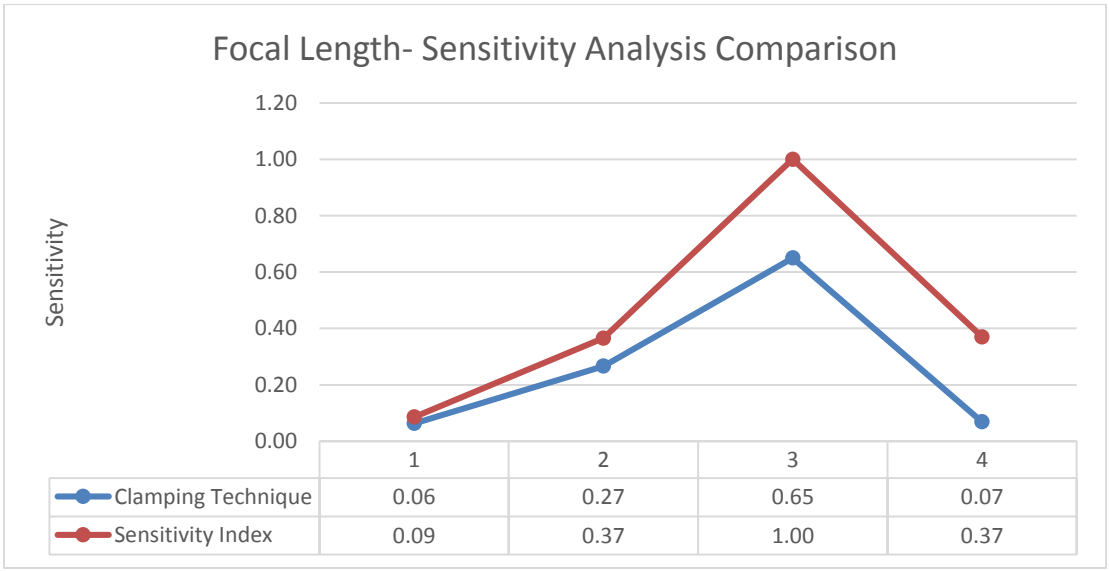

Figure 61: Sensitivity analysis comparison for the focal Length of the lens

From figure 61, it can be determined that the focal length (FL) is the most significant factor for determining the penetration (P) for the clad bead generated with a single pass of 420 steel.

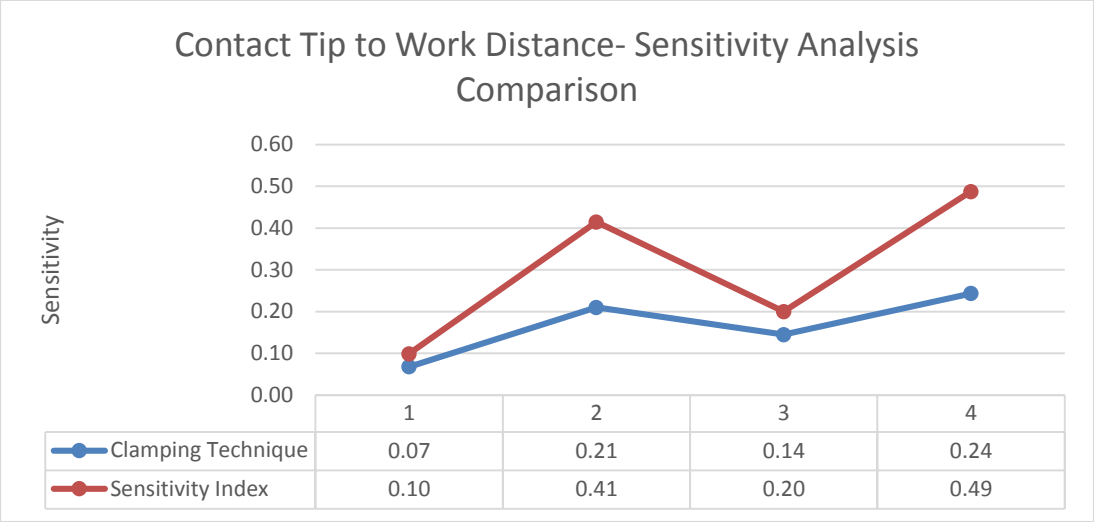

Figure 62: Sensitivity analysis comparison for the contact tip to work-piece distance

From figure 62, it can be determined that the contact tip to workpiece distance (CTWD) is the significant factor for determining the reinforcement height (RH) and the percentage dilution (%D) for the clad bead generated with a single pass of 420 steel. However, it should be noted that the numerical value of the parameters (CTWD and % D) is less than 0.5 (50%), hence CTWD is not the most significant factor in determining RH and %D.

7.2.2 Analysis of Variance

The second approach utilized for finding the significant factors for the laser cladding process for this thesis work is the analysis of variance (ANOVA) technique. The analysis of variance technique refers to a technique that helps study the effects of the parameters and their interactions prevalent in a system. The ANOVA analysis is performed to test the goodness of fit and validate the model developed using the neural network approach.

The ANOVA test is performed to evaluate the statistical significance of the fitted second order quadratic model. The factors (responses) involved in this model are the width, the penetration, the reinforcement height, and the percentage dilution. According to the ANOVA analysis, “if the F – ratio values of the developed models do not exceed the standard tabulated values for a desired level of confidence (95%) and the calculated p-

values of the developed model exceed the standard values for a desired level of confidence (95%) then the models are said to be adequate within the confidence limit" [28] [87] [88].

In other words, if the calculated p-value is less than 0.05, the factor is observed to be significant in the model. On the other hand, if the calculated p-value is greater than 0.05, it indicates that the impact of the factor is really insignificant to the model. The testing hypothesis set up for the ANOVA model, for the purpose of this thesis is as follows [89]:

H_0=there is no interactions between process parameters and shape parameters

H_1=there is significant/relevant interactions between process parameters and shape parameters

Note- the ANOVA analysis does not provide a detailed mathematical evaluation of how much or which interactions between means differ. Some of the assumptions that are put in place while setting up the ANOVA analysis are as follows [90]:

1) Each group defined for ANOVA analysis is normal – this assumption is checked by generating the histogram plots or the normal quantile plots, and thus proving that the groups are normally distributed in the dataset.
2) The standard deviation and/or the variance of each group is approximately equal – this assumption is checked by calculating the ratio of the largest to the smallest factor standard deviation. This ratio is less than 2:1 which hold the assumption valid.
3) The errors generated are independent – this assumption is checked by graphing an interaction plot among the error values to prove that there are no inter-dependencies among manufacturing and shape parameters.
4) The expected values of the errors are zero- this assumption is check by calculating the error values.

ANOVA works on the principle of measuring the sources of variation in the sample set and hence, comparing the group sizes. The two variations that are measured are as follows [90]:

1) Variation between groups –this is a mathematical calculation of the difference between the group mean in comparison to the overall mean. It is mathematically calculated using equation 34,

$$V = (X_i - X)^2 \tag{34}$$

Here, X_i is the mean of the group

X is the overall mean

i is the group

2) Variation within groups –this is a mathematical calculation of the difference between the values in comparison to the group mean. It is mathematically calculated using equation 35,

$$V = \left(X_{ij} - X_i\right)^2 \tag{35}$$

Here, X_{ij} is the value of the numerical data

X_i is the mean of the group

i is the group, j is the value for individual component

Hence, the F-ratio is the comparison of variation between the groups to variation within the groups. The greater the value of the F-ratio, the greater the difference in the means of the groups. Thus, indicating a failed null hypothesis. For the purpose of this thesis work, an ANOVA analysis for shape factors W, RH, P and % D are presented in tables 15, 16, 17, and 18, which display the significant manufacturing parameters relative to the shape characteristics for a single pass of 420 steel. Similar ANOVA analysis can be generated for the various overlap configurations. Table 22, displays an ANOVA analysis for the width (W).

Table 22: Analysis of variance for the bead width

Source	DF	Seq SS	Adj SS	Adj MS	F	P	Significance
Regression	20	12.4823	12.4823	0.62412	9.05	0.000	
Linear	5	10.2727	5.1618	1.03237	14.97	0.000	

FR	1	0.0975	0.0002	0.00016	0.00	0.962	
PW	1	6.5597	4.0030	4.00301	58.05	0.000	Significant*
FL	1	0.5828	0.4832	0.48319	7.01	0.010	Significant
LS	1	3.0299	1.0743	1.07431	15.58	0.000	Significant*
CTWD	1	0.0028	0.0843	0.08431	1.22	0.273	
Square	5	0.8748	0.8748	0.17495	2.54	0.036	Significant
FR*FR	1	0.0020	0.0005	0.00045	0.01	0.936	
PW*PW	1	0.1365	0.0931	0.09311	1.35	0.249	
FL*FL	1	0.2699	0.2825	0.28251	4.10	0.047	Significant
LS*LS	1	0.4571	0.4287	0.42868	6.22	0.015	Significant
CTWD*CTWD	1	0.0091	0.0091	0.00914	0.13	0.717	
Interaction	10	1.3349	1.3349	0.13349	1.94	0.055	
FR*PW	1	0.0008	0.0008	0.00075	0.01	0.917	
FR*FL	1	0.1764	0.1764	0.17642	2.56	0.114	
FR*LS	1	0.1210	0.1210	0.12100	1.75	0.190	
FR*CTWD	1	0.1355	0.1355	0.13547	1.96	0.165	
PW*FL	1	0.4701	0.4701	0.47005	6.82	0.011	Significant
PW*LS	1	0.0403	0.0403	0.04025	0.58	0.447	
PW*CTWD	1	0.1576	0.1576	0.15755	2.28	0.135	
FL*LS	1	0.1838	0.1838	0.18377	2.67	0.107	
FL*CTWD	1	0.0059	0.0059	0.00585	0.08	0.772	
LS*CTWD	1	0.0438	0.0438	0.04380	0.64	0.428	
Residual Error	69	4.7577	4.7577	0.06895			
Lack-of-Fit	4	1.1485	1.1485	0.28713	5.17	0.001	
Pure Error	65	3.6092	3.6092	0.05553			
Total	89	17.2400					

Here, total factors- 20

Significant factors- 7 (P- value <0.05)

Most significant factors- 2 (P-value =0.000)

Linear- PW, LS

Square- N/A

Interaction- N/A

Table 23, displays an ANOVA analysis for the reinforcement height (RH)

Table 23: Analysis of variance for the bead reinforcement height

Source	DF	Seq SS	Adj SS	Adj MS	F	P	Significance
Regression	20	5.26521	5.26521	0.263260	28.47	0.000	
Linear	5	3.97716	1.12200	0.224400	24.27	0.000	
FR	1	1.86889	0.48261	0.482609	52.19	0.000	Significant*
PW	1	0.00196	0.02513	0.025134	2.72	0.104	
FL	1	0.06378	0.00630	0.006304	0.68	0.412	
LS	1	1.81134	0.48261	0.482609	52.19	0.000	Significant*
CTWD	1	0.23120	0.11130	0.111304	12.04	0.001	Significant
Square	5	0.73676	0.73676	0.147352	15.94	0.000	
FR*FR	1	0.17341	0.24252	0.242517	26.23	0.000	Significant*
PW*PW	1	0.06921	0.07196	0.071962	7.78	0.007	Significant
FL*FL	1	0.18432	0.17246	0.172458	18.65	0.000	Significant*
LS*LS	1	0.00006	0.00546	0.005464	0.59	0.445	
CTWD*CTWD	1	0.30976	0.30976	0.309760	33.50	0.000	Significant*
Interaction	10	0.55128	0.55128	0.055128	5.96	0.000	
FR*PW	1	0.05467	0.05468	0.054675	5.91	0.018	Significant
FR*FL	1	0.02521	0.02521	0.025208	2.73	0.103	
FR*LS	1	0.00000	0.00000	0.000000	0.00	1.000	
FR*CTWD	1	0.05741	0.05741	0.057408	6.21	0.015	Significant
PW*FL	1	0.06163	0.06163	0.061633	6.67	0.012	Significant
PW*LS	1	0.06308	0.06307	0.063075	6.82	0.011	Significant
PW*CTWD	1	0.04813	0.04813	0.048133	5.21	0.026	Significant
FL*LS	1	0.05201	0.05201	0.052008	5.62	0.021	Significant
FL*CTWD	1	0.09013	0.09013	0.090133	9.75	0.003	Significant

LS*CTWD	1	0.09901	0.09901	0.099008	10.71	0.002	Significant
Residual Error	69	0.63802	0.63802	0.009247			
Lack-of-Fit	4	0.34900	0.34900	0.087249	19.62	0.000	
Pure Error	65	0.28903	0.28903	0.004447			
Total	89	5.90323					

Here, Total Factors- 20

Significant factors- 15 (P- value <0.05)

Most Significant factors- 5 (P-value= 0.000)

Linear- FR, LS

Square- FR, FL, CTWD

Interaction- N/A

Table 24, displays an ANOVA analysis for the penetration (P)

Table 24: Analysis of variance for the bead penetration

Source	DF	Seq SS	Adj SS	Adj MS	F	P	Significance
Regression	20	5.23570	5.23570	0.26178	52.12	0.000	
Linear	5	4.86596	2.68319	0.53664	106.85	0.000	
FR	1	1.04401	0.37262	0.37262	74.19	0.000	Significant*
PW	1	2.89441	1.49353	1.49353	297.37	0.000	Significant*
FL	1	0.00492	0.01043	0.01043	2.08	0.154	
LS	1	0.90900	0.43530	0.43530	86.67	0.000	Significant*
CTWD	1	0.01361	0.07207	0.07207	14.35	0.000	Significant*
Square	5	0.15590	0.15590	0.03118	6.21	0.000	
FR*FR	1	0.00623	0.02102	0.02102	4.19	0.045	Significant
PW*PW	1	0.00463	0.00102	0.00102	0.20	0.653	
FL*FL	1	0.01322	0.01604	0.01604	3.19	0.078	
LS*LS	1	0.08651	0.10382	0.10382	20.67	0.000	Significant*
CTWD*CTWD	1	0.04531	0.04531	0.04531	9.02	0.004	Significant
Interaction	10	0.21384	0.21384	0.02138	4.26	0.000	
FR*PW	1	0.00677	0.00677	0.00677	1.35	0.250	

FR*FL	1	0.02042	0.02042	0.02042	4.07	0.048	Significant
FR*LS	1	0.04025	0.04025	0.04025	8.01	0.006	Significant
FR*CTWD	1	0.02475	0.02475	0.02475	4.93	0.030	Significant
PW*FL	1	0.00227	0.00227	0.00227	0.45	0.504	
PW*LS	1	0.00775	0.00775	0.00775	1.54	0.218	
PW*CTWD	1	0.05672	0.05672	0.05672	11.29	0.001	Significant
FL*LS	1	0.00880	0.00880	0.00880	1.75	0.190	
FL*CTWD	1	0.00585	0.00585	0.00585	1.17	0.284	
LS*CTWD	1	0.04025	0.04025	0.04025	8.01	0.006	Significant
Residual Error	69	0.34655	0.34655	0.00502			
Lack-of-Fit	4	0.09453	0.09453	0.02363	6.09	0.000	
Pure Error	65	0.25203	0.25203	0.00388			
Total	89	5.58225					

Here, Total Factors- 20

Significant factors- 12 (P- value <0.05)

Most Significant factors- 5 (P-value= 0.000)

Linear- FR, PW, LS, CTWD

Square- LS

Interaction- N/A

Table 25, displays an ANOVA analysis for the percentage dilution (D %)

Table 25: Analysis of variance for the bead percentage dilution

Source	DF	Seq SS	Adj SS	Adj MS	F	P	Significance
Regression	20	16941.2	16941.2	847.06	130.69	0.000	
Linear	5	15214.4	7772.5	1554.51	239.85	0.000	
FR	1	6743.3	2930.6	2930.62	452.17	0.000	Significant*
PW	1	7886.4	3993.5	3993.47	616.16	0.000	Significant*
FL	1	102.3	25.3	25.30	3.90	0.052	
LS	1	432.8	34.2	34.19	5.28	0.025	Significant
CTWD	1	49.7	1.5	1.50	0.23	0.632	

Square	5	1221.5	1221.5	244.30	37.69	0.000	
FR*FR	1	610.4	789.4	789.38	121.79	0.000	Significant*
PW*PW	1	27.6	15.9	15.87	2.45	0.122	
FL*FL	1	71.3	59.4	59.41	9.17	0.003	Significant
LS*LS	1	111.8	179.5	179.48	27.69	0.000	Significant*
CTWD*CTWD	1	400.4	400.4	400.35	61.77	0.000	Significant*
Interaction	10	505.3	505.3	50.53	7.80	0.000	
FR*PW	1	65.2	65.2	65.18	10.06	0.002	Significant
FR*FL	1	0.1	0.1	0.12	0.02	0.891	
FR*LS	1	66.5	66.5	66.46	10.25	0.002	Significant
FR*CTWD	1	22.4	22.4	22.38	3.45	0.067	
PW*FL	1	52.4	52.4	52.43	8.09	0.006	Significant
PW*LS	1	70.5	70.5	70.53	10.88	0.002	Significant
PW*CTWD	1	0.0	0.0	0.01	0.00	0.976	
FL*LS	1	1.0	1.0	0.97	0.15	0.700	
FL*CTWD	1	217.6	217.6	217.58	33.57	0.000	Significant*
LS*CTWD	1	9.7	9.7	9.66	1.49	0.226	
Residual Error	69	447.2	447.2	6.48			
Lack-of-Fit	4	214.3	214.3	53.58	14.96	0.000	
Pure Error	65	232.9	232.9	3.58			
Total	89	17388.4					

Here, Total Factors- 20

Significant factors- 12 (P- value <0.05)

Most Significant factors- 6 (P-value= 0.000)

Linear- FR, PW

Square- FR, LS, CTWD

Interaction- FL*CTWD

A summary of the number of significant factors for the shape characteristics are provided in table 26,

Table 26: Summary of significant factors through ANOVA analysis

Response Variable (Y)	Total Factors	Number of Significant Factors (P- value<0.05)	Number of Most Significant Factors (P- value=0.000)
Percent Dilution (%D)	20	12	6
Width (W)	20	7	2
Reinforcement Height (RH)	20	15	5
Penetration (P)	20	12	5

7.2.3 Validation of ANOVA

The significant factors determined by the sensitivity analysis clamping technique are validated using the sensitivity index technique (through attaining similar results). To validate the ANOVA analysis technique a model statistic summary is presented in table 27, for the various response variables (shape parameters). Here, the statistical summary is generated for a single pass of 420 steel and similar results can be generated for the overlap model configurations.

Table 27: Statistical summary of ANOVA analysis for model verification

Model Summary : Bead Width (W)			
Std Dev.	0.440123	(R^2)	92.40
Mean	4.159222	Adjusted (R^2)	94.40
% C.V.	10.58186	Predicted (R^2)	94.58
Model Summary : Bead Reinforcement Height (RH)			
Std Dev.	0.257543	(R^2)	89.19
Mean	0.864556	Adjusted (R^2)	86.06
% C.V.	29.78908	Predicted (R^2)	91.97
Model Summary : Bead Penetration (W)			
Std Dev.	0.250443	(R^2)	93.79
Mean	0.428333	Adjusted (R^2)	91.99
% C.V.	58.46928	Predicted (R^2)	89.57
Model Summary: Bead Percentage Dilution (%D)			
Std Dev.	13.97769	(R^2)	97.43
Mean	21.46451	Adjusted (R^2)	96.68
% C.V.	65.11999	Predicted (R^2)	95.84

From the presented statistical summary, it can be concluded that the coefficients of correlations (R^2) for all response variables possess a value in excess of 90% (0.90 approx.), which stimulates confidence in the generated ANOVA models. Also, the predicted and adjusted (R^2) values for respective response variable(s) are in agreement with the R^2 value, which again validates the fitness of the model developed. [88]

In the presented statistical summary, mean refers to the overall average of the individual shape parameter (response variable) for each of the model and is mathematically calculated through equation 36,

$$\mu = \frac{1}{n} * \sum_{i=1}^{n} x_i \tag{36}$$

Here, μ denotes the average of each response variable

n is the number of terms/specimens collected for that variable

x_i is the value of individual term

The standard deviation refers to the root mean square error (square root of pure experimental error) and is mathematically expressed as equation 37

$$Std.Dev = Sqrt(MS_{Pure\ Error}) \tag{37}$$

Here, the square root of pure experimental error is mathematically computed through equation 38,

$$MS_{Pure\ Error} = \frac{SS_{Pure\ Error}}{DF_{Pure\ Error}} \tag{38}$$

Here, $SS_{Pure\ Error}$ is the sum of squares of pure experimental error (ANOVA analysis)

$DF_{Pure\ Error}$ is the degree of freedom of pure experimental error (ANOVA analysis)

Finally, the percentage C.V. or otherwise referred to as the coefficient of variation, is the measurement of the error in each of the analysis model. The value of the percentage C.V. is mathematically generated by the following mathematical equation 39

$$\%\ C.V. = \frac{Std.Dev}{Mean} * 100 \tag{39}$$

It is observed that the lower the value of percentage C.V., the lower the chance of error in the system. In other words, the experimentation performed at the sponsor facility holds precise and reliable with a lower value of percentage C.V. Through the statistical analysis summary, it is determined that the error due to any experimental noise factor is less than 10 percent.

7.3 Contour and Surface Plots

"To fit a regression model using two or more continuous predictors (shape parameters), it is always useful to generate a graphical visualization of the fitted surface. The terms contour plot and surface plot refer to generation of specialized surface plot(s) which are utilized in the analysis of the response surface methodology experimental design. The contour and the surface plots are generally plotted between two factors. In the case of

more than two factors, a series of plots are generated with a multiple combination of factors (two at a time). The application of such plots is to determine the optimal settings that aid in maximizing or minimizing the desired response variable of design. Also, these plots help in determining the settings (for factors) that can result in the response variables hitting a pre-determined target value. [91]. Note- while plotting the contour plots, the z (Cartesian axis) is kept constant for representing a two dimensional format.

Through the development of the analytical method for a 2^{nd} order equation, it can be observed that the individual manufacturing parameters and the interactions affect the shape geometry of the clad bead either directly or indirectly. The purpose of generating the contour and surface plots is to illustrate the effect of these combination and interactions of the manufacturing parameters on the shape parameters. A contour plot provides a two-dimensional view in which all points that contain the same responses are connected. This connection of response points aids in generating the contour lines that form boundaries to the constant surfaces. On the other hand, a surface plot provides a three-dimensional view which provides a more accurate (real-time) representation of the response surface. [92]

For the purpose of this thesis work, figure 63 presents various contour plots for percentage dilution (response variable). These plots display linear and non-linear trends among the five interacting manufacturing parameters (FR, PW, FL, LS, and CTWD). The contour plots are generated using the MINITAB software workspace with the following constant values (table 28).

Table 28: Constant factors for generating contour and surface plots

Manufacturing Parameters	Constant Values
Feed rate (FR)	20 g/min
Power (PW)	3 KW
Focal length of the lens (FL)	405 mm
Laser speed (LS)	10 mm/sec
Contact tip to workpiece distance(CTWD)	23 mm

The constant values are generally the center values of the system (as designed in the RSM experimentation technique). Note- the constant value of power (PW) is chosen as

3 KW over 2.5 KW (center value RSM); due to the fact that there is no physical clad bead generation at 2.5 KW power.

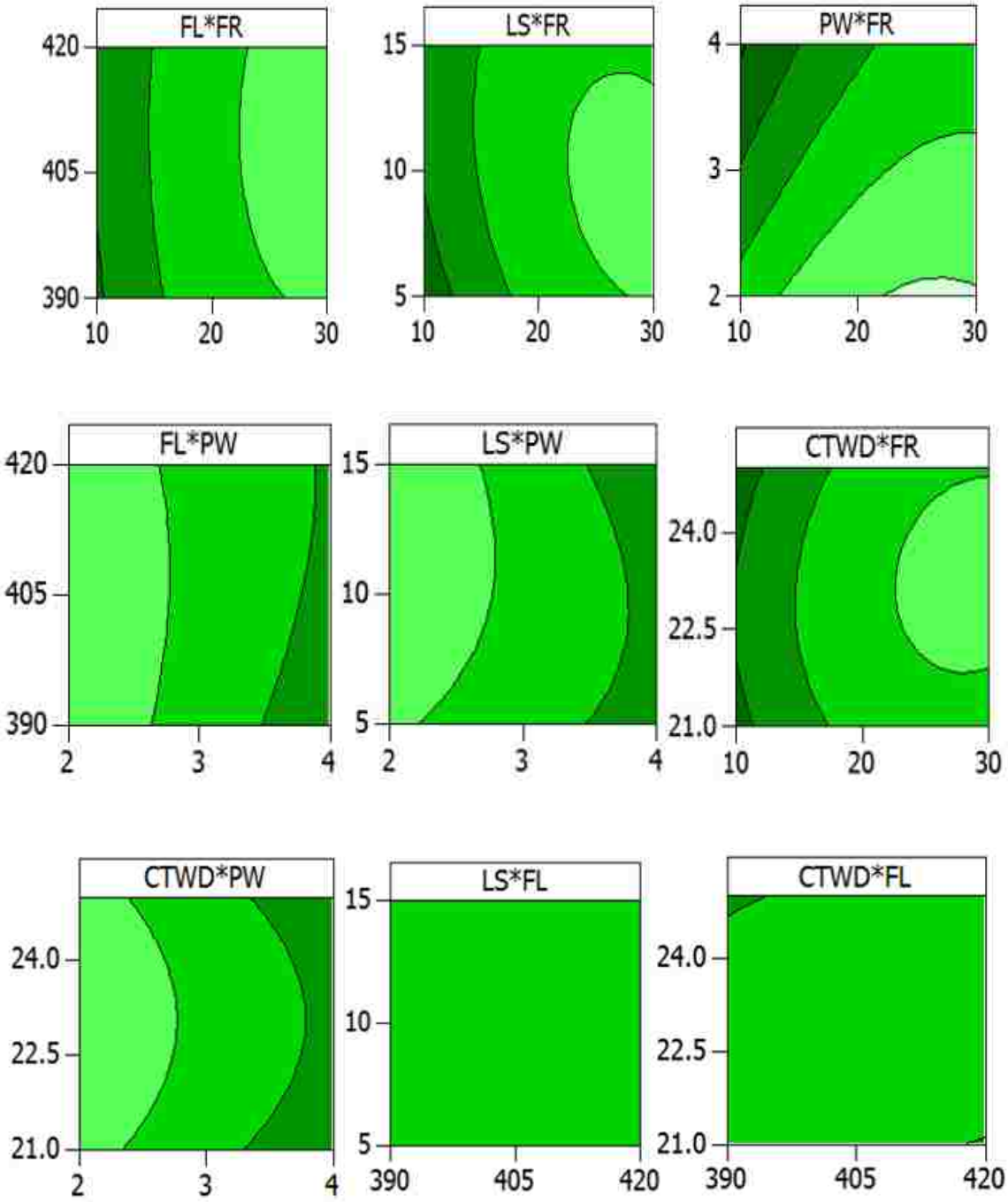

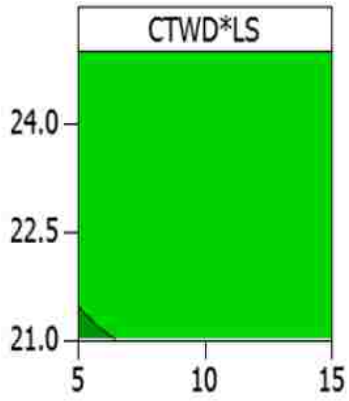

Figure 63: Contour plots for the percentage dilution objective function

These contour plots are interpreted for the response on percentage dilution using the following legend, presented table 29. A clear co-relation to the significant factors calculated using the ANOVA analysis and the sensitivity analysis is observed with the generated plots.

Table 29: Legend for contour & surface plots for the percentage dilution

Percentage Dilution (%D)	Colour
< 0	
0 – 20	
20 – 40	
40 - 60	
60 – 80	
>80	

Similarly, figure 64, presents surface plots for the percentage dilution (response variable). Again interaction among the five manufacturing parameters (FR, PW, FL, LS, and CTWD) generates a response surface that relates to the results derived from the

ANOVA analysis as well as the sensitivity analysis earlier. The surface plots are also generated using the MINITAB software workspace with the same constant values as the contour plots.

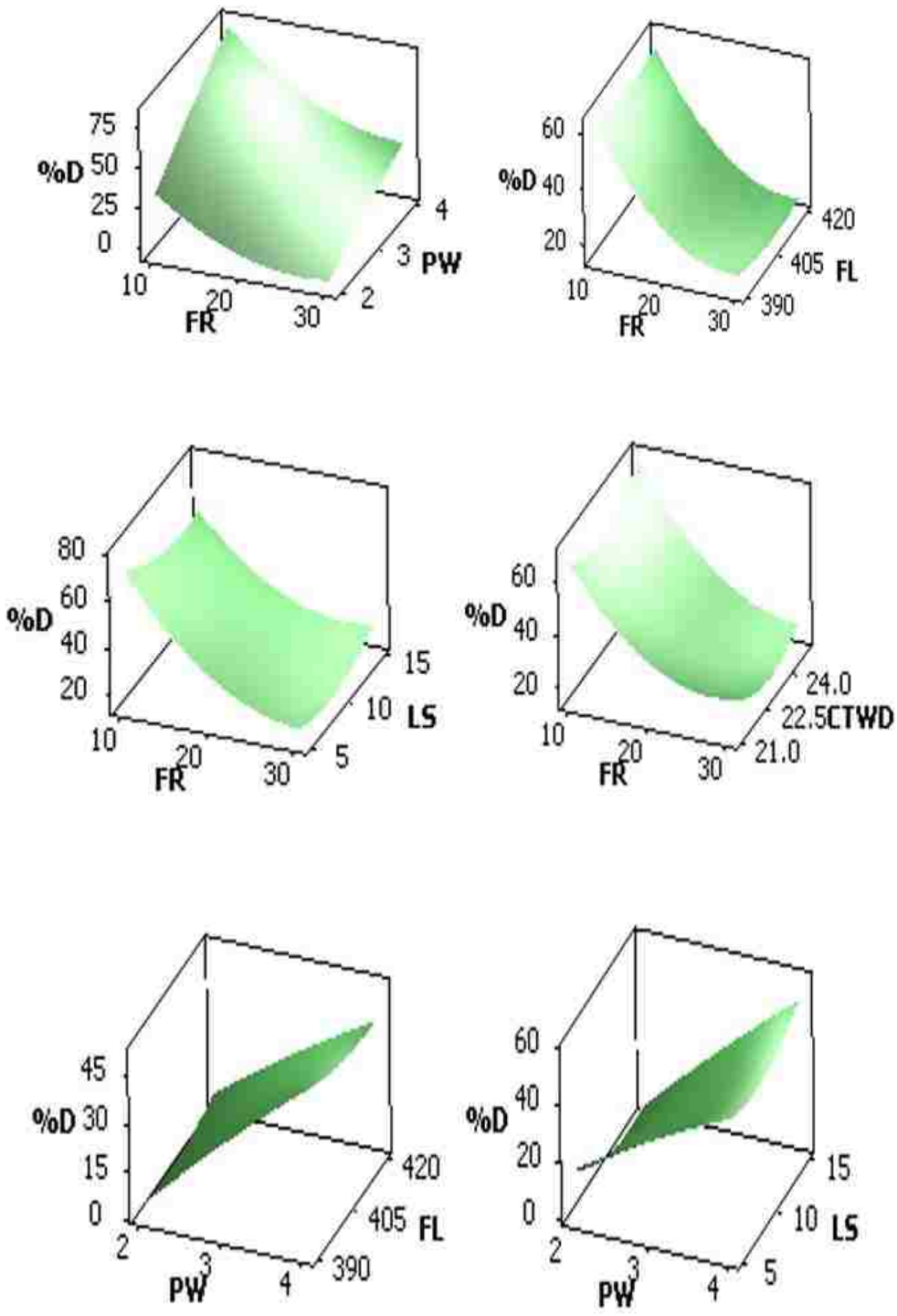

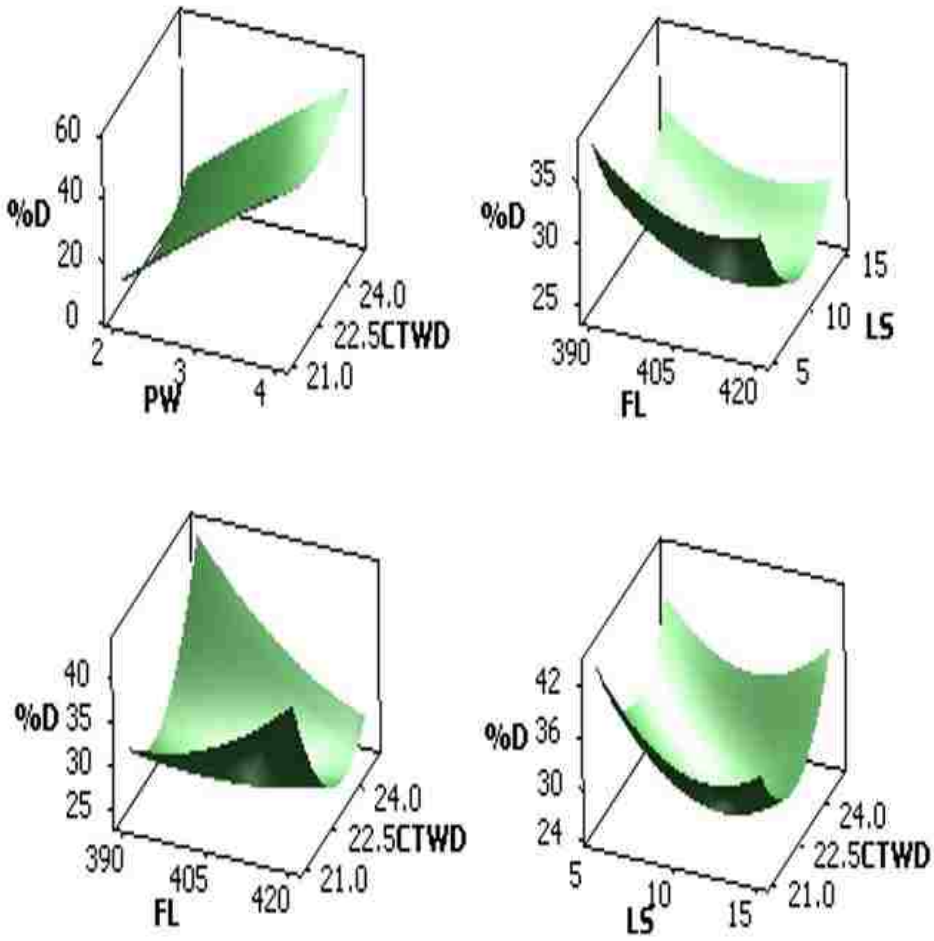

Figure 64: Surface plots for the percentage dilution objective function

All the generated plots (surface and contour) presented in this sub-section are created for a single pass of 420 steel for the laser cladding operation. Similar plots predicting interactions among the various manufacturing parameters can be created for the overlap configurations." [89]:

7.4 Single and Multi Variable Optimization

"The final step after determining the contour and surface trends is to quantify the optimal settings for the laser cladding process. This section focuses on using an optimization tool to determine the optimal settings for the single objective and the multi objective optimization processes. The single objective optimization process refers to

finding the optimal setting of the manufacturing parameters (factors) that aid in achieving a single objective (i.e. targeting a single shape characteristic at one time). On the other hand, in the multi objective optimization process, the optimal settings for the various manufacturing parameters are achieved with satisfying multiple objectives present in the system (i.e. targeting multiple shape parameters at one time).

For the purpose of this thesis, a response optimizer application is used based off the MINITAB workspace. The response optimization tool aids in identifying a certain combination of input variable settings that help in targeting a single response or multiple responses. MINITAB, helps in calculating the optimal input variable parameters and presents a visual plot of the deviation from an initial solution. This visual tool thus allows an interactive change of the input variable settings to perform the sensitivity analysis and the improvement of the initial solution. [92]

The optimization process through the response optimizer in MINITAB is initiated by providing a set of starting points so that an optimal combination of process factors can be obtained. The optimizer tool presented here provides two solution types i.e. a local solution and a global solution. The local solution is defined as the best combination factor settings for particular set of starting points while the global solutions is the best combination of factor settings for the desired response variables i.e. the optimal setting for all the local points. [28]

As an example, the dataset of a single pass of 420 steel (for the laser cladding operation) is used to optimize the following single objective response variable.

1) Objective: minimize percent dilution (%D)
   Optimum process parameters (results):

   FR=10 g/min
   PW=2 KW
   FL=390 mm
   LS=5 mm/sec
   CTWD=21 mm

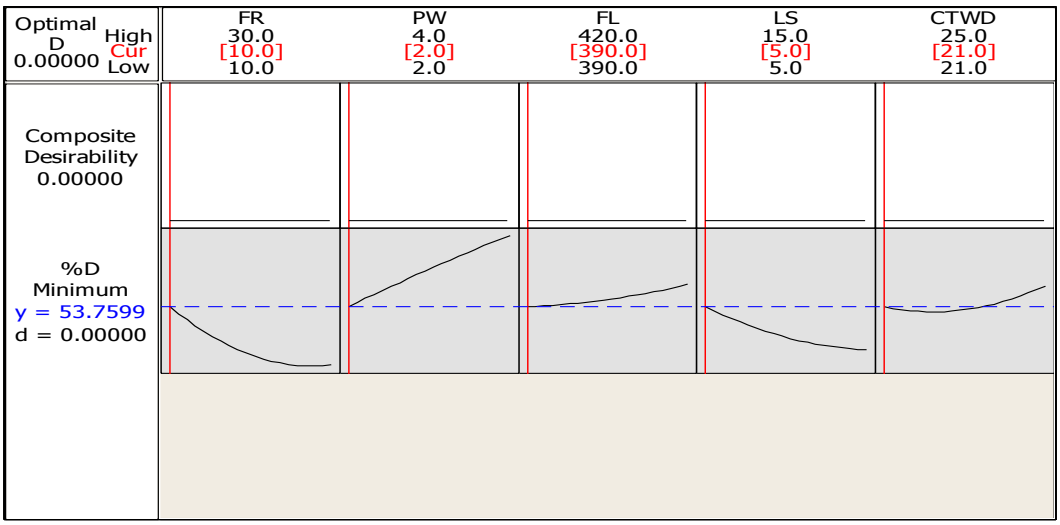

Figure 65: Single objective optimization to minimize percentage dilution

2) Objective: maximize bead width (W)

Optimum process parameters (Results):

FR=30 g/min

PW=4 KW

FL=420 mm

LS=5 mm/sec

CTWD=21 mm

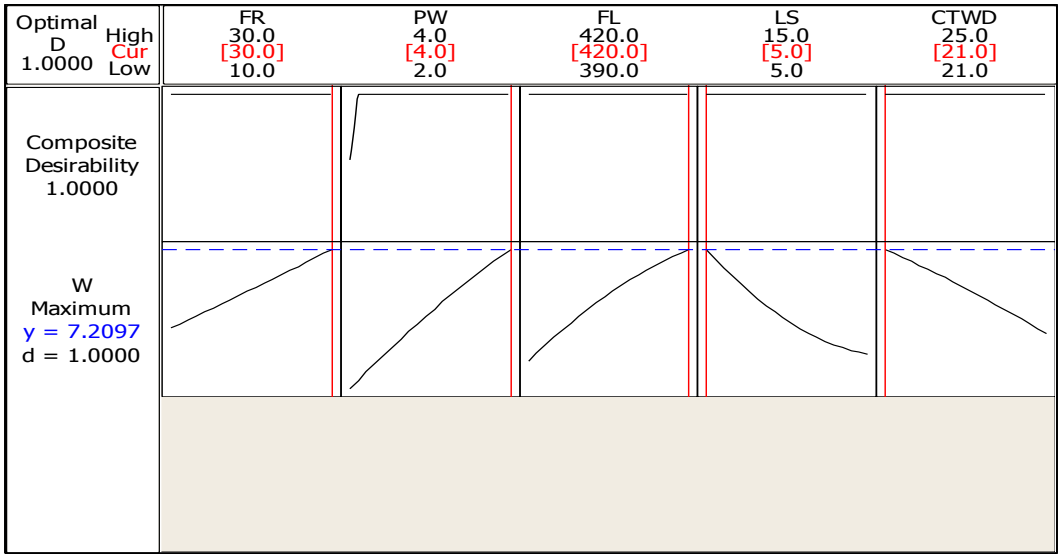

Figure 66: Single objective optimization to maximize width

3) Objective: minimize bead penetration (P)

Optimum process parameters (Results):

FR=15.65 g/min

PW=2 KW

FL=420 mm

LS=15 mm/sec

CTWD=21.36 mm

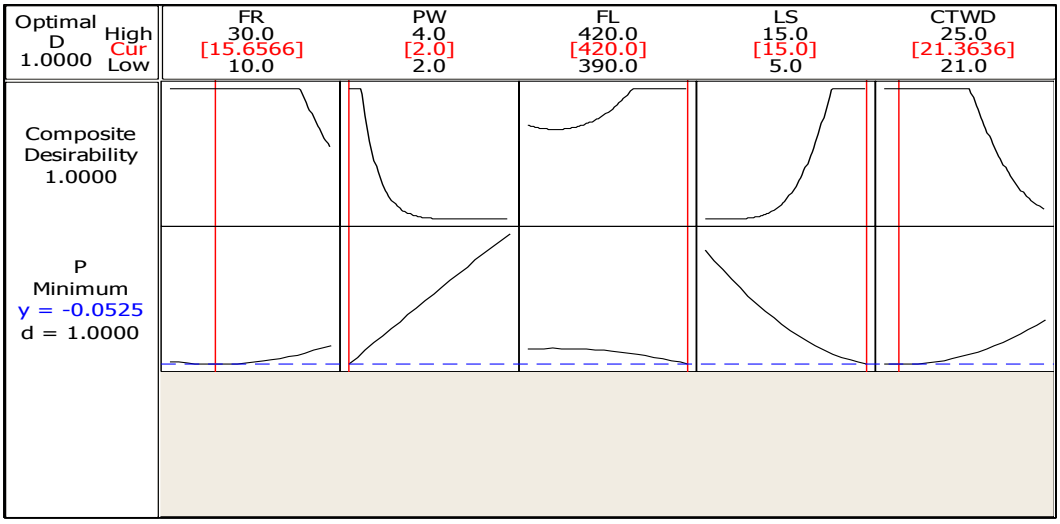

Figure 67: Single objective optimization to minimize penetration

4) Objective: maximize reinforcement height (RH)

Optimum process parameters (Results):

FR=30 g/min

PW=2 KW

FL=405.15 mm

LS=5 mm/sec

CTWD=21.68 mm

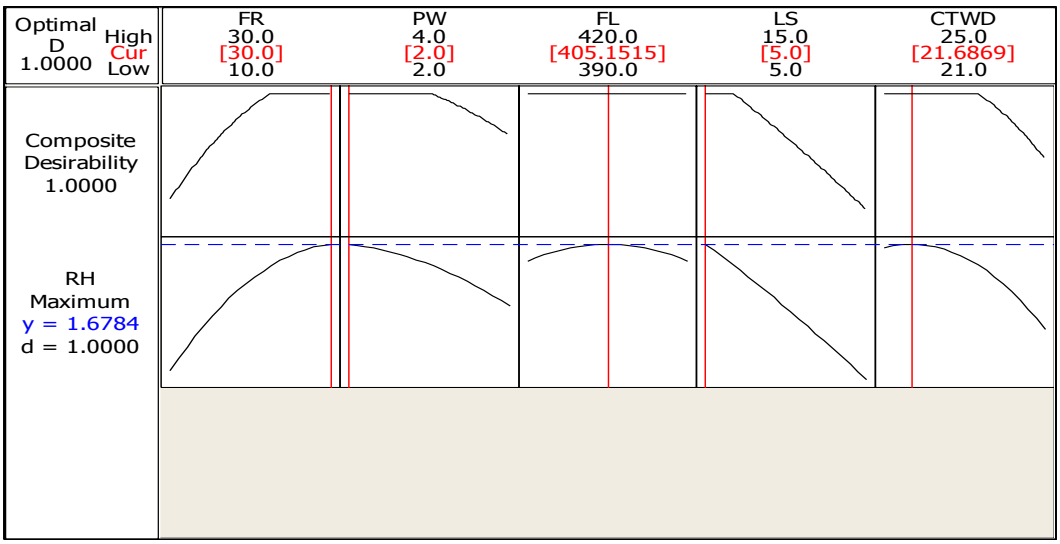

Figure 68: Single objective optimization to maximize reinforcement height

Also as an example, the dataset of the single pass of 420 steel (for the laser cladding operation) is used to optimize the multi objective response variable.

Objective: minimize percent dilution (%D); maximize bead width (W); minimize bead penetration (P); and maximize reinforcement height (RH)

Optimum process parameters (results):

FR=29.39 g/min

PW=2 KW

FL=406.06 mm

LS=8.23 mm/sec

CTWD=22.93 mm

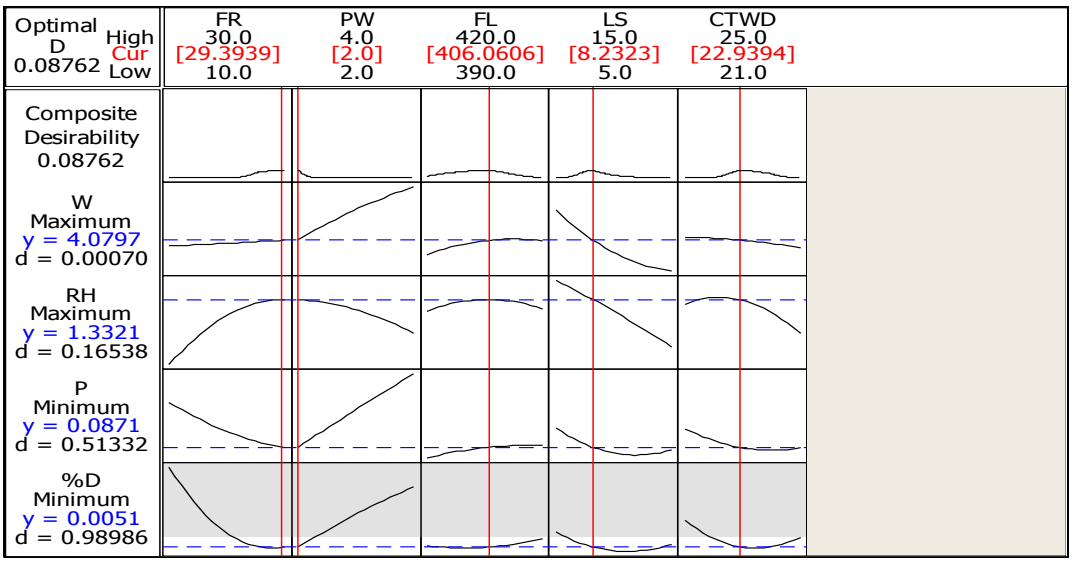

Figure 69: Multiple objective optimization representation

The visual representations (figures 65, 66, 67, 68, and 69), show deviation of the manufacturing parameters from an initial solution (constant values kept at center point of the RSM experimentation). These graphs can further be generated for the various overlap configurations and their interactions to attain the optimal setting of parameters for the desired objective functions." [89]:

CHAPTER 8

CLASSIFICATION OF THE LASER CLADDING DATASET

Classification is a process that refers to categorizing or grouping of the data points from a vast data population so that different classes or sub-categories can be identified according to the group features or common traits. For the process of classification, a K-mean clustering technique is applied to this research and various clusters are generated to determine the bead shape structure of each sub-category. In clustering, the common traits are shared among the data points in each sub-set. The clusters are separated using a distance measure. The distance measure generally determines the shape of the cluster according to the similarity between two elements of the dataset.

There are many approaches to finding the distance measure, but the distance measure approach applied for this thesis is the Euclidean distance approach (also called 2-norm distance). In simple terms, the Euclidean distance is the distance between the two vectors defined by a Pythagorean Theorem [93]. The mathematical expression for calculating the Euclidean distance is present in equation 40,

$$d(x, y) = \sum_{i=1}^{p} |x_i - y_i| \tag{40}$$

Here x, y are two points and the Euclidean distance is the line segment that joins x and y.

The position of a point in the Euclidean n-space is known as the Euclidean vector. For such a case, x and y are the two vectors starting from the origin of the defined space. The tips of these vectors indicate the points x and y respectively.

K-mean clustering algorithm partitions the dataset into k-clusters based on common attributes. Note- it assumes that all (k) clusters exhibit Gaussian distributions. The objective of performing a k-cluster classification is to minimize the intra-cluster variance. The intra cluster variance is minimized by reducing the squared errors of data points in all the present clusters [94]. The mathematical expression for minimizing the squared errors is presented in equation 41,

$$E = \sum_{i=1}^{k} \sum_{p \epsilon C_i} |p - m_i|^2 \quad (41)$$

Here, E is the defined sum of square errors of all data points

P is the given element

m_i is the mean of the cluster

C_i is the defined cluster

K is a positive integer

8.1 K- Mean Clustering

Figure 70 shows the working of a k-mean clustering algorithm.

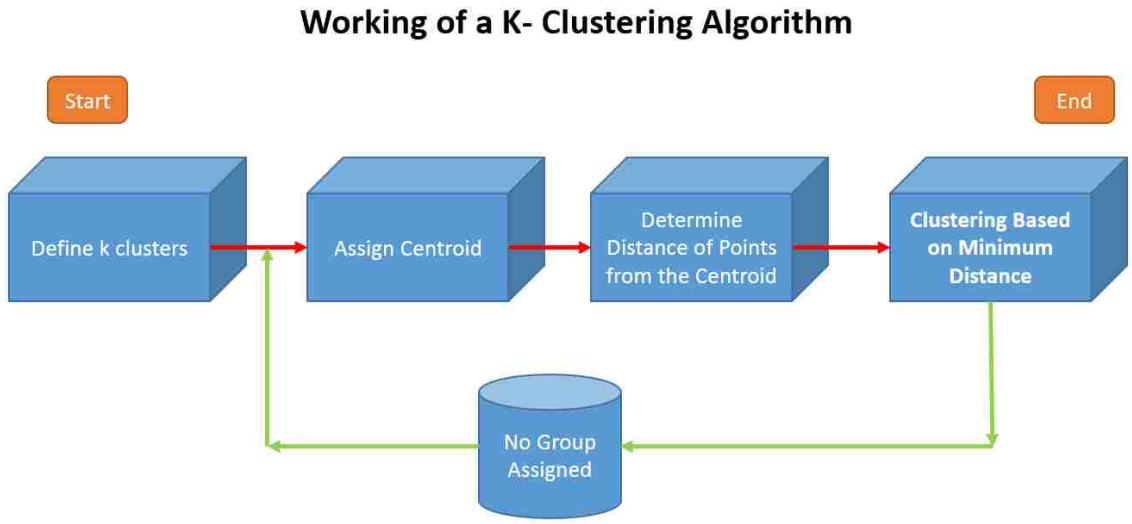

Figure 70: K-mean clustering approach- schematic diagram

As defined earlier, the algorithm follows a basic four step approach which is presented as follows [94]:

1) Defining k clusters – this is the first step in the clustering of the data through k-mean clustering algorithm. This step involves making a decision on the number of clusters involved in the data set according to the mean values.
2) Assigning centroid – once the numbers of clusters are defined, the first k training sample is taken as the single element cluster. Also, each of the remaining samples

(N-k) are assigned to the cluster with the nearest centroid. Finally, re-computation of the centroid of gaining cluster is performed once the training sample is added to the cluster.

3) Determine distance of the data points from the centroid – this step involves calculating the distance of the training sample from the centroid of each cluster. Note – if the training sample is not in the cluster with the smallest distance (closest centroid), the training sample is moved to the closest centroid cluster. After movement of the training sample, the centroid of both clusters (losing sample and gaining sample) are updated.
4) Clustering based on minimum distance- step 3 is repeated until all the training samples are assigned to the cluster with the minimum distance to the centroid of that cluster i.e. convergence is achieved and no new switch of the training samples are possible.

For the purpose of this thesis work, the MINITAB software application is used to perform the k-mean clustering of the data points according to the various shape parameters (width, reinforcement height, penetration and percentage dilution). There are five sets of clusters defined in the dataset indicating the different ranges of the shape parameters calculated from the bead's geometrical structure. To demonstrate the clustering process, the training samples (data points) of a single pass of 420 steel are utilized. Table 30 shows the statistical summary of the five clusters defined along with the minimized sum of squared error values.

Table 30: Statistical summary for (k=5) clusters

Number of Clusters	Number of Observations	Sum of Squares (within a cluster)	Average Distance from Centroid	Maximum Distance from Centroid
Cluster1	16	45.480	1.469	2.753
Cluster2	18	51.877	1.517	2.818
Cluster3	18	119.025	2.200	5.278
Cluster4	23	85.994	1.603	4.440
Cluster5	15	34.300	1.358	2.700

Table 31 provides a breakdown of the various clusters along with their centroid values (mean values) for the various shape characteristics.

Table 31: A summary of centroid distances for (k=5) clusters

Response Variable	Cluster1	Cluster2	Cluster3	Cluster4	Cluster 5	Grand Centroid
W (mm)	4.1813	4.3156	4.4783	4.0065	3.7993	4.1592
RH (mm)	0.8250	0.9472	0.6661	0.8765	1.0273	0.8646
P (mm)	0.5225	0.4456	0.7783	0.2761	0.1207	0.4283
D (%)	26.4322	19.3785	45.0653	12.9739	3.3667	21.4645

It can be observed that the five clusters have different centroids (mean values) for the observations in those clusters. Table 32, displays the distances between the various cluster centroids for the clustering algorithm.

Table 32: A summary of intra-cluster distances for (k=5) clusters

	Cluster1	Cluster2	Cluster3	Cluster4	Cluster5
Cluster1	0.0000	7.0565	18.6379	13.4618	23.0731
Cluster2	7.0565	0.0000	25.6910	6.4146	16.0236
Cluster3	18.6379	25.6910	0.0000	32.0995	41.7109
Cluster4	13.4618	6.4146	32.0995	0.0000	9.6119
Cluster5	23.0731	16.0236	41.7109	9.6119	0.0000

A silhouette plot is presented (figure 71) to provide the measure of closeness of the data points from one cluster to another. This graph is plotted within the ranges of [+1, -1]. Here, the closeness of data points to (+1) indicates that they are very distant from the neighboring cluster points. A measure of (0) indicates that the points are not distinctly observed in a cluster and a measure of (-1) indicates that the points are assigned to a wrong cluster due to interactions or interdependencies between the response variables.

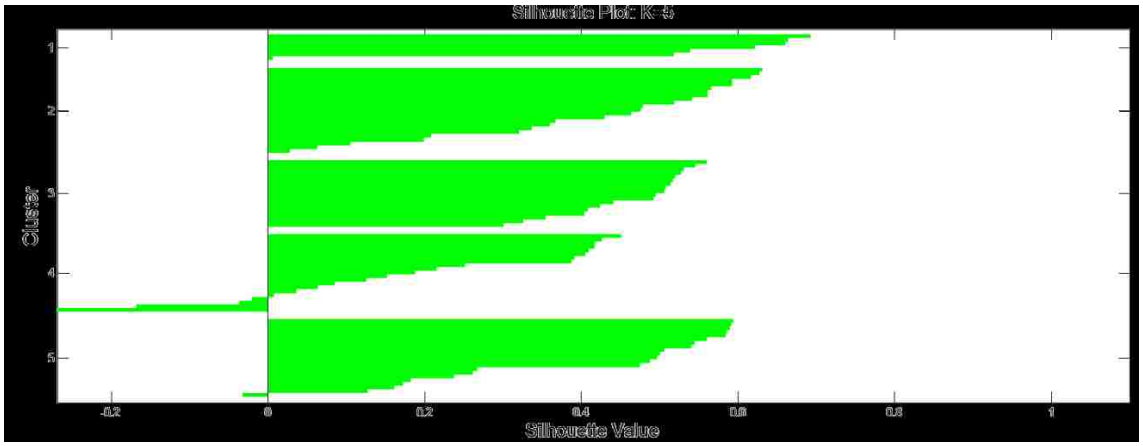

Figure 71: Silhouette plot for (k=5) clusters

The table 32 aids in visualizing the proximity of the clusters from one another. Note- the distance from a cluster to another is always repeated twice in the table for correct classification i.e. distance from cluster 1 to 2 should be the same as the distance of cluster 2 to 1.

For a visual representation of cluster classification, a dendrogram is generated according to the average linkage (mean) and the Euclidean distance between the centroids of the five clusters. A dendrogram (also known as the hierarchical cluster) is a cluster plot that provides a visual representation of spot co-relation data. The spot clusters are created by joining the spots with the help of the joint points (also known as the nodes). Each node has a right and a left branch for a spot cluster. The height of the node is the Euclidean distance between the right and left sub spot clusters. The y-axis of the graph indicates the distance values between the spots or clusters while the x- axis possesses the spot points [95]. The distance measure between two spot clusters is calculated using the mathematical expression presented in equation 42,

$$D = 1 - C \tag{42}$$

Here, D is the Euclidean distance value

C is the co-relation value

If the clusters have a high co-relation value (i.e. close to 1), then the distance value is closer to the zero value. Thus, creating highly correlated clusters near the bottom of the dendrogram plot. Similarly, the lower the co-relation value the greater the distance value between the spot clusters. A larger distance value relates to a larger cluster. It should be noted that it is difficult to interpret the distance of spot points with large cluster sizes [95]. Figure 72, displays the dendrogram generated for the 420 steel single pass spot points (i.e. division of data in 5 groups).

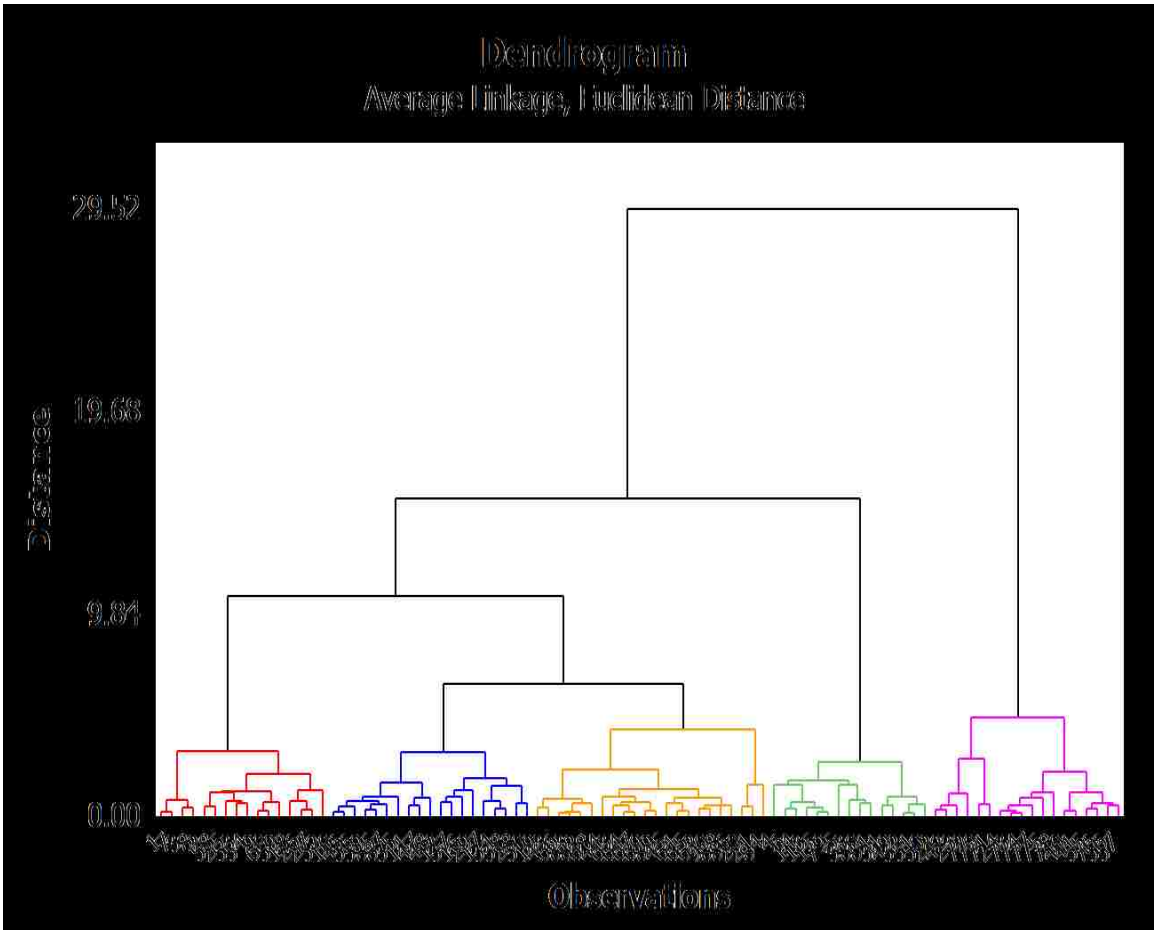

Figure 72: Dendrogram plot for (k=5) clusters

After studying the dendrogram plot and the MINITAB software analysis, table 33 is generated to help identify and classify the clad bead's shape according to the bead geometry/ structure.

Table 33: Standardization table for shape parameters (K=5)

Shape	Cluster	Points	W (mm)		RH (mm)		P (mm)		D (%)	
			Max	Min	Max	Min	Max	Min	Max	Min
A	1	16	5.13	3.77	1.27	0.61	0.79	0.38	29.18	24.04
B	2	18	5.20	3.69	1.51	0.61	0.71	0.26	22.17	16.97
C	3	18	5.04	4.00	0.91	0.43	1.06	0.60	48.57	39.79
D	4	23	4.39	3.59	1.16	0.43	0.39	0.10	16.16	8.57
E	5	15	5.08	3.03	1.36	0.73	0.31	0.02	6.04	1.11

The shapes (A-J) are presented in appendix K, for reference.

8.2 Optimal K Clusters

According to the literature, the optimal number of clusters (k) is generally defined using the clustering algorithm function through the k-mean clustering approach. The clustering algorithm used to determine an optimal number of cluster(s) is the Calinski-Harabasz criterion algorithm. The Calinski Harabasz algorithm (also known as the variance ratio criterion), is defined as the ratio between the overall between cluster variance to the overall within cluster variance [96]. The algorithm can be mathematically expressed as equation 43

$$VRC_k = \frac{SS_B}{SS_W} * \frac{(N-k)}{(k-1)} \tag{43}$$

Here, VRC_k is the variance ratio criterion

SS_B is the overall between cluster variance

SS_W is the overall within cluster variance

K is the number of optimal clusters

N is the total number of observations/ data points

The overall between cluster variance is mathematically calculated as (equation 44)

$$SS_B = \sum_{i=1}^{k} n_i \, \|m_i - m\|^2 \tag{44}$$

Here, k is the number of clusters

m_i is the centroids of each cluster i

m is the overall mean of the data set

$\|m_i - m\|$ is the Euclidean distance between two vectors

While the overall within cluster variance is calculated as (equation 45)

$$SS_W = \sum_{i=1}^{k} \sum_{x=c_i} \|x - m_i\|^2 \tag{45}$$

Here, k is the number of clusters

X is the data point

c_i is the ith cluster

m_i is the centroid of each cluster i

$||x-m_i||$ is the Euclidean distance between two vectors

Note- to obtain a well-defined cluster, the VRC ratio criterion should have a large between cluster variance and a small within cluster variance. The optimal clusters are obtained by maximizing the VRC ratio with respect to the k clusters [96]. A graph plot is generated to determine the optimal number of clusters (k), and the highest index point that (largest Calinski- Harbasz value) corresponds to in optimal cluster conditions. For the 420 steel single pass data, it can be observed that 10 clusters are optimal from the graph plot presented in figure 73.

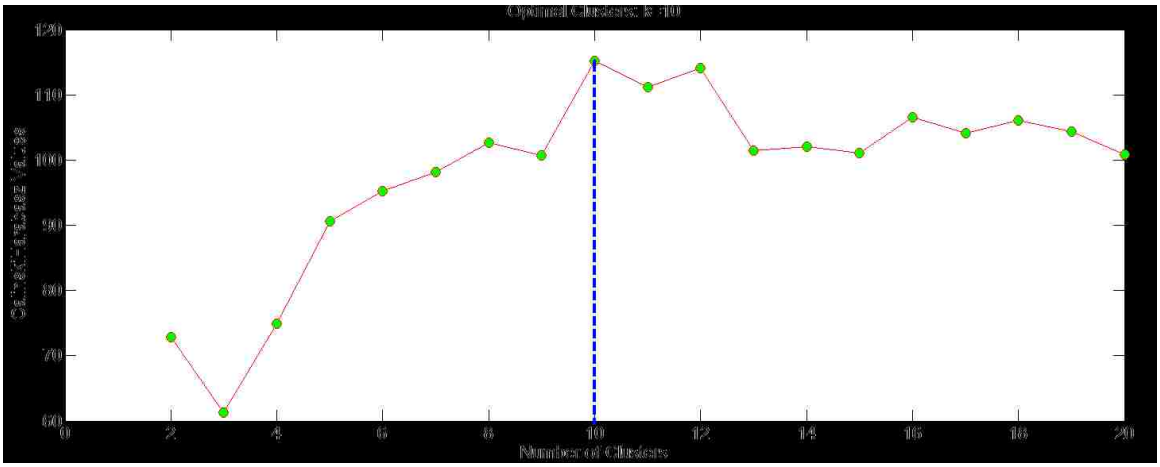

Figure 73: Calinski- Harbasz Scree Plot

Re-division of the data points into 10 clusters provides the following information presented in table (s) 34, 35, and 36.

Table 34: Statistical summary for (k=10) optimal clusters

Number of Clusters	Number of Observations	Sum of Squares (within a cluster)	Average Distance from Centroid	Maximum Distance from Centroid
Cluster1	4	0.6851	0.4075	0.4761
Cluster2	12	16.0262	1.0713	1.6942
Cluster3	15	34.2997	1.3581	2.7003
Cluster4	10	7.5926	0.7484	1.6503
Cluster5	9	10.7929	1.0457	1.4448
Cluster6	19	28.5351	1.0958	1.9910
Cluster7	3	1.6882	0.6936	1.0227
Cluster8	4	1.1459	0.4853	0.8205
Cluster9	12	17.3055	1.1135	1.9441
Cluster10	2	0.1736	0.2946	0.2946

Table 35: A summary of centroid distances for (k=10) optimal clusters

Response Variable	Cluster1	Cluster2	Cluster3	Cluster4	Cluster5	Cluster6	Cluster7
W (mm)	3.9725	4.2508	3.7993	4.0530	4.5611	4.0395	3.8333
RH (mm)	0.6650	0.8783	1.0273	0.8590	1.0478	0.8974	0.7133
P (mm)	0.4900	0.533	0.1506	0.3780	0.5044	0.2895	0.1833
D (%)	28.7396	25.6631	3.3667	17.7983	20.7767	13.3968	9.2336
Response Variable	Cluster8	Cluster9	Cluster10	Grand Centroid			
W (mm)	4.7375	4.3942	4.4650	4.1592			
RH (mm)	0.7300	0.6625	0.5600	0.8646			
P (mm)	0.7750	0.8050	0.6250	0.4283			
D (%)	42.8316	46.6439	40.0608	21.4645			

Table 36: A summary of intra-cluster distances for (k=10) clusters

	CL1	CL2	CL3	CL4	CL5	CL6	CL7	CL8	CL9	CL10
CL1	0.00	3.09	23.37	10.94	7.99	15.34	19.50	14.11	17.91	11.33
CL2	3.09	0.00	22.30	7.86	4.89	12.27	16.43	17.17	20.98	14.40
CL3	25.37	22.03	0.00	14.43	17.43	10.03	5.87	39.48	43.28	36.70
CL4	10.94	7.86	14.43	0.00	3.02	4.40	8.57	25.04	28.85	22.26
CL5	7.99	4.89	17.43	3.02	0.00	7.40	11.57	22.05	25.87	19.29
CL6	15.34	12.27	10.03	4.40	7.40	0.00	4.17	29.44	33.25	26.67
CL7	19.50	16.43	5.87	8.57	11.57	4.17	0.00	33.61	37.41	30.83
CL8	14.11	17.17	39.48	25.04	22.05	29.44	33.61	0.00	3.82	2.79
CL9	17.91	20.98	43.28	28.87	25.87	33.25	37.41	3.82	0.00	6.58
CL10	11.33	14.40	36.70	19.29	19.29	26.67	30.83	2.79	6.58	0.00

Figure 74 presents the various scatter plots to represent the optimal clusters (k=10) for the single pass 420 steel data points. Note: as there are 10 clusters and 4 shape factors, the plots cannot be represented in a 3D format due to a 4D nature, hence, multiple 2D plots are presented. Also, the values are normalized between ranges of [-1, +1] for a true representation of clusters according to the bead's geometry structures.

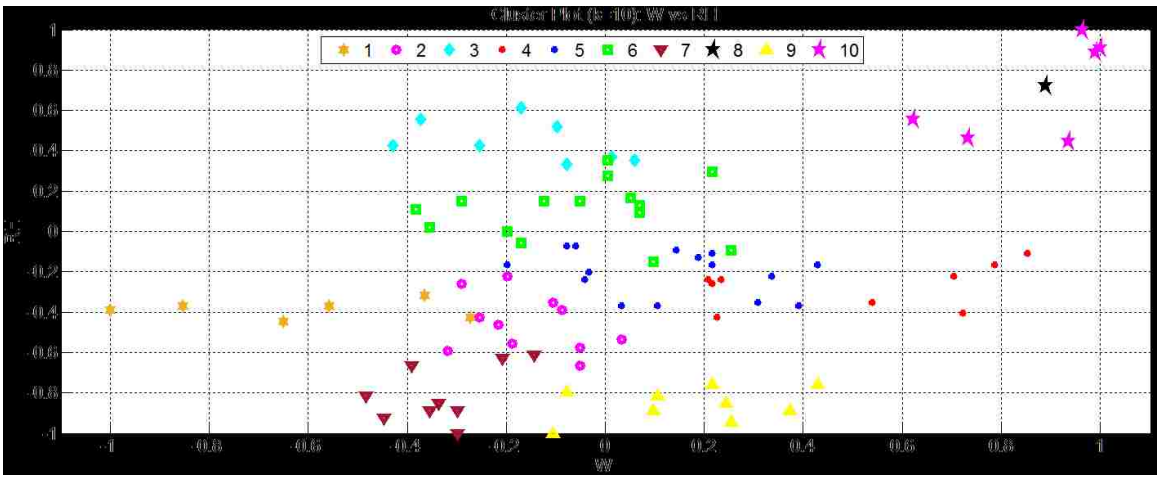

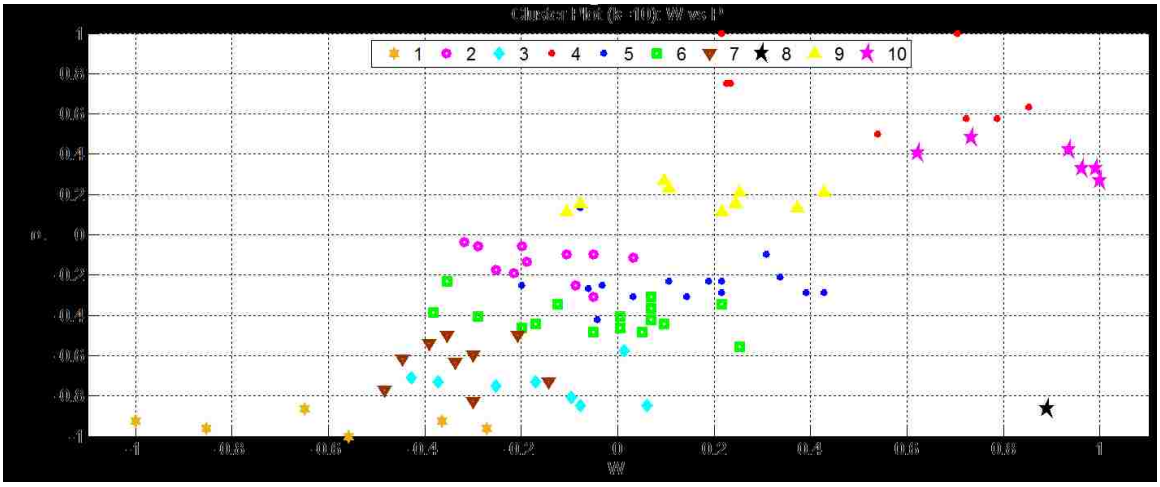
1 2 3 4 5 6 7 8 9 10
W

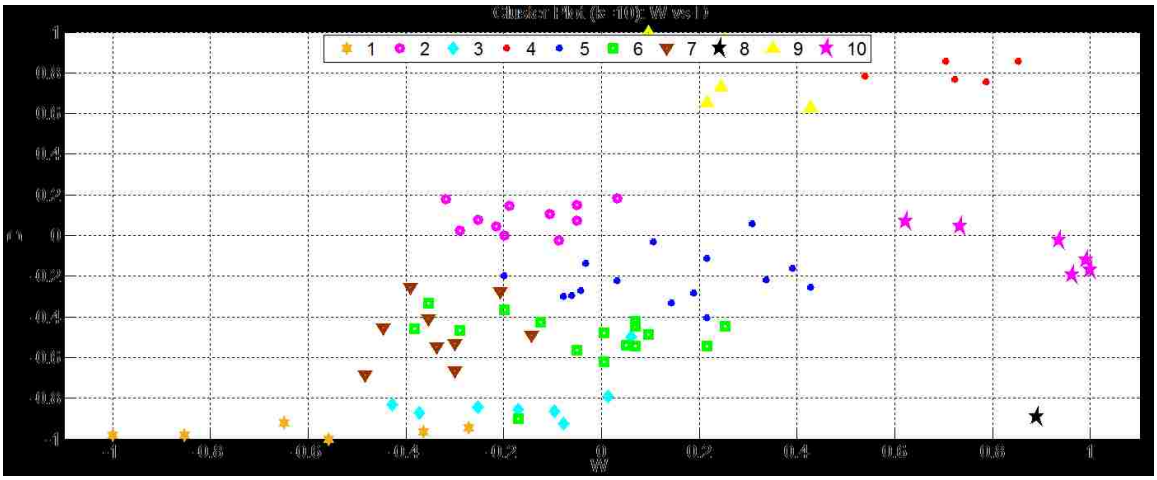
1 2 3 4 5 6 7 8 9 10
W

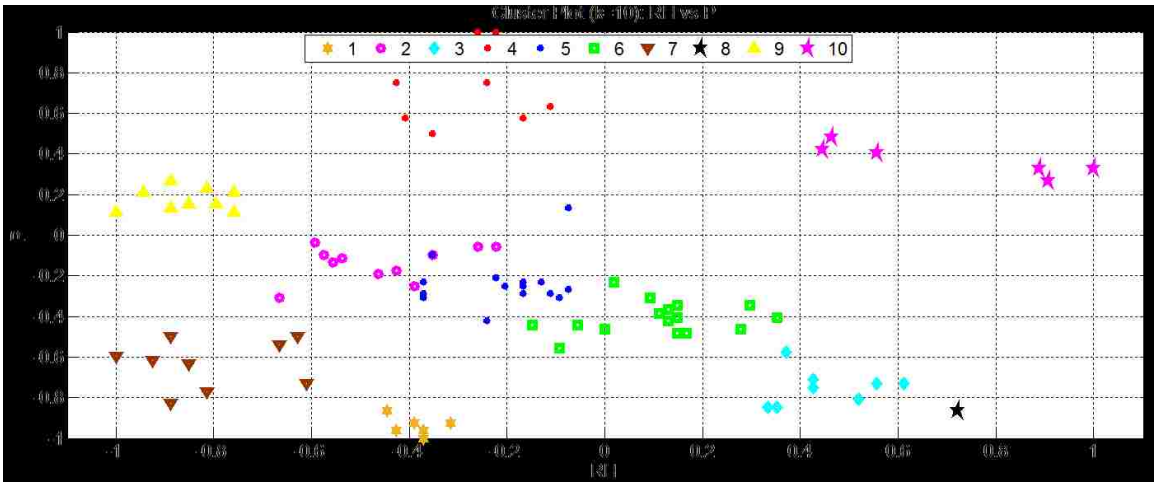
1 2 3 4 5 6 7 8 9 10

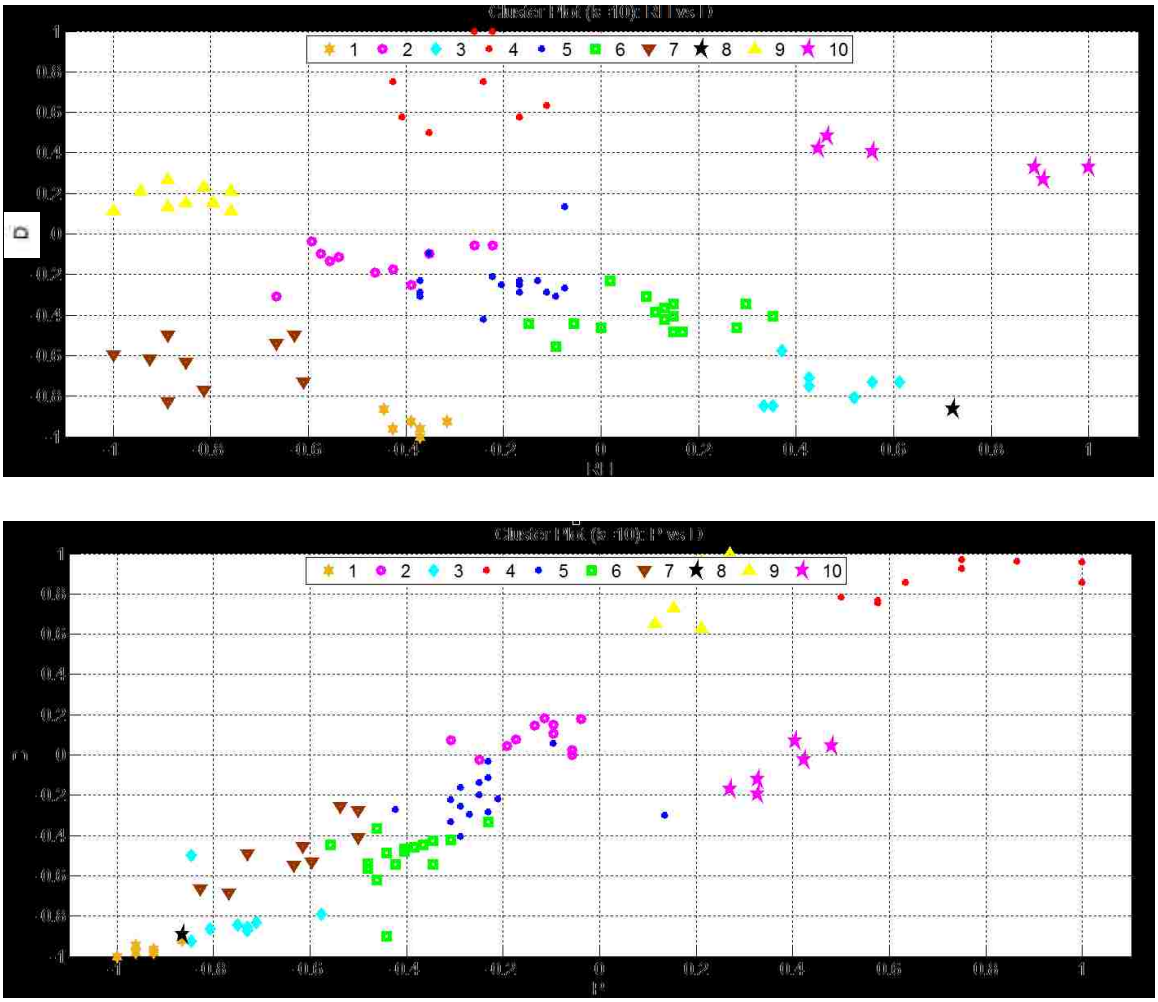

Figure 74: Graphical representation of the optimal (k=10) clusters

A silhouette plot is again presented (figure 75) to provide a measure of the closeness of the points from one cluster to another. This graph is plotted within the ranges of [+1, -1]. Here, the closeness of the data points to (+1) indicate they are very distant from the neighboring cluster points. A measure of (0) indicates that points are not distinctly in a cluster and a measure of (-1) indicates that points are assigned to a wrong cluster due to interaction or interdependencies between the response variables. In case of 10 optimal cluster the silhouette plot shows the greatest closeness to a +1 measure as compared to the 5 cluster case illustrated earlier. This indicates the clusters are distinctively away from each other. The values close to -1 are considered skewed points of the data sets.

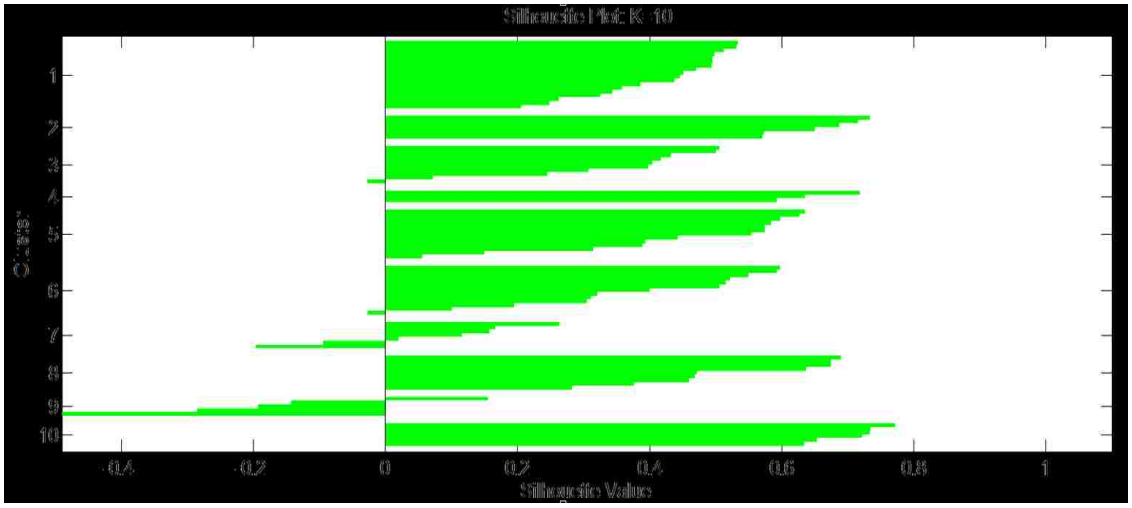

Figure 75: Silhouette plot for (k=10) optimal clusters

The visual representation of the dendrogram plot is displayed in figure 75 for re-classification of the data points in 10 clusters.

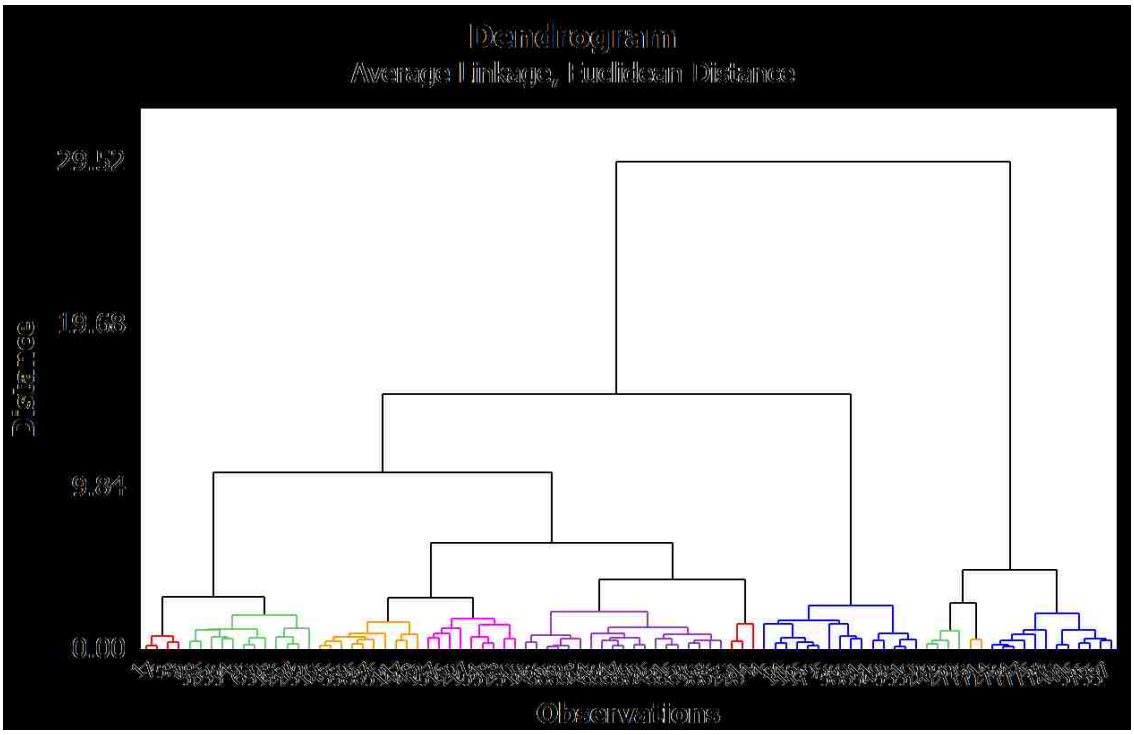

Figure 76: Dendrogram plot for (k=10) optimal clusters

After studying the dendrogram plot and the MINITAB software analysis, table 37 is generated to help identify and classify the clad bead shape according to the bead geometry/ structure.

Table 37: Standardization table for shape parameters (K=10)

Shape	Cluster	Points	W (mm)		RH (mm)		P (mm)		D (%)	
			Max	Min	Max	Min	Max	Min	Max	Min
A	1	4	4.15	3.77	0.68	0.65	0.52	0.47	29.18	28.27
B	2	12	5.13	3.80	1.27	0.61	0.79	0.38	27.33	24.04
C	3	15	5.08	3.03	1.36	0.73	0.31	0.02	6.04	1.11
D	4	10	4.58	3.69	0.98	0.61	0.61	0.26	18.81	16.16
E	5	9	5.20	3.90	1.51	0.77	0.71	0.38	22.17	19.52
F	6	19	4.39	3.63	1.16	0.43	0.39	0.10	15.20	11.41
G	7	3	4.12	3.59	1.12	0.49	0.30	0.11	10.12	8.57
H	8	4	4.97	4.38	0.88	0.51	0.84	0.62	43.39	42.14
I	9	12	5.04	4.00	0.91	0.43	1.06	0.60	48.57	45.13
J	10	2	4.58	4.35	0.56	0.56	0.65	0.60	40.33	39.79

The Shapes (A-J) are presented in Appendix L. The table 37, can be used to identify the bead shape according to the multi-objective responses (shape characteristics). To utilize this novel standardized procedure, the user would start off by selecting the value for the percent dilution as the first option and then moving on to defining the three basic shape parameters within a boundary condition.

CHAPTER 9

DISCUSSION

This thesis work presents eight different artificial neural network (ANN's) models for prediction of the bead's geometry from the manufacturing parameters and vice versa. Out of the eight proposed models, two of the models are focused on the single pass bead generation process with a 420 steel clad powder. Whereas the other six models pay much closer attention to the overlap bead generation (40%, 50%, and 60%) process with a 420 steel clad powder. The error in the system for all eight models is minimal (within a 5 percent window), hence, confident predictions for the desired parameters can be made for production purposes.

It is observed that the target values supplied to the various neural networks (for a supervised learning) superimpose the network output values when plotted, hence, this trend provides a confidence in the model developed. Although, it should be noted that the network generalization is lower for the backward networks created (shape parameters to manufacturing parameters). This is basically due to the nature of data being mapped while training the backward networks.

Training backward networks involves mapping of continuous data to discreet data. The continuous data comprises of various shape parameters (unique in nature), that are mapped to the five classes of manufacturing parameters coded between the [-2, 2] range. When a set of unique shape parameters are mapped to a class, the network assigns that class to those shape parameters. If while training a similar set of shape parameters are noticed by the network, instead of assigning the data to either of the five classes, the network introduces a new class by averaging the results. This averaging of results causes decrease in the overall accuracy of the network and increases the generalization errors. It is recognized that the averaging condition for this thesis work occurs due to the closeness of numerical values for the continuous data set (inputs- shape parameters) giving rise to network errors.

Generalization of the network plays a vital role in making successful predictions during a simulation process. This is due to the fact that generalization avoids conditions

for over fitting of the data points. Over fitting occurs if the error value in the data set while training is forced to be a small numerical value. In such a case, the network performs exceptionally well for the training set as it memorizes the set as a training example. However, once an unknown test data set (simulation process) within the input parameter range is introduced to the trained network, it becomes difficult for the network to adapt to the new conditions. Hence, making the network brittle and not generalized. To avoid such over fitting conditions, one of the listed techniques in this sub-section can be utilized [97].

1) Defining a large network architecture – the goal is to define a network that can encompass the entire training process and provide an adequate fit. This is generally the most recommended process out of the two solutions listed in this sub-section. A drawback to this solution is that the adequate number of neurons for a particular application that can provide an acceptable fit should be known. As the network architecture is developed with a trial and error method for the best fit, it is very difficult to find the exact number of neurons that can provide the best fit [97].

2) Regularization – this solution involves improving the overall performance algorithm of the network architecture to avoid over fitting of a dataset. For the networks defined in this thesis work the performance function used is a mean square error (MSE) function. Regularization process enforces a smoothness factor to the mean square error function to decrease generalization errors. The smoothness factor may vary for various network architectures such as fixing the number of parameters in a model, blocking the parameters or improving the algorithm. One example of improving algorithm is presented in equation 46 [97].

$$MSEREG = (g * MSE) + (1 - g) * MSW \quad (46)$$

Here, MSEREG is the new performance function

g is the improved performance ration

MSW is the mean sum of squares of the network weights and bias values

MSE is the performance function with high generalization errors

CHAPTER 10

CONCLUSIONS

The laser cladding process is a non-linear multi-variable process relevant to the additive manufacturing technique. Both the process and shape parameters play an important role in defining the geometry of the clad bead; however, due to the highly coupled nature of the process there are many interdependencies among the parameters giving rise to the non-linearity behaviour in the overall bead structure. The presented research proves effective in setting up a methodology and proposing a meta-structure (artificial intelligence model) for predicting the bead shape parameters with the manufacturing parameters and vice-versa. This goal is achieved through accomplishing the following vital steps and methodologies:

1) Establishment of an experimental approach for a time efficient and financially viable data collection for the key bead shape parameters through the response surface methodology (DOE tool). Therefore, subsequent experimental work should follow this methodology.
2) Development of a cognitive artificial intelligence system for confident predictions for a single pass and an overlap pass configuration through the artificial neural networks (MATLAB tool). More experimental work needs to be performed prior to determining whether a general ANN model can be used for multiple materials, or whether there needs to be ANN-material-system sets.
3) Proof of the relative interactions between the manufacturing parameters and the geometrical properties of the clad bead structure through the sensitivity analysis (CT, SI) and analysis of variance (ANOVA) techniques. Therefore, non-linear relationship between the shape and the process parameters are determined which aids in manipulating the bead structure through ANN network designed.
4) Optimization of the manufacturing parameters to obtain the desired clad bead geometry through the response optimizer (MINITAB tool). Therefore, optimal process parameters are determined for the desired bead geometry for obtaining higher yield levels.

5) Classification of the clad bead structure (shape analysis) as a means of standardizing the clad beads to exhibit the class characteristics through K- mean clustering approach. Therefore, determining similar trends within a defined class to which the beads belong. This helps in overall decision making while selecting a class to manipulate the bead dimensions.

CHAPTER 11

FUTURE WORK

The thesis work presented provides a standard to improvise an experimental strategy for the data collection process towards the laser cladding process. It uses a design of experiments (DOE) approach to design an experimentation set with the help of a response surface methodology (RSM) central composite design. Furthermore, an artificial intelligence system is established to successfully predict the shape parameters or the manufacturing parameters (according to network architecture) within a 95^{th} percentile confidence range for a single pass as well as overlap configurations of the 420 steel clad powder. Through the use of the response surface methodology approach, various relations between the shape and the manufacturing parameters are also determined. These relations are verified using various sensitivity analysis approaches to determine the significant factors relevant to the laser cladding process. The relations among parameters are then visualized using the surface and the contour plots for their respective objective functions. An optimization resolver tool is adopted to provide optimized results for the various single objective and multi objective functions for both single and overlap passes. Lastly, a k-mean clustering approach is applied to the manufacturing operations (single pass and overlap) to determine an optimal number of clusters in each data set. This clustering approach helps categorize the bead shape according to the various cluster characteristics and aids in standardizing the laser cladding process for shape parameters.

To expand the scope of the knowledge in the additive manufacturing (AM) sector, the future work should involve:

1) Other experimentation strategies (such as Taguchi) and development of artificial intelligence systems for a layered manufacturing approach. Figure 77 (source: industry sponsor. [4]; designer- Mr. Syed Saqib), displays an image of the layered manufacturing technique using the laser cladding operation.

2) This research helps in determining the relations between the shape and the manufacturing parameters, but various mechanical and material properties such as the heat affected zones (HAZ), the strength of the generated bead (tensile and

compressive strengths), the finite element analysis (yield points of materials) etc. should be studied for several manufacturing configurations for the laser cladding process.

3) The research presented in this thesis uses a single material i.e. the 420 steel clad powder (low carbon ferrous material). Other materials with high carbon (such as H13 steel) and non-ferrous (such as tungsten carbide) characteristics should be studied to incorporate a re-configurability principle in the overall manufacturing system to be able to adapt to different materials.

4) Various fill strategies (such as 45degrees, zig-zag, orthogonal, or honey comb) while positioning the beads should be thoroughly studied to obtain the desirable properties while generating a layered three dimensional part.

5) The artificial intelligence model should be overextended by including the various constant parameters such as the nozzle angle or the shielding gas type etc.to confidently predict more settings for the manufacturing parameters relevant to the laser cladding process.

Figure 77: A 3-dimensional part generation by laser cladding operation [4]

REFERENCES/BIBLIOGRAPHY

[1] Dictionary.com, LLC, "Manufacture," 2014. [Online]. Available: http://dictionary.reference.com/browse/manufacture.

[2] Merriam-Webster, Incorporated, "Manufacture," 2013. [Online]. Available: http://www.merriam-webster.com/dictionary/manufacture.

[3] D. M. C. Santos, A. E. M. Pertence, H. B. Campos and P. R. Cetlin, "The development of 3D models through rapid prototyping concepts," *Journal of Materials Processing Technology,* vol. 169, no. 1, p. 1–4, 2005.

[4] Whitfield Welding Inc., "Media Gallery," Whitfield Welding, 2013. [Online]. Available: http://www.whitfieldwelding.com/Media.aspx. [Accessed 29 05 2014].

[5] Gosiger, "Why You Should Consider Trochoidal Milling," Gosiger, 2012. [Online]. Available: http://info.gosiger.com/news/bid/152475/Why-You-Should-Consider-Trochoidal-Milling#emart-form-anchor. [Accessed 29 05 2014].

[6] Schott. F., "http://en.wikipedia.org/wiki/File:SchlichtenDrehen.jpg," Schlichtbearbeitung beim Drehen von Aluminium, 07 05 2008. [Online]. Available: http://en.wikipedia.org/wiki/File:SchlichtenDrehen.jpg. [Accessed 29 05 2014].

[7] T. T. Wohlers, "Wohlers report 2009: state of the industry annual worldwide progress report," Wohlers Associates, Fort Collins,Col, 2009.

[8] A. Gebhardt, Rapid Prototyping, vol. 1, Hanser Publications, 2003.

[9] D. Bak, "Rapid prototyping or rapid production? 3D printing processes move industry towards the latter," *Assembly Automation,* vol. 23, no. 4, pp. 340-345, 2003.

[10] BCF replications Ltd., "The Practical Applications of Rapid Prototyping and the Possibilities for Tomorrow," BCF replications Ltd., [Online]. Available: http://bcf-replication.tripod.com/. [Accessed 29 05 2014].

[11] Ziad. A., "How designers can get the most out of additive manufacturing," Quickparts Solutions, 3D Systems Atlanta, Ga., 29 10 2013. [Online]. Available: http://machinedesign.com/3d-printing/how-designers-can-get-most-out-additive-manufacturing. [Accessed 29 05 2014].

[12] K.I., Arshak; E.G., Moore; C., Cunniffe and L.M., Cavanagh, "Using Design of Experiment to Investigate the Effects of Conducting Polymer Composite Sensor

Composition on the Response to an Homologous Series of Alcohols," in *PROC. 25th INTERNATIONAL CONFERENCE ON MICROELECTRONICS (MIEL 2006),*, BELGRADE, SERBIA AND MONTENEGRO, 2006.

[13] L. K. Pan, C. C. Wang, Y. C. Hsiso and K. C. Ho, "Optimization of Nd-YAG laser welding onto magnesium," *J. of Optics & Laser Technology*, pp. 33-42, 2004.

[14] M., Buragohain; C., Mahanta, "Modelling of Thermal Power Plant using Full Factorial Design based ANFIS," in *Cybernetics and Intelligent Systems*, Bangkok, 2006.

[15] V. K. Gupta and R. S. Parmar, "Fractional factorial technique to predict dimensions of the weld bead in automatic," *IE(I) Journal-MC*, pp. pp.67-75, 1989.

[16] Z. Zhang, "Comparison about the Three Central Composite Designs with Simulation," in *International Conference on Advanced Computer Control*, Singapore, 2008.

[17] A., Khawas; A, Banarjee; S., Mukhopadhyay., "A Response Surface Method for Design Space Exploration and Optimization of Analog Circuits," in *2011 IEEE Computer Society Annual Symposium on VLSI*, Chennai, 2011.

[18] A.A., Giunta; V., Balabanov; D., Haim; B., Grossman; W.H., Mason; L.T., Watson; R.T., Haftka., "WING DESIGN FOR A HIGH-SPEED CIVIL TRANSPORT USING A DESIGN OF EXPERIMENTS METHODOLOGY," *American Institute of Aeronautics and Astronautics*, pp. 1-16, 1996.

[19] K., Andersen; G.E., Cook; K., Ramaswamy; G., Karsai., "Artificial neural networks applied to arc welding process modeling and control," in *Conference Record of the 1989 IEEE Industry Applications Society Annual Meeting*, 1989.

[20] K., Andersen; G.E., Cook; G., Karsai; K., Ramaswamy., "Artificial neural networks applied to arc welding process modeling and control," *IEEE Transactions on Industry Applications*, vol. 26, no. 5, pp. 824-830, 1990.

[21] S., Datta; D.K., Pratihar, "Modeling of metal inert gas welding process using radial basis function neural networks," in *World Congress on Nature Biologically Inspired Computing*, NaBIC, 2009.

[22] F., Meriaudeau; F., Truchetet; D., Grevey; A.B., Vannes, "Laser cladding process and image processing," *Journal of Lasers in Engineering*, vol. 6, no. 3, pp. 161-187, 1997.

[23] F., Meriaudeau; F., Truchetete; C., Dumont; E., Renier; P., Bolland, "Acquisition and image processing system able to optimize laser cladding process," in *3rd International Conference on Signal Processing (ICSP)*, 1996.

[24] E.H., Amara; L., Achab; O., Boumia, "Numerical modelling of the laser cladding process using a dynamic mesh approach," in *Advanced Optoelectronics and Lasers, 2005. Proceedings of CAOL 2005. Second International Conference on*, Crimea, 2005.

[25] Z, Xiong; Q.B., Zhang; Y., Zeng X., "Effects of Process Parameters of Laser Cladding on the Deformation," in *2011 Fourth International Conference on Intelligent Computation Technology and Automation*, 2011.

[26] L., Song; J., Mazumder, "Feedback control of melt pool temperature during laser cladding process," *Control Systems Technology, IEEE Transactions on,* vol. 19, no. 6, pp. 1349-1356, 2011.

[27] T., Stewart; W., Stiver D., "Thermal optimization of electronic systems using design of experiments based on numerical inputs," in *Semiconductor Thermal Measurement and Management Symposium, 2004. Twentieth Annual IEEE*, 2004.

[28] P. Sreeraj, "Optimization of weld bead geometry for stainless steel cladding deposited by GMAW," *American Journal of Engineering Research (AJER),* vol. 2, no. 5, pp. 178-187, 2013.

[29] A., Jahan; Y., Ismail M.; R., Noorossana, "Multi response optimization in design of experiments considering capability index in bounded objectives method," *Journal of Scientific and Industrial Research,* vol. 69, pp. 11-16, 2010.

[30] M., Kumar; S., Verma; P.P., Singh., "Data clustering in sensor networks using ART," in *Fourth International Conference on Wireless Communication and Sensor Networks*, Allahbad, 2008.

[31] S.S.R., Abidi; J., Ong, "A data mining strategy for inductive data clustering: a synergy between self-organising neural networks and K-means clustering techniques," in *TENCON 2000. Proceedings*, Kuala Lampur, 2000.

[32] S., Alam; G., Dobbie; Y.S., Koh; P., Riddle, "Clustering heterogeneous web usage data using Hierarchical Particle Swarm Optimization," in *IEEE Symposium on Swarm Intelligence (SIS), 2013*, Singapore, 2013.

[33] Farlex Inc., "Cladding," Farlex Inc., 2013. [Online]. Available: http://www.thefreedictionary.com/cladding. [Accessed 29 05 2014].

[34] K., Komvopoulos; K., Nagarathnam, "Processing and Characterization of Laser-Cladded Coating Materials," *Journal of Engineering Materials and Technology*, vol. 112, no. 2, pp. 131-143, 1990.

[35] F., Schneider M., "Laser cladding with powder: effect of some machining parameters on clad properties," Print Partners Ipskamp, Enschede, Enschede, Netherlands, 1998.

[36] R. MacIntyre, "Laser Hardsurfacing of Gas Turbine Blade Shroud Interlocks," in *LIM-1*, 1983.

[37] M. Eboo and A. Lindemanis, "Advances In Lasercladding Technology," in *Proc. ICALEO'83 SPIE*, 1983.

[38] P.A., Carvalho; N., Braz; M.M., Pontinha; M.G.S., Ferreira; W.M., Steen; R., Vilar; K.G., Watkins, "Automated Workstation for Variable- Its Use for Rapid Alloy Scanning,," in *Surface and Coatings Technology*, Liverpool, UK, 1995.

[39] M. Weck and J. Schön, "Integration prozeßspecifischer Sensoren und Aktoren in das Strahlführungssystem - Arbeitskopf mit Wechselobjektiv für das Oberflächenveredeln," in *Materialbearbei-tung mit CO2-Laserstrahlen höchster Leistung*, 1994.

[40] V. Weerasinghe, "Laser Cladding of Flat Plates," 1984.

[41] E.A., Metzbower; Pierpoint, E.R.; Hartman, K., "Hardfacing Using a CW laser," in *Proc. ICALEO*, 1986.

[42] A., Jonnalagadda; S., Scharek, "Laser Solutions Short Courses," in *ICALEO 30th International Congress on Applications of Lasers & Electro-Optics*, MI, USA & Dresden, Germany.

[43] Dictionary.com, LLC, "Laser- Collins English Dictionary - Complete & Unabridged 10th Edition," Dictionary.com, 2009. [Online]. Available: http://dictionary.reference.com/browse/laser. [Accessed 14 05 2014].

[44] OPTECH Consulting Inc., "Major Findings of the Fiber Laser Report," OPTECH Consulting, 03 03 2009. [Online]. Available: http://www.optech-consulting.com/html/fiberlaserreport.html. [Accessed 14 05 2014].

[45] OPTECH Consulting Inc., "GLobal MArket for Lasers for Material Processing and Share of Fiber Lasers," OPTECH Consulting, 2012. [Online]. Available: http://www.optech-consulting.com/html/laserprocessingmarkets.html. [Accessed 14 05 2014].

[46] E. Stiles, "IPG Photonics Fiber Lasers: The Flexible Tool for High Power Laser Welding," in *AWS New Welding Technologies Conference*, 2010.

[47] K. R. Spring, T. J. Fellers and M. W. Davidson, "Introduction to Lasers," Olympus: Microscopy Resource Center, 2012. [Online]. Available: http://www.olympusmicro.com/primer/lightandcolor/lasersintro.html. [Accessed 29 05 2014].

[48] Houghton Mifflin Company, "Semiconductor Laser," The American Heritage® Dictionary of the English Language, Fourth Edition, 2000. [Online]. Available: http://www.thefreedictionary.com/semiconductor+laser. [Accessed 14 05 2014].

[49] D. R. Paschotta, "Diode-pumped Lasers," RP Photonics consulting GmbH, 2006. [Online]. Available: http://www.rp-photonics.com/diode_pumped_lasers.html. [Accessed 14 05 2014].

[50] R. Aldrich, "Laser Fundamentals," Naval Surface Warfare Center, Dahlgren Division, 1995. [Online]. Available: http://www.fas.org/man/dod-101/navy/docs/laser/fundamentals.htm. [Accessed 14 05 2014].

[51] Materialgeeza, "Laser Cladding System Setup," 17 05 2008. [Online]. Available: http://en.wikipedia.org/wiki/File:Laser_Cladding_System_setup.jpg. [Accessed 29 05 2014].

[52] S., Funderburk R., "Key Concepts in Welding Engineering- A look at heat input," *Welding Innovation*, vol. XVI, no. 1, pp. 1-4, 1999.

[53] Husson D, Poeppel S, and Stannard S, "Cladding and Additive Manufacturing Using Laser Applied Powder® Processes," in *AWS New Welding Technologies*, 2010.

[54] Kumar. V., "Development and characterization of Fluxex for submerged Arc Welding," Punjabi University, Patiala, India, 2010.

[55] S.R., Gupta; N., Arora, "Influence of flux basicity index on weld bead geometry and HAZ submerged arc welding," *Indian Welding Journal*, vol. 24, no. 3, pp. 127-133, 1991.

[56] L.J., Yang; R.S., Chandel; M.J., Bibby, "The effects of process variables on the bead width of submerged-arc weld deposits," *Journal of Materials Processing Technology*, vol. 29, no. 1, pp. 133-134, 1992.

[57] V., Gunaraj; N., Murugan, "Prediction and Comparison of the Area of the Heat Affected Zone for the Bead-no-Plate and Bead-on-Joint in Submerged Arc Welding of Pipes," *Journal of Materials Processing Technology*, vol. 95, no. 1-3, pp. 246-261, 1999.

[58] J.C., McGlone, "Weld bead geometry prediction-A review," *Metal Construction*, vol. 14, no. 7, pp. 378-384, 1982.

[59] J., Cornu, Advanced Welding Systems, vol. 2, London: IFS Publications, 1988.

[60] Air Liquide, "Welding terms and Definitions," American Welding Society , 2001.

[61] J., Manuel; R.S., Tavares., "Measurement of Welding Dilution from Images using Active Contours," in *SEECCM - 2nd South East European Conference on Computational Mechanics*, Porto, Portugal, 2009.

[62] G.J, Bruck, "High Power Laser Beam Cladding," *Journal of Meterials*, vol. 39, no. 2, pp. 10-13, 1987.

[63] N., Coniglio; C.E., Cross; T., Michael; M., Lammers, "Defining a Critical Weld Dilutio to avoid Solidification Cracking in Aluminium," in *1st International Conference on Welding Technologies*, Ankara, Turkey, 2009.

[64] D. C. Montgomery, "Response Surface Methodologgy," in *Design of Experiments* , Arizona, John Wiley & Sons, 2009, pp. 417-485.

[65] D. W. Gernjak, "Solar Photo- Fenton Treatment of EU Priority Substances.," 2006.

[66] R., Box G. E. P.: Draper N., Empirical model-building and response surfaces, Wiley, 1987.

[67] D. C. Montgomery, "Response Surface Methodologgy," in *Design of Experiments*, Arizona, John Wiley & Sons Inc., 2009, pp. 417-485.

[68] A.I., Khuri; S., Mukhopadhyay, "Response surface methodology," *Advanced Review*, vol. 2, pp. 128-148, 2010.

[69] GEP, Box; JS., Hunter, "Multifactor experimental," *Ann Math Stat*, pp. 195-241, 1957.

[70] J., Hughes, "A Tutorial on the Application of Experimental Designs to Development of Chromatographic Methods," School of Applied Science, RMIT University, Melbourne , Australia, 2007.

[71] S. Tandon, G. Kanshal and S. and Gupta, "Effect of Flux Characteristics on HAZ during Submerged Arc Welding," in *Proceedings of the International Conference on Welding Technology*, Roorkee, India, 1988.

[72] N. Mohan and S. Pandey, "Modeling for Element Transfer in Submerged Arc Welding," in *Proceedings of International Conference on Mechanical Engineering in Knowledge Age*, New Delhi, India, 2005.

[73] S. Gupta and P. Gupta, "Investigation into flux consumption in submerged arc welding," *Indian Welding Journal,* vol. 21, no. 3, pp. 365-369, 1988.

[74] M. Aksoy, M. Ero and N. Orhan, "Effect of coarse initial grain size on microstructure and mechanical properties of weld metal and HAZ of a low carbon steel," *Material Science and Engineering,* vol. 269, no. 1, pp. 1-9, 1999.

[75] C.E, Jackson; Shrubsall, A. E., "Control of penetration and melting ratio with welding technique," *Welding Journal,* vol. 32, no. 4, pp. 172-178, 1953.

[76] S., Samarasinghe., Neural Networks for Applied Sciences and ENgineering- From Fundamentals to complex Pattern REcognition, Boca Raton, New York: Auerbach Publications- Taylor & Francis Group, LLC, 2006.

[77] Q., Jarosz., "Neuron," 2009. [Online]. Available: http://en.wikipedia.org/wiki/File:Neuron_Hand-tuned.svg. [Accessed 29 05 2014].

[78] K. Aggarwal, R. Urbanic and A. L. , "A Methodology for Investigating and Modelling Laser Clad Bead Geometry and Process Parameter Relationships," *SAE International Journal of Materials and Manufacturing,* vol. 7, no. 2, pp. 269-279, 2014.

[79] S. Haykin, Neural Networks: A Comprehensive Foundation, New York: MacMillan College Publishing, 1994.

[80] V. Cheung and k. Cannons, "An introduction to Neural Networks," University of Manitoba (Electrical and Computing Engineering), Winipeg, 2002.

[81] J. C. Principe, N. R. Euliano and W. C. Lefebvre, Neural and Adaptive Systems, New York: John Whiley & Sons Inc., 2000.

[82] Houghton Mifflin Company, "The Free Dictionary," The American Heritage® Science Dictionary, 2005. [Online]. Available: http://www.thefreedictionary.com/degree+of+freedom. [Accessed 18 05 2014].

[83] R. Rojas, Neural Networks, Berlin: Springer-Verlang, 1996.

[84] C. Souza, "Neural Network Learning by the Levenberg-Marquardt Algorithm with Bayesian Regularization," 18 11 2009. [Online]. Available: http://crsouza.blogspot.ca/2009/11/neural-network-learning-by-levenberg_18.html.. [Accessed 18 05 2014].

[85] L., Aggarwal; K., Aggarwal; R.J., Urbanic, "Use of artificial neural networks for the development of an inverse kinematic solution and visual identification of singularity zone(s)," in *Variety Management in Manufacturing. Proceedings of the 47th CIRP Conference on Manufacturing Systems*, Windsor, Ontario, 2014.

[86] P., McCollum, "An Introduction to Back-Propagation Neural Networks," Encoder- The Newsletter of the Seatle Robotics Society, 2004. [Online]. Available: http://www.seattlerobotics.org/encoder/nov98/neural.html. [Accessed 18 05 2014].

[87] T. Kannan and Yoganath, "Effect of process parameters on clad bead geometry and shape relationships of stainless steel cladding deposited by GMAW," *International Journal of Manufacturing Technology*, vol. 47, pp. 1083-1095, 2010.

[88] V. Kumar, J. Khamba and N. Mohan, "Chapter – 5 Effect of welding parameters on bead geometry and flux consumption," in *Development and characterization of fluxes for submerged arc welding*, Patiala, India, Punjabi University, 2011, pp. 101-158.

[89] K., Aggarwal; L., Aggarwal; R., Urbanic J., "Identifying relative importance of input parameter(s) in developing predictive model for Laser Cladding process," in *Proceedings of ASME 2014 International Mechanical Engineering Congress & Exposition*, Montreal, Quebec, Canada, 2013.

[90] R., Pruim, "ANOVA: Analysis of Variation," Calvin College, 1999.

[91] U.S. Commerce Department, "DOE contour plot," NIST Engineering Statistics Handbook, 01 06 2013. [Online]. Available: http://www.itl.nist.gov/div898/handbook/eda/section3/eda33a1.htm. [Accessed 27 05 2014].

[92] Minitab Inc., "Contour and Surface Plots. Retrieved from Minitab 17 Documentation - Getting started with Minitab 17," Minitab Inc.,

http://www.minitab.com/uploadedFiles/Documents/getting-started/Minitab17_GettingStarted-en.pdf.

[93] J., Aleshunas, "K- Means Clustering," Webster University, 2006. [Online]. [Accessed 30 05 2014].

[94] Han J., Kamber M., Data Mining: Concepts and Techniques, San Francisco: Elsevier Inc., 2..6.

[95] TotalLab Limited, "Correlation Analysis," TotalLab- Life Science Analysis Essential, 2013. [Online]. Available: http://www.totallab.com/products/samespots/support/faq/dendrogram.aspx. [Accessed 30 02 2014].

[96] The MathWorks, Inc., "clustering.evaluation.CalinskiHarabaszEvaluation class," Math Works- Accelerating the pace of engineering and science, 1994. [Online]. Available: http://www.mathworks.com/help/stats/clustering.evaluation.calinskiharabaszevaluation-class.html. [Accessed 2 06 2014].

[97] The MathWorks, Inc., "How can I improve generalization for my Neural Network?," MATLAB Central, 2013. [Online]. Available: http://www.mathworks.com/matlabcentral/answers/97718-how-can-i-improve-generalization-for-my-neural-network. [Accessed 30 05 2014].

APPENDICES

Appendix A: Published papers- acceptance letters
SAE Paper

Dear Kush,

Thank you for your correspondence requesting permission to reprint SAE paper 2014-01-0737 – which you co-authored – in your MASc thesis titled 'Investigation of Laser Clad Bead Geometry to Process Parameter Configuration for Tool Path Generation, Simulation, and Optimization" for University of Windsor. ON, Canada.

Permission is hereby granted, and subject to the following conditions:

Permission is for this one-time single use only. New requests are required for further use or distribution of the SAE material.

The following credit statement must appear on the paper: "Reprinted with permission Copyright © 2014 SAE International. This paper may not be printed, copied, distributed or forwarded without prior permission from SAE."

We also request that you credit the original source (author, paper number and SAE) in the reference section of your thesis.

This permission does not cover any third party copyrighted work which may appear in the material requested.

Please feel free to contact me if you need further assistance. Good luck with your thesis!

Best regards,

Terri Kelly

Intellectual Property Rights Administrator

SAE INTERNATIONAL
400 Commonwealth Drive
Warrendale, PA 15096
o +1.724.772.4095
f +1.724-776-9765
e terri@sae.org
www.sae.org

CIRP CMS Paper

Dear Kush Aggarwal,

Elsevier is very pleased to announce that starting from February 1st, 2014 Procedia journal will be published under Creative commons license, in particular under Creative Commons Attribution Non-Commercial No Derivatives license (CC-BY-NC-ND). CC-BY-NC-ND license gives the authors similar rights to the ones under Procedia Exclusive License agreement.

Under CC-BY-NC-ND the authors would retain:
• Copyright of the article
• Patent, trademark and other intellectual property rights in the article
• The right for proper attribution and credit for the published work
• The right to reuse their own work in the same way readers can as defined by CC-BY-NC-ND license.

Under CC-BY-NC-ND the users are allowed to copy and distribute the article, provided this is not done for commercial purposes and the article is not changed or edited in any way. The author must be attributed and must not be represented as endorsing the use made of the work. This also does not allow users to text or data mine the article. You are invited to visit Elsevier open access page to learn more: http://www.elsevier.com/about/open-access/open-access-policies/oa-license-policy?a=133551.

Please share this information with Procedia authors. The authors will automatically receive a copy of creative commons license that they will need to sign and send back by email to Elsevier.
Kind Regards,
Jeniv

Jeniv Praveen Kumar
Journal Manager - Global Journals Production
Elsevier India
(A division of Reed Elsevier India Pvt. Ltd.)
International Tech Park | Crest – 12th Floor | Taramani Road | Taramani | Chennai 600 113 | India
Tel: +91 44 42994854 |
E-mail: j.praveenkumar@elsevier.com; url: www.elsevier.com
Line Manager: L.Rajaram@elsevier.com

RP Journal Paper

Dear Kush Aggarwal,

Manuscript ID RPJ-02-2014-0025 entitled "Analysis of laser cladding bead morphology for developing additive manufacturing travel paths" which you submitted to the Rapid Prototyping Journal, has been reviewed. The comments of the reviewer(s) are included at the bottom of this letter.

The reviewer(s) have recommended publication, but also suggest some revisions to your manuscript. Therefore, I invite you to respond to the reviewer(s)' comments and revise your manuscript.

To revise your manuscript, log into http://mc.manuscriptcentral.com/rpj and enter your Author Center, where you will find your manuscript title listed under "Manuscripts with Decisions." Under "Actions," click on "Create a Revision." Your manuscript number has been appended to denote a revision.

You will be unable to make your revisions on the originally submitted version of the manuscript. Instead, revise your manuscript using a word processing program and save it on your computer. Please also highlight the changes to your manuscript within the document by using the track changes mode in MS Word or by using bold or colored text.

Once the revised manuscript is prepared, you can upload it and submit it through your Author Center.

When submitting your revised manuscript, you will be able to respond to the comments made by the reviewer(s) in the space provided. You can use this space to document any changes you make to the original manuscript. In order to expedite the processing of the revised manuscript, please be as specific as possible in your response to the reviewer(s).

IMPORTANT: Your original files are available to you when you upload your revised manuscript. Please delete any redundant files before completing the submission.

Because we are trying to facilitate timely publication of manuscripts submitted to the Rapid Prototyping Journal, your revised manuscript should be uploaded as soon as possible. If it is not possible for you to submit your revision in a reasonable amount of time, we may have to consider your paper as a new submission.

Once again, thank you for submitting your manuscript to the Rapid Prototyping Journal

and I look forward to receiving your revision.

Sincerely,
Prof. David Bourell
Regional Editor, Rapid Prototyping Journal
dbourell@mail.utexas.edu

ASME Paper

Congratulations Kush Aggarwal!

The draft you have submitted to IMECE has been accepted. The final version will be eligible for publication in the conference proceedings, provided all required materials and forms are submitted by the stated deadline.

Your paper information is as follows:

Paper Number: IMECE2014-37719
Paper Title: IDENTIFYING RELATIVE IMPORTANCE OF THE INPUT PARAMETER(S) FOR DEVELOPING PREDICTIVE MODEL FOR LASER CLADDING PROCESS

Please incorporate the reviewer comments and my comments into your final version. The detailed comments of the reviewers are available at
the http://www.asmeconferences.org/congress2014 web site. Please log in as Returning Author to see these comments.

--- My Comments ---

Acceptable. Please make appropriate revisions, and submit final paper.

--- End Comments ---

When you have completed your final version, please login to your IMECE author account and submit it online. You will receive on-screen confirmation of your submission, as well as an e-mail confirmation.

The maximum number of technical publications, presentations only, and posters that an individual can be an author or co-author for is limited to 6, which includes a maximum of 4 technical publications. The exception to this policy requires the recommendation by the responsible topic chair and track chair, and the approval of the Congress Technical Program Chair.

Congratulations again and thank you for your interest and participation in IMECE.

http://www.asmeconferences.org/congress2014

Appendix B: Single pass forward network results

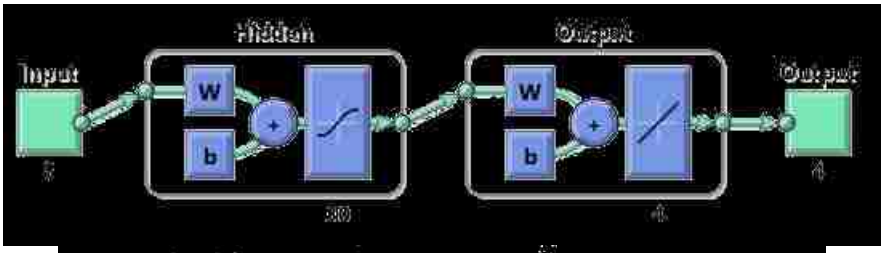

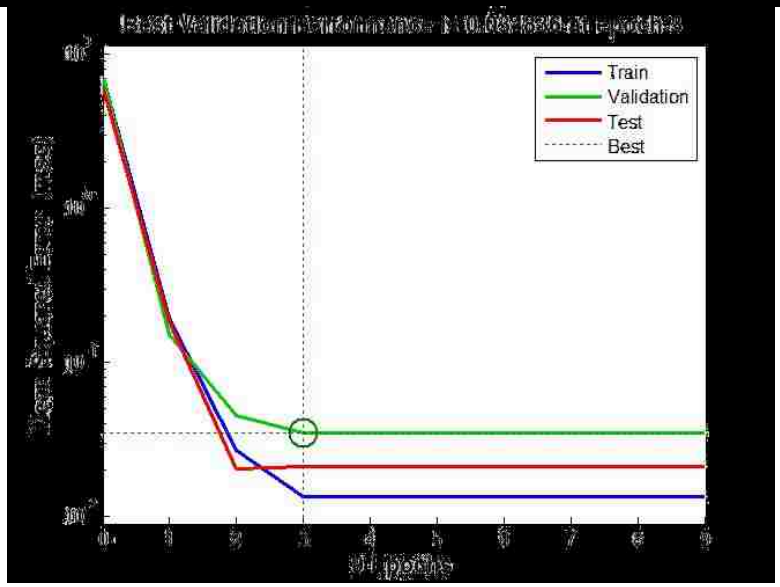

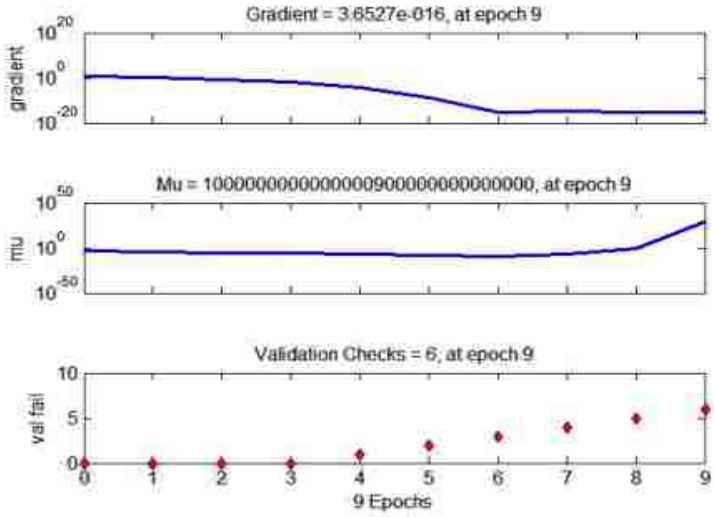

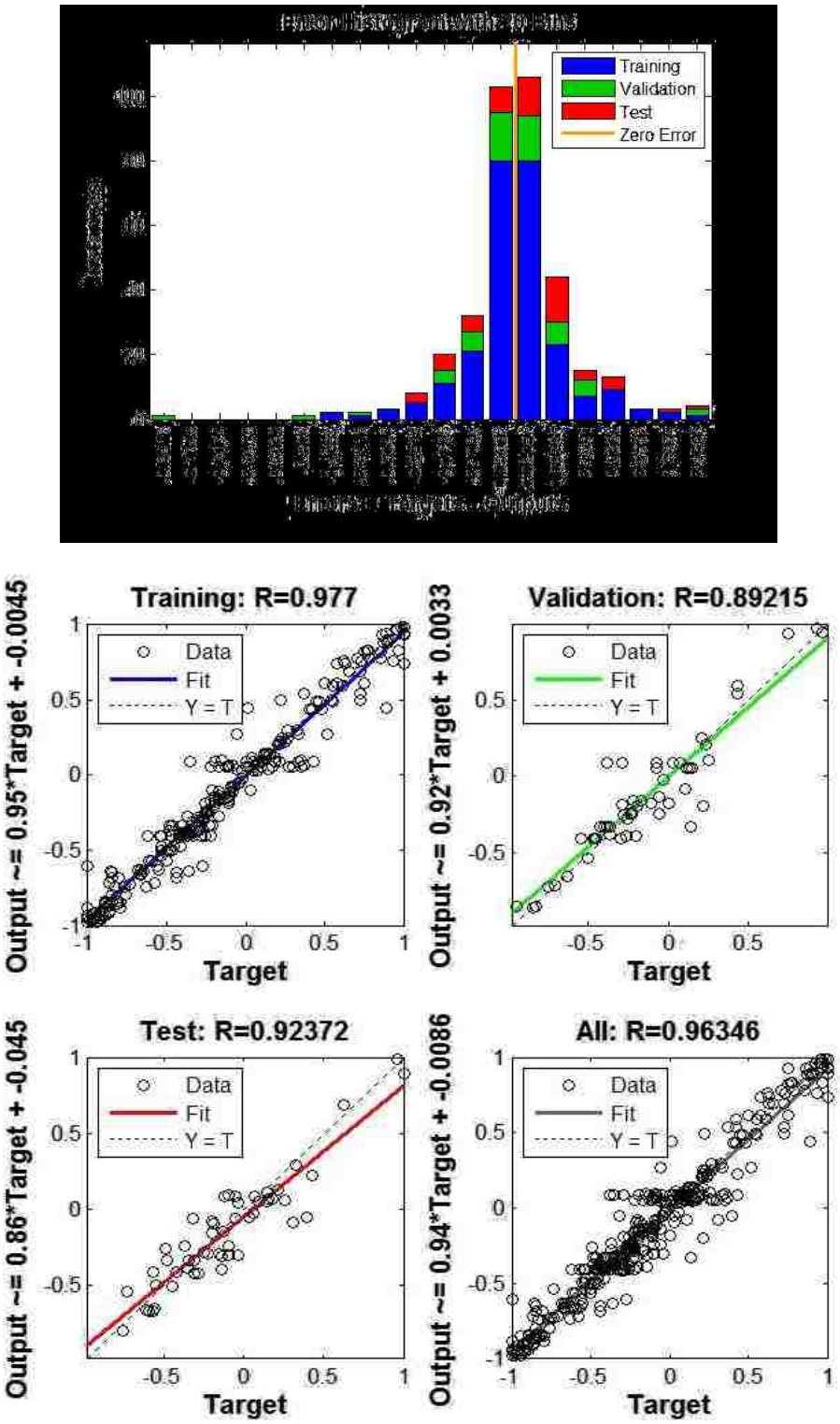

Figure 78: Training results for the single pass forward network

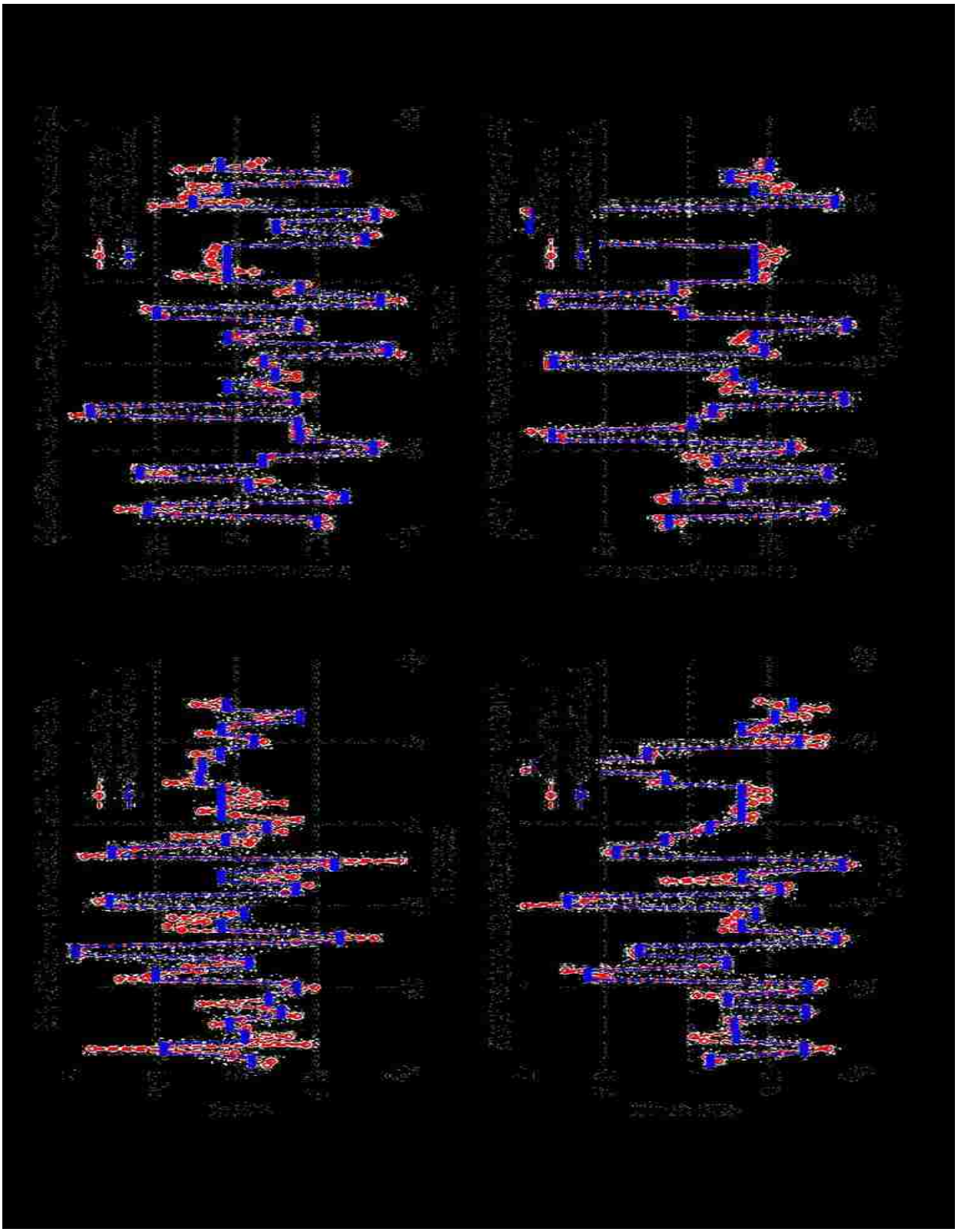

Figure 79: Training output vs network output plots for the single pass 420 steel forward network

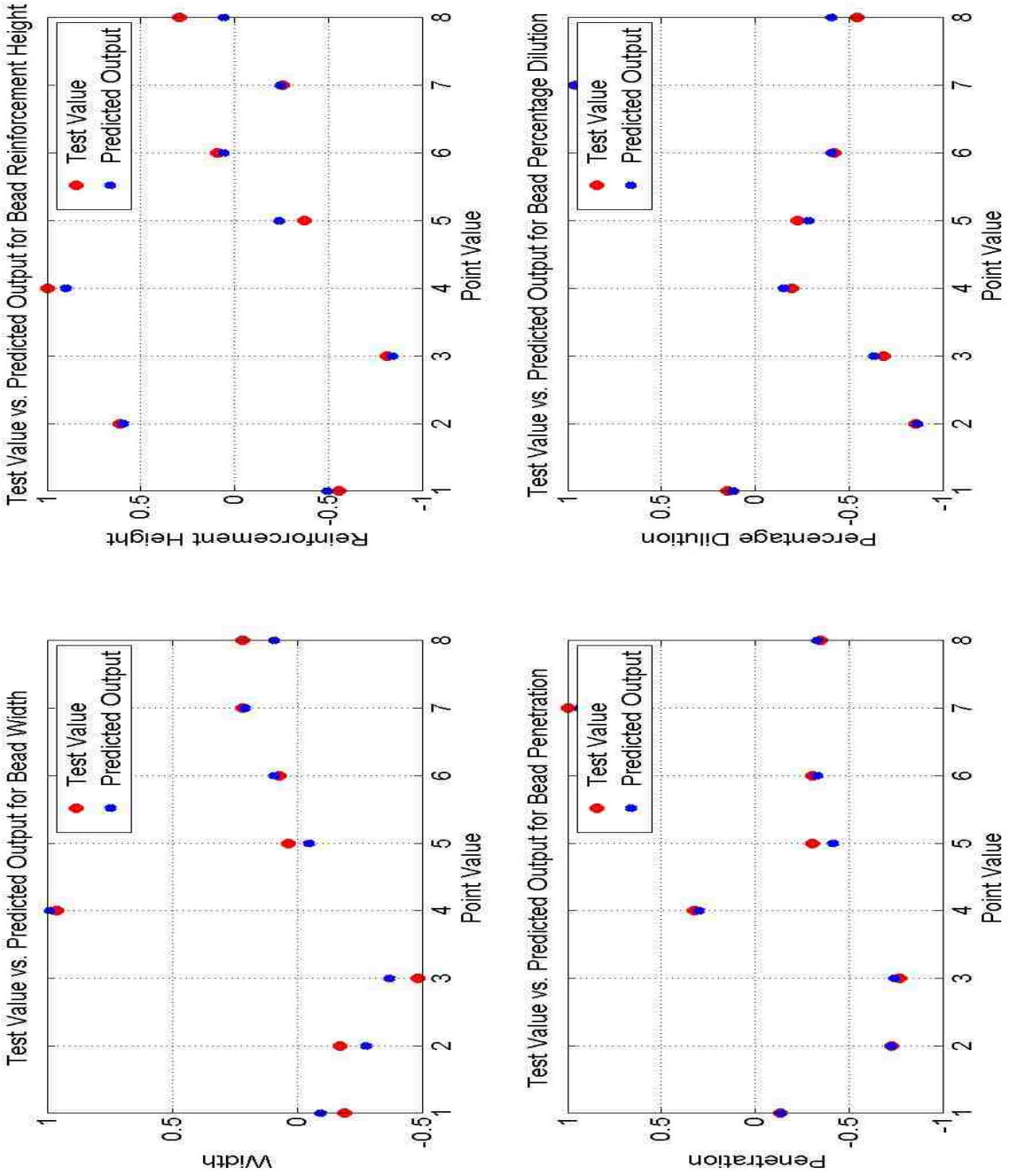

Figure 80: Test output vs predicted output plots for the single pass forward network

Appendix C: Single pass backward network results

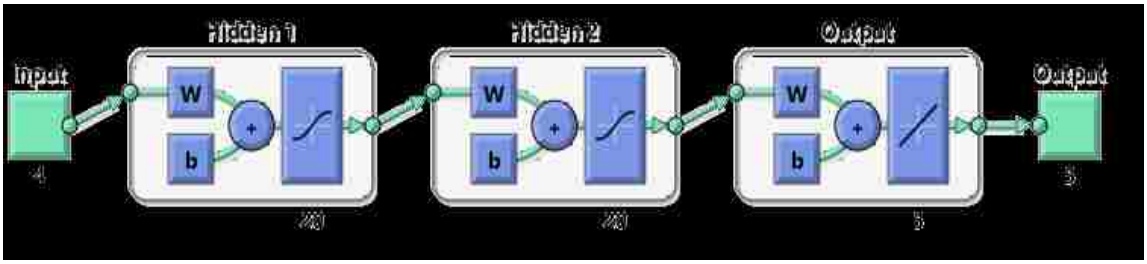

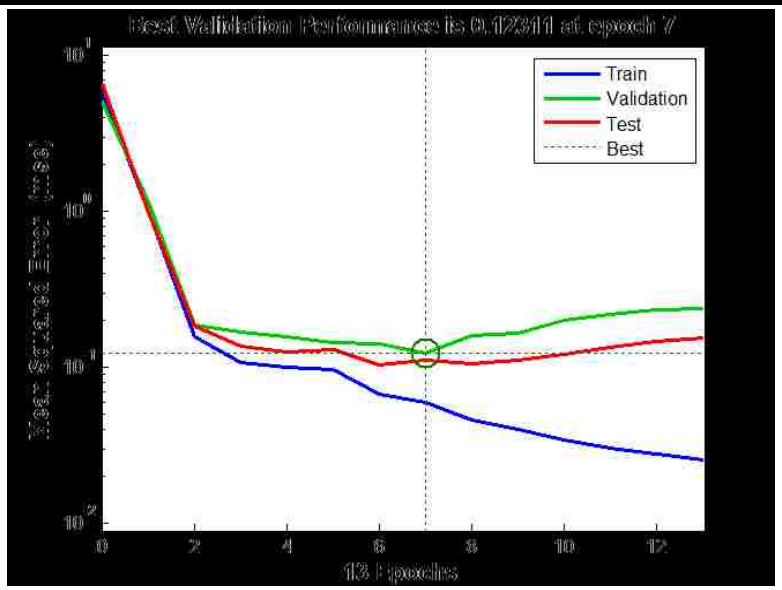

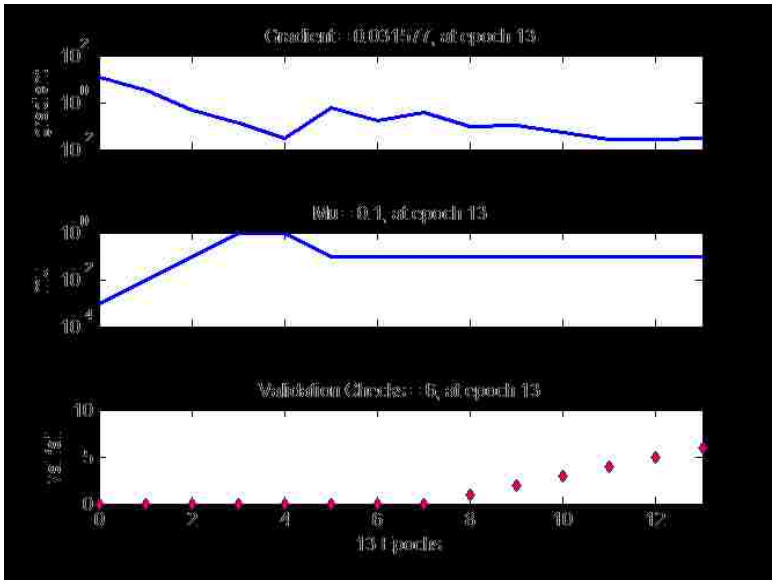

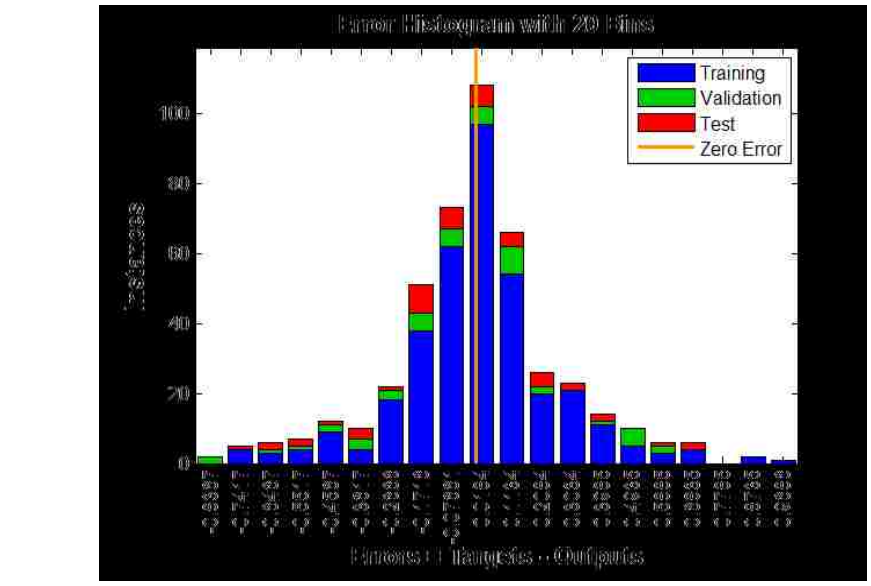

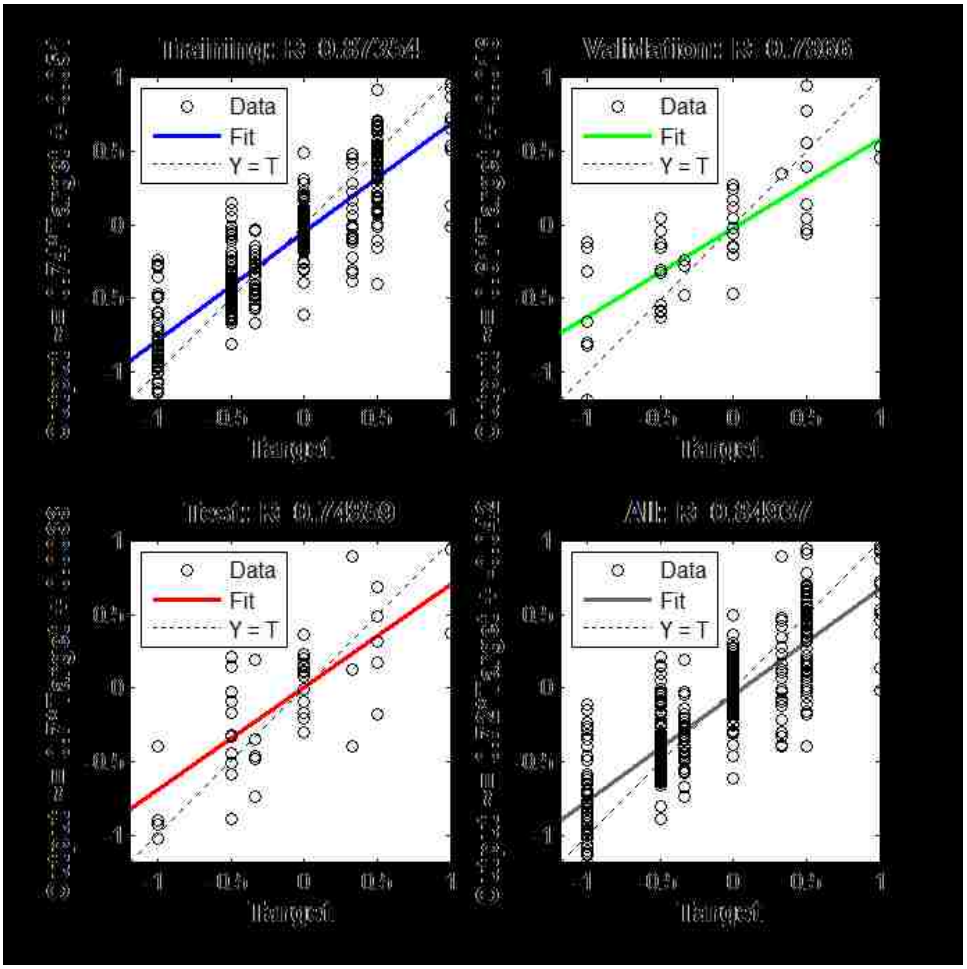

Figure 81: Training results for the single pass backward network

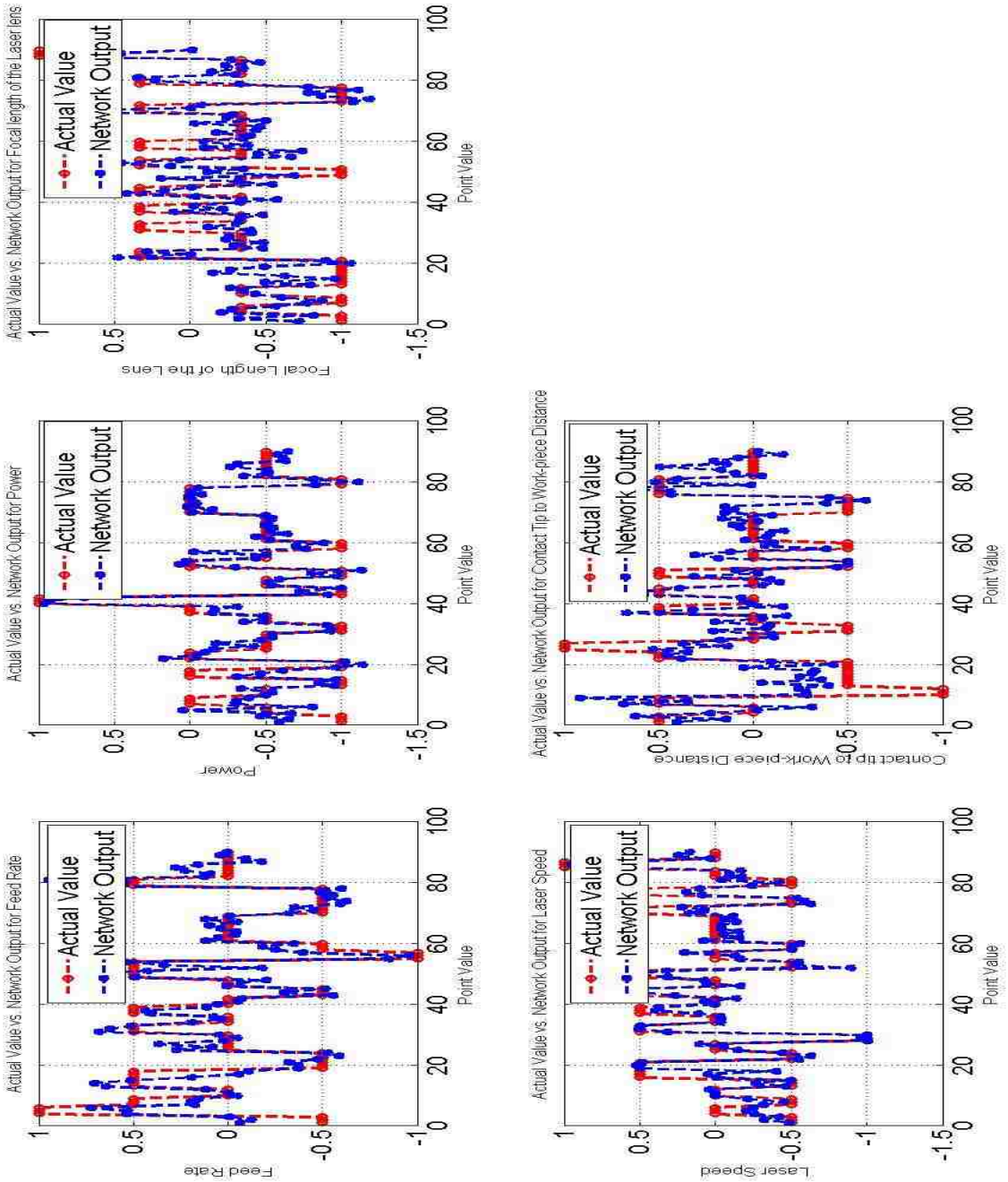

Figure 82: Training output vs network output plots for the single pass 420 steel backward network

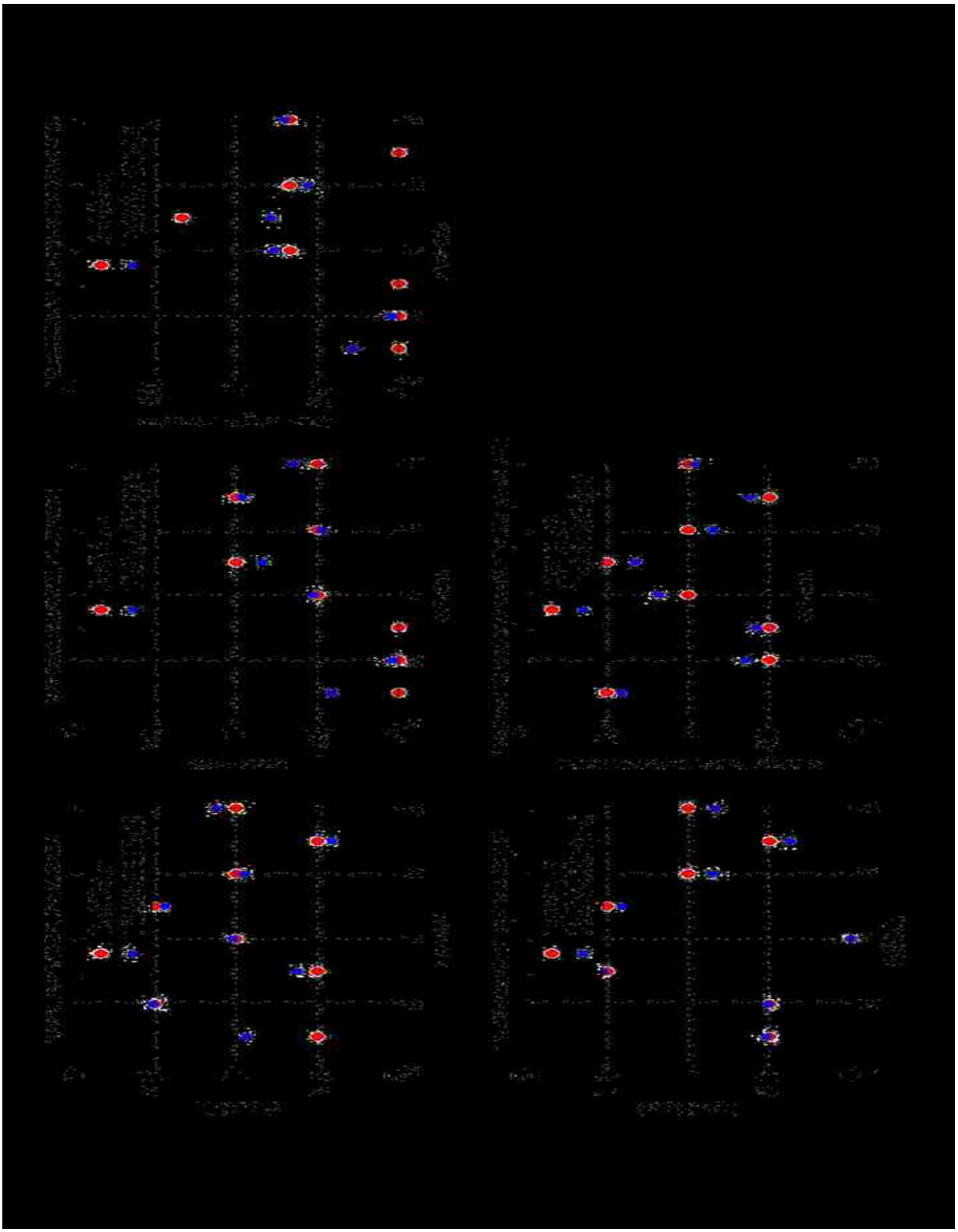

Figure 83: Test output vs predicted output plots for the single pass backward network

Appendix D: 40% overlap configuration forward network results

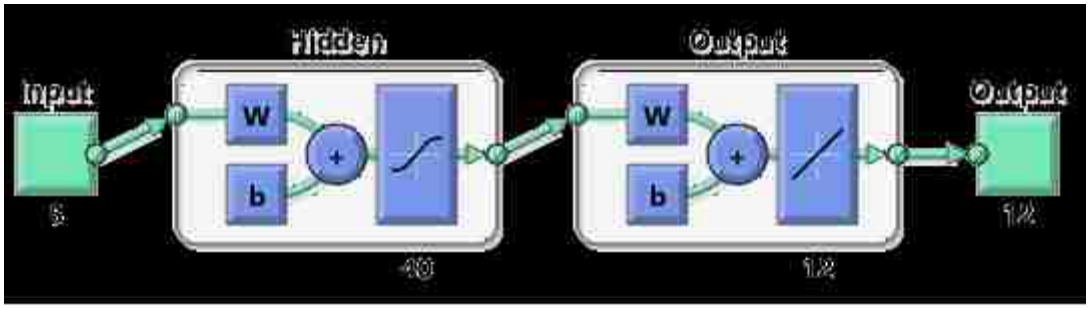

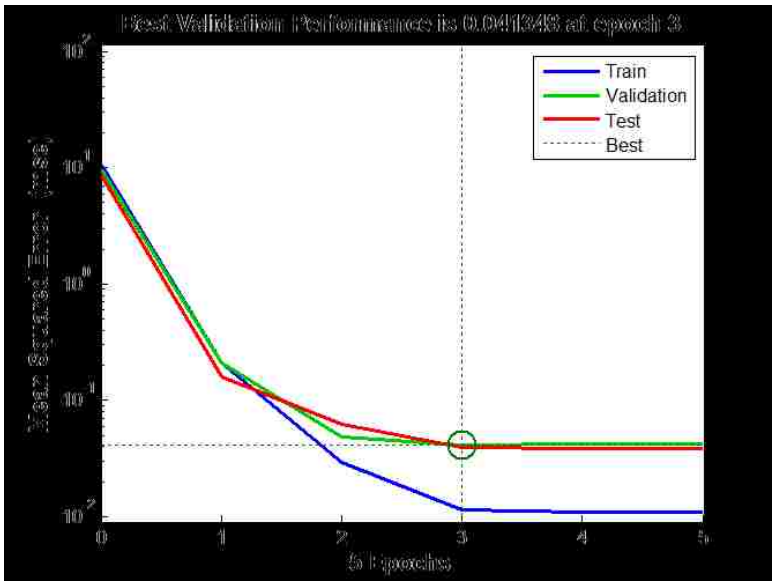

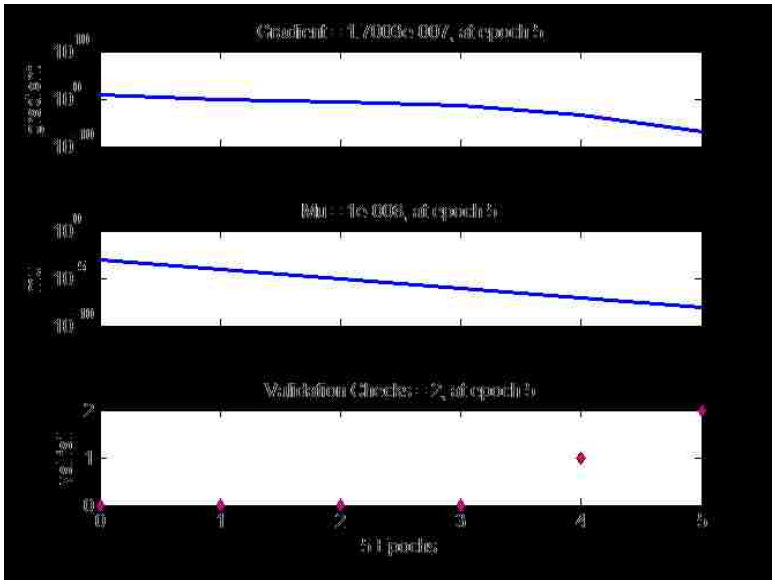

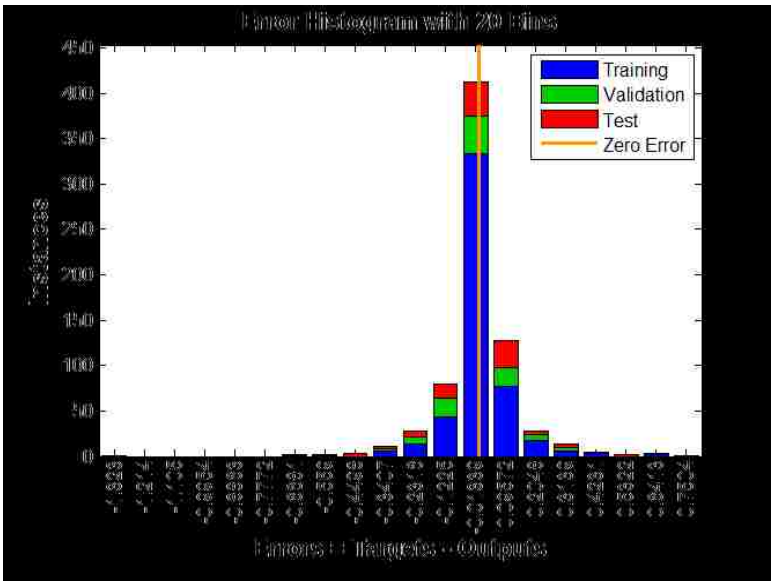

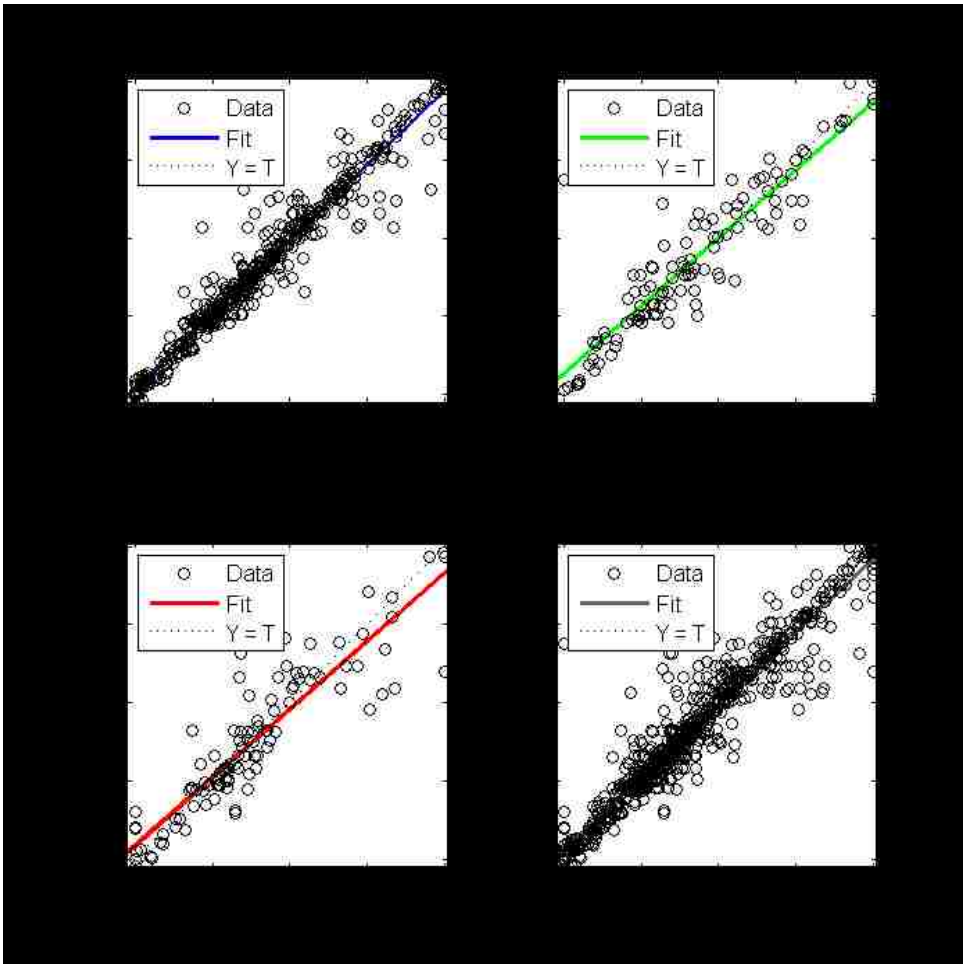

Figure 84: Training results for the 40% overlap pass forward network

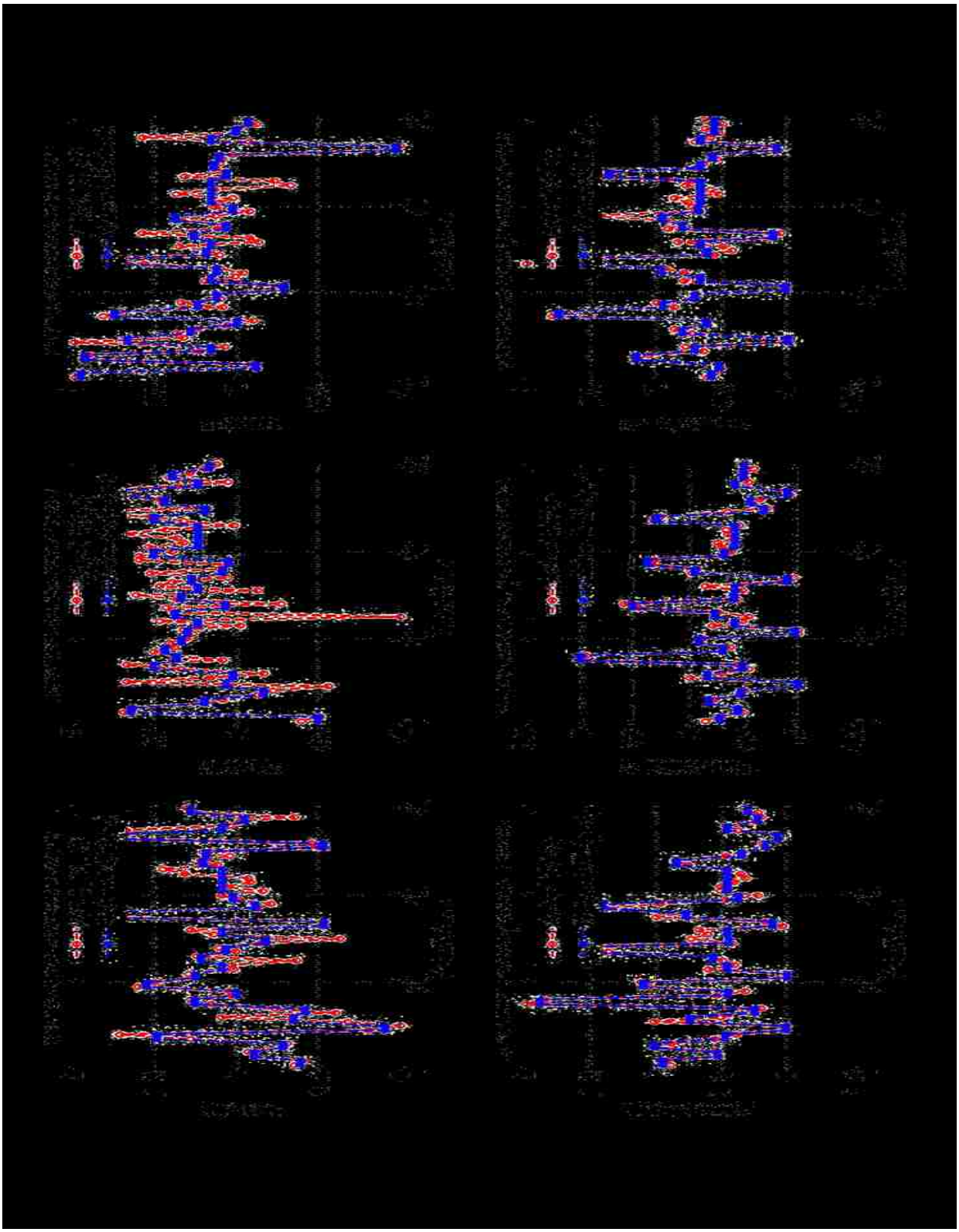

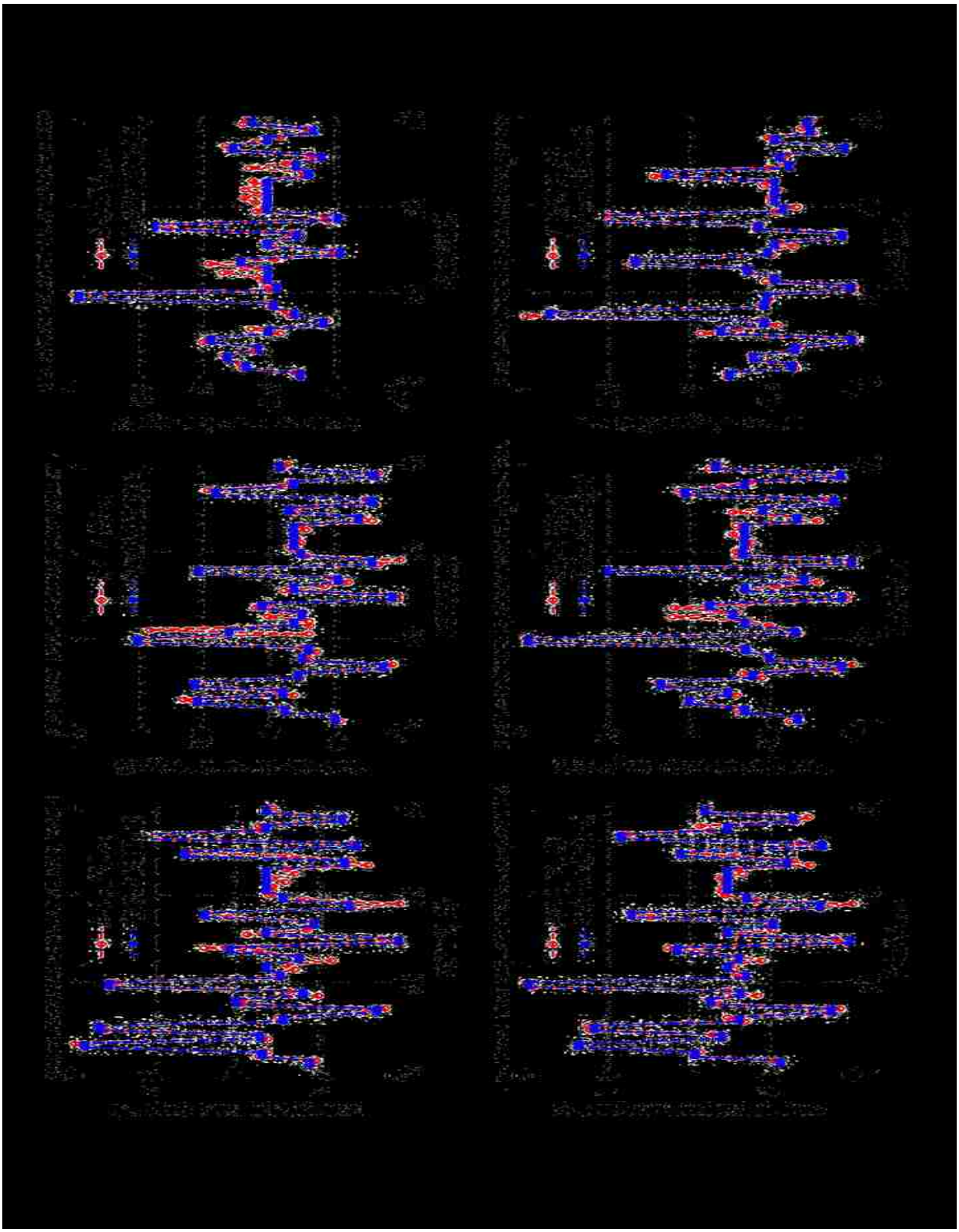

Figure 85: Training output vs network output plots for the 40% overlap pass forward network

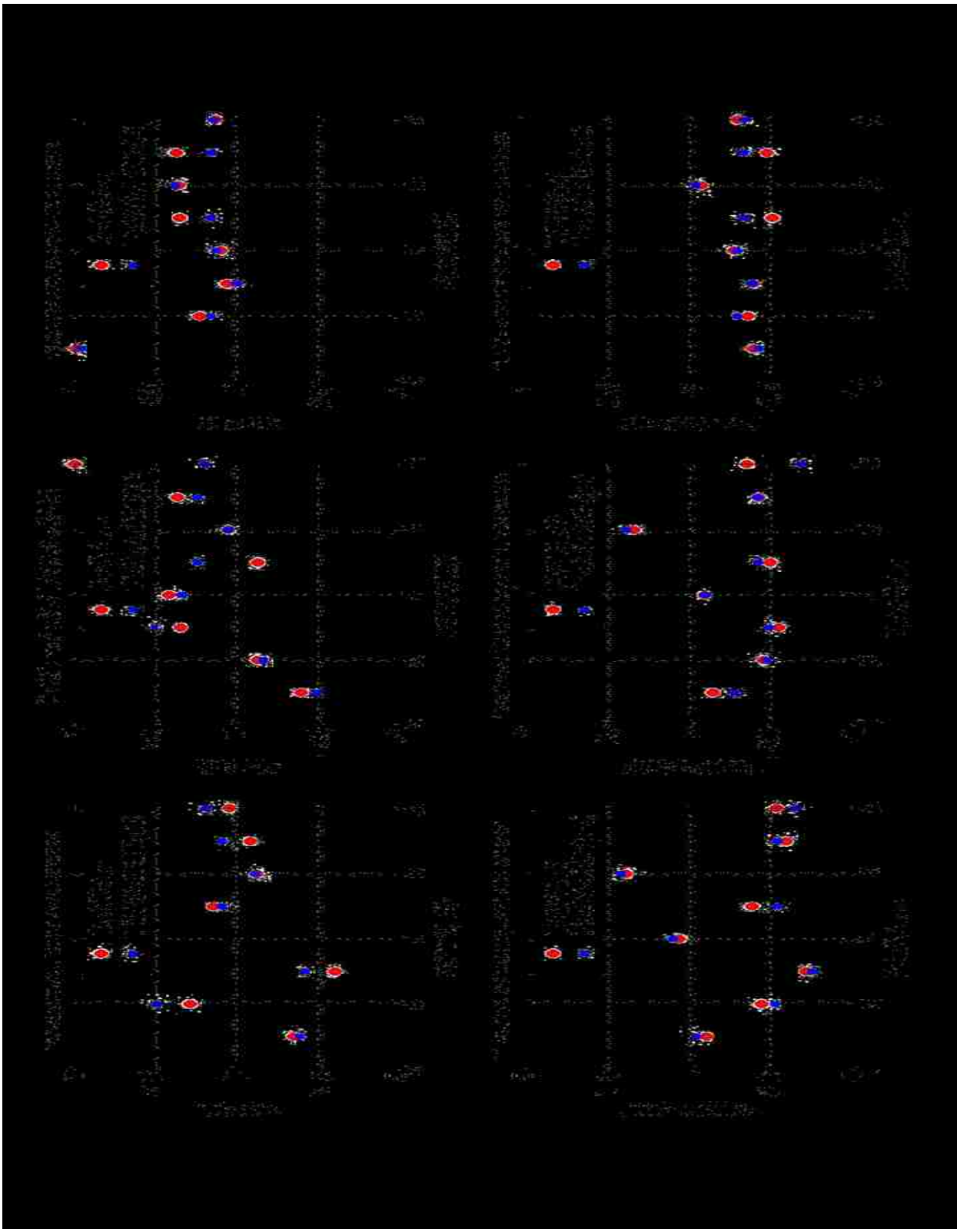

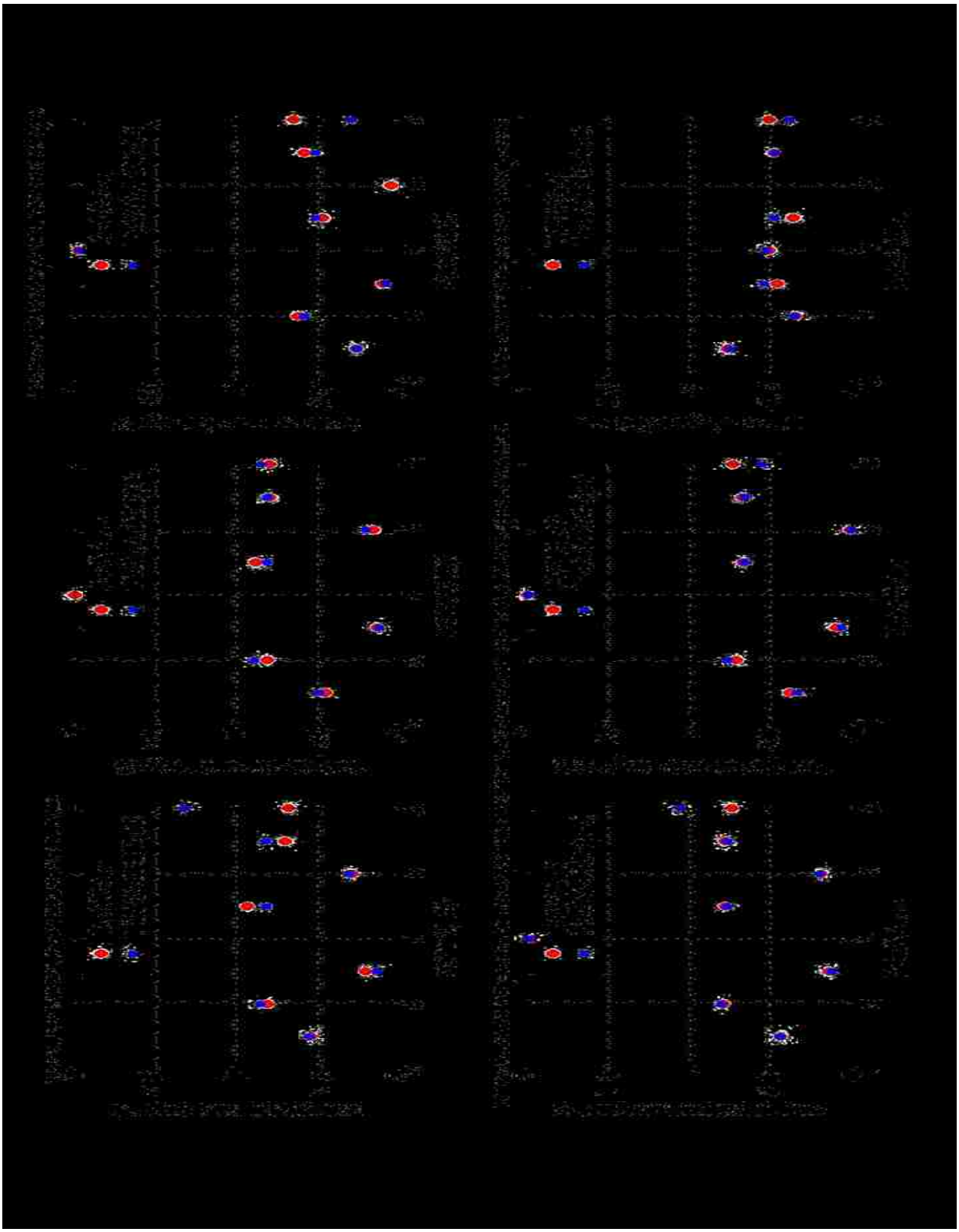

Figure 86: Test output vs predicted output plots for the 40% overlap pass forward network

Appendix E: 50% overlap configuration forward network results

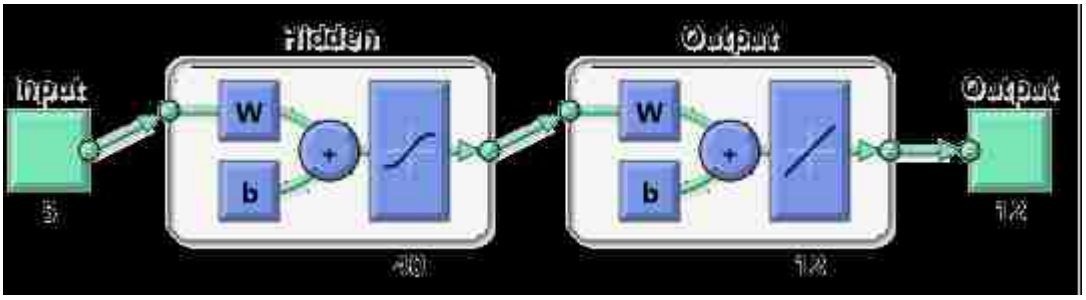

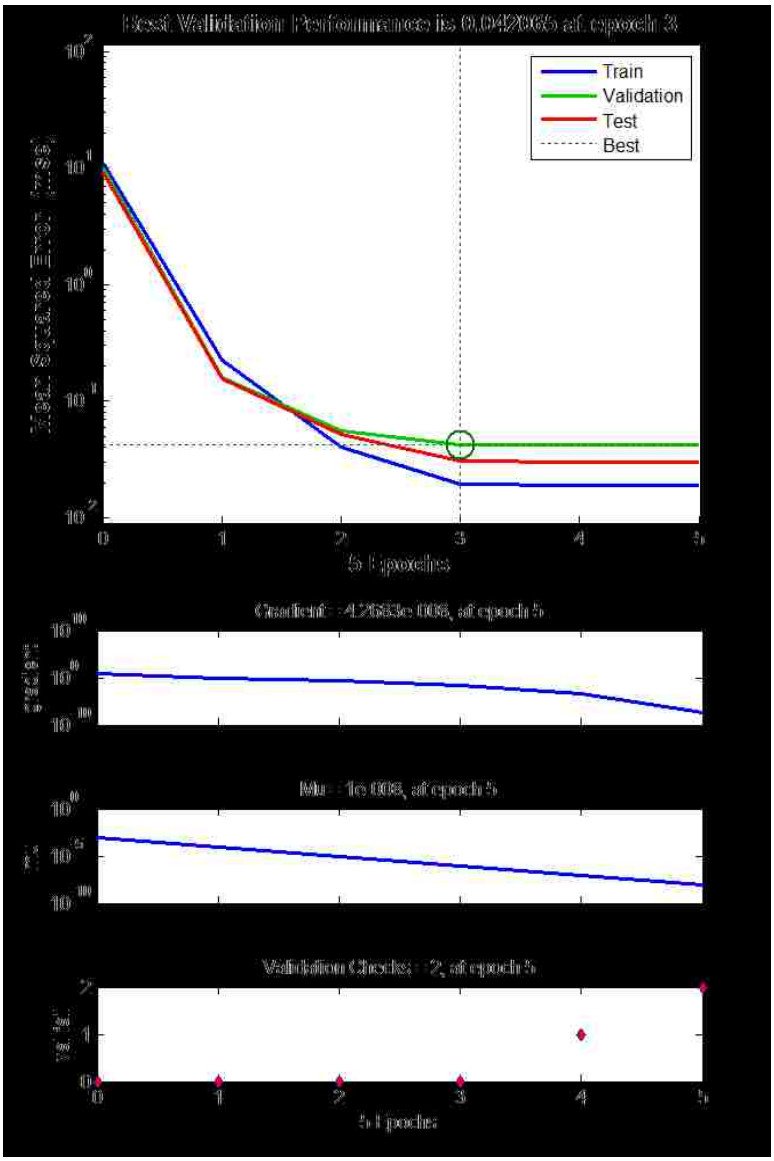

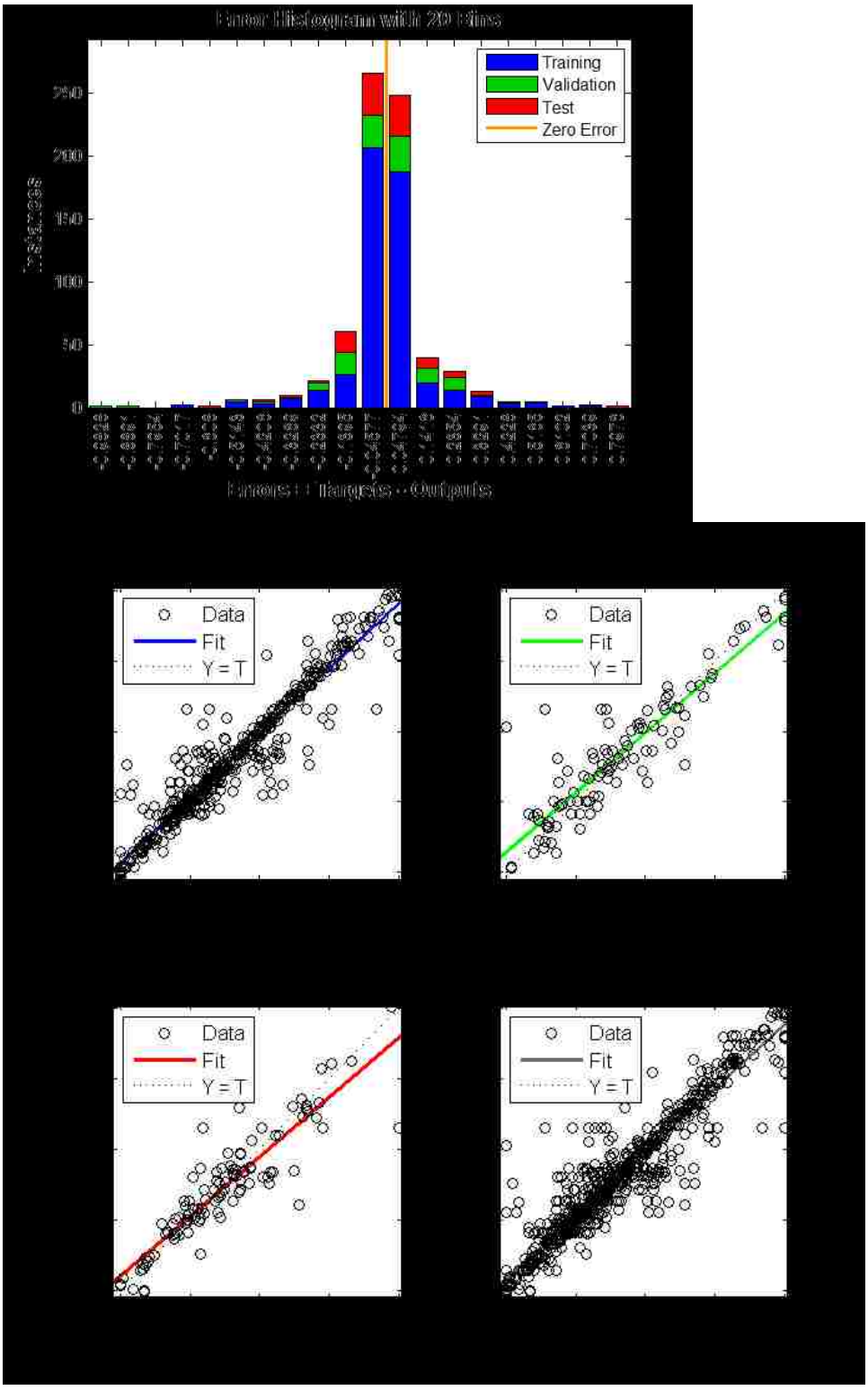

Figure 87: Training results for the 50% overlap pass forward network

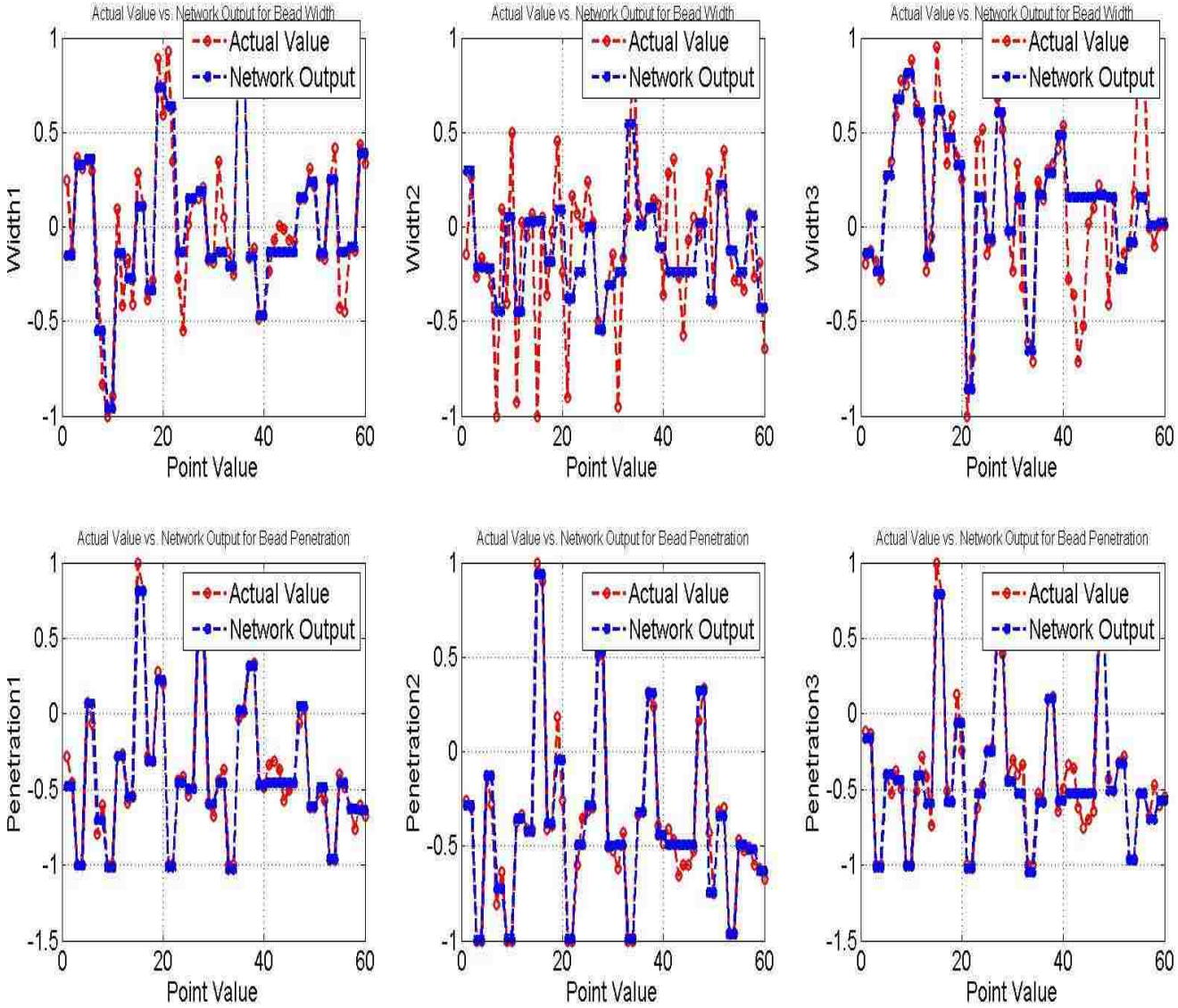
Actual Value vs. Network Output for Bead Width
Actual Value
Network Output
Width1
Point Value
Actual Value vs. Network Output for Bead Width
Actual Value
Network Output
Width2
Point Value
Actual Value vs. Network Output for Bead Width
Actual Value
Network Output
Width3
Point Value
Actual Value vs. Network Output for Bead Penetration
Actual Value
Network Output
Penetration1
Point Value
Actual Value vs. Network Output for Bead Penetration
Actual Value
Network Output
Penetration2
Point Value
Actual Value vs. Network Output for Bead Penetration
Actual Value
Network Output
Penetration3
Point Value

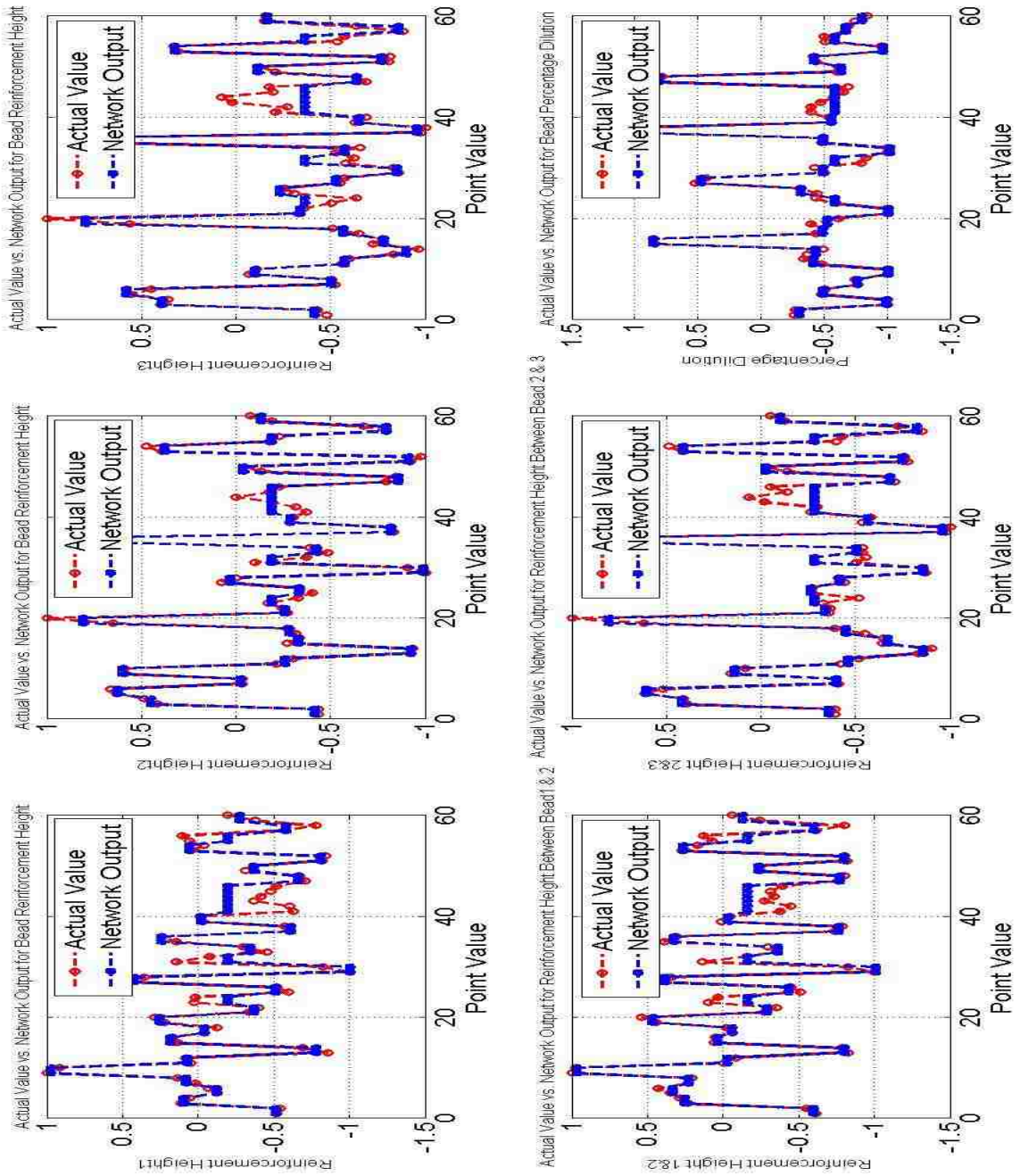

Figure 88: Training output vs network output plots for the 50% overlap pass forward network

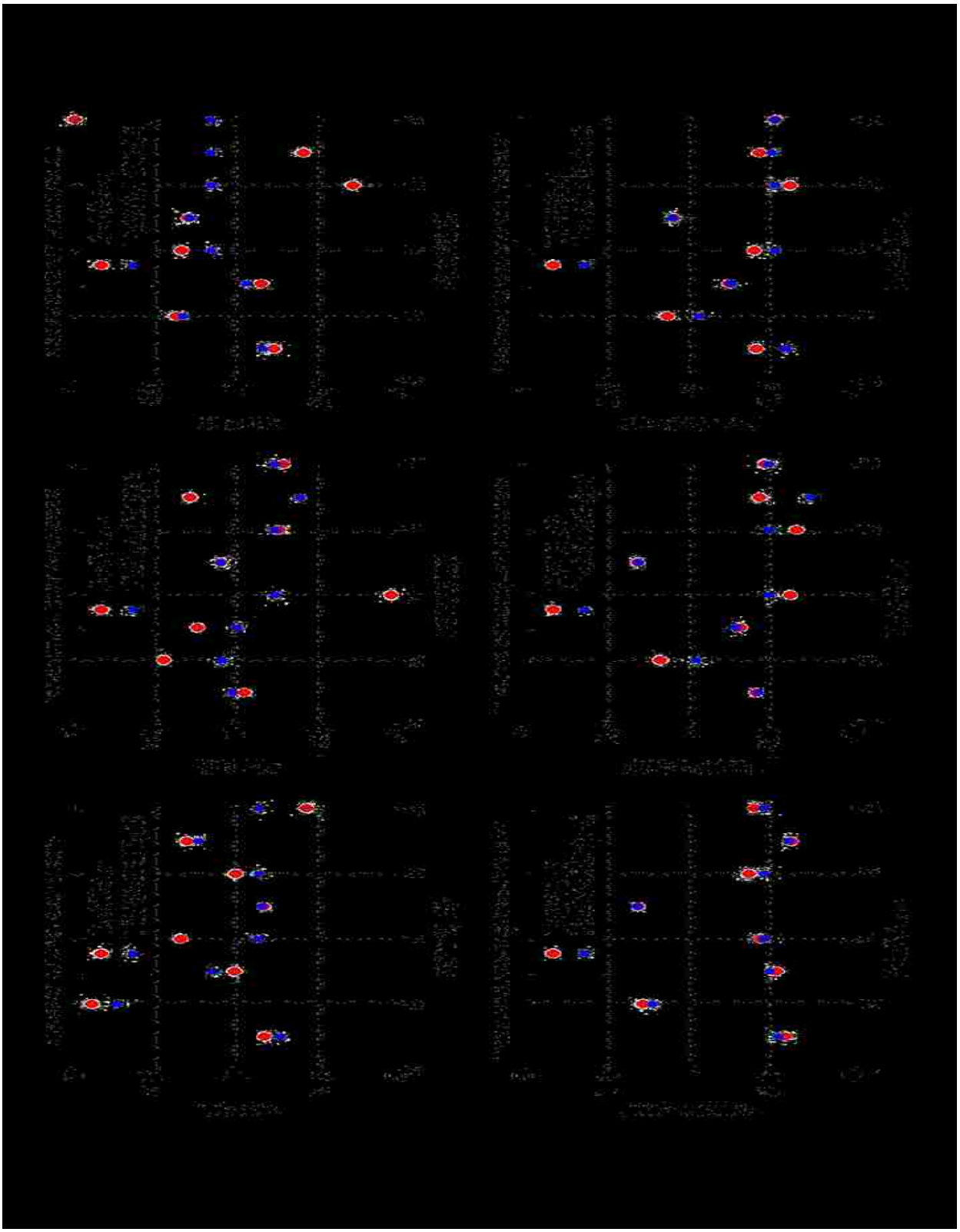

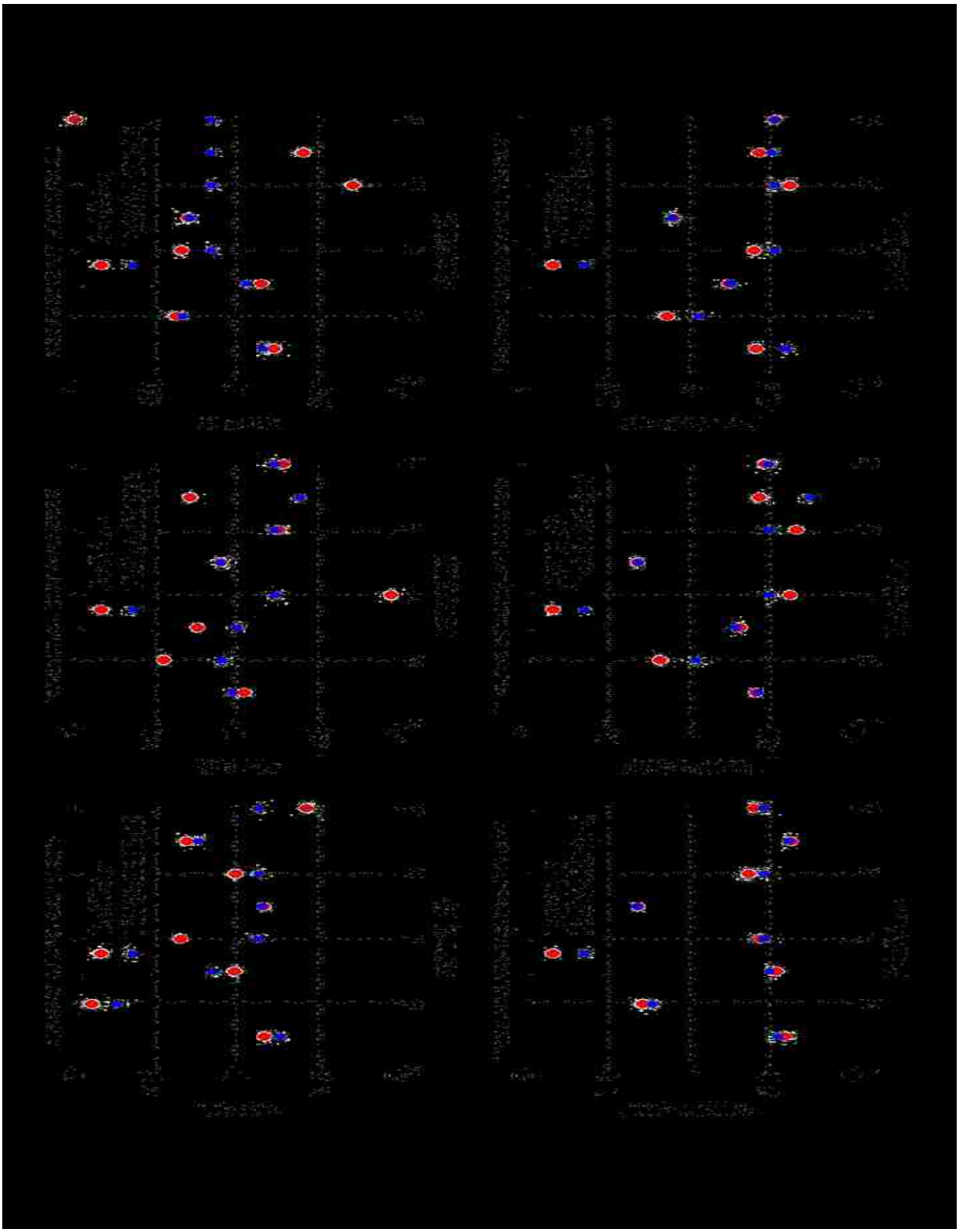

Figure 89: Test output vs predicted output plots for the 50% overlap pass forward network

Appendix F: 60% overlap configuration forward network results

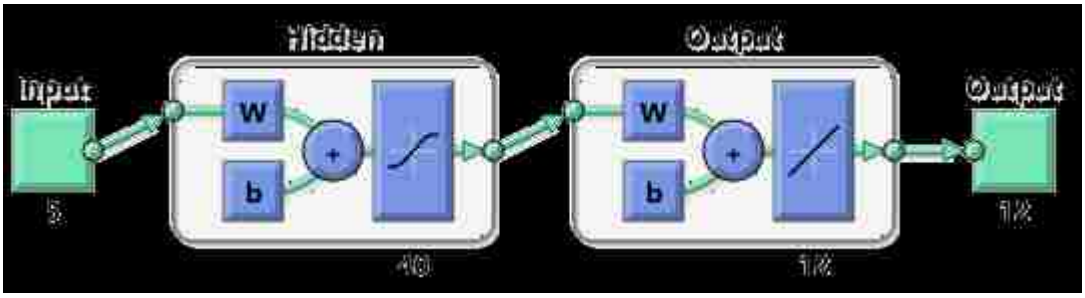

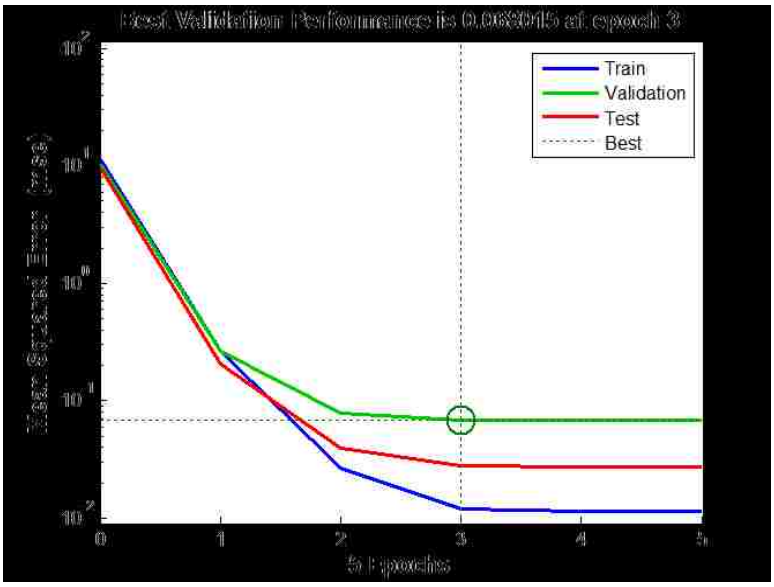

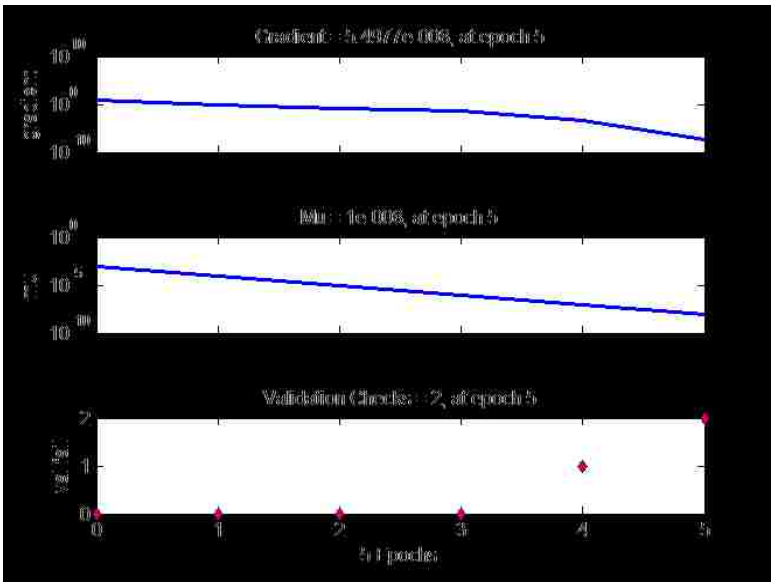

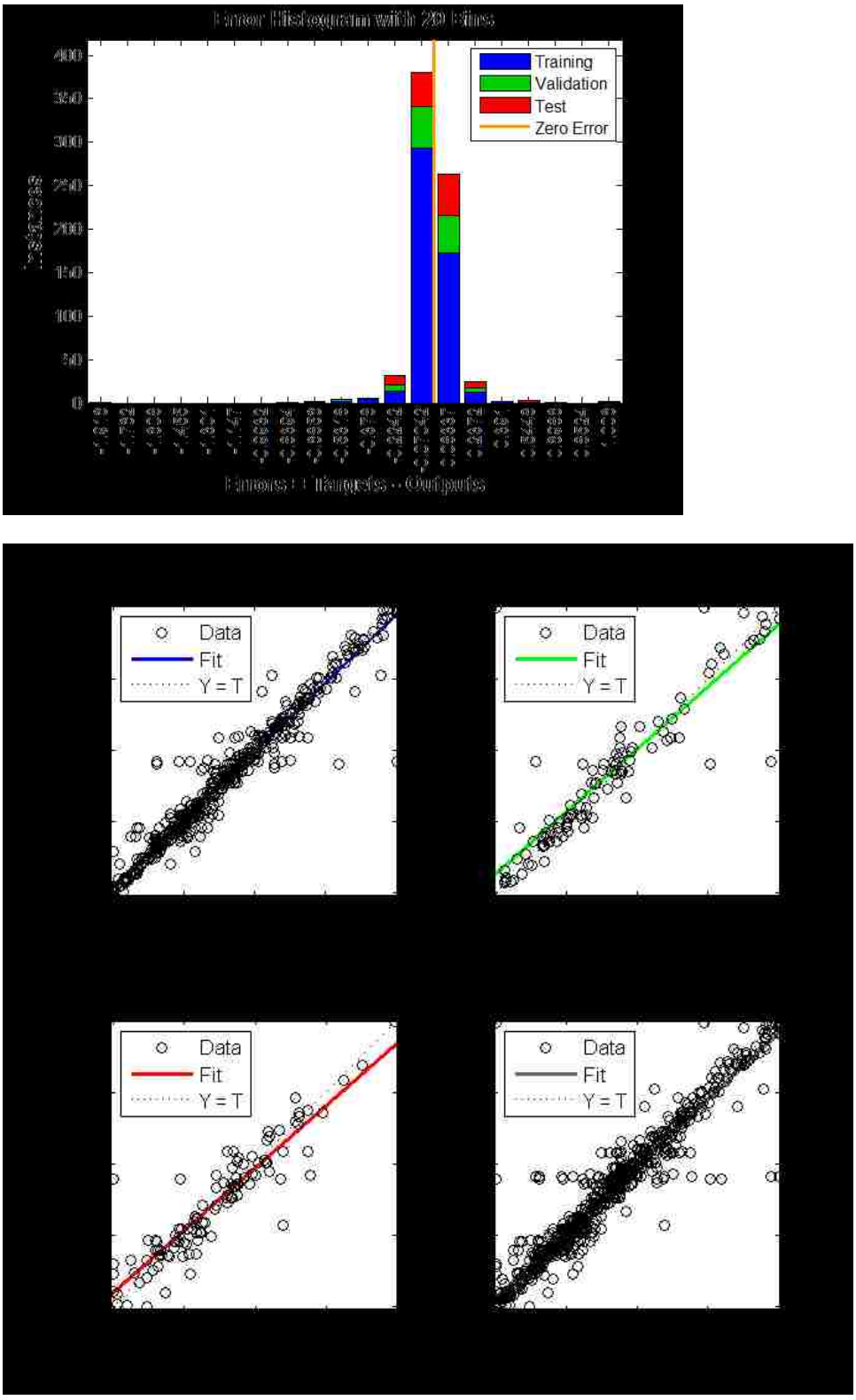

Figure 90: Training results for the 60% overlap pass forward network

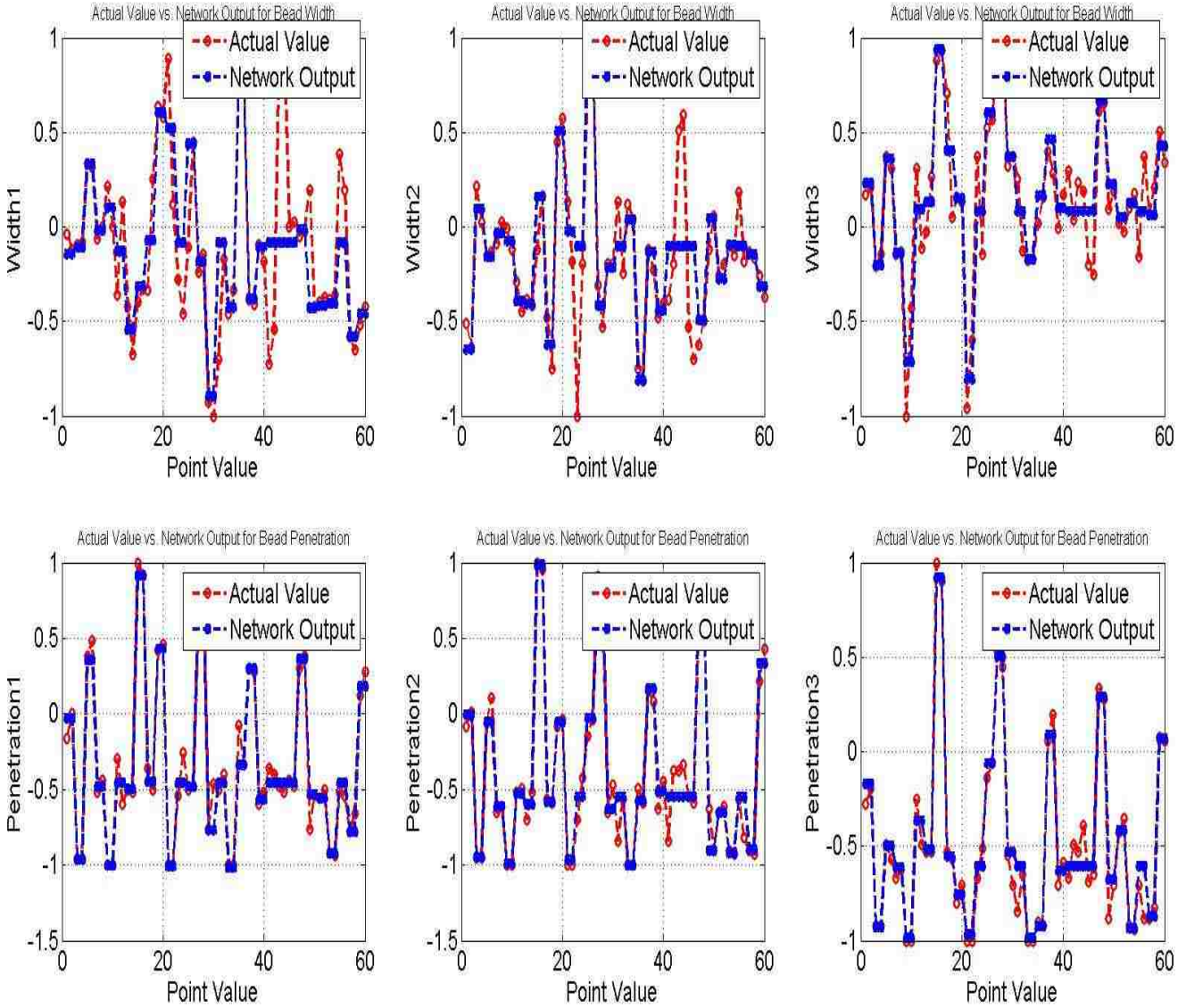
Actual Value vs. Network Output for Bead Width
Actual Value
Network Output
Width1
Point Value
Actual Value vs. Network Output for Bead Width
Actual Value
Network Output
Width2
Point Value
Actual Value vs. Network Output for Bead Width
Actual Value
Network Output
Width3
Point Value
Actual Value vs. Network Output for Bead Penetration
Actual Value
Network Output
Penetration1
Point Value
Actual Value vs. Network Output for Bead Penetration
Actual Value
Network Output
Penetration2
Point Value
Actual Value vs. Network Output for Bead Penetration
Actual Value
Network Output
Penetration3
Point Value

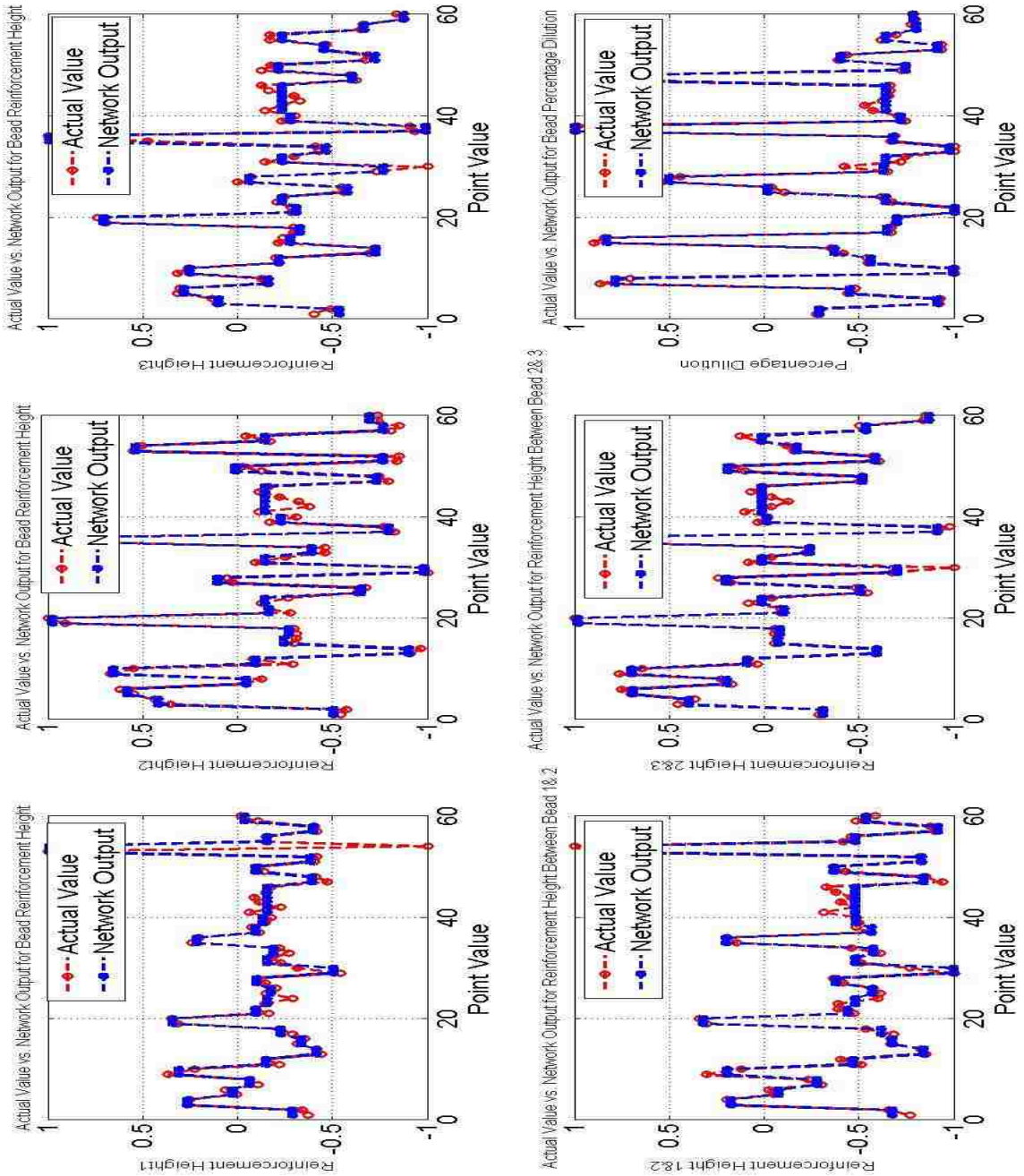

Figure 91: Training output vs network output plots for the 60% overlap pass forward network

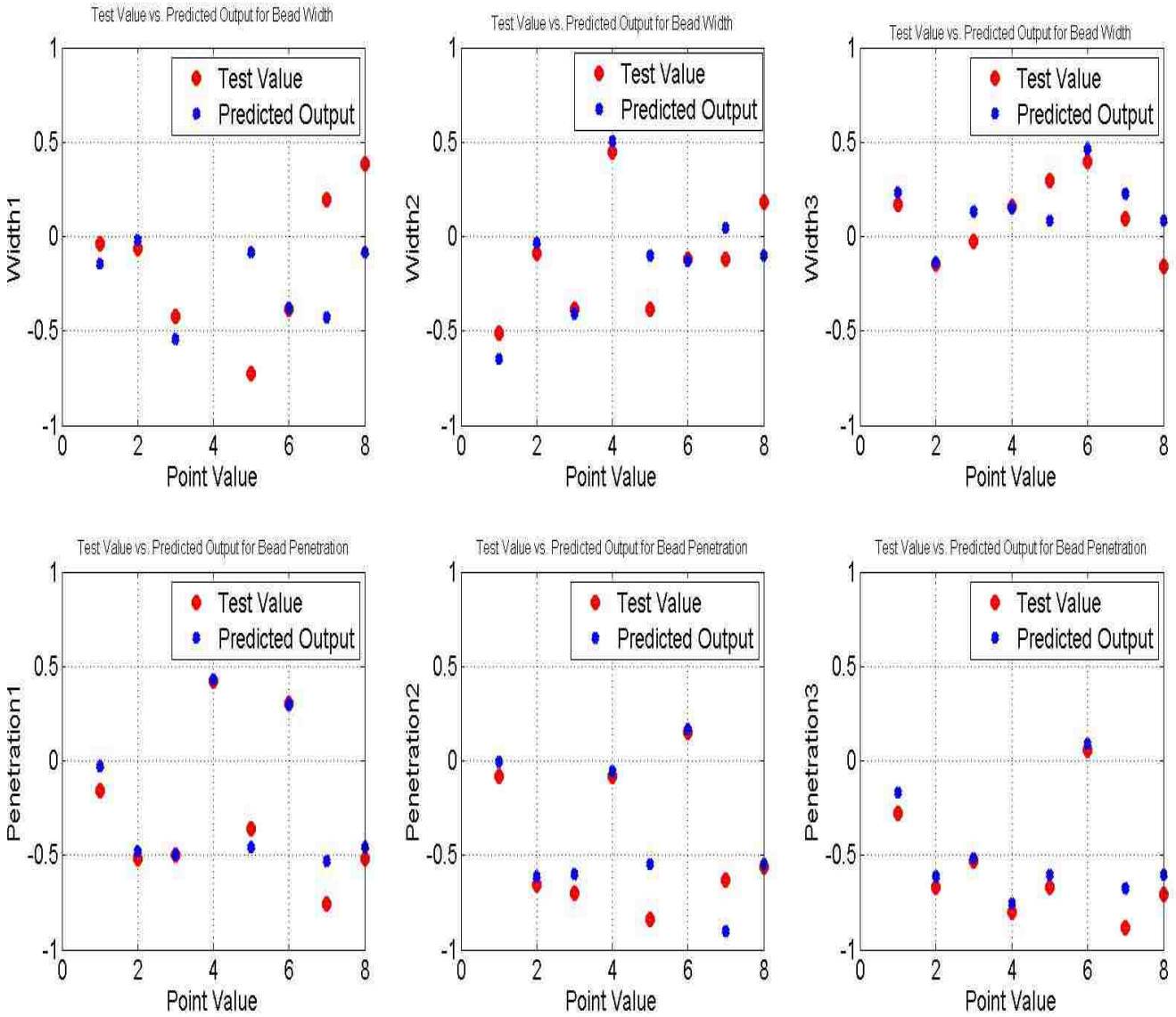
Test Value vs. Predicted Output for Bead Width
Test Value
Predicted Output
Width1
Point Value
Test Value vs. Predicted Output for Bead Width
Test Value
Predicted Output
Width2
Point Value
Test Value vs. Predicted Output for Bead Width
Test Value
Predicted Output
Width3
Point Value
Test Value vs. Predicted Output for Bead Penetration
Test Value
Predicted Output
Penetration1
Point Value
Test Value vs. Predicted Output for Bead Penetration
Test Value
Predicted Output
Penetration2
Point Value
Test Value vs. Predicted Output for Bead Penetration
Test Value
Predicted Output
Penetration3
Point Value

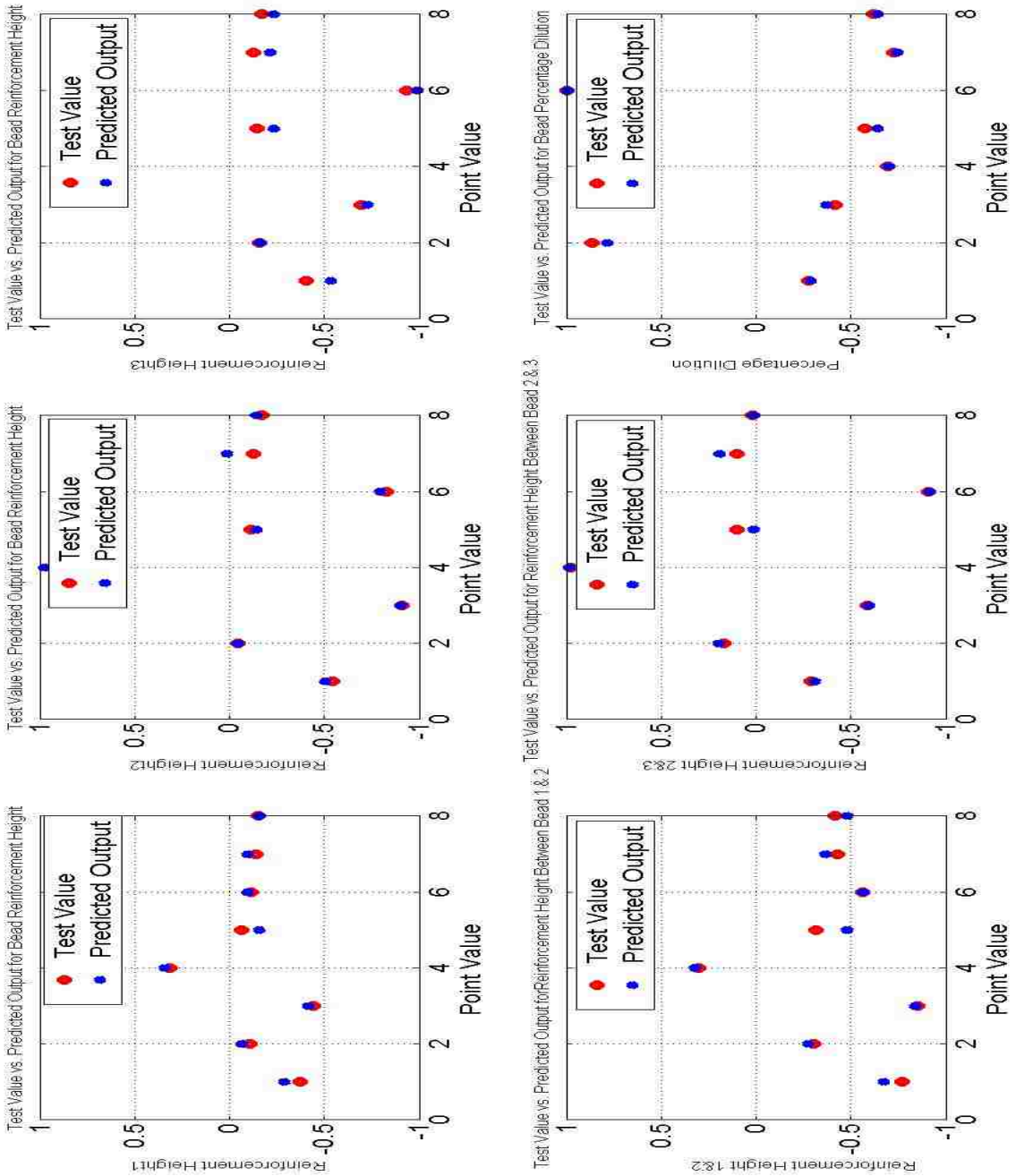

Figure 92: Test output vs predicted output plots for the 60% overlap pass forward network

Appendix G: 40% overlap configuration backward network results

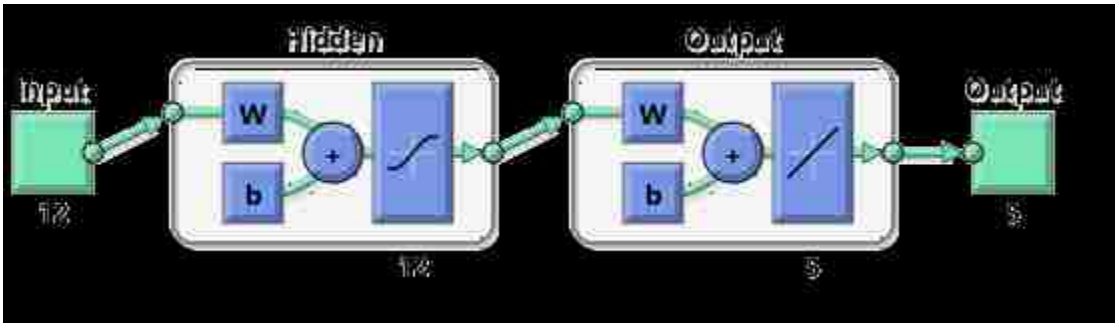

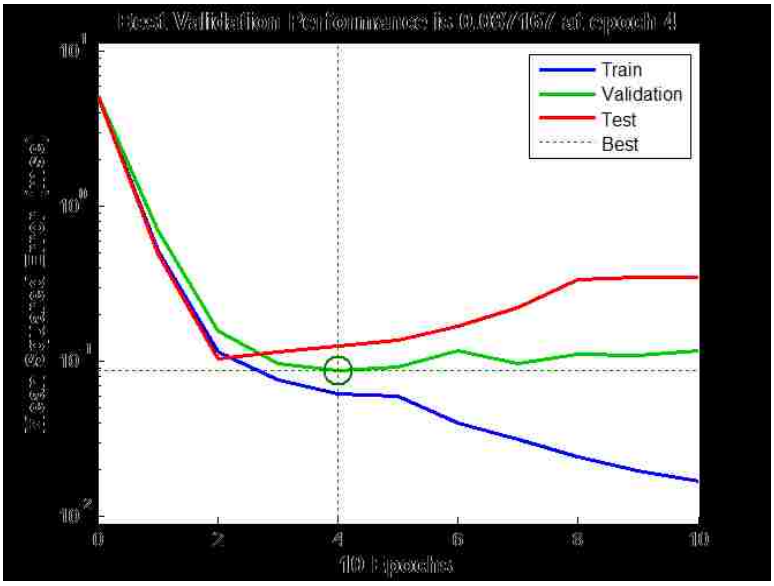

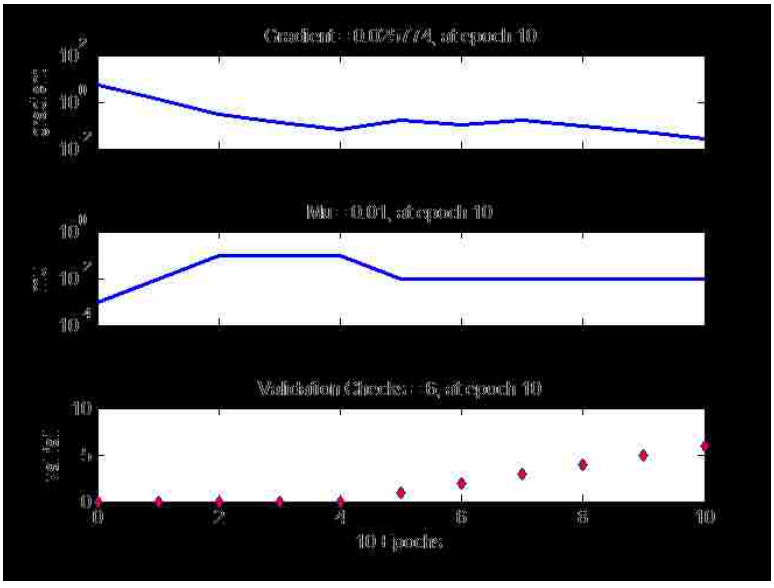

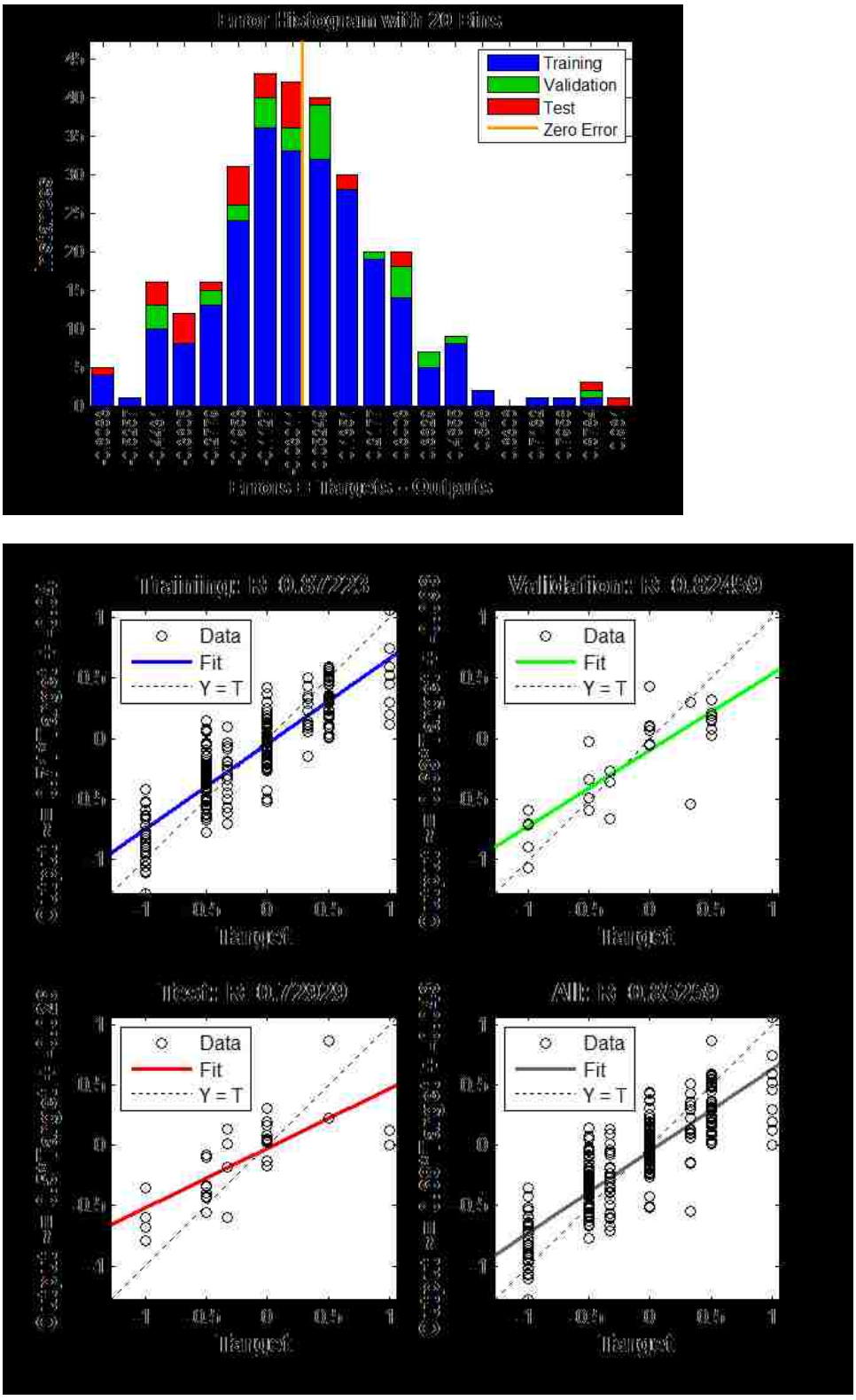

Figure 93: Training results for the 40% overlap pass backward network

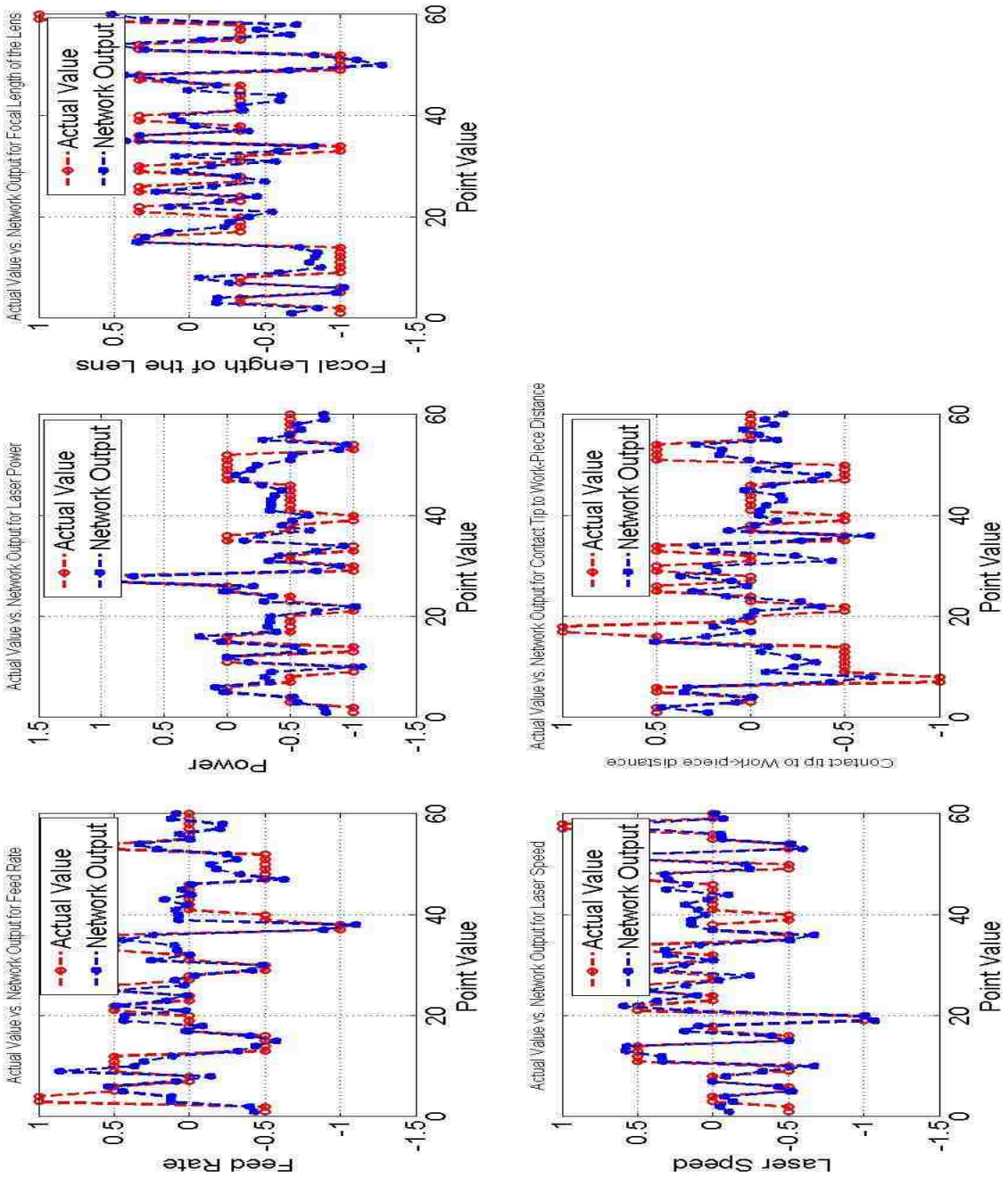

Figure 94: Training output vs network output plots for the 40% overlap pass backward network

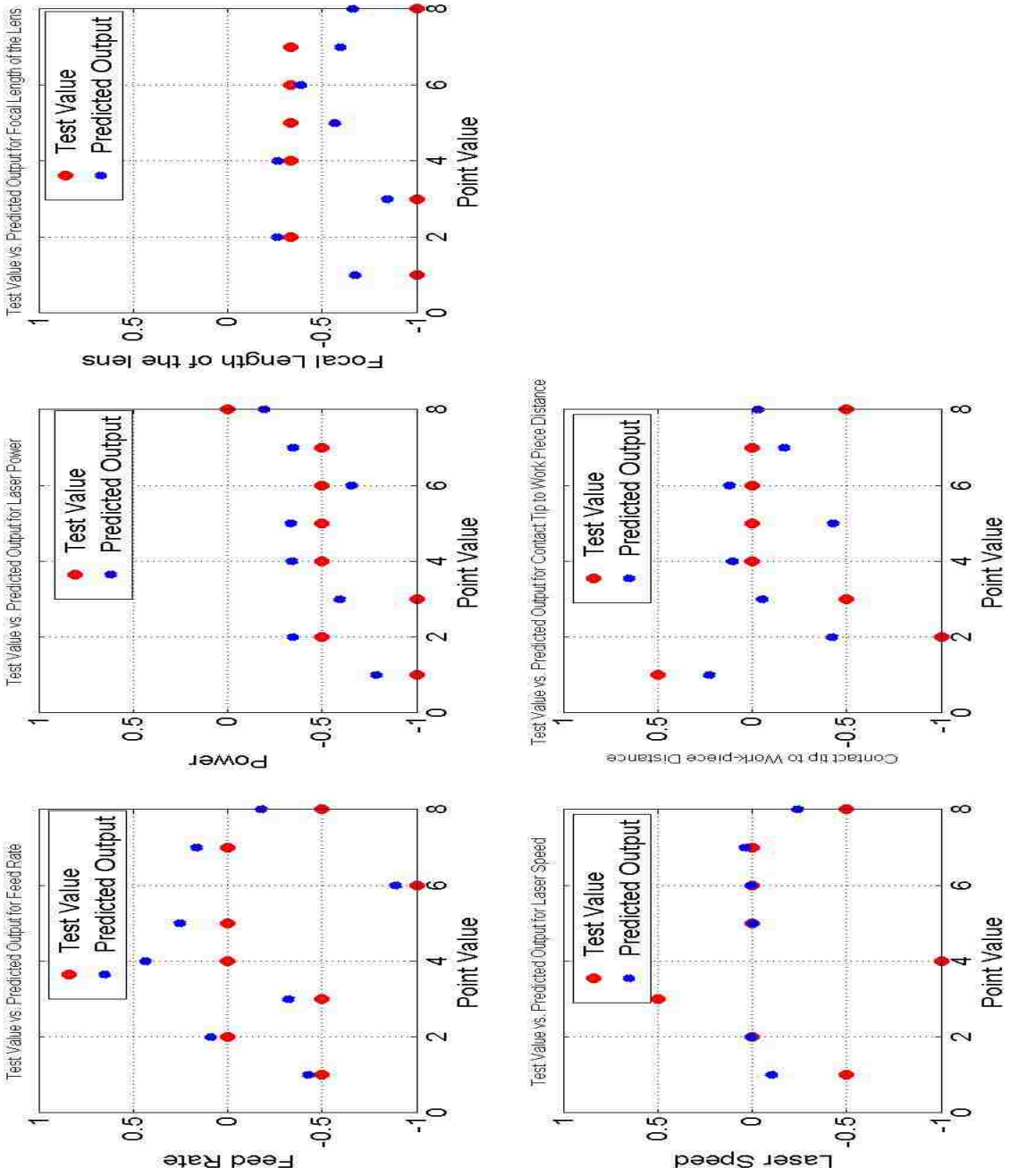

Figure 95: Test output vs predicted output plots for the 40% overlap pass backward network

Appendix H: 50% overlap configuration backward network results

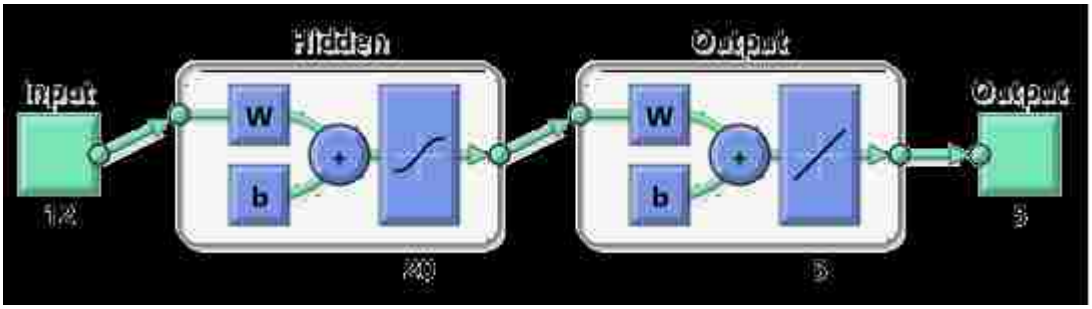

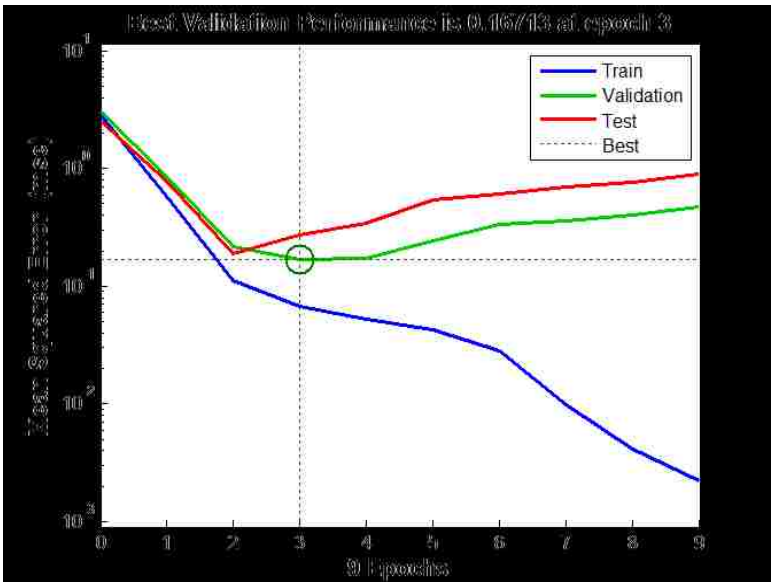

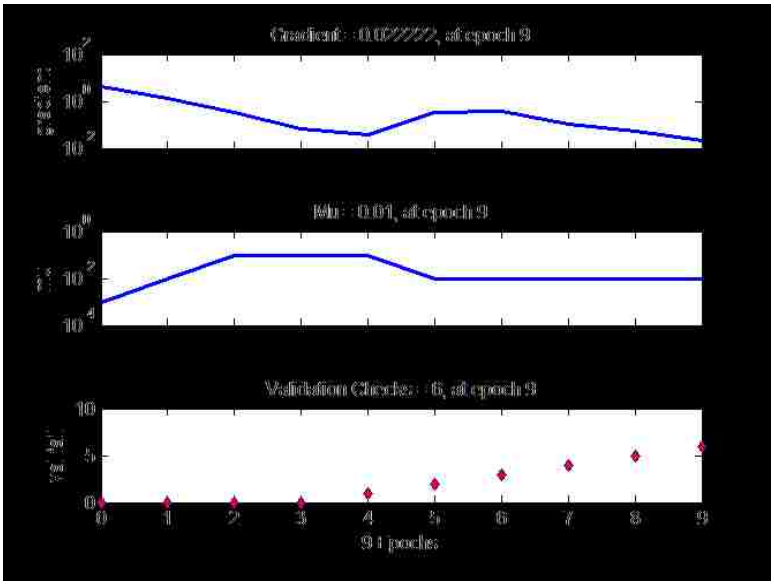

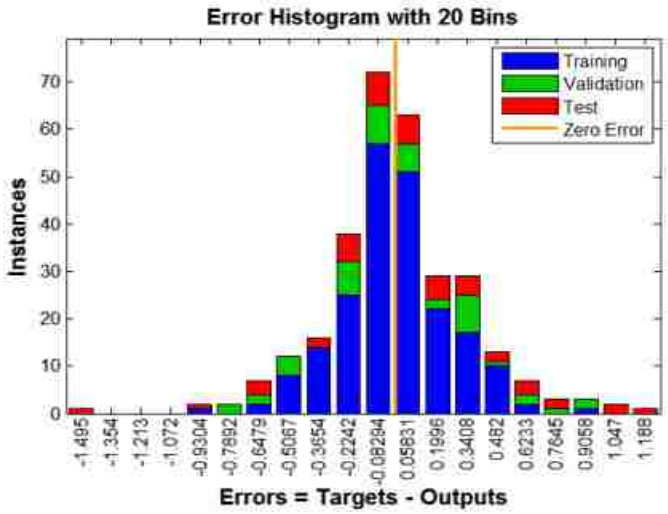

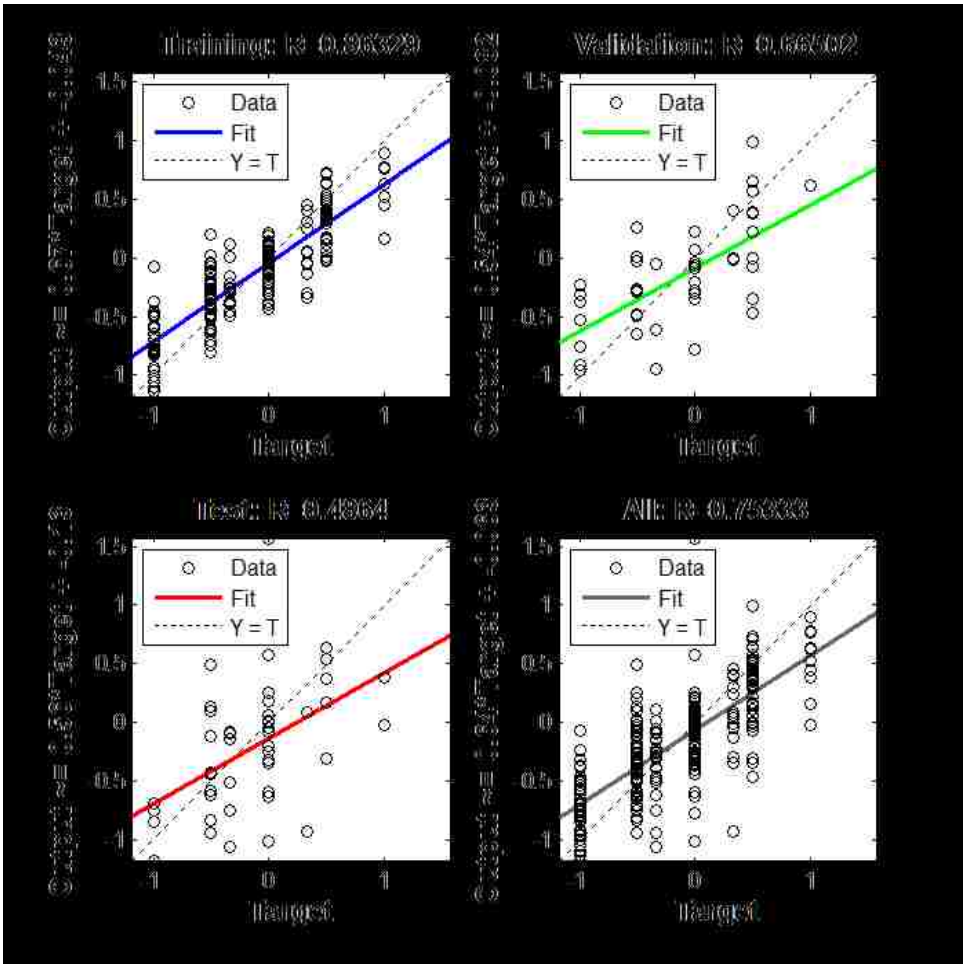

Figure 96: Training results for the 50% overlap pass backward network

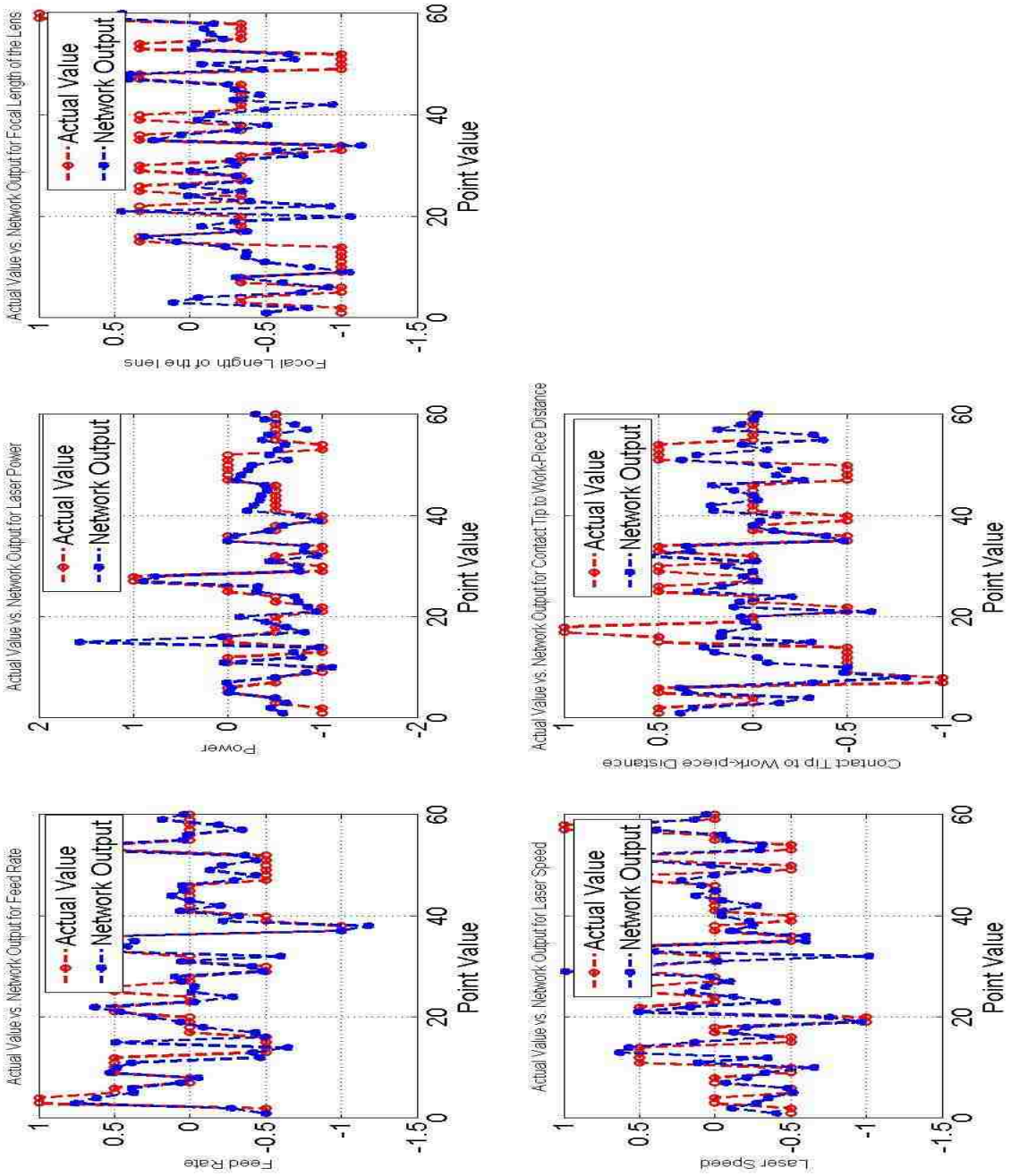

Figure 97: Training output vs network output plots for the 50% overlap pass backward network

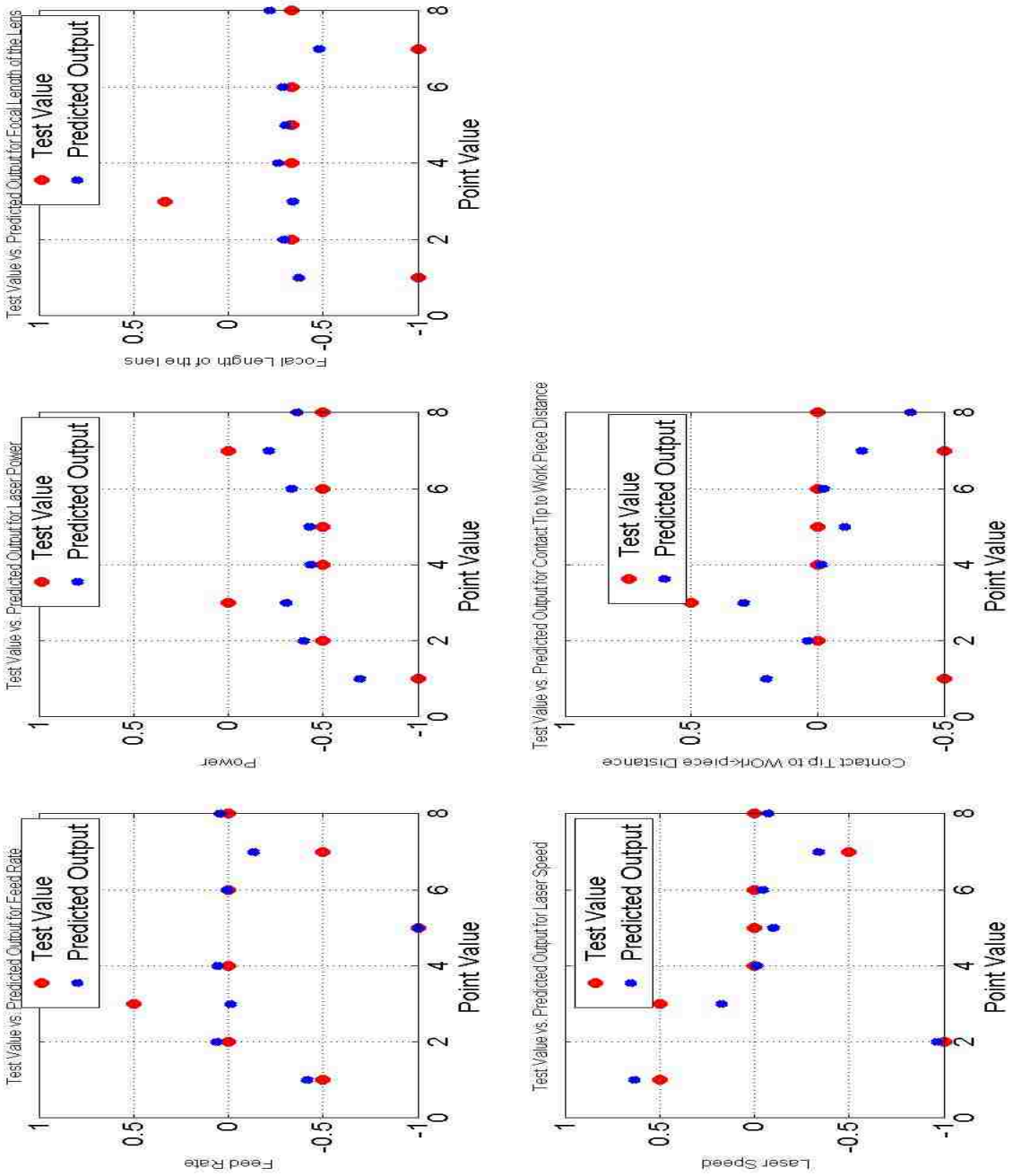

Figure 98: Test output vs predicted output plots for the 50% overlap pass backward network

Appendix I: 60% overlap configuration backward network results

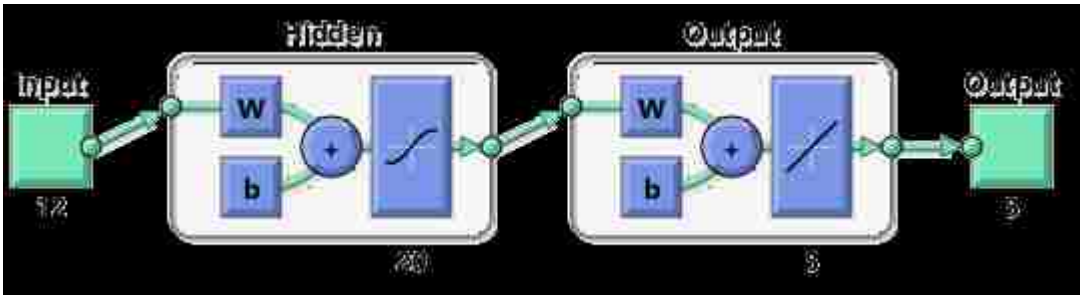

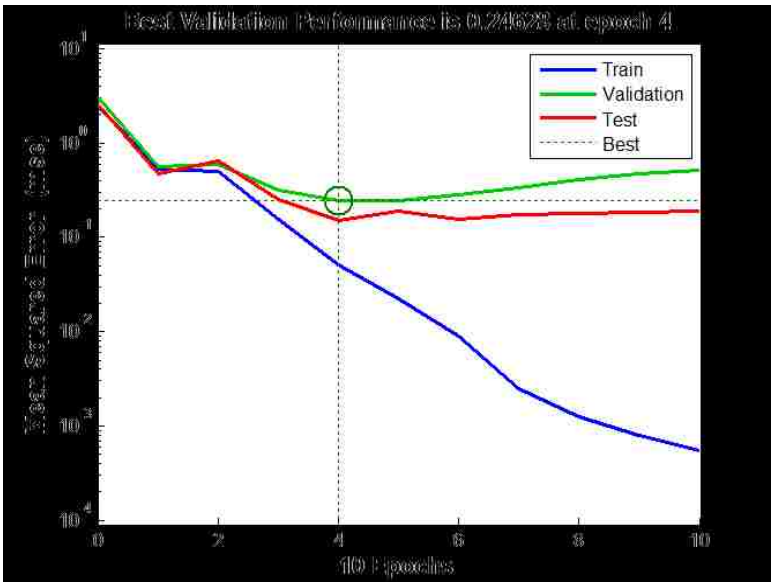

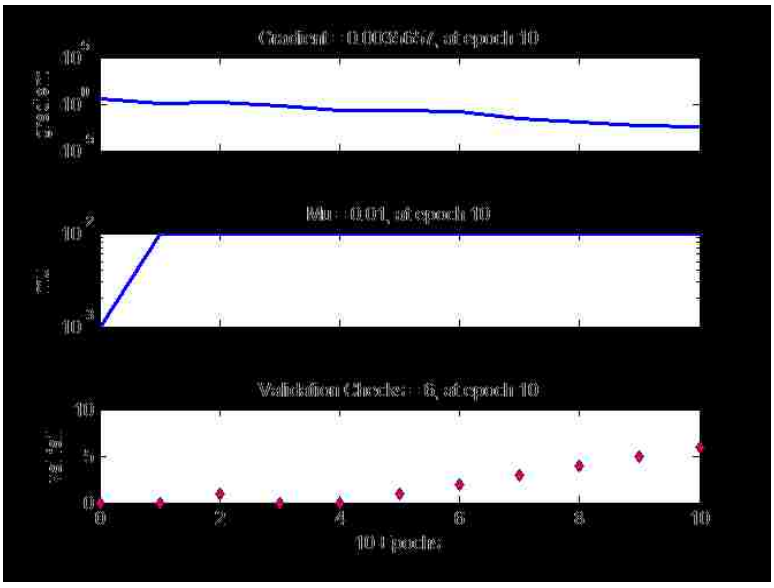

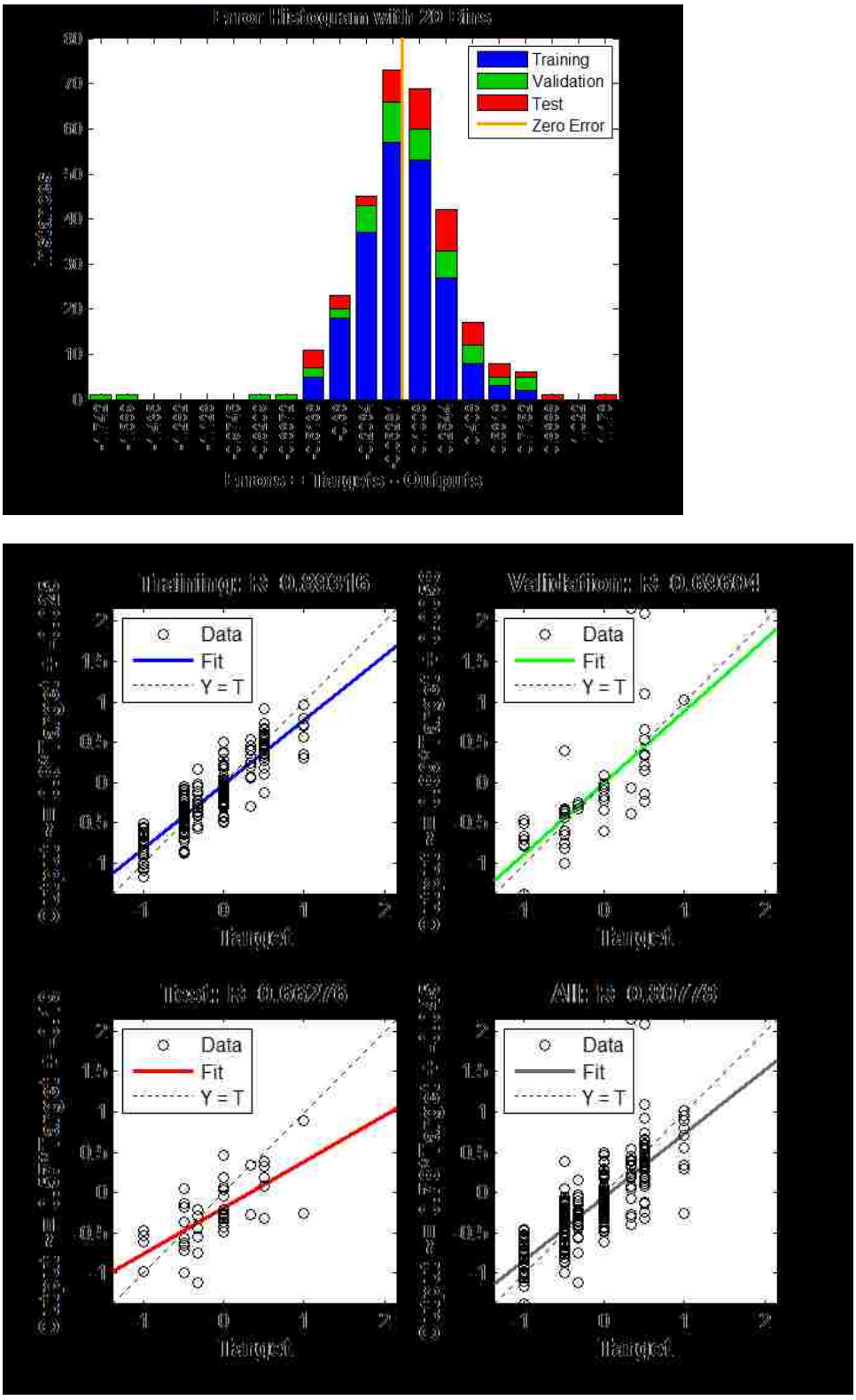

Figure 99: Training results for the 60% overlap pass backward network

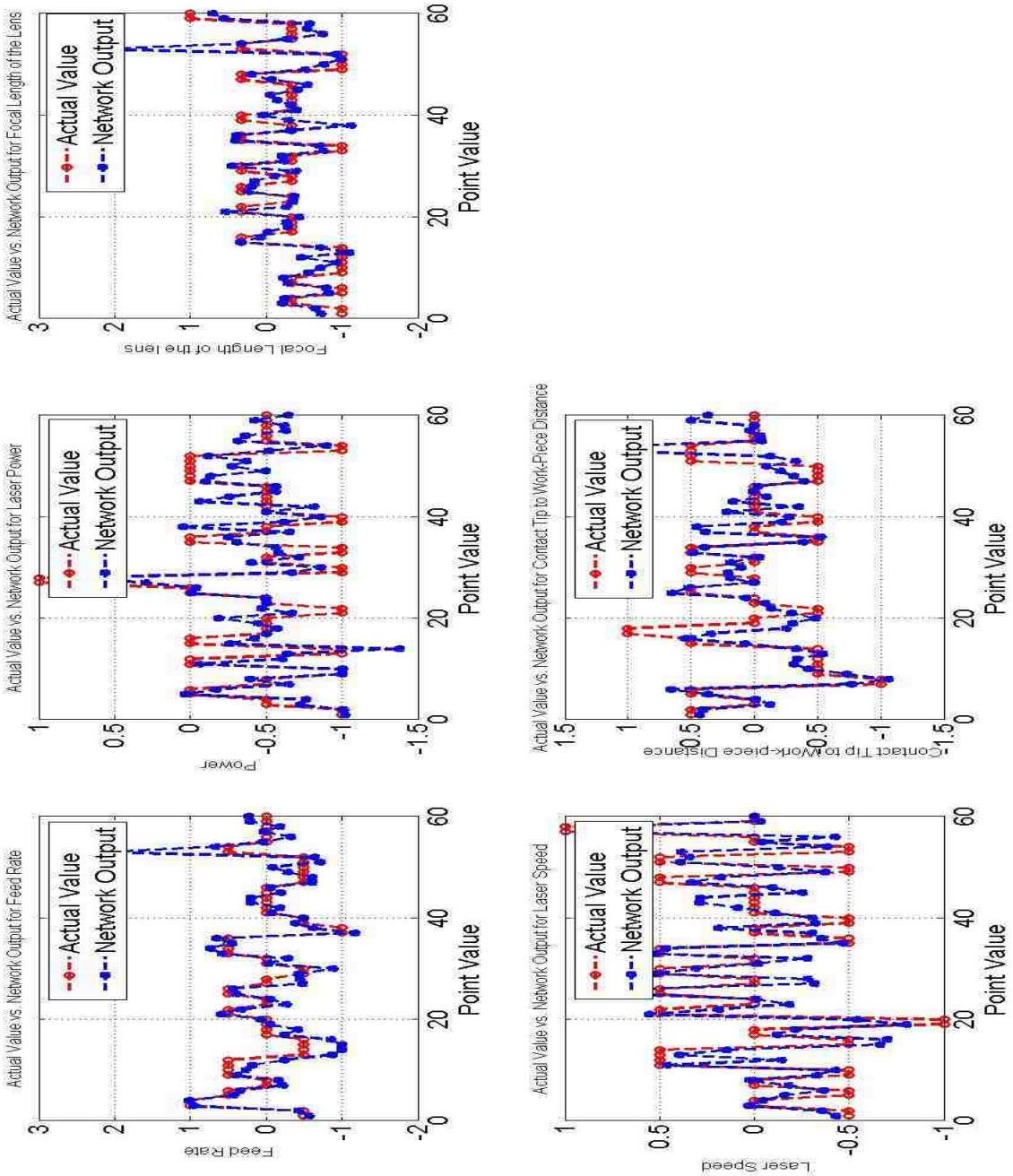

Figure 100: Training output vs network output plots for the 60% overlap pass backward network

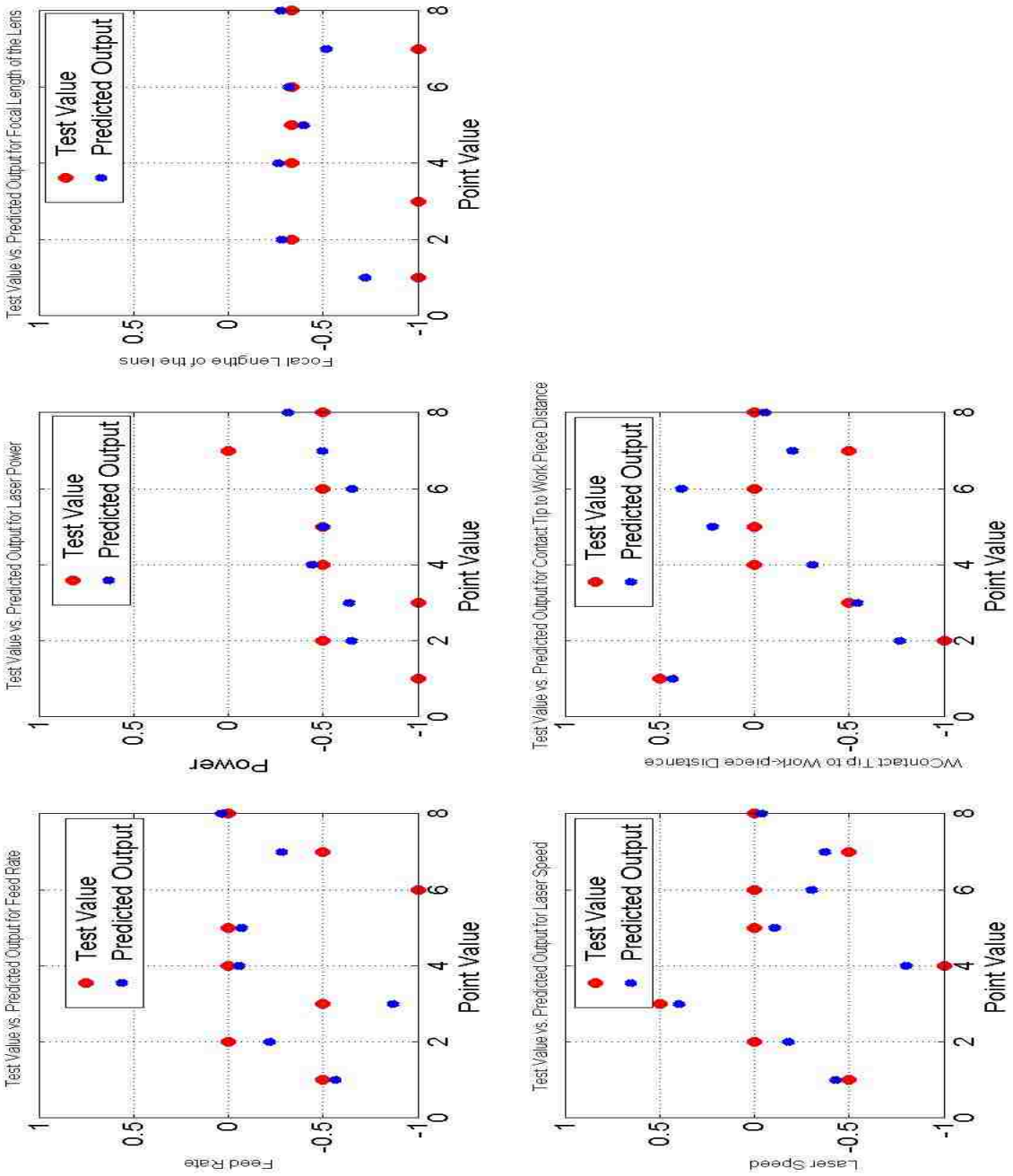

Figure 101: Test output vs predicted output plots for the 60% overlap pass backward network

Appendix J: Significant factors overlap configuration

Table 38: Analysis of variance results for the 40% overlap configurations

Analysis of Variance for W1

Source	DF	Seq SS	Adj SS	Adj MS	F	P
Regression	20	5.28481	5.28481	0.264240	10.14	0.000
Linear	5	3.11995	1.63814	0.327628	12.57	0.000
FR	1	0.06021	0.10136	0.101359	3.89	0.056
PW	1	0.20393	0.00010	0.000101	0.00	0.951
FL	1	1.96767	0.19743	0.197428	7.58	0.009
LS	1	0.67213	0.75761	0.757613	29.07	0.000
CTWD	1	0.21601	0.55163	0.551635	21.17	0.000
Square	5	0.76103	0.76103	0.152206	5.84	0.000
FR*FR	1	0.19602	0.17562	0.175623	6.74	0.013
PW*PW	1	0.21284	0.17036	0.170361	6.54	0.015
FL*FL	1	0.32704	0.33149	0.331492	12.72	0.001
LS*LS	1	0.00011	0.00112	0.001122	0.04	0.837
CTWD*CTWD	1	0.02502	0.02502	0.025023	0.96	0.333
Interaction	10	1.40383	1.40383	0.140383	5.39	0.000
FR*PW	1	0.01711	0.01711	0.017112	0.66	0.423
FR*FL	1	0.55125	0.55125	0.551250	21.15	0.000
FR*LS	1	0.00101	0.00101	0.001013	0.04	0.845
FR*CTWD	1	0.04351	0.04351	0.043512	1.67	0.204
PW*FL	1	0.03251	0.03251	0.032513	1.25	0.271
PW*LS	1	0.09680	0.09680	0.096800	3.71	0.061
PW*CTWD	1	0.29645	0.29645	0.296450	11.38	0.002
FL*LS	1	0.20161	0.20161	0.201613	7.74	0.008
FL*CTWD	1	0.04351	0.04351	0.043513	1.67	0.204
LS*CTWD	1	0.12005	0.12005	0.120050	4.61	0.038
Residual Error	39	1.01633	1.01633	0.026060		
Lack-of-Fit	4	0.04509	0.04509	0.011273	0.41	0.803
Pure Error	35	0.97124	0.97124	0.027750		
Total	59	6.30114				

Analysis of Variance for W2

Source	DF	Seq SS	Adj SS	Adj MS	F	P
Regression	20	0.96411	0.96411	0.048206	1.40	0.179
Linear	5	0.06593	0.35116	0.070232	2.04	0.094
FR	1	0.00907	0.09628	0.096276	2.80	0.102
PW	1	0.02920	0.12381	0.123813	3.60	0.065
FL	1	0.02738	0.07417	0.074174	2.16	0.150
LS	1	0.00007	0.10436	0.104363	3.04	0.089
CTWD	1	0.00021	0.00074	0.000742	0.02	0.884
Square	5	0.12795	0.12795	0.025590	0.74	0.595
FR*FR	1	0.05204	0.04599	0.045990	1.34	0.254
PW*PW	1	0.00513	0.00396	0.003957	0.12	0.736
FL*FL	1	0.03835	0.03767	0.037671	1.10	0.301
LS*LS	1	0.00982	0.00576	0.005762	0.17	0.684
CTWD*CTWD	1	0.02261	0.02261	0.022613	0.66	0.422
Interaction	10	0.77023	0.77023	0.077023	2.24	0.035
FR*PW	1	0.13005	0.13005	0.130050	3.79	0.059
FR*FL	1	0.00031	0.00031	0.000313	0.01	0.925
FR*LS	1	0.16245	0.16245	0.162450	4.73	0.036
FR*CTWD	1	0.07801	0.07801	0.078013	2.27	0.140
PW*FL	1	0.18911	0.18911	0.189113	5.50	0.024
PW*LS	1	0.07220	0.07220	0.072200	2.10	0.155
PW*CTWD	1	0.00781	0.00781	0.007813	0.23	0.636
FL*LS	1	0.11761	0.11761	0.117613	3.42	0.072
FL*CTWD	1	0.00605	0.00605	0.006050	0.18	0.677
LS*CTWD	1	0.00661	0.00661	0.006613	0.19	0.663
Residual Error	39	1.33979	1.33979	0.034354		
Lack-of-Fit	4	0.25324	0.25324	0.063309	2.04	0.110
Pure Error	35	1.08655	1.08655	0.031044		
Total	59	2.30390				

Analysis of Variance for W3

Source	DF	Seq SS	Adj SS	Adj MS	F	P
Regression	20	7.28443	7.28443	0.36422	9.99	0.000
Linear	5	2.94225	2.08411	0.41682	11.44	0.000
FR	1	0.29141	0.09575	0.09575	2.63	0.113
PW	1	0.90654	1.68080	1.68080	46.11	0.000
FL	1	1.30160	0.00605	0.00605	0.17	0.686
LS	1	0.34003	0.05907	0.05907	1.62	0.211
CTWD	1	0.10267	0.09470	0.09470	2.60	0.115
Square	5	0.30895	0.30895	0.06179	1.70	0.159
FR*FR	1	0.00254	0.00043	0.00043	0.01	0.915
PW*PW	1	0.15186	0.13958	0.13958	3.83	0.058
FL*FL	1	0.11613	0.11394	0.11394	3.13	0.085
LS*LS	1	0.00509	0.00191	0.00191	0.05	0.820
CTWD*CTWD	1	0.03333	0.03333	0.03333	0.91	0.345
Interaction	10	4.03323	4.03323	0.40332	11.06	0.000
FR*PW	1	0.32401	0.32401	0.32401	8.89	0.005
FR*FL	1	1.24031	1.24031	1.24031	34.03	0.000
FR*LS	1	0.14851	0.14851	0.14851	4.07	0.050
FR*CTWD	1	0.53561	0.53561	0.53561	14.69	0.000
PW*FL	1	0.80011	0.80011	0.80011	21.95	0.000
PW*LS	1	0.05951	0.05951	0.05951	1.63	0.209
PW*CTWD	1	0.13781	0.13781	0.13781	3.78	0.059
FL*LS	1	0.58861	0.58861	0.58861	16.15	0.000
FL*CTWD	1	0.17111	0.17111	0.17111	4.69	0.036
LS*CTWD	1	0.02761	0.02761	0.02761	0.76	0.389
Residual Error	39	1.42156	1.42156	0.03645		
Lack-of-Fit	4	0.10590	0.10590	0.02647	0.70	0.594
Pure Error	35	1.31567	1.31567	0.03759		
Total	59	8.70599				

Analysis of Variance for P1

Source	DF	Seq SS	Adj SS	Adj MS	F	P
Regression	20	5.14233	5.14233	0.25712	24.51	0.000
Linear	5	3.17383	2.62590	0.52518	50.07	0.000
FR	1	0.42563	0.08132	0.08132	7.75	0.008
PW	1	1.97040	1.93944	1.93944	184.91	0.000
FL	1	0.05296	0.11338	0.11338	10.81	0.002
LS	1	0.61653	0.55543	0.55543	52.96	0.000
CTWD	1	0.10830	0.02671	0.02671	2.55	0.119
Square	5	0.45415	0.45415	0.09083	8.66	0.000
FR*FR	1	0.19206	0.22132	0.22132	21.10	0.000
PW*PW	1	0.05985	0.07689	0.07689	7.33	0.010
FL*FL	1	0.15047	0.15336	0.15336	14.62	0.000
LS*LS	1	0.05036	0.04685	0.04685	4.47	0.041
CTWD*CTWD	1	0.00141	0.00141	0.00141	0.13	0.716
Interaction	10	1.51435	1.51435	0.15144	14.44	0.000
FR*PW	1	0.16245	0.16245	0.16245	15.49	0.000
FR*FL	1	0.28125	0.28125	0.28125	26.82	0.000
FR*LS	1	0.09245	0.09245	0.09245	8.81	0.005
FR*CTWD	1	0.18301	0.18301	0.18301	17.45	0.000
PW*FL	1	0.25561	0.25561	0.25561	24.37	0.000
PW*LS	1	0.12251	0.12251	0.12251	11.68	0.001
PW*CTWD	1	0.00720	0.00720	0.00720	0.69	0.412
FL*LS	1	0.00661	0.00661	0.00661	0.63	0.432
FL*CTWD	1	0.00720	0.00720	0.00720	0.69	0.412
LS*CTWD	1	0.39605	0.39605	0.39605	37.76	0.000
Residual Error	39	0.40904	0.40904	0.01049		
Lack-of-Fit	4	0.10307	0.10307	0.02577	2.95	0.034
Pure Error	35	0.30597	0.30597	0.00874		
Total	59	5.55137				

Analysis of Variance for P2

Source	DF	Seq SS	Adj SS	Adj MS	F	P
Regression	20	3.52506	3.52506	0.17625	55.51	0.000
Linear	5	2.31001	1.54513	0.30903	97.33	0.000
FR	1	0.65333	0.20470	0.20470	64.47	0.000
PW	1	1.38347	1.18174	1.18174	372.20	0.000
FL	1	0.11797	0.15602	0.15602	49.14	0.000
LS	1	0.13441	0.15400	0.15400	48.50	0.000
CTWD	1	0.02083	0.00419	0.00419	1.32	0.258
Square	5	0.23735	0.23735	0.04747	14.95	0.000
FR*FR	1	0.10953	0.11431	0.11431	36.00	0.000
PW*PW	1	0.00018	0.00145	0.00145	0.46	0.503
FL*FL	1	0.11981	0.12048	0.12048	37.95	0.000
LS*LS	1	0.00711	0.00632	0.00632	1.99	0.166
CTWD*CTWD	1	0.00071	0.00071	0.00071	0.23	0.638
Interaction	10	0.97770	0.97770	0.09777	30.79	0.000
FR*PW	1	0.08000	0.08000	0.08000	25.20	0.000
FR*FL	1	0.24851	0.24851	0.24851	78.27	0.000
FR*LS	1	0.02645	0.02645	0.02645	8.33	0.006
FR*CTWD	1	0.04500	0.04500	0.04500	14.17	0.001
PW*FL	1	0.23805	0.23805	0.23805	74.98	0.000
PW*LS	1	0.02101	0.02101	0.02101	6.62	0.014
PW*CTWD	1	0.00151	0.00151	0.00151	0.48	0.494
FL*LS	1	0.03920	0.03920	0.03920	12.35	0.001
FL*CTWD	1	0.00045	0.00045	0.00045	0.14	0.709
LS*CTWD	1	0.27751	0.27751	0.27751	87.41	0.000
Residual Error	39	0.12383	0.12383	0.00318		
Lack-of-Fit	4	0.00218	0.00218	0.00054	0.16	0.959
Pure Error	35	0.12165	0.12165	0.00348		
Total	59	3.64889				

Analysis of Variance for P3

Source	DF	Seq SS	Adj SS	Adj MS	F	P
Regression	20	3.73505	3.73505	0.18675	40.51	0.000
Linear	5	2.90391	1.84395	0.36879	79.99	0.000
FR	1	0.56550	0.14560	0.14560	31.58	0.000
PW	1	2.18316	1.56813	1.56813	340.12	0.000
FL	1	0.07892	0.08250	0.08250	17.89	0.000
LS	1	0.04877	0.06554	0.06554	14.22	0.001
CTWD	1	0.02755	0.04131	0.04131	8.96	0.005
Square	5	0.14986	0.14986	0.02997	6.50	0.000
FR*FR	1	0.02807	0.03203	0.03203	6.95	0.012
PW*PW	1	0.00122	0.00332	0.00332	0.72	0.402
FL*FL	1	0.09810	0.09878	0.09878	21.43	0.000
LS*LS	1	0.00720	0.00433	0.00433	0.94	0.338
CTWD*CTWD	1	0.01526	0.01526	0.01526	3.31	0.077
Interaction	10	0.68128	0.68128	0.06813	14.78	0.000
FR*PW	1	0.09353	0.09353	0.09353	20.29	0.000
FR*FL	1	0.19375	0.19375	0.19375	42.02	0.000
FR*LS	1	0.00633	0.00633	0.00633	1.37	0.248
FR*CTWD	1	0.00945	0.00945	0.00945	2.05	0.160
PW*FL	1	0.13650	0.13650	0.13650	29.61	0.000
PW*LS	1	0.01853	0.01853	0.01853	4.02	0.052
PW*CTWD	1	0.02050	0.02050	0.02050	4.45	0.041
FL*LS	1	0.00578	0.00578	0.00578	1.25	0.270
FL*CTWD	1	0.00003	0.00003	0.00003	0.01	0.938
LS*CTWD	1	0.19688	0.19688	0.19688	42.70	0.000
Residual Error	39	0.17981	0.17981	0.00461		
Lack-of-Fit	4	0.00580	0.00580	0.00145	0.29	0.882
Pure Error	35	0.17402	0.17402	0.00497		
Total	59	3.91486				

Analysis of Variance for RH1

Source	DF	Seq SS	Adj SS	Adj MS	F	P
Regression	20	8.83954	8.83954	0.44198	31.61	0.000
Linear	5	7.42345	2.03450	0.40690	29.10	0.000
FR	1	2.37630	0.24799	0.24799	17.73	0.000
PW	1	0.12171	0.03466	0.03466	2.48	0.123
FL	1	0.08024	0.08248	0.08248	5.90	0.020
LS	1	4.82601	1.53302	1.53302	109.63	0.000
CTWD	1	0.01920	0.07891	0.07891	5.64	0.023
Square	5	0.50229	0.50229	0.10046	7.18	0.000
FR*FR	1	0.20703	0.15280	0.15280	10.93	0.002
PW*PW	1	0.01439	0.01636	0.01636	1.17	0.286
FL*FL	1	0.04756	0.04360	0.04360	3.12	0.085
LS*LS	1	0.23089	0.21909	0.21909	15.67	0.000
CTWD*CTWD	1	0.00242	0.00242	0.00242	0.17	0.680
Interaction	10	0.91380	0.91380	0.09138	6.53	0.000
FR*PW	1	0.16245	0.16245	0.16245	11.62	0.002
FR*FL	1	0.11045	0.11045	0.11045	7.90	0.008
FR*LS	1	0.19220	0.19220	0.19220	13.74	0.001
FR*CTWD	1	0.01361	0.01361	0.01361	0.97	0.330
PW*FL	1	0.10351	0.10351	0.10351	7.40	0.010
PW*LS	1	0.00211	0.00211	0.00211	0.15	0.700
PW*CTWD	1	0.16245	0.16245	0.16245	11.62	0.002
FL*LS	1	0.06301	0.06301	0.06301	4.51	0.040
FL*CTWD	1	0.03920	0.03920	0.03920	2.80	0.102
LS*CTWD	1	0.06480	0.06480	0.06480	4.63	0.038
Residual Error	39	0.54535	0.54535	0.01398		
Lack-of-Fit	4	0.19387	0.19387	0.04847	4.83	0.003
Pure Error	35	0.35148	0.35148	0.01004		
Total	59	9.38489				

Analysis of Variance for RH2

Source	DF	Seq SS	Adj SS	Adj MS	F	P
Regression	20	8.71091	8.71091	0.43555	16.44	0.000
Linear	5	7.75893	2.35934	0.47187	17.81	0.000
FR	1	3.37610	1.03870	1.03870	39.21	0.000
PW	1	0.11370	0.03843	0.03843	1.45	0.236
FL	1	0.07125	0.00018	0.00018	0.01	0.935
LS	1	4.04260	1.27459	1.27459	48.12	0.000
CTWD	1	0.15527	0.00022	0.00022	0.01	0.929
Square	5	0.51078	0.51078	0.10216	3.86	0.006
FR*FR	1	0.26780	0.19279	0.19279	7.28	0.010
PW*PW	1	0.01374	0.01998	0.01998	0.75	0.390
FL*FL	1	0.00058	0.00018	0.00018	0.01	0.935
LS*LS	1	0.22832	0.22591	0.22591	8.53	0.006
CTWD*CTWD	1	0.00033	0.00033	0.00033	0.01	0.912
Interaction	10	0.44121	0.44121	0.04412	1.67	0.124
FR*PW	1	0.03445	0.03445	0.03445	1.30	0.261
FR*FL	1	0.03713	0.03713	0.03713	1.40	0.244
FR*LS	1	0.02940	0.02940	0.02940	1.11	0.299
FR*CTWD	1	0.00945	0.00945	0.00945	0.36	0.554
PW*FL	1	0.07703	0.07703	0.07703	2.91	0.096
PW*LS	1	0.00300	0.00300	0.00300	0.11	0.738
PW*CTWD	1	0.15540	0.15540	0.15540	5.87	0.020
FL*LS	1	0.07125	0.07125	0.07125	2.69	0.109
FL*CTWD	1	0.01088	0.01088	0.01088	0.41	0.525
LS*CTWD	1	0.01320	0.01320	0.01320	0.50	0.484
Residual Error	39	1.03302	1.03302	0.02649		
Lack-of-Fit	4	0.41425	0.41425	0.10356	5.86	0.001
Pure Error	35	0.61877	0.61877	0.01768		
Total	59	9.74393				

Analysis of Variance for RH3

Source	DF	Seq SS	Adj SS	Adj MS	F	P
Regression	20	9.4730	9.47300	0.47365	12.65	0.000
Linear	5	7.6732	2.89768	0.57954	15.47	0.000
FR	1	2.6696	1.36107	1.36107	36.34	0.000
PW	1	0.2211	0.08638	0.08638	2.31	0.137
FL	1	0.1351	0.04567	0.04567	1.22	0.276
LS	1	4.4287	1.35908	1.35908	36.29	0.000
CTWD	1	0.2187	0.07678	0.07678	2.05	0.160
Square	5	1.4482	1.44816	0.28963	7.73	0.000
FR*FR	1	0.3967	0.28658	0.28658	7.65	0.009
PW*PW	1	0.0718	0.04614	0.04614	1.23	0.274
FL*FL	1	0.0532	0.06044	0.06044	1.61	0.212
LS*LS	1	0.8853	0.81161	0.81161	21.67	0.000
CTWD*CTWD	1	0.0411	0.04114	0.04114	1.10	0.301
Interaction	10	0.3516	0.35162	0.03516	0.94	0.510
FR*PW	1	0.0300	0.03001	0.03001	0.80	0.376
FR*FL	1	0.0465	0.04651	0.04651	1.24	0.272
FR*LS	1	0.0703	0.07031	0.07031	1.88	0.178
FR*CTWD	1	0.0015	0.00151	0.00151	0.04	0.842
PW*FL	1	0.0231	0.02311	0.02311	0.62	0.437
PW*LS	1	0.0153	0.01531	0.01531	0.41	0.526
PW*CTWD	1	0.0028	0.00281	0.00281	0.08	0.786
FL*LS	1	0.0015	0.00151	0.00151	0.04	0.842
FL*CTWD	1	0.0120	0.01201	0.01201	0.32	0.574
LS*CTWD	1	0.1485	0.14851	0.14851	3.97	0.053
Residual Error	39	1.4607	1.46072	0.03745		
Lack-of-Fit	4	1.0740	1.07400	0.26850	24.30	0.000
Pure Error	35	0.3867	0.38672	0.01105		
Total	59	10.9337				

Analysis of Variance for RH12

Source	DF	Seq SS	Adj SS	Adj MS	F	P
Regression	20	7.12673	7.12673	0.35634	46.38	0.000
Linear	5	6.31222	1.75232	0.35046	45.62	0.000
FR	1	2.14630	0.39014	0.39014	50.78	0.000
PW	1	0.17248	0.05475	0.05475	7.13	0.011
FL	1	0.00016	0.00735	0.00735	0.96	0.334
LS	1	3.96175	1.26500	1.26500	164.65	0.000
CTWD	1	0.03152	0.01110	0.01110	1.44	0.237
Square	5	0.47308	0.47308	0.09462	12.32	0.000
FR*FR	1	0.21306	0.16296	0.16296	21.21	0.000
PW*PW	1	0.00005	0.00008	0.00008	0.01	0.918
FL*FL	1	0.00648	0.00516	0.00516	0.67	0.417
LS*LS	1	0.24626	0.22884	0.22884	29.78	0.000
CTWD*CTWD	1	0.00723	0.00723	0.00723	0.94	0.338
Interaction	10	0.34143	0.34143	0.03414	4.44	0.000
FR*PW	1	0.05695	0.05695	0.05695	7.41	0.010
FR*FL	1	0.03445	0.03445	0.03445	4.48	0.041
FR*LS	1	0.12375	0.12375	0.12375	16.11	0.000
FR*CTWD	1	0.00525	0.00525	0.00525	0.68	0.413
PW*FL	1	0.02703	0.02703	0.02703	3.52	0.068
PW*LS	1	0.00003	0.00003	0.00003	0.00	0.952
PW*CTWD	1	0.05528	0.05528	0.05528	7.19	0.011
FL*LS	1	0.02153	0.02153	0.02153	2.80	0.102
FL*CTWD	1	0.01240	0.01240	0.01240	1.61	0.211
LS*CTWD	1	0.00475	0.00475	0.00475	0.62	0.436
Residual Error	39	0.29963	0.29963	0.00768		
Lack-of-Fit	4	0.11658	0.11658	0.02915	5.57	0.001
Pure Error	35	0.18305	0.18305	0.00523		
Total	59	7.42637				

Analysis of Variance for RH23

Source	DF	Seq SS	Adj SS	Adj MS	F	P
Regression	20	7.32060	7.32060	0.36603	20.22	0.000
Linear	5	6.25079	2.22684	0.44537	24.60	0.000
FR	1	1.79027	0.99323	0.99323	54.86	0.000
PW	1	0.30648	0.16387	0.16387	9.05	0.005
FL	1	0.16869	0.10597	0.10597	5.85	0.020
LS	1	3.90450	1.01541	1.01541	56.08	0.000
CTWD	1	0.08085	0.01497	0.01497	0.83	0.369
Square	5	0.71270	0.71270	0.14254	7.87	0.000
FR*FR	1	0.40057	0.31070	0.31070	17.16	0.000
PW*PW	1	0.02630	0.01676	0.01676	0.93	0.342
FL*FL	1	0.00262	0.00396	0.00396	0.22	0.642
LS*LS	1	0.28309	0.27862	0.27862	15.39	0.000
CTWD*CTWD	1	0.00011	0.00011	0.00011	0.01	0.937
Interaction	10	0.35711	0.35711	0.03571	1.97	0.064
FR*PW	1	0.05363	0.05363	0.05363	2.96	0.093
FR*FL	1	0.01240	0.01240	0.01240	0.69	0.413
FR*LS	1	0.06390	0.06390	0.06390	3.53	0.068
FR*CTWD	1	0.00525	0.00525	0.00525	0.29	0.593
PW*FL	1	0.02820	0.02820	0.02820	1.56	0.219
PW*LS	1	0.05865	0.05865	0.05865	3.24	0.080
PW*CTWD	1	0.00025	0.00025	0.00025	0.01	0.906
FL*LS	1	0.00228	0.00228	0.00228	0.13	0.725
FL*CTWD	1	0.00878	0.00878	0.00878	0.48	0.490
LS*CTWD	1	0.12375	0.12375	0.12375	6.84	0.013
Residual Error	39	0.70610	0.70610	0.01811		
Lack-of-Fit	4	0.47631	0.47631	0.11908	18.14	0.000
Pure Error	35	0.22979	0.22979	0.00657		
Total	59	8.02670				

Analysis of Variance for D

Source	DF	Seq SS	Adj SS	Adj MS	F	P
Regression	20	6868.00	6868.00	343.40	78.21	0.000
Linear	5	4315.33	3036.28	607.26	138.30	0.000
FR	1	1824.07	725.94	725.94	165.33	0.000
PW	1	2244.35	2129.19	2129.19	484.92	0.000
FL	1	73.12	242.50	242.50	55.23	0.000
LS	1	67.02	85.90	85.90	19.56	0.000
CTWD	1	106.78	95.14	95.14	21.67	0.000
Square	5	788.92	788.92	157.78	35.94	0.000
FR*FR	1	652.86	632.82	632.82	144.13	0.000
PW*PW	1	7.01	10.58	10.58	2.41	0.129
FL*FL	1	125.29	124.36	124.36	28.32	0.000
LS*LS	1	3.70	3.47	3.47	0.79	0.379
CTWD*CTWD	1	0.06	0.06	0.06	0.01	0.904
Interaction	10	1763.75	1763.75	176.38	40.17	0.000
FR*PW	1	46.44	46.44	46.44	10.58	0.002
FR*FL	1	341.79	341.79	341.79	77.84	0.000
FR*LS	1	117.48	117.48	117.48	26.76	0.000
FR*CTWD	1	92.57	92.57	92.57	21.08	0.000
PW*FL	1	460.45	460.45	460.45	104.87	0.000
PW*LS	1	12.60	12.60	12.60	2.87	0.098
PW*CTWD	1	1.39	1.39	1.39	0.32	0.577
FL*LS	1	26.99	26.99	26.99	6.15	0.018
FL*CTWD	1	60.42	60.42	60.42	13.76	0.001
LS*CTWD	1	603.63	603.63	603.63	137.48	0.000
Residual Error	39	171.24	171.24	4.39		
Lack-of-Fit	4	101.51	101.51	25.38	12.74	0.000
Pure Error	35	69.73	69.73	1.99		
Total	59	7039.24				

From table 38, the following table 39 presents' results for the most significant factors relevant to the 40% overlaps for the 420 steel operating processes. (Note- most significant factors are the factors with P-value =0.00; other significant factors are factors with P-value < 0.05).

Table 39: Most significant factors for the 40% overlap configurations

Shape Parameter	Linear Significance	Squared Significance	Quadratic Significance
W1	LS, CTWD	N/A	FR*FL
W2	N/A	N/A	N/A
W3	PW	N/A	FR*FL; FR*CTWD; PW*FL; FL*LS
P1	PW; LS	FR^2; FL^2	FR*PW; FR*FL; FR* CTWD; PW* FL; LS *CTWD
P2	FR; PW; FL; LS	FR^2; FL^2	FR*PW; FR*FL; PW*FL; LS*CTWD
P3	FR; PW; FL	FL^2	FR*PW; FR*FL; PW*FL; LS*CTWD
RH1	FR; LS	LS^2	N/A
RH2	FR; LS	N/A	N/A
RH3	FR; LS	LS^2	N/A
RH12	FR; LS	FR^2; LS^2	FR*LS
RH23	FR; LS	FR^2; LS^2	N/A
D	FR; PW; FL; LS; CTWD	FR^2; FL^2	FR*FL; FR*LS; FR*CTWD; PW*FL; LS*CTWD

Similarly, most significant factors are generated for 50% and 60% overlap configurations (table 40 and 41), for the 420 steel clad powder

Table 40: Most significant factors for the 50% overlap configurations

Shape Parameter	Linear Significance	Squared Significance	Quadratic Significance
W1	FR; LS	LS^2	FR*FL; PW*LS
W2	N/A	N/A	N/A
W3	N/A	N/A	FR*FL
P1	FR; PW; LS	FL^2	FR*PW; FR*FL; PW*FL; LS*CTWD
P2	FR; PW; FL; LS; CTWD	LS^2	FR*FL; PW*FL; LS*CTWD
P3	FR; PW; FL	N/A	FR*FL; LS*CTWD
RH1	PW; LS	N/A	FR*FL
RH2	FR; LS	N/A	FR*LS
RH3	FR; LS	LS^2	FR*LS
RH12	FR; LS	N/A	FR*FL
RH23	FR; LS	LS^2	FR*FL; FR*LS
D	FR; PW; FL	FR^2	FR*FL; PW*FL; LS*CTWD

Table 41: Most significant factors for the 60% overlap configurations

Shape Parameter	Linear Significance	Squared Significance	Quadratic Significance
W1	LS, CTWD	N/A	FR*FL
W2	N/A	N/A	N/A
W3	PW	N/A	FR*FL; FR*CTWD; PW*FL; FL*LS
P1	FR; PW; FL; LS	N/A	FR*FL; PW*FL; LS*CTWD
P2	FR; PW; FL	FL^2	FR*FL; PW*FL;LS*CTWD
P3	FR; PW; FL; CTWD	FL^2	FR*FL; FR*LS; PW*FL; PW*CTWD; LS*CTWD
RH1	FR; PW; FL; LS; CTWD	FL^2; LS^2	PW*LS; FL*CTWD
RH2	FR; FL; LS; CTWD	FL^2; LS^2	FR*LS
RH3	FR; PW; FL; LS; CTWD	FL^2; LS^2	PW*LS; FL*CTWD
RH12	FR; LS	FR^2	FR*PW; FR*LS; PW*FL
RH23	FR; PW; FL; LS; CTWD	FR^2; FL^2; LS^2	PW*LS; FL*CTWD
D	PW; FR	FR^2; $CTWD^2$	PW*FL; LS*CTWD

Appendix K: Surface, contour & optimization results: overlap configuration

The figure(s) 102 and 103 represent contour and surface plots respectively for percentage dilution (response variable) among five manufacturing parameters (FR, PW, FL, LS, and CTWD) for a 40% overlap configuration. The contour plots are generated using MINITAB software workspace with constant values.

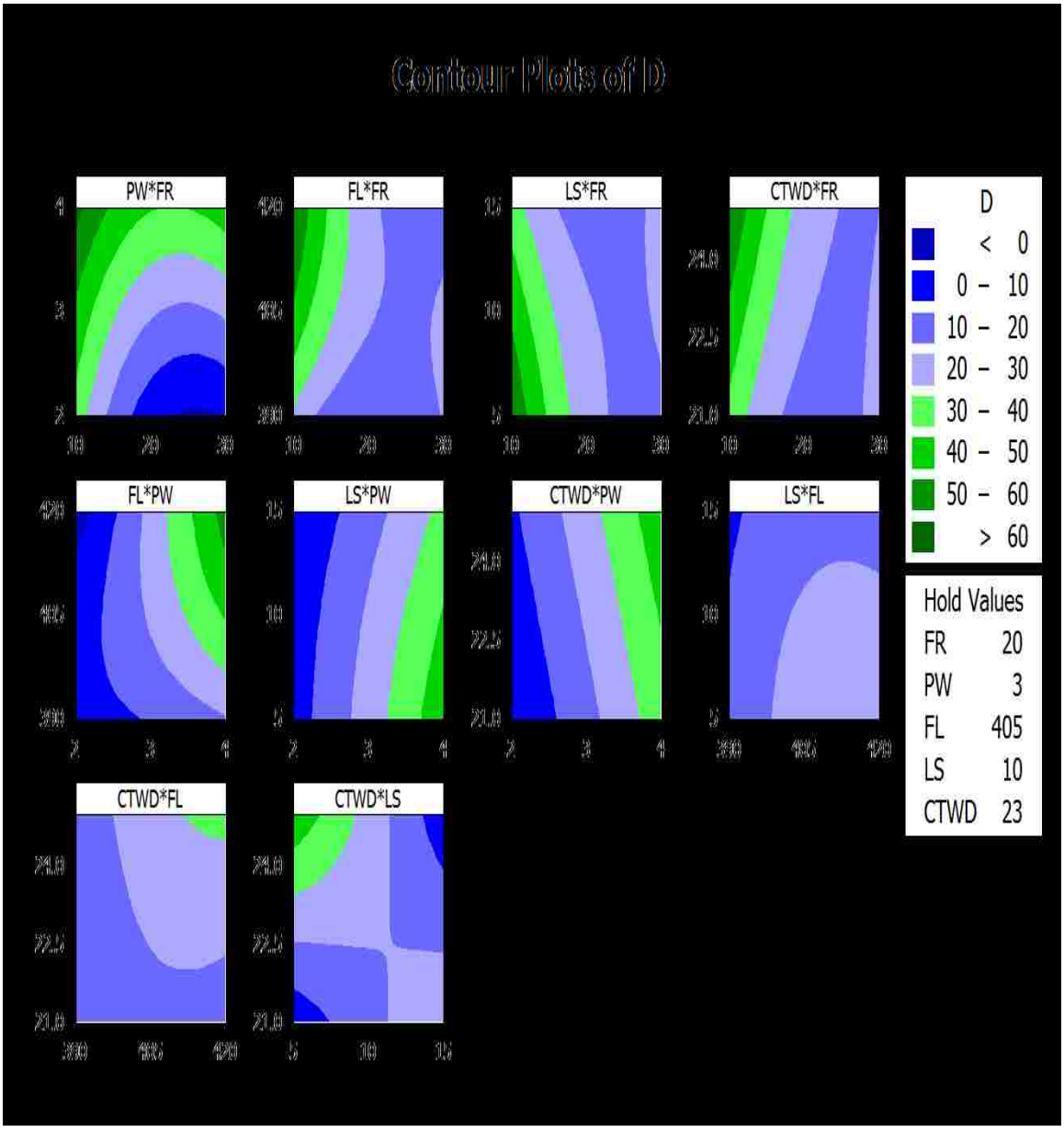

Figure 102: Contour plots: percentage dilution for 40% overlap pass

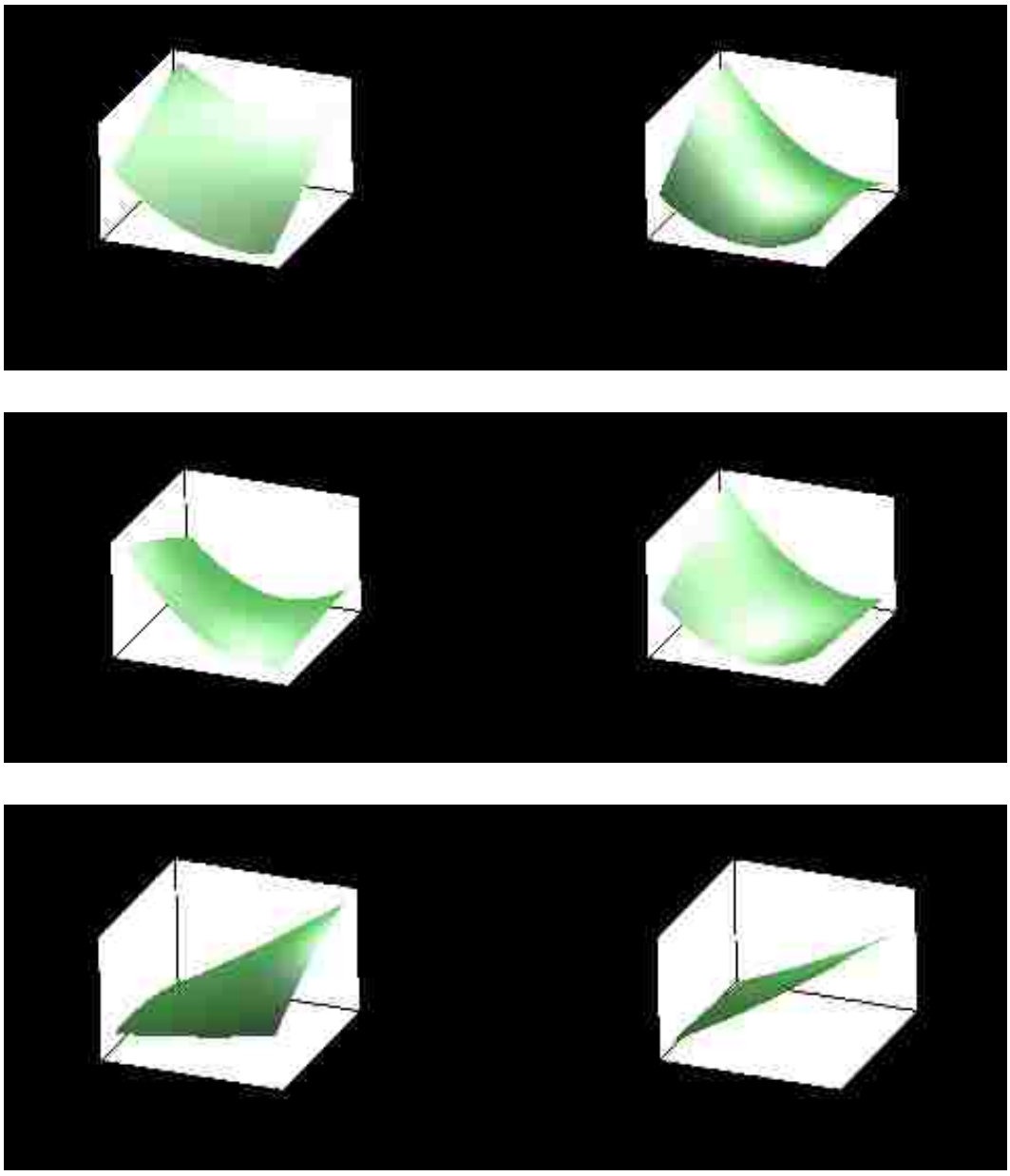

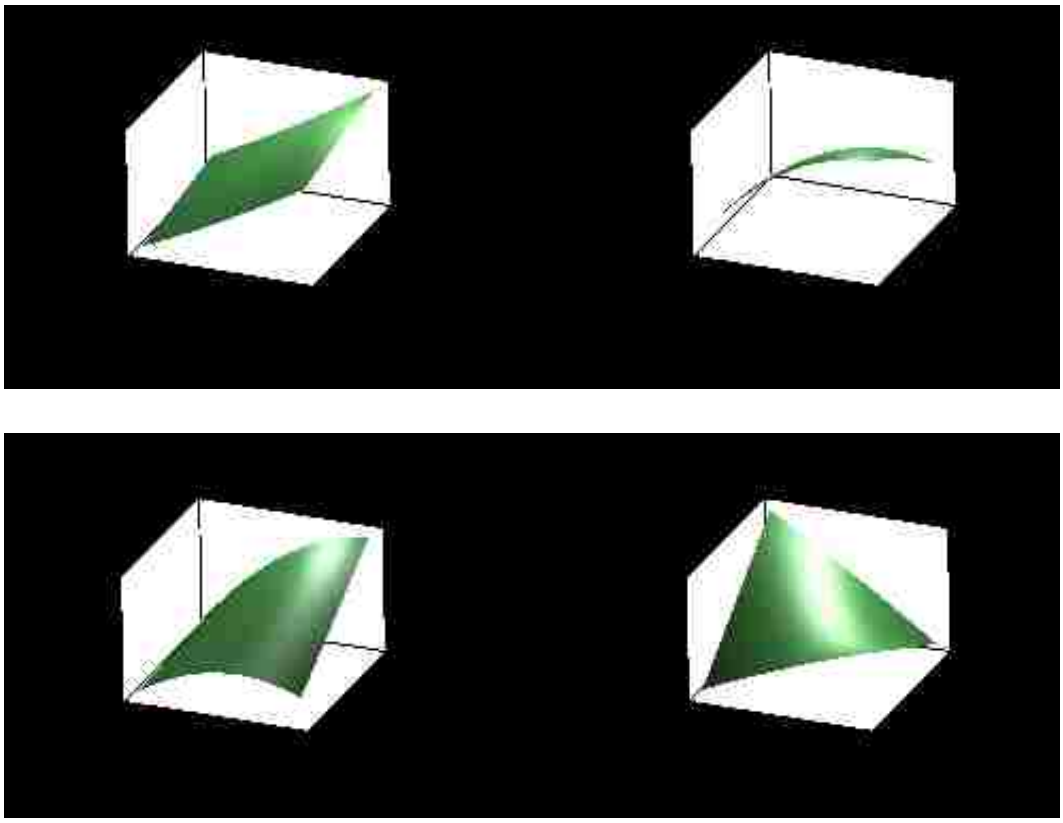

Figure 103: Surface plots: percentage dilution for 40% overlap pass

Similar plots are generated for 50% and 60% overlap configurations.

A multi-objective function plot is presented in figure 104which represents the optimal values of the manufacturing parameters according to the shape parameters for the 40% overlap configurations. The objective of this function is to maximize all widths (W1, W2, W3); minimize all penetrations (P1, P2, P3), Maximize all reinforcement heights (RH1, RH2, RH3, RH12, RH23) and minimize percentage dilution (D%).

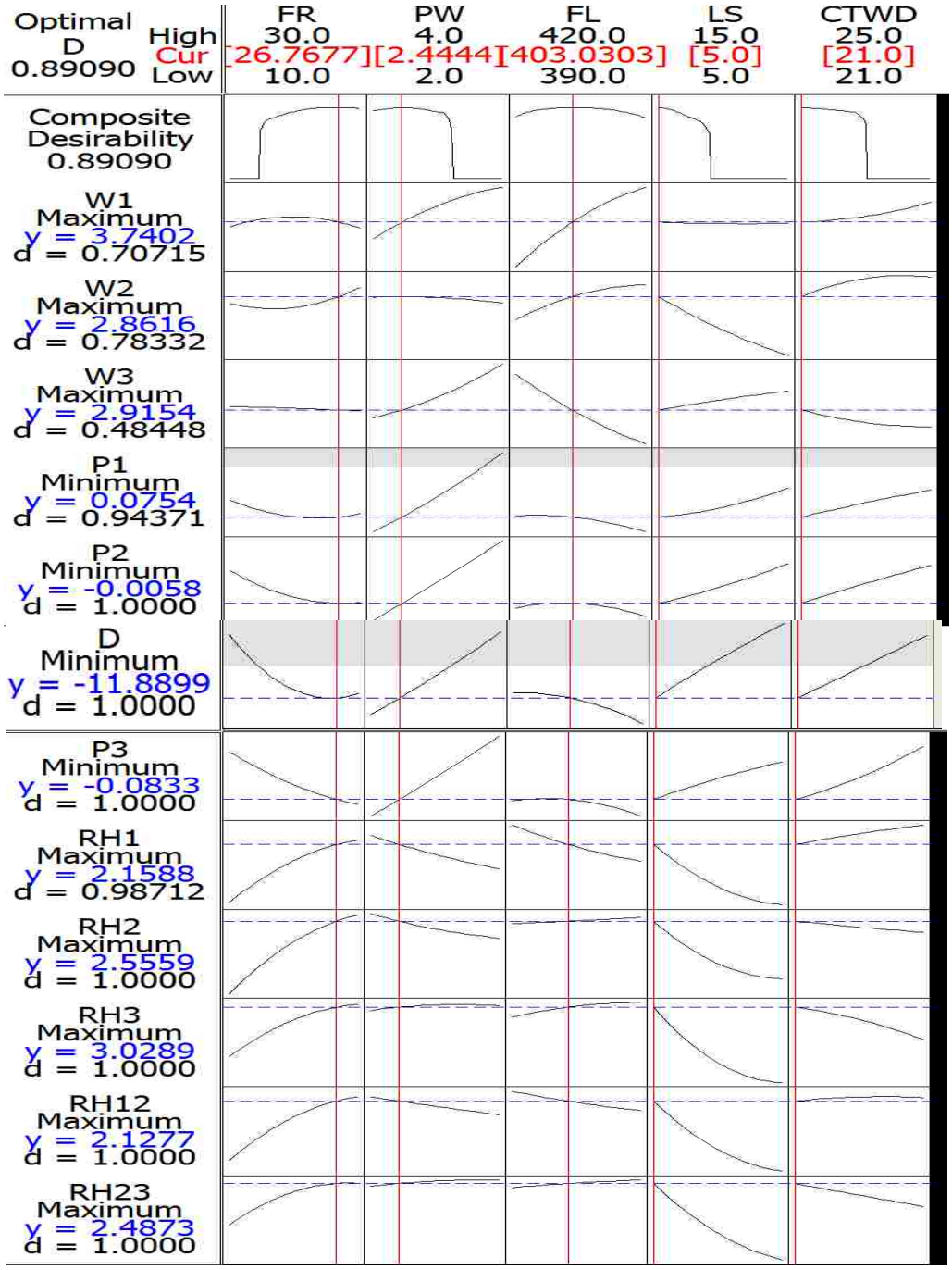

Figure 104: Multiple-objective optimization plot for 40% overlap pass

Multiple- single objective optimized results can be also generated using the MINITAB tool. It should be noted that the optimal results for the single objective optimization for the process parameters will be different from the multi objective optimization results. Similarly, optimization plots (single and multi-objective) can be generated for 50% and 60% overlap configurations.

Appendix L: Cluster (K=5) - shape analysis

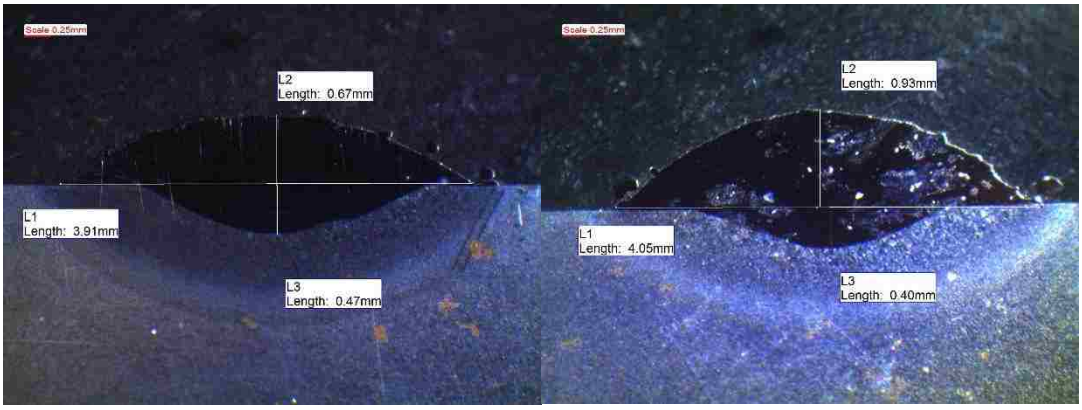

(A) (B)

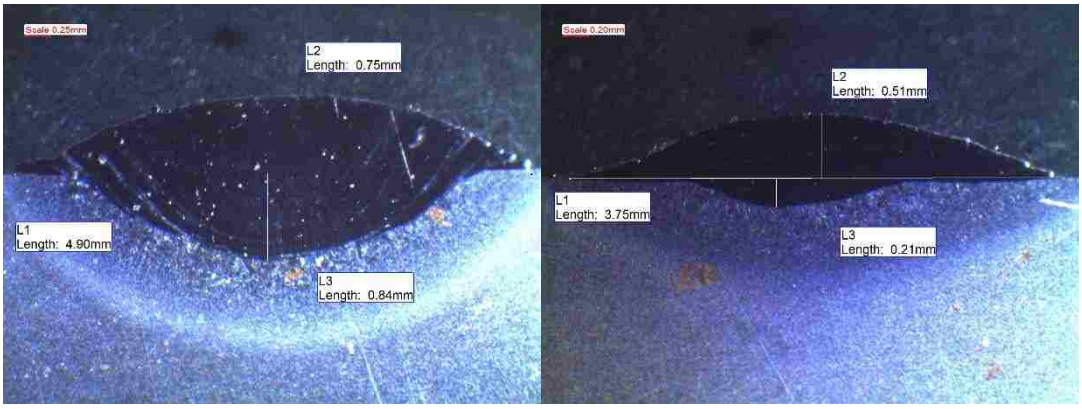

(C) (D)

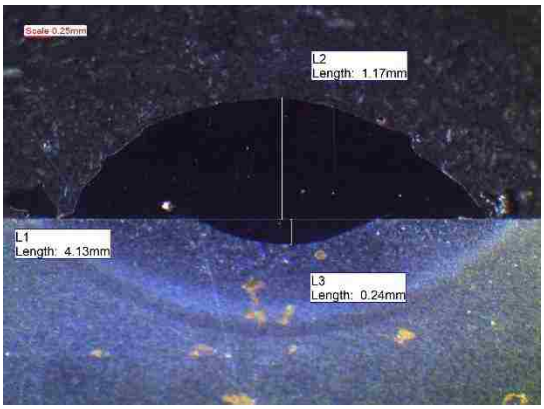

(E)

Figure 105: Bead shapes (A-E) for k=5 clusters

Appendix M: Cluster (K=10) - shape analysis

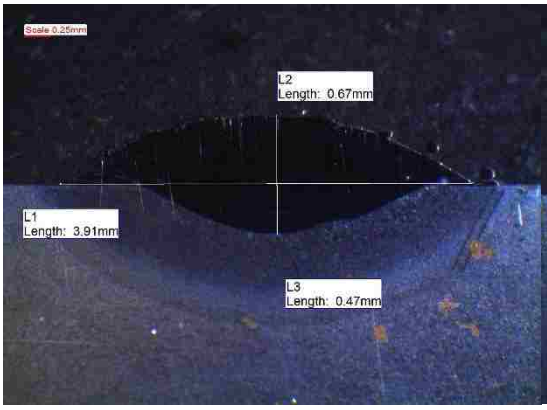

(A)

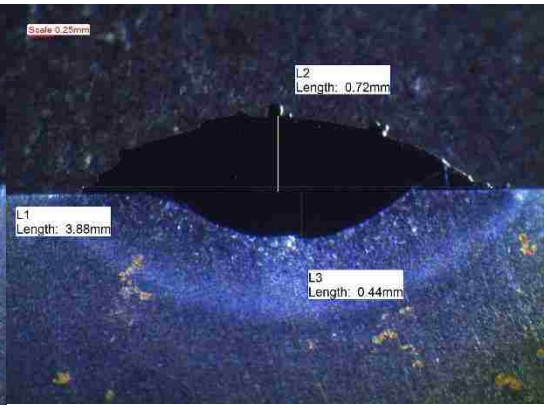

(B)

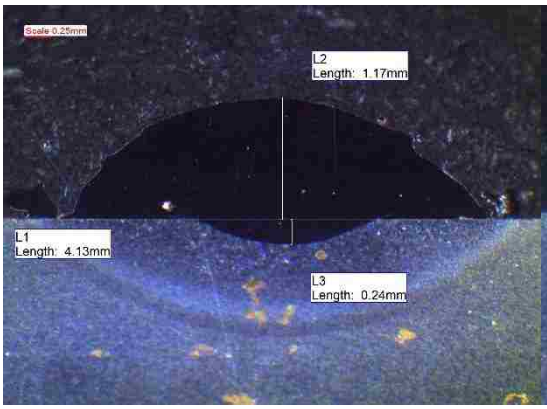

(C)

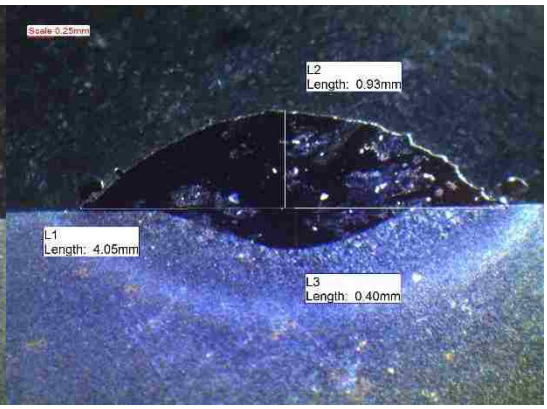

(D)

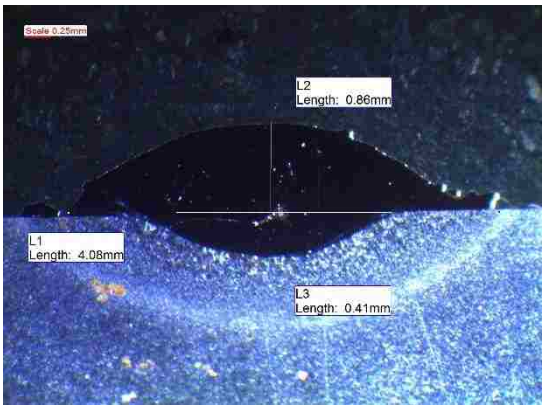

(E)

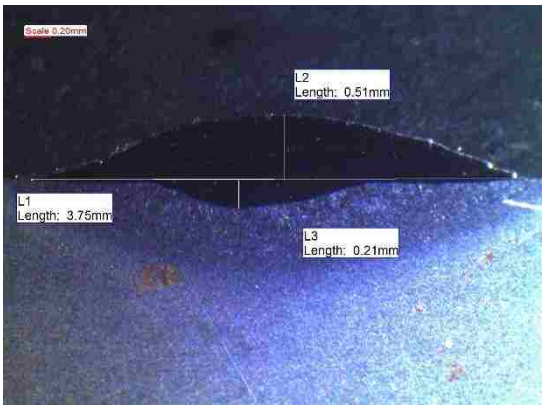

(F)

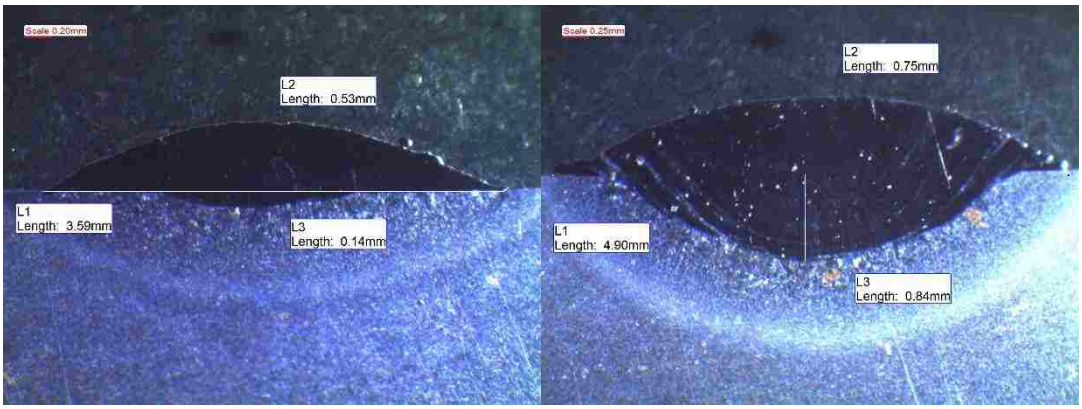

(G) (H)

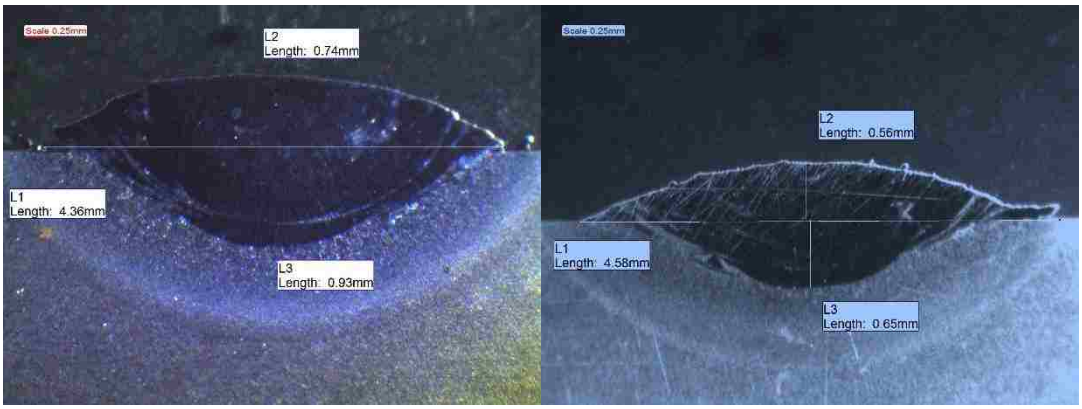

(I) (J)

Figure 106: Bead shapes (A-J) for k=10 optimal clusters

VITA AUCTORIS

NAME:	Kush Aggarwal
PLACE OF BIRTH:	Rohtak, Haryana, India
YEAR OF BIRTH:	1991
EDUCATION:	University of Windsor, M.A.Sc. Mechanical Engineering, Windsor, ON, 2014
	University of Windsor, B.A.Sc. Honours Industrial Engineering With Minor in Business Administration Co-Operative Education, Windsor, ON, 2012
	Lawrence Technological University, Black Belt Lean Six Sigma- Certification, Detroit, MI, 2014
	Lawrence Technological University, Green Belt Lean Six Sigma- Certification, Detroit, MI, 2014